

8  
2 (mit)

NATIONAL AERONAUTICS AND SPACE ADMINISTRATION

*Technical Memorandum 33-605*

*3-D Multilateration: A Precision Geodetic Measurement System*

*P. R. Escobal  
K. M. Ong  
O. H. von Roos  
M. S. Shumate  
R. M. Jaffe  
H. F. Fliegel  
P. M. Muller*

6  
(NASA-CR-132251) THREE-D MULTILATERATION:  
A PRECISION GEODETIC MEASUREMENT SYSTEM  
(Jet Propulsion Lab.) 316 p HC \$18.00  
N73-24412  
CSCL 08E  
Unclas  
G3/13 04172

**JET PROPULSION LABORATORY  
CALIFORNIA INSTITUTE OF TECHNOLOGY  
PASADENA, CALIFORNIA**

March 15, 1973

REPRODUCED BY  
U.S. DEPARTMENT OF COMMERCE  
NATIONAL TECHNICAL  
INFORMATION SERVICE  
SPRINGFIELD, VA 22161

NATIONAL AERONAUTICS AND SPACE ADMINISTRATION

*Technical Memorandum 33-605*

*3-D Multilateration: A Precision Geodetic  
Measurement System*

*P. R. Escobal*

*K. M. Ong*

*O. H. von Roos*

*M. S. Shumate*

*R. M. Jaffe*

*H. F. Fliegel*

*P. M. Muller*

**JET PROPULSION LABORATORY  
CALIFORNIA INSTITUTE OF TECHNOLOGY  
PASADENA, CALIFORNIA**

March 15, 1973

PRECEDING PAGES BLANK NOT FILMED

## PREFACE

The work described in this report was performed by the Mission Analysis Division of the Jet Propulsion Laboratory.

## ACKNOWLEDGMENTS

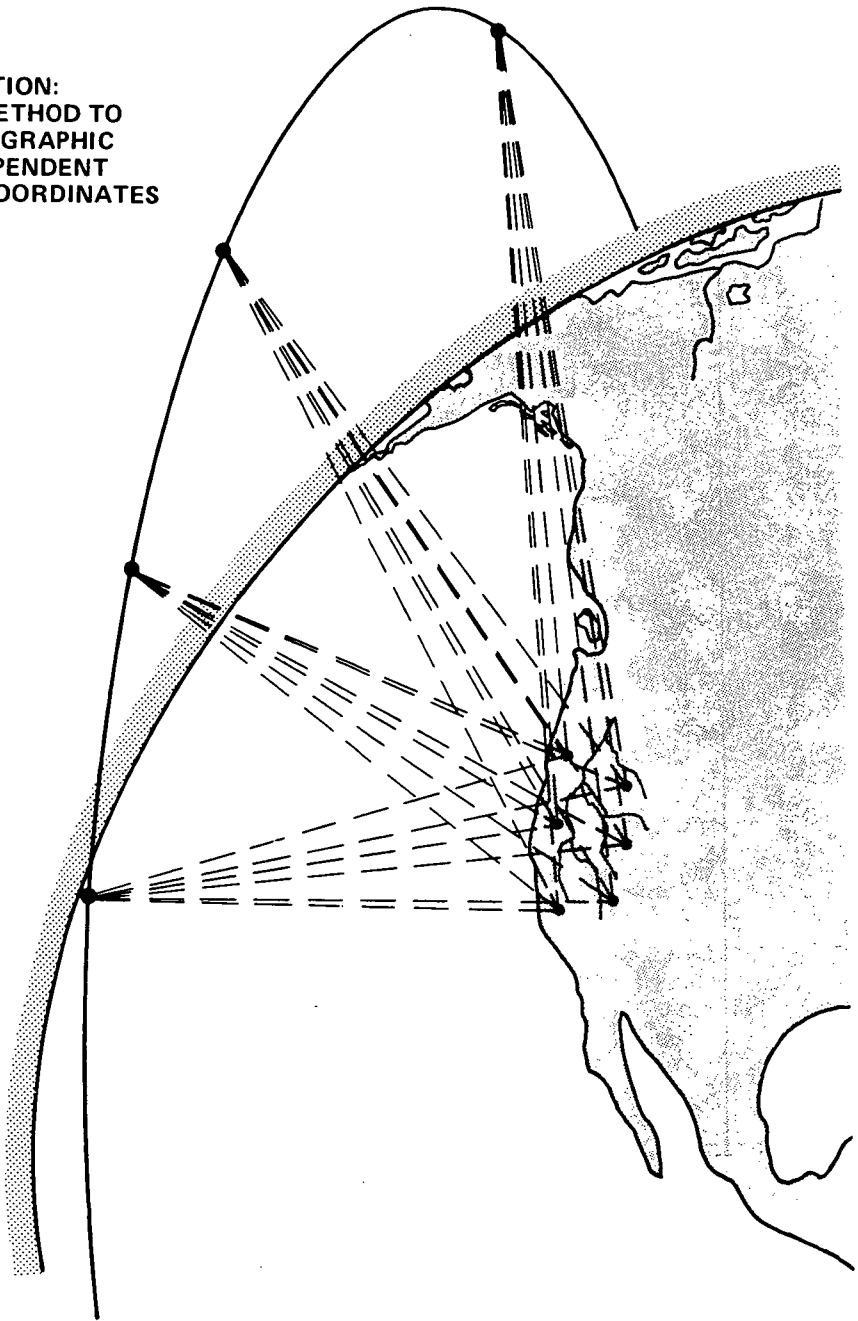
Many suggestions improving the quality of this report were provided by scientists not directly attached to the primary project team. The authors of this report wish to thank all of these contributors. Specifically, the contributions of Leon Knopoff to Section VI need special mention; as do the contributions of Clarence R. Allen, Don L. Anderson, and James H. Whitcomb to Appendix L. Similarly R. J. Wallace is to be thanked for material presented in Section IX.

Other contributors to be cited are H. D. Mc Ginness, B. D. Mulhall, A. W. Newberry, W. M. Peterschmidt and R. A. Zanteson.

After the completion of this report the authors attention was drawn to the independent work by G. Blaha dealing with singularities peculiar to critical ranging networks. The reader is directed to [P. 1] for further information.

**Preceding page blank**

**3-D MULTILATERATION:  
A GEOMETRIC METHOD TO  
DETERMINE GEOGRAPHIC  
POSITIONS INDEPENDENT  
OF SATELLITE COORDINATES**



## CONTENTS

I	SUMMARY . . . . .	1-1
	1.1 Applications of the 3-D Multilateration Technique . . . . .	1-1
	1.2 Description of the 3-D Multilateration Technique . . . . .	1-3
	1.3 Three Systems Using Multilateration Techniques . . . . .	1-4
	1.4 Hardware System and Accuracy Demonstration . . . . .	1-9
	1.5 Analysis of System Errors . . . . .	1-10
	1.6 Anticipated Performance of the Proposed Systems . . . . .	1-12
	1.7 Operational Considerations . . . . .	1-14
	1.8 Comparison with Other Techniques . . . . .	1-15
	1.9 Conclusions . . . . .	1-18
II	HISTORY OF PROJECT . . . . .	2-1
	2.1 Background . . . . .	2-1
	2.2 Recent Developments . . . . .	2-2
III	INTRODUCTION AND COMPARISON TO OTHER SYSTEMS . . . . .	3-1
	3.1 The Geodolite . . . . .	3-1
	3.2 Tiltmeters and Gravimeters . . . . .	3-3
	3.3 The Goddard Laser Ranging System . . . . .	3-4
	3.4 Very Long Baseline Interferometry . . . . .	3-6
	3.5 Comparison of the 3-D Multilateration Technique with the Described Systems . . . . .	3-7
IV	COORDINATE SYSTEMS FOR RANGING EXPERIMENTS . . . . .	4-1
	4.1 Inertial Systems . . . . .	4-1
	4.2 Determination of Station Coordinates . . . . .	4-4
	4.3 Generalized Geometric Coordinate System . . . . .	4-4
	4.4 Adopted Geometric Topocentric Coordinate System . . . . .	4-6
	4.5 Station Coordinate Relationships . . . . .	4-7

CONTENTS (contd)

V	EXPECTED SYSTEM ACCURACIES FOR REAL WORLD CONFIGURATIONS . . . . .	5-1
	5.1 Six-Station Configuration: A System for All Baselines . . . . .	5-2
	5.2 Four Station Configuration: Intercontinental Baselines . . . . .	5-13
	5.3 Collinear Three-Station Configuration: Very Short Baselines . . . . .	5-14
	5.4 Ultimate System Accuracy . . . . .	5-16
VI	GEOLOGICAL APPLICATIONS OF MULTILATERATION: STATION LOCATION SELECTION . . . . .	6-1
	6.1 Critical Components of Earthquake Estimation . . . . .	6-2
	6.2 Plate Tectonics . . . . .	6-5
	6.3 Questions of Primary Interest . . . . .	6-8
	6.4 Earth/Ocean Tide Calibration . . . . .	6-13
	6.5 Concluding Remarks . . . . .	6-15
VII	GENERAL THEORY OF MULTILATERATION . . . . .	7-1
	7.1 Necessary Conditions for the Solution of Range-Only Systems . . . . .	7-2
	7.2 Derivation and Method of Solution of Multilateration Equations . . . . .	7-7
	7.3 Sensitivity Analysis of the Multistation Solution . . . . .	7-11
	7.4 Fundamental Cause and Removal of System Degeneracies . . . . .	7-15
	7.5 Three-Station Solution: A Degenerate but Solvable Configuration . . . . .	7-19
VIII	OPERATIONAL CONSIDERATIONS . . . . .	8-1
	8.1 Orbit Element Selection. . . . .	8-2
	8.2 Viewing Windows . . . . .	8-7
	8.3 Data Smoothing . . . . .	8-11
	8.4 Simultaneous Data Determination . . . . .	8-15
	8.5 Atmospheric Laser Corrections . . . . .	8-20
	8.6 Trajectory Generation Using Geometric Principles . . . . .	8-23

CONTENTS (contd)

	8.7 Weather Constraints . . . . .	8-31
	8.8 Safety Considerations . . . . .	8-36
IX	LASER RANGING HARDWARE STUDY . . . . .	9-1
	9.1 Present Systems . . . . .	9-1
	9.2 Improved Approach to Laser Ranging. . . . .	9-7
	9.3 Experimental Program . . . . .	9-13
	9.4 Demonstration Laser Ranging System . . . . .	9-24
	9.5 Transportable Laser Tracking Station . . . . .	9-46
X	RECOMMENDATIONS AND FUTURE ACTIVITIES . . . . .	10-1
	10.1 Recommended System Configuration . . . . .	10-1
	10.2 Program Plan . . . . .	10-3
	10.3 Future Study Areas. . . . .	10-7
	10.4 Project Recommendations . . . . .	10-12
	REFERENCES . . . . .	11-1
	GLOSSARY . . . . .	12-1
APPENDIX A	COMPUTATIONAL ALGORITHMS FOR GEOMETRIC LASER RANGING . . . . .	A-1
APPENDIX B	DEGENERACIES IN MULTILATERATION THEORY . . . . .	B-1
APPENDIX C	OBTAINING BASELINES USING ONLY 3 STATIONS . . . . .	C-1
APPENDIX D	INVERSE TRILATERATION: A METHOD OF STATION LOCATION . . . . .	D-1
APPENDIX E	TIMING REQUIREMENTS . . . . .	E-1
APPENDIX F	EXPECTED DATA ACCURACY. . . . .	F-1
APPENDIX G	CURVE FITTING TECHNIQUE WITH RATIONAL FUNCTIONS . . . . .	G-1
APPENDIX H	LASER PULSE SHAPE DEGRADATION BY MULTIPLE REFLECTION FROM CORNER REFLECTORS MOUNTED ON A SATELLITE . . . . .	H-1
APPENDIX I	SIGNAL STRENGTH FLUCTUATIONS IN A LASER RANGING SYSTEM DUE TO OPTICAL INTERFERENCE BETWEEN THE MANY REFLECTORS ON A SATELLITE : . . . . .	I-1

CONTENTS (contd)

APPENDIX J TRANSFORMATION OF COORDINATES . . . . .	J-1
APPENDIX K MULTILATERATION SYSTEM BIAS STUDY . . . . .	K-1
APPENDIX L EARTHQUAKE HAZARD ESTIMATION ALONG THE SAN ANDREAS FAULT ZONE FROM A LONG-BASELINE STRAIN NET . . . . .	L-1
APPENDIX M PHYSICAL CONSTANTS . . . . .	M-1
APPENDIX N ABERRATION AND FRESNEL DIFFRACTION . . . . .	N-1

TABLES

5-1	Adopted coordinates in kilometers of the San Andreas Fault stations . . . . .	5-4
5-2	The average errors, $\epsilon$ , and the standard deviations, $\sigma$ , of the coordinates of the San Andreas Fault stations in centimeters assuming 1 cm normal random errors in ranging . . . . .	5-5
5-3	Adopted coordinates in kilometers of the continental stations . . . . .	5-7
5-4	The average, $\epsilon$ , and the standard deviation, $\sigma$ , of station coordinate errors in centimeters for the continental stations, assuming 1 cm normal random error in ranging . . . . .	5-7
5-5	The average, $\epsilon$ , and the standard deviation, $\sigma$ , in centimeters of the errors in the station coordinates of the intercontinental configuration (origin assumed to be at Mexico City) . . . . .	5-10
5-6	The average, $\epsilon$ , and the standard deviation, $\sigma$ , in centimeters of the errors in the station coordinates of the second intercontinental configuration (origin assumed to be at Kaneohe) . . . . .	5-10
5-7	Average, $\epsilon$ , and standard deviation, $\sigma$ , in station locations for the airplane system in Los Angeles (origin assumed to be at San Fernando) . . . . .	5-11
5-8	Average, $\epsilon$ , and standard deviation, $\sigma$ , in centimeters of station coordinate errors for the four-station inter- continental system (origin assumed to be at Mexico City) . . . . .	5-13
5-9	Accuracy of the 3-station system as a function of the misalignment $Y_3$ from the X-axis . . . . .	5-16

TABLES (contd)

7-1	Summary of conditions . . . . .	7-2
7-2	Parametric solution of inequality . . . . .	7-4
8-1	Error sources . . . . .	8-27
8-2	The probability, given n stations, each of which has probability p of acquiring useful ranges on a given pass of the satellite, that at least 6 stations will acquire ranges . . . . .	8-34
8-3	The probability, given n stations, each of which has probability p of acquiring ranges on a given pass of the satellite, that at least 4 stations will acquire useful ranges . . . . .	8-35
9-1	Performance parameters of several laser ranging systems . . . . .	9-5
9-2	Mode locked ruby laser characteristics . . . . .	9-9
9-3	Characteristics of RCA C31034 photomultiplier tube . . . . .	9-16
9-4	High resolution time interval meters . . . . .	9-21
9-5	Measurement of time-interval meter interpolator error . . . . .	9-24
9-6	Constant fraction discriminator characteristics . . . . .	9-39
9-7	Experimental ranging system accuracy . . . . .	9-45
9-8	Description of terms and typical values for equation (9.5.1) . . . . .	9-47
9-9	Tracking mount errors . . . . .	9-53
9-10	Design cost . . . . .	9-59
9-11	Equipment cost . . . . .	9-60
9-12	Network support equipment . . . . .	9-60
K-1	The average error $\epsilon$ and the standard deviation $\sigma$ of the coordinates of the San Andreas Fault stations in centimeters, assuming 1 cm standard deviation normal random errors in ranging and 1 cm standard deviation bias for each station . . . . .	K-3

## FIGURES

1-1	Applications of 3-D multilateration . . . . .	1-2
1-2	Two basic components of overall system . . . . .	1-3
1-3	Six station solution . . . . .	1-5
1-4	Four station solution . . . . .	1-6
1-5	Three station solution . . . . .	1-7
1-6	Geometric coordinate system . . . . .	1-11
4-1	Inertial coordinate system . . . . .	4-2
4-2	Geometric coordinate system . . . . .	4-5
4-3	Geometric topocentric coordinate system . . . . .	4-7
5-1	The adopted coordinate system for 6 stations along the San Andreas fault . . . . .	5-3
5-2	The continental station network . . . . .	5-6
5-3	An intercontinental network . . . . .	5-9
5-4	The 6 station airplane system in the Los Angeles area . . . . .	5-12
5-5	Misalignment of station 3 in the collinear three-station system . . . . .	5-14
6-1	Strain as a function of time . . . . .	6-2
6-2	Strain versus time . . . . .	6-4
6-3	Large earthquakes and associated faulting in the California and Nevada region . . . . .	6-9
6-4	Earth/moon tides . . . . .	6-14
7-1	Degeneracies causing system malfunction . . . . .	7-5
7-2	A station measuring the range between itself and an orbiting satellite . . . . .	7-7
7-3	Fundamental equation . . . . .	7-16
8-1	Orientation elements . . . . .	8-4
8-2	Superposition to rise/set functions . . . . .	8-7
8-3	Range history as a function of time . . . . .	8-15
8-4	Polar view of the orbital path of a trilaterated satellite, T, and a dynamically determined satellite, D . . . . .	8-24
8-5	Schematic orbit determination process . . . . .	8-25
8-6	Orbital paths as a function of initial conditions . . . . .	8-26
8-7	Sequential processing of data . . . . .	8-29

## FIGURES (contd)

9-1	Block diagram of a typical laser satellite ranging system currently in use . . . . .	9-3
9-2	Sampling oscilloscope display of the average shape of the dark current pulse from an RCA C31034 photomultiplier tube. . .	9-17
9-3	Block diagram of a high resolution time interval meter. . . . .	9-19
9-4	Diagram of experimental apparatus for testing for time interval meter interpolator errors . . . . .	9-22
9-5	Photograph of the demonstration laser ranging system, showing the optical assembly, laser pulse generator, power supplies, constant fraction timing discriminator, and time interval meter. . . . .	9-26
9-6	Block diagram of the demonstration laser ranging system. . . . .	9-27
9-7(a)	Optical assembly with covers in place . . . . .	9-28
9-7(b)	Optical assembly with covers removed . . . . .	9-29
9-8	Pulse generator circuit for providing short duration, fast rise time pulses to a gallium-aluminum-arsenide diode laser . . . . .	9-31
9-9	Gallium-aluminum-arsenide diode laser mount . . . . .	9-33
9-10	Sampling oscilloscope trace of the electrical pulse driving the diode laser . . . . .	9-34
9-11	Photomultiplier tube socket wiring schematic . . . . .	9-35
9-12	Close-up photograph of the photomultiplier tube socket wiring, showing details of the output cable connection to the tube socket pins . . . . .	9-36
9-13	Time domain reflectometer display of the PMT output circuit . . . . .	9-38
9-14	Sampling oscilloscope trace of the electrical signal from an RCA C31034 PMT . . . . .	9-41
9-15	Variation of the response time of an RCA C31034 PMT with signal level . . . . .	9-43
9-16	Diagram of the major optical components in a proposed transportable laser ranging system. . . . .	9-51
9-17	Artist's sketch of the optical mount assembly diagrammed in Figure 9-16 . . . . .	9-52
9-18	Artist's sketch of a complete transportable laser ranging system, showing the optical mount in its transporter . . . . .	9-55
9-19	Block diagram of a transportable laser ranging station. . . . .	9-57

FIGURES (contd)

B-1	An operational flow diagram for the discovery and avoidance of degeneracies . . . . .	B-9
C-1	Three station collinear system . . . . .	C-2
C-2	Physical interpretation of alignment error . . . . .	C-8
D-1	Relation between the physical and the image solutions to the trilateration problem . . . . .	D-4
H-1	Reflectors mounted on spherical satellite . . . . .	H-2
H-2	Pulse shapes . . . . .	H-6
I-1	Probability distribution of dynamic range . . . . .	I-12
J-1	Inertial and geometric coordinate systems . . . . .	J-1
L-1	Large earthquakes and associated faulting in the California and Nevada region . . . . .	L-3
L-2	Schematic graph of a real station displacement rate $\underline{r}$ and two displacement measurements with errors $\pm \underline{a}$ and $\pm \underline{b}$ respectively and with intervening time interval $\underline{i}$ . . . . .	L-6
L-3	Major faults, lithospheric plates, and proposed stations for the initial long-baseline strain net in Southern California . . . . .	L-8
N-1	The idealized configuration for the optical system consisting of a corner reflector and a beam spreading lens . . . . .	N-7
N-2	The mathematical model simulating Fig. N-1. Source is the virtual focus of the lens on Fig. N-1. The corner reflector is simulated by a circular aperture of radius $a$ . The far field diffraction pattern is calculated by standard means (Ref. A (N-1)). . . . .	N-7
N-3	Fraunhofer ( $r_o = \infty$ ) and Fresnel diffraction. Explanations in the text . . . . .	N-8

## 3-D MULTILATERATION: A PRECISION GEODETIC MEASUREMENT SYSTEM

### ABSTRACT

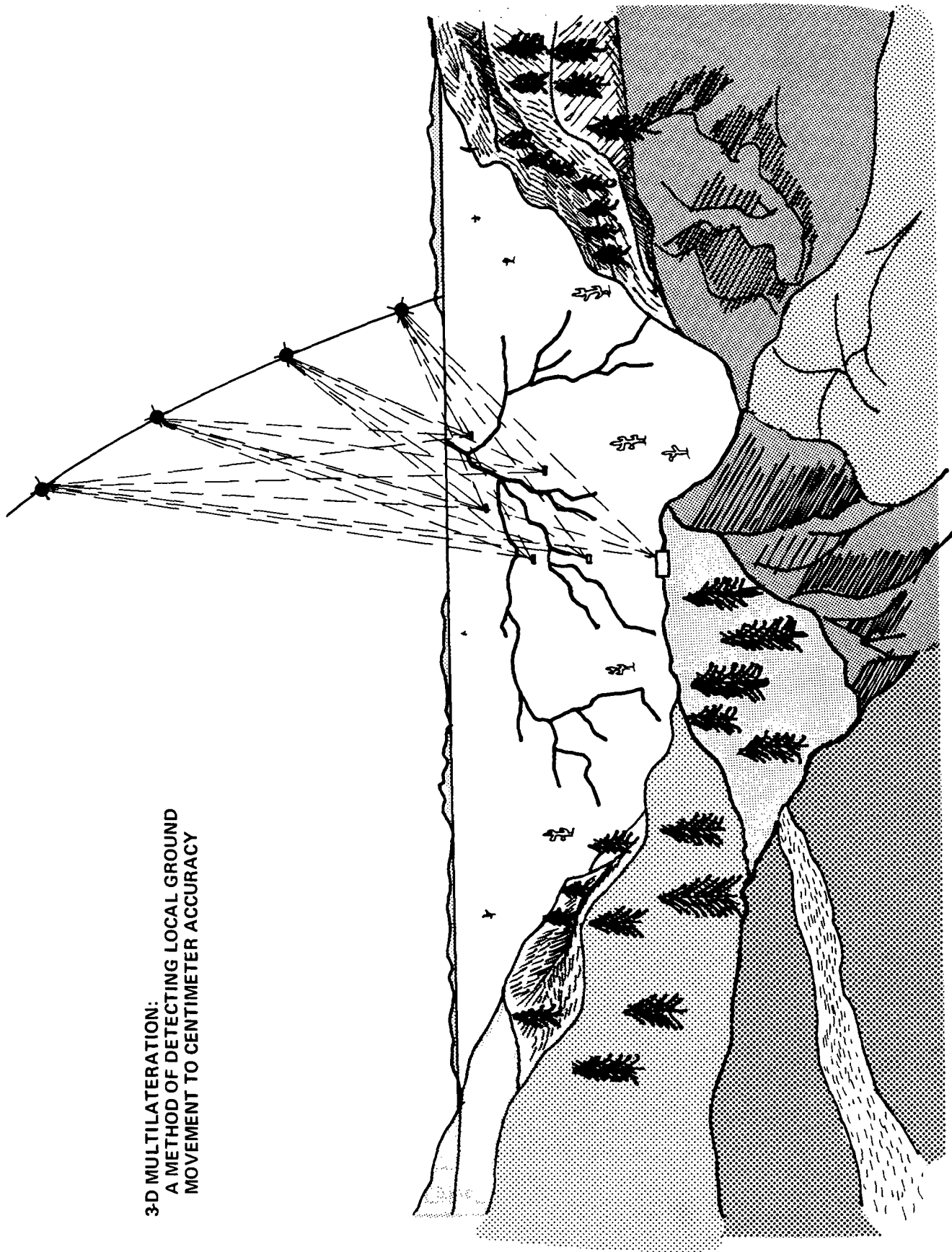
The systems analysis and laboratory demonstration described in this report indicate that a new technique of satellite geodesy, to be called 3-D Multilateration, can determine the relative three dimensional coordinates of ground stations within 1 centimeter over baselines of 20 to 10,000 kilometers. With this high accuracy, several crucial geodetic applications become possible. These applications include: earthquake hazards assessment, precision surveying, plate tectonics, and orbital applications.

Achievement of such accuracy can be attained through use of pulsed lasers to obtain simultaneous slant-ranges between an ensemble of ground stations and a moving retroreflector whose trajectory is known a-priori only to the accuracy necessary for aiming the lasers. Specifically, the positions of the satellite or airplane carried retroreflectors are eliminated from the equations which govern determination of station locations. However, once the station locations are determined, the trajectory of the retroreflector can be obtained as a direct by-product.

Numerical analysis has shown that suitably chosen multistation configurations result in well-conditioned solutions, with very small error magnification of the inherent ranging errors occasioned by the hardware subsystem.

Laboratory tests have demonstrated that a laser hardware subsystem with a ranging accuracy of 3 centimeters can be built from commercially available components. By 1975, at the latest, an accuracy level of 1 centimeter can be achieved. Costs of the proposed systems are lower than other proposed systems on a station construction and implementation basis.

3-D MULTILATERATION:  
A METHOD OF DETECTING LOCAL GROUND  
MOVEMENT TO CENTIMETER ACCURACY



## SECTION I

### SUMMARY

$\Sigma$  This Section briefly summarizes the basic concepts and investigations of the 3-D Multilateration system study performed at JPL under contract number NASA 7-100. The Summary Section is intended to be a detachable unit from the main body of this report.

#### 1.1 APPLICATIONS OF THE 3-D MULTILATERATION TECHNIQUE

Earthquakes are the result of sudden slips between two blocks of the Earth's crust. The entire Earth is covered by large blocks which may be in steady motion relative to each other at points distant from their boundaries. At the boundaries, i. e. , at seismic zones, the blocks are held together by friction. When the driving stresses exceed the breaking strength of the frictional contact, abrupt motion ensues and an earthquake occurs. However, the Earth is a deformable body and in the earthquake case, it deforms non-elastically in creep. Creep strains build up in regions astride earthquake faults, and are relieved, at least in part, by the occurrence of an earthquake on the fault. Occasionally, some creep is observed on the faults themselves. A knowledge of the strain configuration in the Earth's crust, both at a fault and at points distant from the fault, is an essential ingredient to a program of learning how to estimate the location and the epoch of major earthquakes. There are no specific problems in the measurement of creep along faults, since the motion takes place over relatively short distances. To evaluate the strain accumulation in a large region surrounding a fault, it is necessary to measure precisely the relative motion of points in various parts of this region. If this motion is to be evaluated within a period of one to two years, it will be

necessary to measure distances as large as 10,000 km with an accuracy of 3 cm or better. Until this moment there has been no technique capable of making such measurements.

In this report a new technique, 3-D Multilateration, will be described. This technique appears to provide not only a one centimeter distance measurement accuracy capability, but also determines each station position in three dimensions and thereby allows evaluation of the different components of strain buildup. Furthermore, since the 3-D Multilateration technique will require only hours to obtain raw data and process this data into geophysically significant information, it may be possible to detect the presence of rapidly occurring ground creep which often gives a premonitory indication of earthquakes.

It should be noted that the 3-D Multilateration technique can be used in geophysical analysis not directly related to earthquake prediction. This technique is sufficiently flexible to permit a wide variety of applications, as illustrated in Figure 1-1.

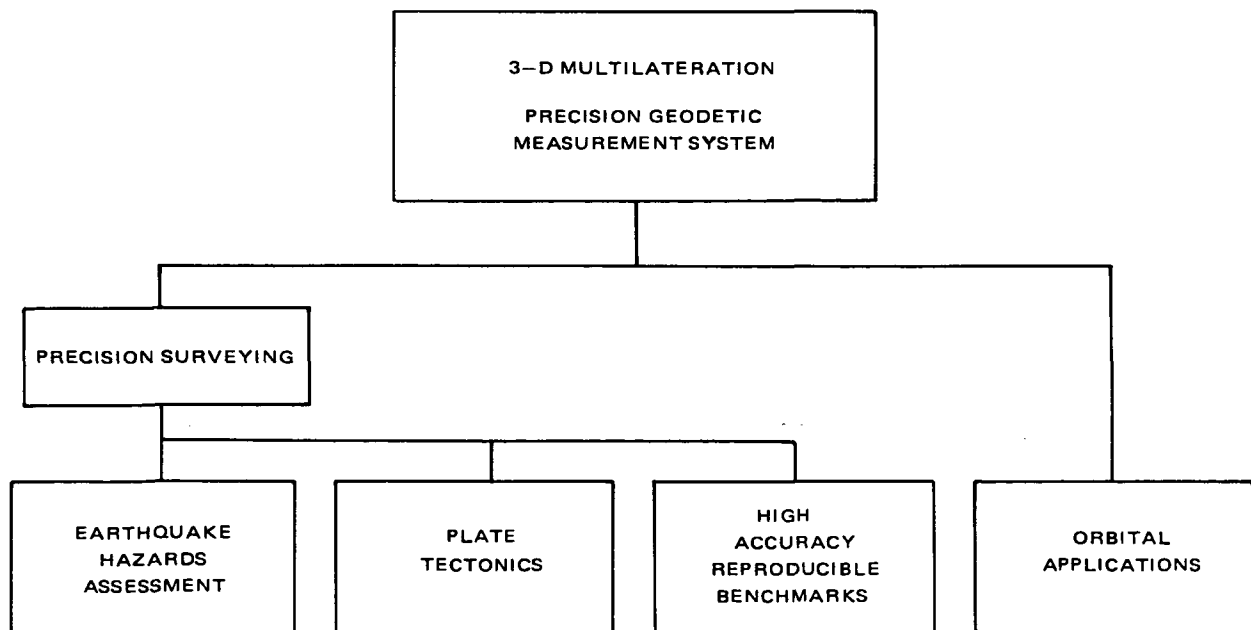


Figure 1-1. Applications of 3-D Multilateration

In summary, if the performance of the 3-D Multilateration technique demonstrated in this report is realized, not only will science be provided with a valuable tool for investigation of tectonic phenomena, but there is a significant possibility that geophysicists will be able to predict the location, and perhaps the approximate time, of future earthquakes.

## 1.2 DESCRIPTION OF THE 3-D MULTILATERATION TECHNIQUE

The 3-D Multilateration technique can be implemented through use of a number of ground stations which nearly simultaneously transmit laser pulses to reflectors on a moving vehicle, e.g., an airplane or a satellite. Each station evaluates station-to-vehicle range by measuring the time interval between transmission of the original pulse and reception of the reflected pulse. Simultaneous range measurements are then processed to yield relative station locations in 3 dimensions.\*

The components which are necessary to define the Precision Geodetic Measurement System are illustrated in Figure 1-2.

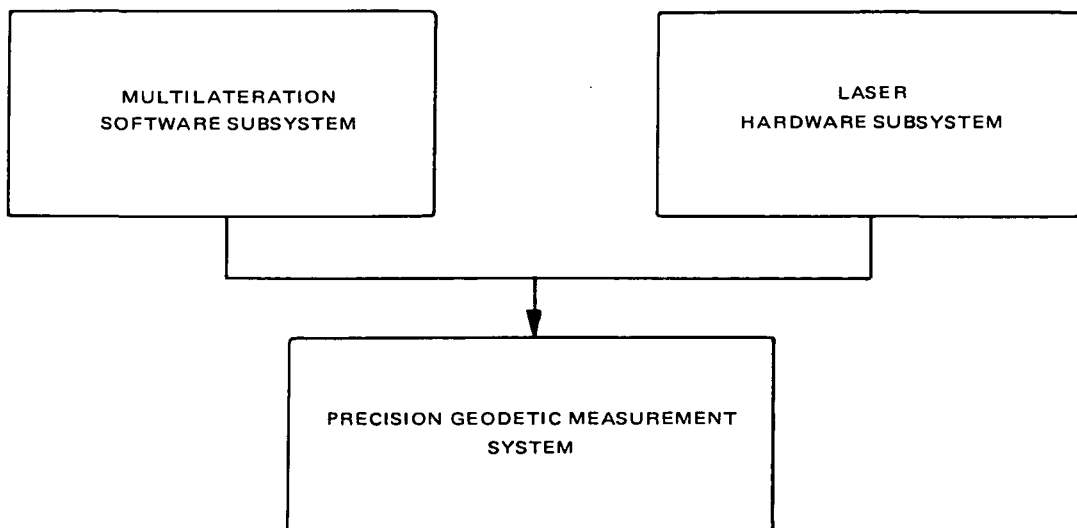


Figure 1-2. Two Basic Components of Overall System

---

\*See Para. 1.5 for definition of the phrase "relative station locations."

An important advantage of multilateration techniques is that no information concerning the vehicle trajectory is required to obtain station coordinates relative to one another. Thus, uncertainty of the satellite ephemeris has no effect on the deduced station coordinates. Indeed, it is possible to determine the trajectory of the vehicle in the coordinate frame of the stations to the centimeter level. In summary two kinds of information are provided by 3-D Multilateration:

- The three-dimensional coordinates of all stations utilized in the operational configuration, and
- The precise positions of the moving retroreflector mounted on the vehicle.

### 1.3 THREE SYSTEMS USING MULTILATERATION TECHNIQUES

Three separate systems, which are possible, will be discussed in this report. These systems will require the use of six, four and three stations for operational implementation. Specifically it is demonstrated that solutions for the station coordinates are possible if:

- Six stations simultaneously make 6 range measurements (between station and vehicle) at four independent times,
- Four stations simultaneously make 4 range measurements at six independent times,
- Three stations (which are aligned) simultaneously make 3 range measurements at two independent times.

The above three solutions give rise to what will be referred to in this report as the 6 station system, the 4 station system, and the 3 station system.

The process of making simultaneous range measurements from any number of stations to a vehicle, i. e., to an airplane or satellite (at a single instant of time) is called a strike. Hence, to obtain a solution for the station coordinates what is required is a sequence (timewise) of strikes. The rules described above are stated as the minimum requirement for a deterministic solution to the 3-D Multilateration problem. A much longer sequence of strikes would be used for purposes of statistical improvement. Hence in more detail there exists:

- The Six Station Solution (Figure 1-3) which states that:

Six ground stations which make a sequence of four or more simultaneous strikes (which are separated in time by any arbitrary duration) to one or two vehicles, will give rise to a mathematically and numerically stable solution for the determination of relative three-dimensional station locations. The station coordinates can be obtained without using the vehicle coordinates within the defining equations, and without any restriction on the distance between the stations. The vehicle position and velocity can be obtained as a by-product of the calculation.

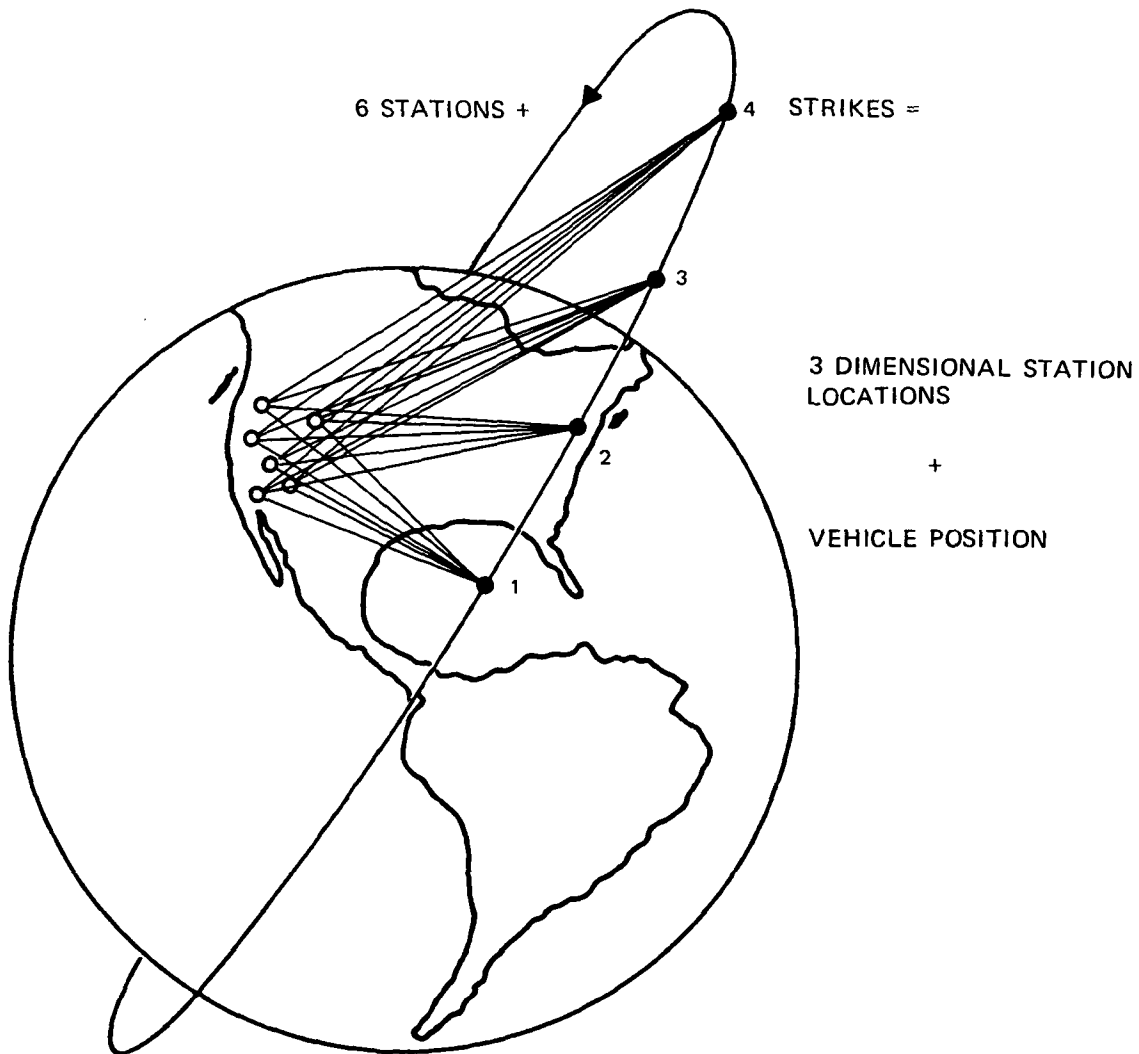


Figure 1-3. Six Station Solution

\* See Para. 1.5 for the definition of relative station locations.

- The Four Station Solution (Figure 1-4) which states that:

A solution for the relative station locations can be obtained by using four ground stations which make a sequence of six or more simultaneous strikes (which are separated in time by any arbitrary duration) to one or more vehicles, if the fourth station is located out of the plane of the other three stations by a reasonably large distance, such as might be obtained in establishing intercontinental reference locations. As with the previous solution the position of the vehicle does not enter into the calculations, but is in fact obtained as a by-product.

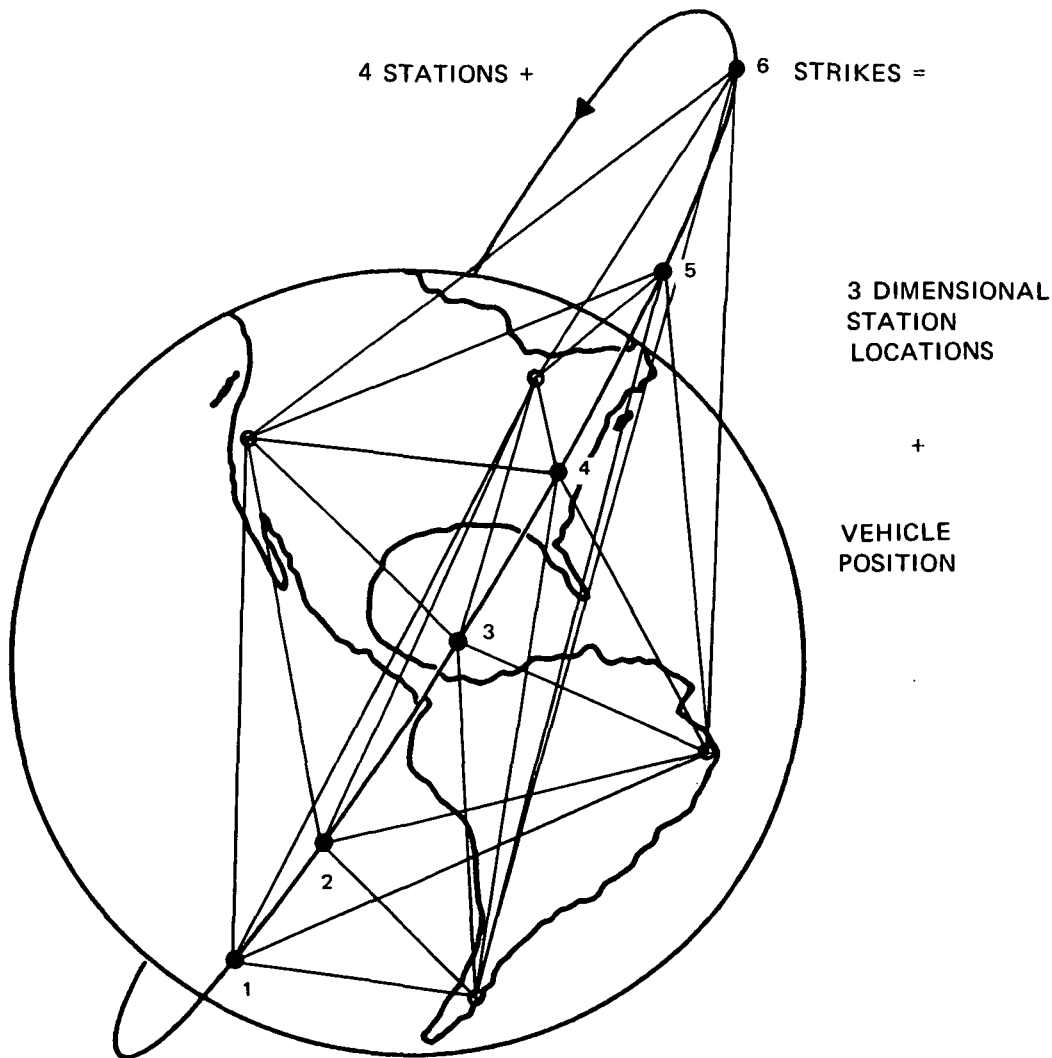


Figure 1-4. Four Station Solution

- The Three Station Solution (Figure 1-5) which states that:

The relative distance between two ground stations can be obtained by aligning a third station in a straight line with respect to the first two stations and taking a sequence of two or more simultaneous strikes (which are separated in time over any arbitrary duration) to a vehicle. Again, no satellite ephemeris information is needed in the calculation of station locations.

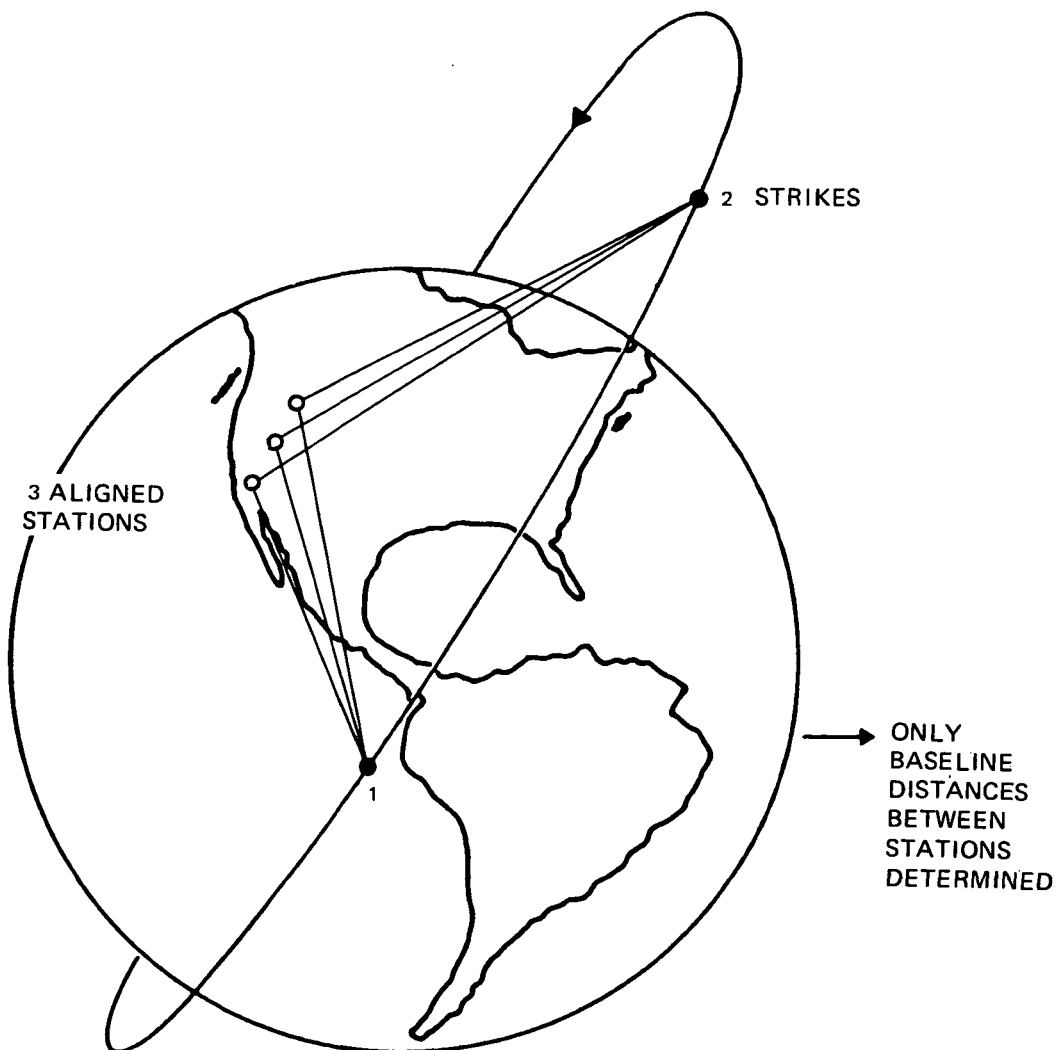
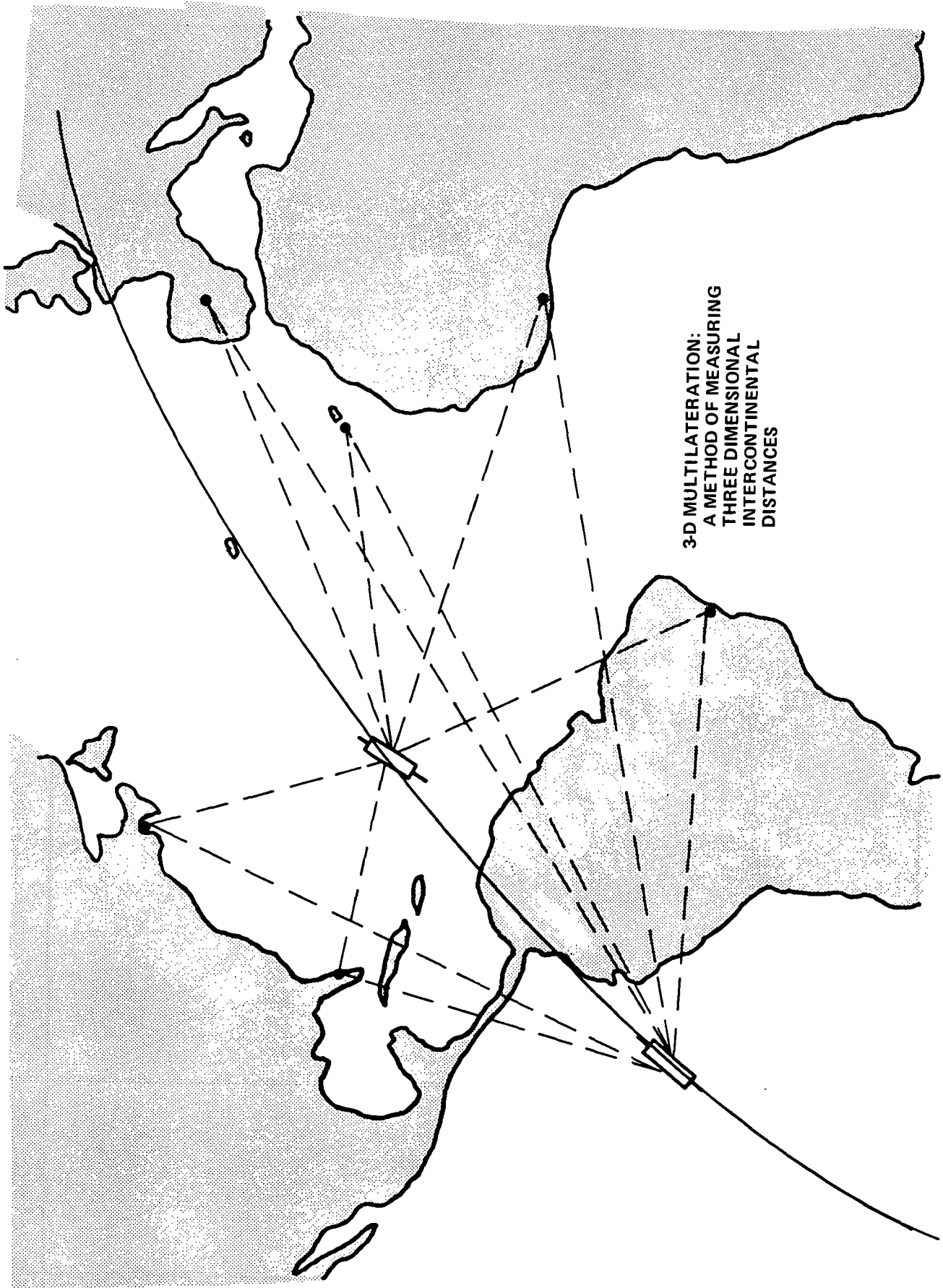


Figure 1-5. Three Station Solution



3-D MULTILATERATION:  
A METHOD OF MEASURING  
THREE DIMENSIONAL  
INTERCONTINENTAL  
DISTANCES

In closing this Section it should be mentioned that other system combinations are possible. For example, in the four station solution it is possible to fix two of the baselines between the stations and arrive at a suitable solution for nearly coplanar configurations. In fact, the four station system previously described, can then be used for local and intercontinental applications. The baselines can be obtained by several methods which will be described shortly. Hence, though not much emphasis is placed upon these systems there also exists a myriad of:

- Hybrid Multilateration Solutions.

These and other solutions can be obtained using range data (as previously described) or by use of range difference data, i. e., the difference in-range between the vehicle and two stations.

#### 1.4 HARDWARE SYSTEM AND ACCURACY DEMONSTRATION

The hardware subsystem for measuring station-to-vehicle ranges is identical for all station configurations. In order to obtain high accuracy range measurements, the subsystem utilizes a new type of pulsed laser. This laser is a mode-locked, Q-spoiled ruby laser, and has the capability of emitting very short duration (0.1 ns or less) light pulses. The subsystem employs a tracking mount to aim transmitting and receiving telescopes at the vehicle. A measurement is made of the duration required for a laser pulse to make a round trip from the station to the vehicle borne retroreflector. This duration, measured with a resolution of 0.1 ns, is used in conjunction with an atmospheric model to calculate the range to the vehicle.

Each ground station contains an X-Y tracking mount for steering the two telescopes, a small computer to direct the tracking mount towards the satellite, timing circuitry, recording equipment and power supplies.

In order to satisfy the requirement for "simultaneous" ranging, the clocks at each station must be synchronized to 3  $\mu$ sec. Such synchronization is easily achievable using low-cost components. Synchronization of laser firing to 1 ms accuracy is adequate and well within the state of the art; variations of laser firing within this range are compensated for by time-tagging range measurements, and interpolating between successive measurements so as to obtain effective simultaneity among stations.

In order to evaluate the measurement errors produced by current hardware, a demonstration ranging subsystem was assembled using commercially available components. The hardware configuration simulated a long distance ranging system over short path lengths by using attenuated return signals. The results obtained with this system show that hardware related errors in range measurement can be made acceptably small, typically less than 2 cm. Future systems, fabricated circa 1975, can be expected to operate with 1 cm ranging accuracy for satellites placed in orbits yielding nominal system efficiency.

#### 1.5 ANALYSIS OF SYSTEM ERRORS

It is emphasized that the system errors caused by the satellite, Earth constants, and orbital perturbations do not enter into the multilateration process. In fact, since the proposed techniques are independent of the location of the retroreflector, the only error sources which enter into these techniques are as follows:

- Multiple reflection error,
- Bias error due to atmospheric delay,
- Random error due to atmospheric turbulence,
- Random equipment measurement error,
- Equipment bias error.

It is shown in this study that a ranging subsystem can be fabricated in which the net effect of these errors will lead to a ranging accuracy of 1 cm.

The geometric coordinate system used in these studies is a relative coordinate system, in which Station 1 is placed at the origin, arbitrary placement of Station 2 fixes the X axis, and arbitrary location of Station 3 defines the X-Y plane of the coordinate system (see Figure 1-6).

This coordinate system can be linked to the inertial geocentric coordinate system only via the geographic coordinates of the first adopted station. The standard deviations in the latitude, longitude and elevation of Station 1, established by other methods distinct from multilateration, are required inputs to the process of computing errors in the inertial coordinate system.

These error sources, however, are not an integral part of the proposed geometric laser ranging technique which has been studied at the Jet Propulsion Laboratory for the determination of relative station locations.

If the method of multilateration is used to determine the trajectory within the standard inertial system, then the following errors must be considered:

- The geographic coordinates of the first station,
- The astrodynamics constants,
- Timing errors.

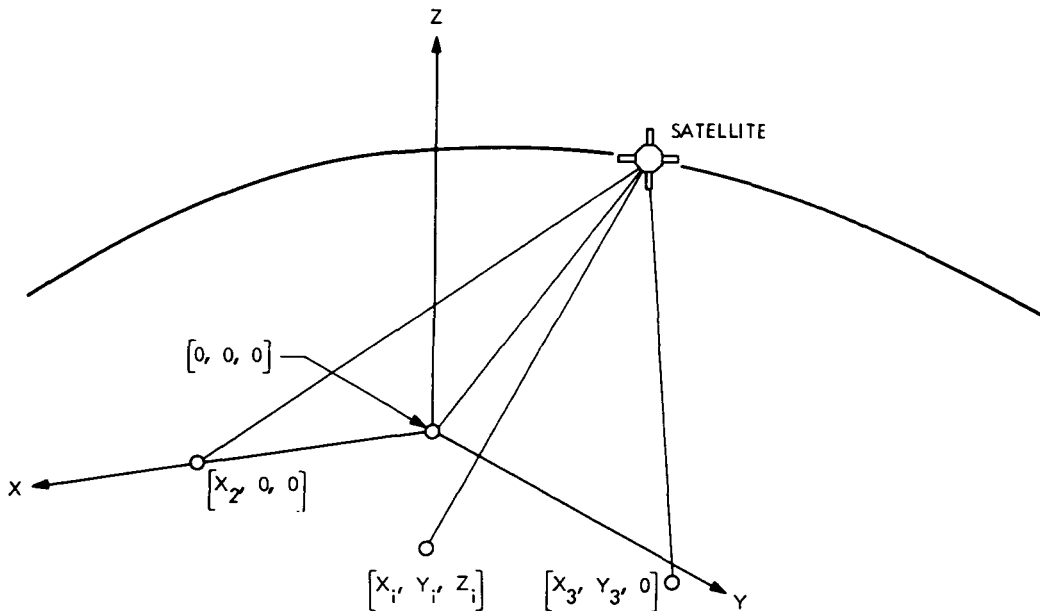


Figure 1-6. Geometric Coordinate System

Specifically, these errors will be transferred only to the coordinates of the orbit in the inertial frame. Hence only the coordinates of the orbit will be corrupted by the analytic process but not the relative station locations.\* If the trajectory of the orbit is determined in the geometric frame these errors will, of course, vanish.

## 1.6 ANTICIPATED PERFORMANCE OF THE PROPOSED SYSTEMS

The comparison of the three proposed systems requires examination of three basic factors:

- System Cost,
- Operational Cost,
- Accuracy.

### 1.6.1 Cost Estimates

Station fabrication costs will be moderate, with each station expected to cost approximately \$275,000 when fabricated in quantities of six.

While operational costs have not been estimated in this report, automatic operation of the hardware subsystem has been included in the preliminary design.

The software subsystem costs are a small fraction of the overall cost due to the inherent simplicity of 3-D Multilateration technique. An operational software system to process the raw data can be developed for \$150,000.

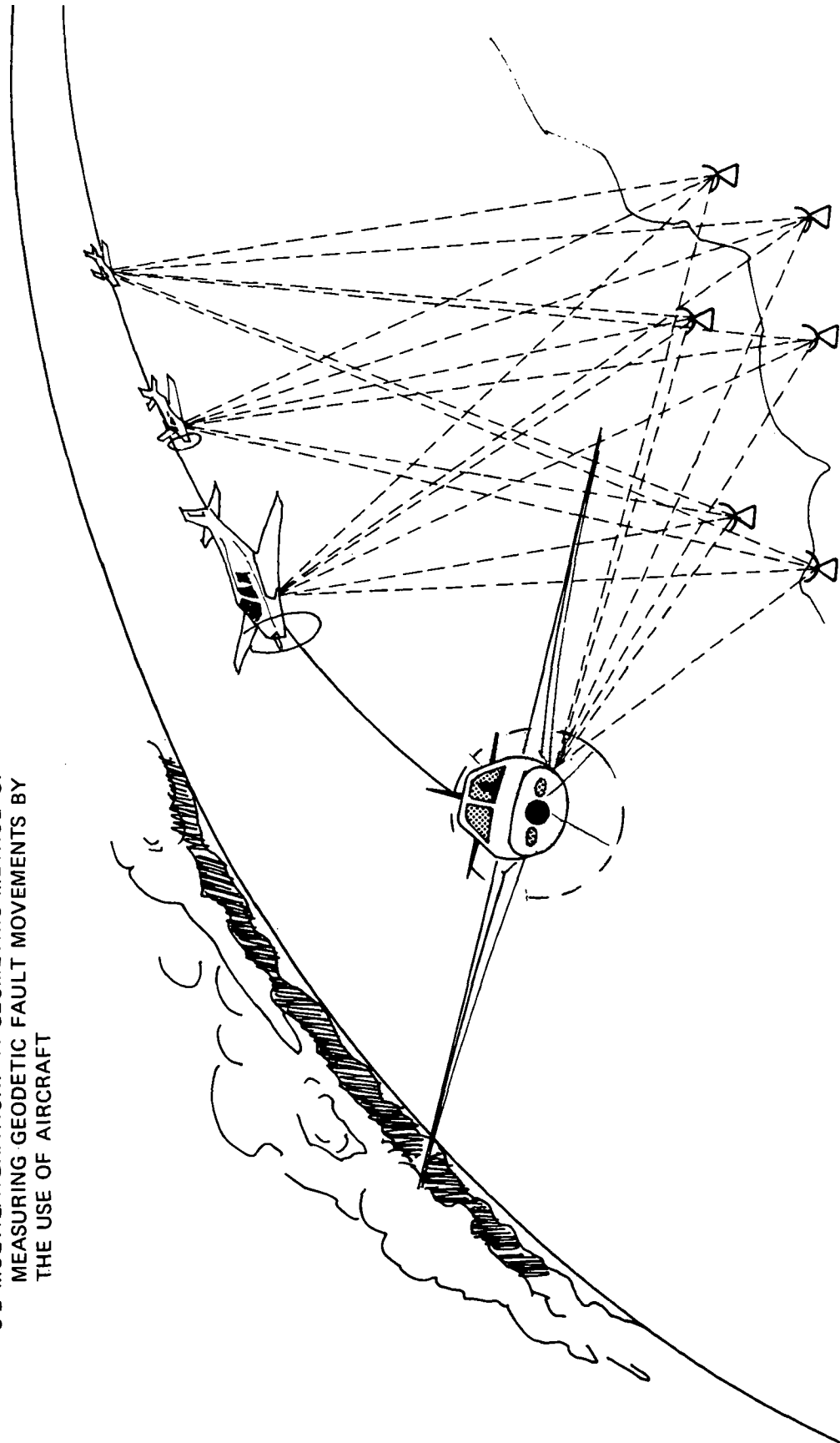
### 1.6.2 Accuracy

It is shown in this report that the three and four station systems have certain limitations. Specifically the three station system will function only if the three stations are collinear. Furthermore, this system determines inter-station baselines only. On the other hand, multilateration systems using four or five stations do not function for local separation between the stations. Specifically, the equations defining the three dimensional coordinates become

---

\*The laboratory units of distance discussed in this report are ultimately dependent on the adopted value for the velocity of light.

3-D MULTILATERATION: A GEOMETRIC METHOD OF  
MEASURING GEODETIC FAULT MOVEMENTS BY  
THE USE OF AIRCRAFT



singular unless the stations are placed at intercontinental distances. However, it is proved that if six or more stations are used to define the system, the inherent mathematical singularity vanishes. This important fact has the effect of increasing the accuracy of the station location determinations whether the six station system is used in a local or global capacity. For observation sets of 100, 1-cm accuracy measurements, the performance of each proposed system is summarized below.

- For the six station system, the errors occasioned upon the three coordinates of each station are of the order of 1 centimeter for well-scattered local and/or global station locations.
- For the four station system, using a wide baseline separation (3000-5000 km) between the stations, an accuracy of the order of 5 to 10 centimeters can be obtained.
- If three stations in a straight line are used to determine the distance between the stations, e. g. , in the three-station system, an accuracy of 3 centimeters can be obtained in determining the baseline between the first two stations.

#### 1.7 OPERATIONAL CONSIDERATIONS

As will be explained, the proposed systems require the use of an elliptic orbit, or two circular orbits. These requirements are not a barrier and are not expensive. The elliptic orbit approach is recommended as the simplest, e. g. , a 400 x 1000 km orbit with inclinations between 45° and 60° is acceptable for stations with 100 to 1000 km separation.

The proposed system outlined herein can be implemented by using a octahedral array of reflectors to achieve a strict point source reflection. The array can be attached to any available satellite whose overall mission objective might be considerably different from the experiments proposed herein.

Atmospheric attenuation is not expected to significantly degrade system performance. Other work (See Section 8) indicates that atmospheric effects can be corrected to a residual error of 2 mm at the zenith, and approximately 1 cm at 70° from the zenith.

Since each station uses small telescopes and a simple tracking mount, the stations can be made transportable and can be moved to various locations. Thus, a single set of stations can be used to map a large number of locations.

It has been already mentioned that synchronization of the laser firing to 1 ms is adequate, and that data-interpolation can be obtained from polynomials. The easily met constraint of the station clock synchronization to 3  $\mu$ sec, which is necessary for time-tagging the observations, presents no problem.

In real time operations the station up-times due to common visibility durations as a function of weather must be considered. Safety considerations, as with all laser systems, must be taken into account; e. g. , it has been shown that laser damage to the unshielded human retina can result if a direct laser strike is sustained by a pilot whose retina crosses the laser beam.

## 1.8 COMPARISON WITH OTHER TECHNIQUES

There are three other techniques which are presently in existence for precision geodetic surveying. They are:

- The Geodolite
- The Goddard Laser Ranging System
- Very Long Baseline Interferometry

Spectra-Physics of Mountain View, California manufactures a laser-ranging device known as the Geodolite which is capable of measuring the distance between points on the Earth's surface. The Geodolite can measure only

line-of-sight distances, but provides excellent accuracy over its severely constrained range. For example, the U.S. Geological Survey has used a Geodolite to measure baselines of 30 km with accuracies of 1 cm or better; however, in order to achieve this accuracy, the USGS combined a number of partially redundant measurements from different benchmarks, and then corrected these raw measurements with temperature and humidity data obtained by overflying the baselines with a helicopter. In summary, although the Geodolite appears to be an excellent device for obtaining high accuracy distance measurements over short baselines, it is not an acceptable tool for measuring the 3-dimensional components of distance over long baselines.\* Consequently, the Geodolite is suitable for investigations similar to those anticipated for our 3-station system, but is completely inapplicable to the long distance, 3-dimensional measurement problems capable of being solved by 6-station system.

The second comparable technique is that developed by Goddard Space Flight Center. The GSFC system also employs laser ranging to a retroreflecting satellite, but requires only two ground stations. Three-dimensional station locations are obtained by combining the station-to-satellite range measurements with a highly precise model of the force field acting upon the satellite. Goddard presently obtains ranging measurements with a standard deviation of approximately 35 cm. The resultant residuals in 3-dimensional station locations have standard deviations of about 50 cm, and the overall accuracy of the station location is about 2 meters. GSFC anticipates improving the accuracy of its laser ranging equipment so as to yield ranging errors of 1-3 cm (similar to the

---

\*Although it would be conceptually possible to augment the Geodolite measurements with measurements of vertical motion provided by tiltmeters or gravimeters, such systems are not feasible in practice (See Section 3).

ranging errors predicted for the proposed systems). However, the Goddard system is extremely sensitive to inaccuracies in modelling the force field acting on the satellite, and it is doubtful if such modelling can be improved sufficiently to permit evaluation of 3-dimensional station locations with accuracies of 10 cm or better in the foreseeable future.

Very Long Baseline Interferometry is a method which by means of measuring radio signals from extragalactic radio sources can deduce station locations. This method has promise. Accuracies of the order of 10 cm are possible. In the 1975 time frame the limit of accuracy will probably approach 5 cm. The disadvantage of this method is its dependence on state of the art frequency standards and digital recording systems and a reliance on major radio tracking facilities. This implies increased cost in real time operations. Furthermore, unlike the 3-D laser ranging system proposed in this report, the VLBI system relies heavily on data processing. The software expenses are at least an order of magnitude larger than those incurred in the 3-D Multilateration process.

However, when VLBI is used to obtain range differences (see Paragraph 1.3) from an orbiting satellite, then the use of multilateration techniques will drastically alter the accuracy and software aspects of VLBI in a positive sense.\*

---

\*The application of range difference multilateration is currently under preliminary investigation.

## 1.9 CONCLUSIONS

A precision geodetic measurement system which enables three dimensional station coordinates to be determined relative to each other within a few centimeters has been demonstrated as being feasible.

It is concluded that a system using lasers and six operational stations has the potential of resolving the coordinates of stations to within 1 cm.

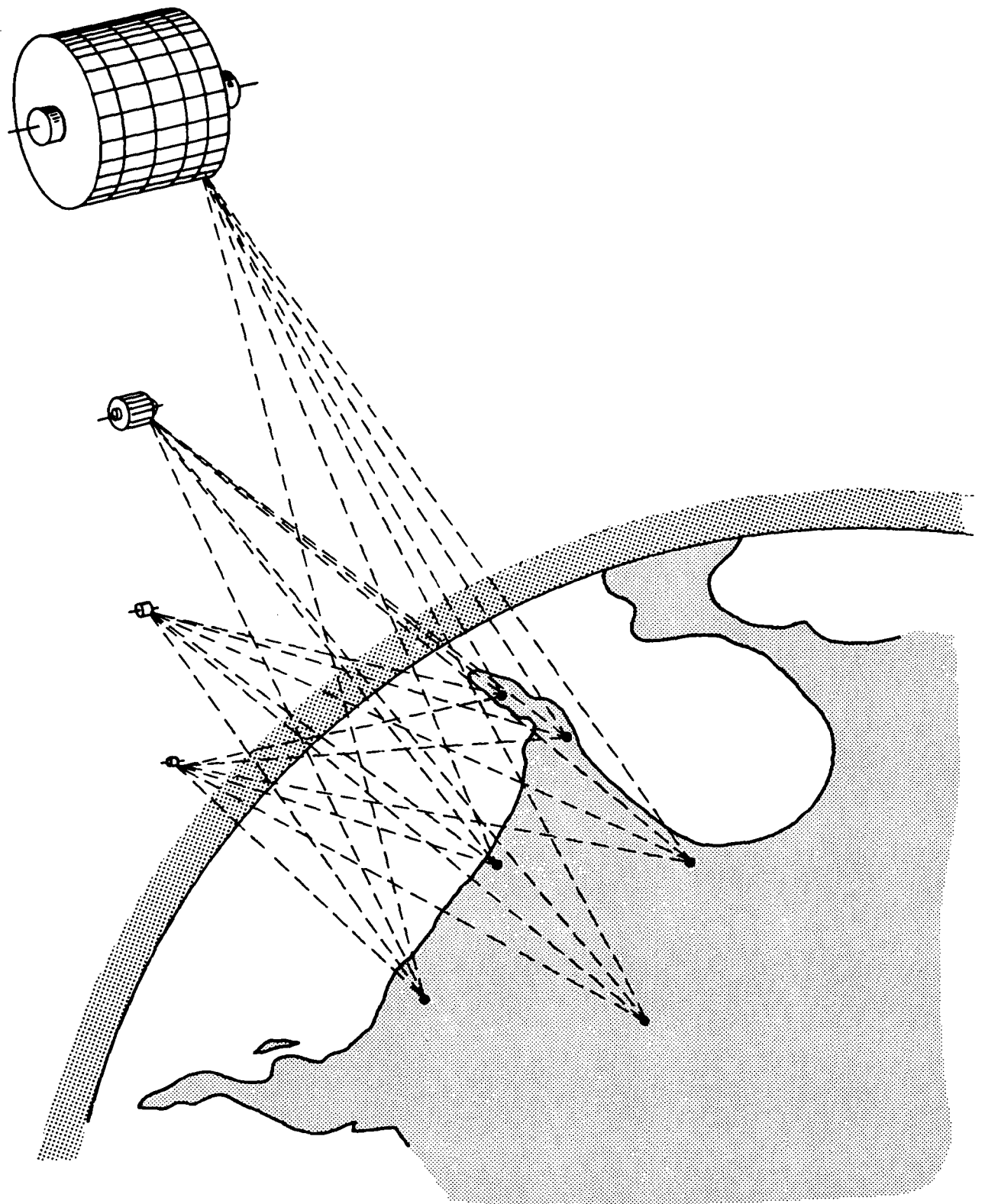
Having established a system which has such powerful resolution potential, serious work can now begin on the development of a workable stress/strain geodetic model. This model would have profound influence in the area of earthquake hazards assessment.

The cost of each laser subsystem has been estimated to be \$275,000. The software development costs for the operational software package that will process the data are inexpensive.

The results of the system analysis performed herein indicate that no pertinent barriers against implementation of such a system exist. In fact since orbits have already been trilaterated using ordinary tracking equipment [1.1], the six station concept could be tested at this date by using an additional three radio tracking stations.

Furthermore many other proposed systems, each with unique advantages, i. e., hybrid methods, are also available to aid in geodetic applications.

3-D MULTILATERATION:  
AN ACCURATE METHOD FOR ORBIT DETERMINATION



## SECTION II

### HISTORY OF PROJECT



The use of geometric principles to determine the ephemeris of a satellite and other related parameters is not a new idea. However, it appears that most geometric techniques were abandoned in favor of dynamical methods due to the natural evolution of the artificial earth satellite.

#### 2.1 BACKGROUND

Late in 1957, the first man-made satellite was lofted into a low Earth orbit. The limited view periods of low satellites as observed by Earth ground stations imposed an important operational constraint, namely: the smaller the number of ground stations, the lower the overall system cost. Operating under this constraint, the idea of using simultaneous geometric ranging from at least three stations in order to trilaterate, that is, to geometrically determine three triangles whose subsequent solution would yield the position of the satellite, was abandoned. Indeed, the dynamic methods of orbit determination were more suited to handling the pressing problem of satellite ephemeris propagation at those early times.

As time passed, satellites were lofted into higher orbits and finally into the practical and useful geosynchronous orbits now so common for satellite communication systems. The geosynchronous equatorial satellite, as is well known, would appear to hang motionless over a given equatorial station. Since ground stations placed on baselines of an intercontinental dimension would have common visibility with respect to each other, this advantage was quickly exploited to yield a communications relay system. Furthermore, at that date, since station nets were well dispersed throughout the globe, visibility of the geosynchronous satellites by at least three stations became a common occurrence. This

advantage was recognized and the geometric method of trilateration came into favor again. Operational software to perform the orbit determination was developed and tested by assuming that the location of the stations relative to the geodetic datum was known. Analysis indicated that the errors in the satellite positions and velocities obtained via trilateration would be smaller than the estimates provided via dynamical theory. This was due to the fact that all the dynamical constants and their corresponding uncertainties were not required in the geometric modeling process.

## 2.2 RECENT DEVELOPMENTS

One of the pressing problems which still remained unanswered until recently was concerned with the manner in which station locations themselves would be determined. In essence, the question arose of how both the position and velocity of the satellite and the three-dimensional station locations could be computed simultaneously.

Early in 1971 some preliminary investigation of this problem was performed at the Jet Propulsion Laboratory because it appeared that by using laser ranging equipment the data, i. e., the ranges between the station and the satellite, could be determined to a high degree of accuracy. The objective was to estimate Earth station positions, at least the relative positions, an order of magnitude more accurately than was presently possible for purposes of geodetic applications.

The results of that investigation showed that if simultaneous ranging is performed from a group of four stations at six independent times, then, in a specially chosen coordinate system, the positions of the four stations and the six trajectory points could be theoretically determined. A second indenture analysis discovered a serious problem: namely the station ground separation

needed to be on an intercontinental scale, because if all four stations were contained in a plane, the mathematical solution becomes singular, i. e., a solution can not be found. Specifically, the geodetically important situation of stations with short baselines in a nearly coplanar configuration, e. g., such as in the region surrounding the San Andreas fault in California, could not be implemented by the four station method.

Subsequent investigations discovered the interesting fact that if two measurements of the range are taken from each of three stations which are all in a straight line, then the distances between the stations could be uniquely determined. This discovery gave rise to the idea of fixing one or more baselines between the stations in the planar four-station system. Analysis showed that this four-station system did not degenerate mathematically once two of the baselines were fixed. Hence, a workable system could be obtained by aligning stations in straight lines and using the mathematically stable straight line solutions to determine the baselines which then would be used to yield the numerically stable four station solution. Such a system is actually possible for short baselines.

More analysis on the geometry peculiar to this problem showed that the addition of two more stations was equivalent to fixing the ground baselines between two sets of stations. Therefore, as was expected and further theoretical and numerical analysis indicated, a six-station configuration permitted simultaneous determination of the station coordinates and the position/velocity of the satellite if at least four simultaneous fixes or strikes are taken by the station net, even if the stations are nearly coplanar. Subsequent analysis has shown that accuracies in station coordinates to a centimeter level can be obtained.

Lately, it has been demonstrated that the systems described herein can also function if only range differences, instead of range only information is available.

Further analysis will no doubt uncover more information relative to the peculiarities of such geometric ranging schemes. Nevertheless, the feasibility of the geometric method for station location determination and ephemeris computation has been clearly established.

## SECTION III

### INTRODUCTION AND COMPARISON TO OTHER SYSTEMS

● In this section other techniques will be discussed which might be used to monitor tectonic motion and implement earthquake hazard assessment. The other techniques to be considered are the Geodolite, Tiltmeters, Gravimeters, very long baseline interferometry (VLBI), and the Goddard Space Flight Center laser ranging system. The salient features of each system will be described first, and then a comparison of the described systems with the 3-D Multilateration technique proposed in this report will be presented.

#### 3.1 THE GEODOLITE

The Geodolite is a laser-ranging device which is capable of measuring the distance between two points on the Earth's surface, but is not capable of resolving this distance into 3-dimensional components. The device is manufactured by Spectra Physics (Mountain View, California) and is currently being used by the U.S. Geological Survey. The Geodolite transmits an amplitude-modulated laser beam to a ground-based reflector; the modulation of the reflected beam is then compared with the modulation of the transmitted beam in order to evaluate the range between transmitter and reflector. The U.S. Geological Survey calculates the distances between benchmarks (reference points on the ground) by grouping the benchmarks into sets of 7, and then using a Geodolite to measure each of the 15 distances between different pairs of the 7 benchmarks. Since the measurements are partially redundant some statistical averaging is possible, and interstation distances up to 30 km can be evaluated with a standard deviation of error which is less than 1 cm. Clearly, the Geodolite provides excellent accuracy over its severely constrained range. However, in order to achieve the quoted accuracy, it is necessary to correct the crude data with temperature

and humidity measurements obtained by flying a helicopter along each path that is measured by the Geodolite.

Although it is conceivable to combine a large number of Geodolite measurements in order to measure distances up to 1000 km, there will be some serious problems. For example, if a distance of 900 km is partitioned into 30 segments of 30 km each, and each segment is measured by using the Geodolite and the U. S. Geologic Survey technique then:

- It will be necessary to measure 450 (30 x 15) separate distances.
- The overall standard deviation of error will be at least:

$$\sqrt{30} \cong 5.5 \text{ cm}^*$$

- To obtain the complete set of measurements will require a great deal of time and rapid crustal deformations (which may give premonition of earthquakes) will be lost.

Furthermore:

- The Geodolite is practical only when measuring distances between points which are elevated with respect to the intervening terrain. (Otherwise the line-of-sight distance will be reduced to a few kilometers, and variations in ground temperature will cause anomalous propagation of the light beam). It is extremely unlikely that the 450 required measurement paths can be chosen so that each path connects points which are elevated with respect to the intervening terrain.

---

\*This assumes that the errors in measuring each of the 30 segments are uncorrelated. If the errors are correlated, the overall standard deviation will be greater than 5.5 cm.

- Since the Geodolite can only measure lateral distance, vertical movement of the benchmarks will not be easily discernible. However, many important strain fields (such as the field related to the 1971 San Fernando earthquake in the Los Angeles area) have vertical components.

### 3.2 TILTMETERS AND GRAVIMETERS

Tiltmeters and gravimeters could conceivably be used in conjunction with a Geodolite so as to provide independent measurements of vertical motion. Both tiltmeters and gravimeters have the capability of detecting vertical ground motions within the order of centimeters. Tiltmeters show only a change in slope, however, and not the amplitude of a vertical ground excursion at any one place. Tilt measurements are thus not directly comparable with the results anticipated from laser retroreflection.

Gravimeters, on the other hand, can detect the amplitude of ground motion because of the change in gravity which results from a change in distance from the center of the Earth. The change in gravity is equal to the magnitude of the "Bouguer correction" for gravity analysis (see Glossary). It is the change in gravity due to a change in elevation when the ground surface moves along with the instrument.

The accurate value of the Bouguer correction at any specific location depends partly upon the local rock density, but it is about 2 microgals.\*

The modern LaCoste-Romberg gravimeters have a sensitivity capsule of reading to one microgal, accuracies of 3  $\mu$ gal with repeated exceedingly careful observations, and 10  $\mu$ gal with ordinary good work. The wideband

---

\*One  $\mu$ gal is an acceleration of  $10^{-6}$  cm/sec<sup>2</sup> and about equal to  $10^{-9}$  g.

accelerometer described by Block and Moore [3.1] also has a sensitivity and accuracy capability of measuring elevation changes of about one centimeter.

Both instruments have a considerable drift rate, however, which is the equivalent of several centimeters per week. Neither instrument could be left by itself to monitor elevation changes at individual stations because the drift rate would make the results uninterpretable at worst and ambiguous at best.

In order to account for instrumental drift rates, a gravimeter program would involve frequent transportation of the reading gravimeter to a base station for calibration, or the continuous transportation of one gravimeter from a base station to the reading stations. Either case would require constant work by a ground staff.

In summary, neither tiltmeters nor gravimeters appear practical for measuring vertical motion to the required accuracy.

### 3.3 THE GODDARD LASER RANGING SYSTEM\*

Goddard Space Flight Center has designed and built a laser ranging system which employs two ground stations and which calculates the geocentric coordinates of one station given the geocentric coordinates of the other station. Each station transmits a laser pulse to a retroreflecting satellite, receives the reflected pulse, and computes station-to-satellite range from the measured value of time between transmission and reception of the laser pulse. The range data from each station is then combined with 1) an extremely detailed model of the forces acting on the satellite, and 2) the assumed geocentric coordinates of one station, in order to yield the geocentric coordinates of the other stations.

---

\*The information presented in this section is based on private communication from Dr. David Smith of GSFC as related to R. Jaffe.

Goddard has tested its system by ranging to satellites at altitudes of 1000 km from stations which are separated by 400 km. The station-to-satellite ranges were measured with a standard deviation (about the measured mean) of about 35 cm. Interstation distance was evaluated with a standard deviation of approximately 25 cm, and the 3-dimensional components of the interstation distance were evaluated with a standard deviation of approximately 50 cm. Goddard's error analysis indicates that interstation distances were calculated with an accuracy of about 2 meters, and that the 3-dimensional components of interstation distances were calculated with an accuracy no better (but not worse) than 2 meters.

Goddard expects to be able to improve the accuracy of its system by utilizing more advanced laser-ranging components, and more sophisticated predictions of the force fields on the satellite. It should be noted that Goddard already employs an extremely sophisticated trajectory program which includes the effects of polar motion, Earth tides, and gravity anomalies. Goddard estimates that its present orbit determination model is accurate to a few meters over a 2-3 day period for a 1000 km altitude satellite. However, the present accuracy of the Goddard technique must be improved by an order of magnitude before the system can be used in the earthquake-hazards applications described in this report.

### 3.4 VERY LONG BASELINE INTERFEROMETRY

This technique [3.2] has its origins in optical and radio astronomy. The technique operates by receiving random radio signals generated by objects external to our own galaxy, typically, quasars and other galaxies. By measuring the difference in time of arrival of identical random signal patterns at a pair of stations, the distance between the stations can be determined.

An error frequently made in projecting the usefulness of this system to geophysical goals is to confuse the angular resolving power of the interferometer with an equivalent linear distance on the Earth's surface. Since the resolving power of an interferometer is given by the ratio of the received wavelength to the distance between the receiving stations, resolutions of  $10^{-8}$  arc seconds are possible. It is not correct to conclude that such resolution alone provides Earth distances to be measured with accuracies of 1 centimeter.

The ability to invert very long baseline interferometry (VLBI) observations into accurate geophysical measurements is limited mainly by Earth atmospheric uncertainties. However, dual frequency VLBI holds significant promise for ionospheric calibrations and water vapor radiometers appear promising for calibrating the wet component of the troposphere. Therefore, VLBI performance at the 10 cm baseline accuracy level is being forecast within a few years and 5 cm or better for the long term.

VLBI possesses the following advantages:

- Capacity to determine three-dimensional station coordinates in a geocentric coordinate system accurate to 10 cm.
- Capacity to operate under virtually all weather conditions.
- Measurements are made relative to a frame of virtually time invariant extragalactic radio sources.

- Portable stations are feasible for remote station utilization. There is no VLBI requirement to build or launch any spacecraft or to transmit from Earth any radio or light signals. VLBI is entirely passive, using only natural radio signals.

Some disadvantages are:

- Water vapor in the atmosphere prevents precise system calibration.
- Software costs are relatively high.
- Some modeling errors are present.

It is interesting to speculate how the present multilateration technique and VLBI might be combined (use of range difference data from a satellite) to overcome some of the inherent disadvantages of each method.

### 3.5 COMPARISON OF THE 3-D MULTILATERATION TECHNIQUE WITH THE DESCRIBED SYSTEMS

The Geodolite appears to be suitable for many of the applications envisioned for the 3-station collinear system. Both the Geodolite and the 3-station system can measure short distances (but not the 3-dimensional components of these distances) with high accuracy and at relatively low cost. The Geodolite has the advantage of requiring considerably less capital investment; however, the Geodolite can measure only line-of-sight distances, and can achieve high accuracy only when its raw measurements are corrected with temperature and humidity data obtained by overflying the baseline with a helicopter. Neither the Geodolite nor the 3-station system are applicable to the most difficult measurement problem in earthquake hazard assessment, viz., accurate evaluation of the 3-dimensional components of strain between widely separated stations.

Tiltmeters and gravimeters initially seemed to offer some promise of augmenting the distance measurement capability of the Geodolite with independent measurements of vertical motion. However, more detailed investigation

revealed that tiltmeters were incapable of directly measuring either distance or motion, while gravimeters were incapable of yielding the requisite accuracy without frequent recalibration.

The Goddard laser ranging system shares many features in common with the 4- and 6-station systems. All systems employ laser ranging, and all systems are capable of measuring the 3-dimensional components of distance between widely separated stations.

The Goddard system has the advantage of requiring fewer stations, and hence requiring a smaller capital investment for a complete operating system. However, Goddard needs approximately 2 months of range measurements to yield accurate output data, whereas JPL systems can yield accurate output data in only hours within reception of the ranging measurements. Consequently, if many locations are to be mapped in a limited period of time, only one of the JPL systems would be needed (since data could be obtained rapidly and the stations then transported to new locations), whereas a number of Goddard systems would be needed. The systems' rapidity of operation is also significant in applications such as detection of sudden ground deformations which often give a premonitory indication of earthquakes, and monitoring of seismic activity during the period immediately following a major earthquake.

Although cost, complexity and time required for observation are all important bases for comparison among systems, the ultimate criterion for system evaluation, at least with regard to earthquake hazard applications, is accuracy. And it is in terms of accuracy that the Goddard system and the 3-D Multilateration technique manifest their most significant differences. The accuracy of the Goddard system is fundamentally dependent upon the accuracy of the satellite force-field model; unless the accuracy of this model is improved 10-fold or more, it is extremely unlikely that Goddard will be able

to achieve station location accuracies of 10 cm or better, regardless of any improvements made in their laser ranging equipment. In contrast, the 3-D Multilateration technique is essentially independent of Earth force fields, and is constrained only by the accuracy of the laser ranging equipment. Since excellent laser ranging accuracies can be achieved using commercially available hardware, the 3-D Multilateration technique will be able to achieve station location accuracies of 1 cm or better. It seems highly improbable that the Goddard system will be able to match this performance in the foreseeable future.

On the other hand VLBI techniques which use the principle of multilateration, wherein the raw data is the time delay between reception of a signal at two stations from a satellite (which is subsequently transformed into the slant range difference between the satellite and each of the two stations) seem to offer a second avenue of approach. Specifically, the geometric principles invoked in this report can be transformed such that range differences instead of range itself become the raw data. Under these transformations it is possible that VLBI might be able to reach to within a few centimeters of the accuracy of the laser ranging system.

## SECTION IV

### COORDINATE SYSTEMS FOR RANGING EXPERIMENTS



In this section, the inertial coordinate system of dynamical astronomy is outlined in order to provide the reader with a means of comparing the coordinate system to be introduced in this study with the standard system. Determination of station coordinates relative to an inertial system briefly is discussed next. Geometric coordinate systems peculiar to laser ranging are discussed and a comparison to the inertial system is made. Finally, the fundamental coordinate system utilized in this study is defined. It is concluded that the geometric coordinate system is a self-consistent system capable of yielding station locations with high accuracy relative to a plane defined by three of the stations. The accuracy with which the true equator can be determined relative to the geometric equator is estimated, and explicit formulas for the transformation of coordinates are discussed.

#### 4.1 INERTIAL SYSTEMS

Newtonian laws are always referred to a conveniently adopted inertial coordinate frame. The system commonly utilized in dynamical astronomy is displayed in Figure 4-1.

In this coordinate system the principle axis,  $x$ , is taken to pass through the true equator and equinox of date. This means that the position of the pole of the Earth has been modeled as accurately as is presently permitted, i. e., all the precession and nutation effects caused by the perturbative action of the Sun and the Moon on the equatorial bulge of the Earth have been incorporated into the coordinate system model. The  $y$  axis is in the true equator (where the equator actually is at a given instant) and the  $z$  axis is taken to

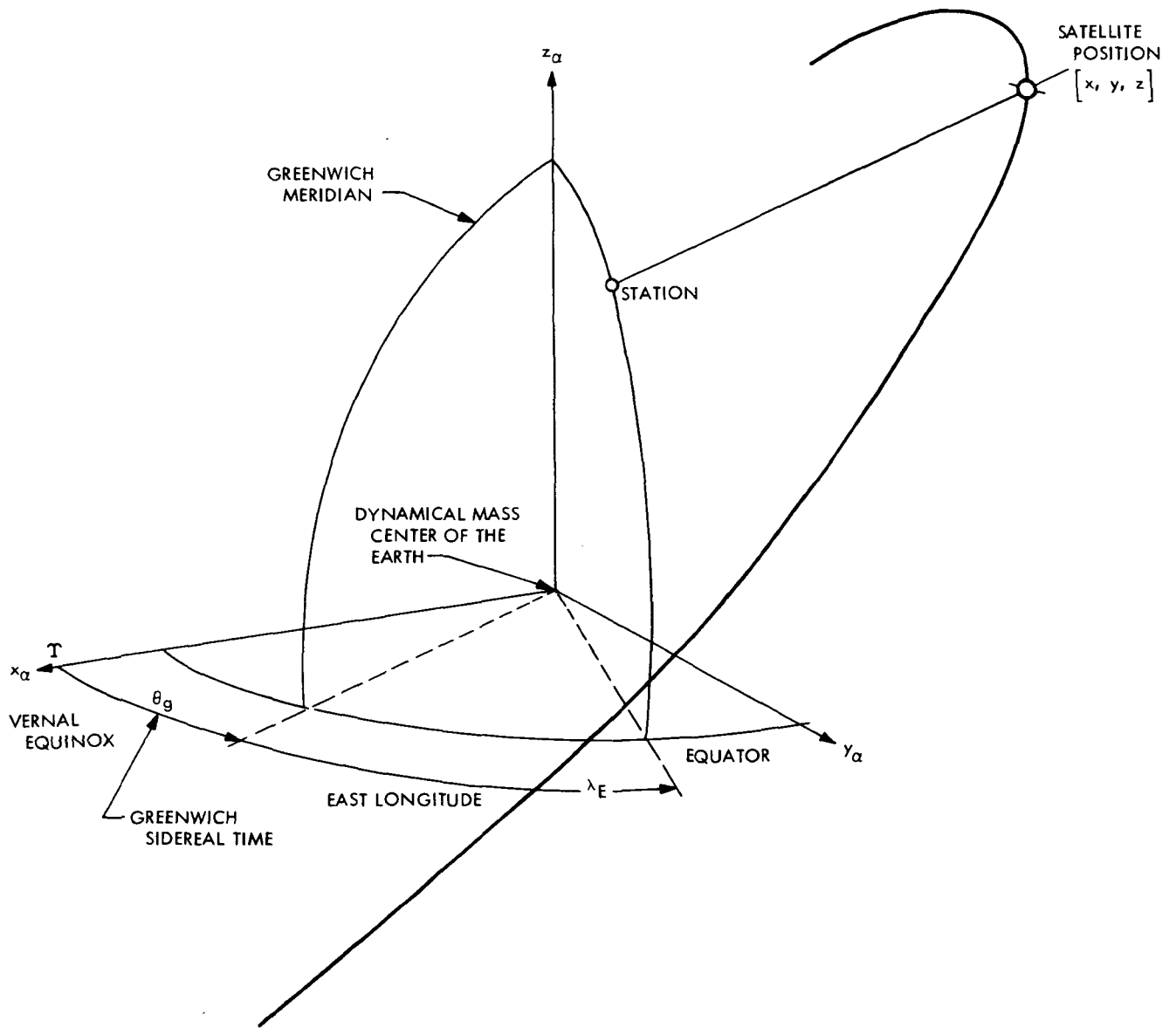


Figure 4-1. Inertial Coordinate System

complete the right handed coordinate system. Thus, the z axis is directed along the best possible estimate of the Earth's angular momentum vector.

In a broad sense, if the wandering of the pole caused by the lack of alignment of the Earth's body fixed system and the Earth's angular momentum vector is neglected, the linkage between a geographically fixed system and the best estimate of an inertial system is the true sidereal time.

On Earth, time is usually reckoned in a mean sense, e.g., as mean sidereal time. To determine the actual or true position, the true sidereal time as opposed to the mean sidereal time must be determined. To determine the true sidereal time, the equation of the equinoxes [4. 1], [4. 2], must be evaluated. This equation is defined as

$$E \equiv \delta\psi \cos (\epsilon_M + \delta\epsilon),$$

where  $\delta\psi$  is the nutation in longitude,  $\delta\epsilon$  is the nutation in obliquity, and  $\epsilon_M$  is the mean obliquity of the ecliptic. From observational astronomy the fundamental constants of these expressions can be obtained, and analytic expressions with time as the independent variable can be derived based upon theory [4. 3], [4. 4]. Once E is evaluated, the true sidereal time,  $\theta_T$  is given as

$$\theta_g = \theta_T = \theta_M + E,$$

where  $\theta_M$ , the mean sidereal time, is given as a polynomial in time [4. 1].

The local sidereal time at any observational station is then taken to be

$$\theta = \theta_T + \lambda_E,$$

where  $\lambda_E$  is the east longitude of the station. The rectangular coordinates of the station from the dynamical origin are then defined in Appendix J.

## 4.2 DETERMINATION OF STATION COORDINATES

If the study objective is to use accurately measured data, e. g. , laser range measurements, in order to determine the locations of ground stations, a few fundamental points must be kept in mind.

First, laser data is taken in a coordinate system with respect to the body-fixed axes of the Earth at any given instant. Second, the satellite position will be computed in the true inertial coordinate system defined previously. Hence, if the satellite ephemeris is used to determine a station coordinate, say, the latitude, that coordinate will be determined relative to the inertial coordinate system.

Therefore to compare the new estimates of station coordinates with the old, the rectangular coordinates of the stations should be transformed back to the body-fixed axes to which geodetic coordinates are referred. The transformations are standard, [4. 1], [4. 5].

However, since the Conventional International Origin of the Earth's body-fixed coordinate system was actually chosen arbitrarily [4. 6], it follows that, if a new method for estimating station coordinates of much higher accuracy becomes available, it might be desirable to adopt a new equatorial position and reference all new station data to such a new benchmark. If the new method should be much better than the old method, a much more consistent set of station coordinate data would be available.

## 4.3 GENERALIZED GEOMETRIC COORDINATE SYSTEM

It will be demonstrated in this study that, if simultaneous range measurements are taken from a suitable number of ground stations to an orbiting satellite, then the rectangular coordinates of the stations can be determined to extremely high accuracy in a suitable coordinate system without knowledge of

the trajectory. Without going into further details let the following coordinate system be examined (Figure 4-2).

In Figure 4.2, the geometric equator is defined by physically positioning two stations to be on the best possible estimate of the equator on a given adopted date. By then adopting the coordinates of these stations by definition to be  $[X_2, 0, 0]$ ,  $[X_3, Y_3, 0]$ , it follows that the geometric equator on this date has been defined relative to some origin  $[0, 0, 0]$ . Hence the X axis passes through  $X_2$ , the Y axis lies in the plane defined by stations 2 and 3, and Z is perpendicular to the plane defined by the X-Y plane.

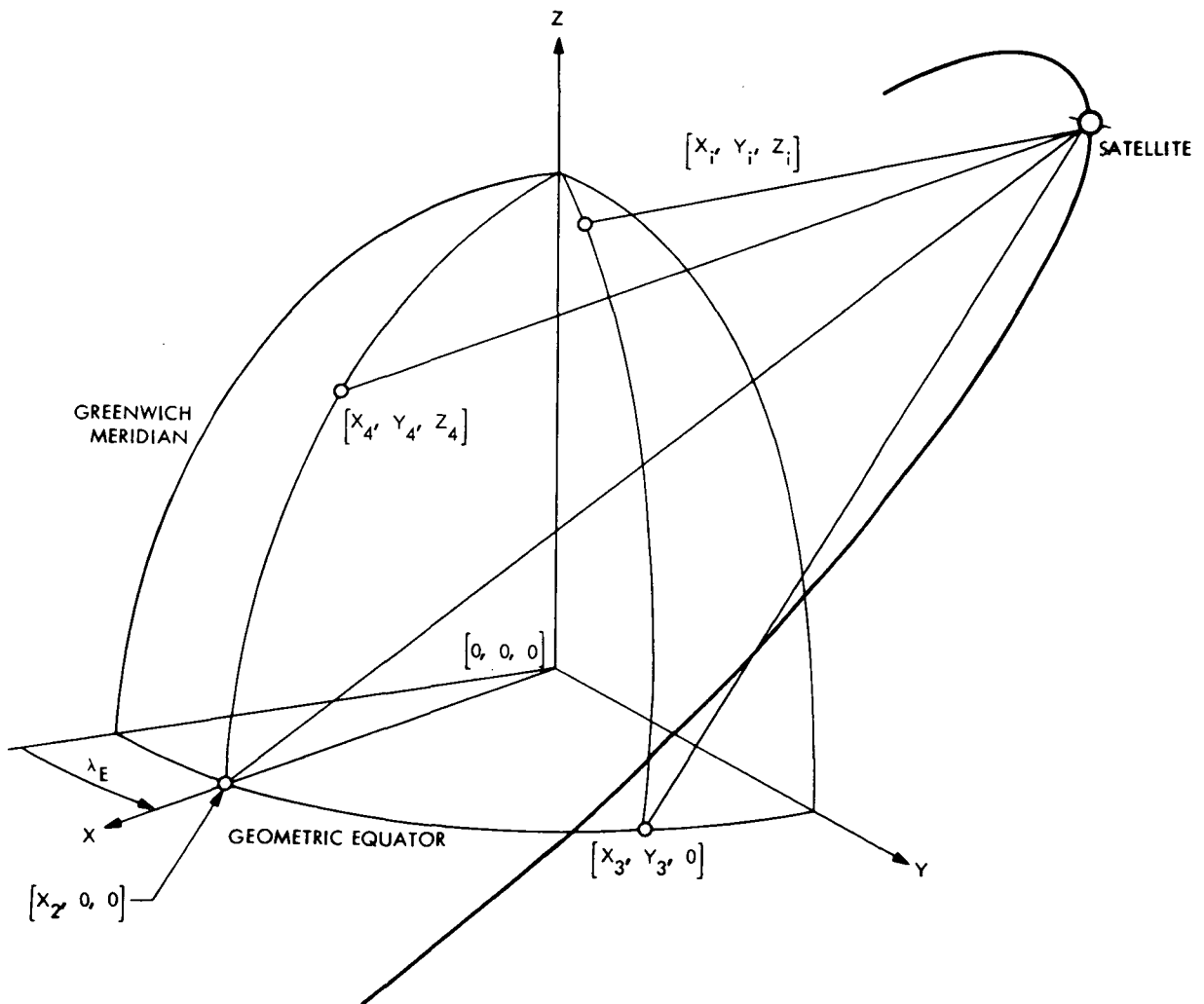


Figure 4.2. Geometric Coordinate System

Since current estimates of station position with respect to the equator can only be accomplished to within a few meters, it follows that the dynamical coordinate system and the geometric system can only be brought into agreement by an error source of this order of magnitude.

It will be seen that, via laser ranging, the coordinates  $[X_2, X_3, Y_3, X_4, Y_4, Z_4, X_i, Y_i, Z_i]$  can be computed within the geometric framework two orders of magnitude more accurately than in the dynamical coordinate system. Furthermore, once the coordinates of the stations are obtained, it follows that the satellite coordinates  $[x, y, z]$  at that instant can be derived. The negative of these coordinates is therefore the location of the origin of the geometric system as viewed by the satellite.

In summary, the geometric system yields station coordinates in a relative framework, in which the accuracy of relative distance measurement is only limited by laser equipment accuracy.

#### 4.4 ADOPTED GEOMETRIC TOPOCENTRIC COORDINATE SYSTEM

The previous discussion indicated that to make the generalized geometric system agree with the standard astronomical system, the longitude of station 2 with respect to the Greenwich meridian would have to be precisely known. Furthermore, stations 2 and 3 would have to lie precisely on the equatorial plane. Since exact alignments of this sort are not possible, it makes sense to adopt some well known surface station as the origin of a topocentric system to be used in laser ranging studies. This origin will of course have errors in latitude, longitude and elevation relative to the inertial astronomical system of a few meters, i. e., a bias-like error in the coordinates with respect to the adopted origin of the dynamical center.\* The adopted topocentric system

---

\*The origin of the dynamical system cannot be defined to any greater accuracy than the origin of the generalized geometric system.

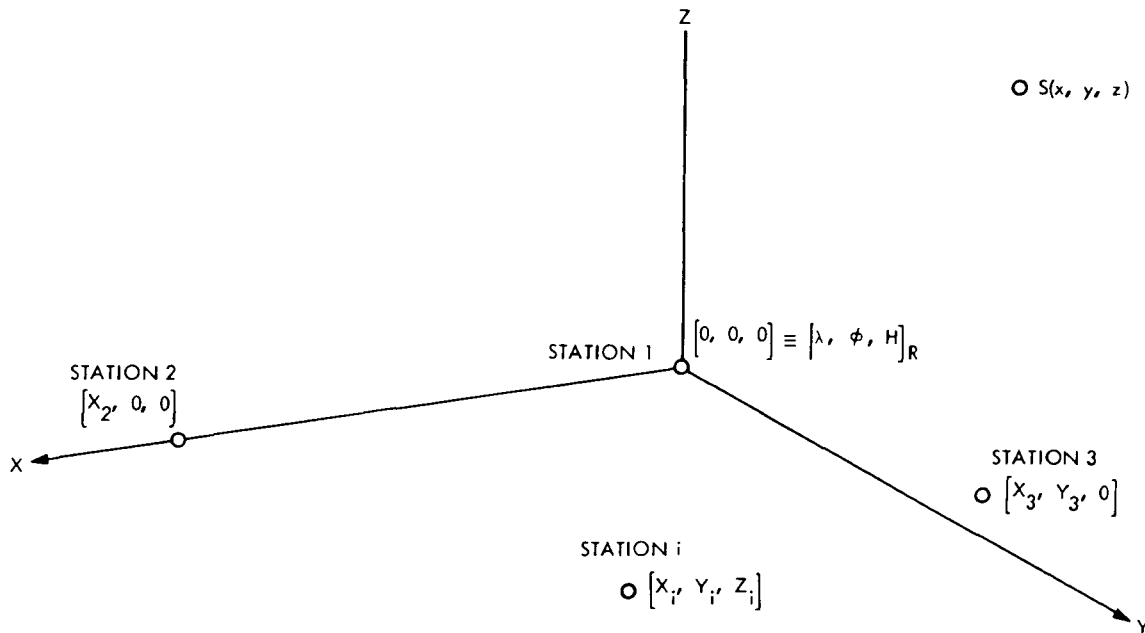


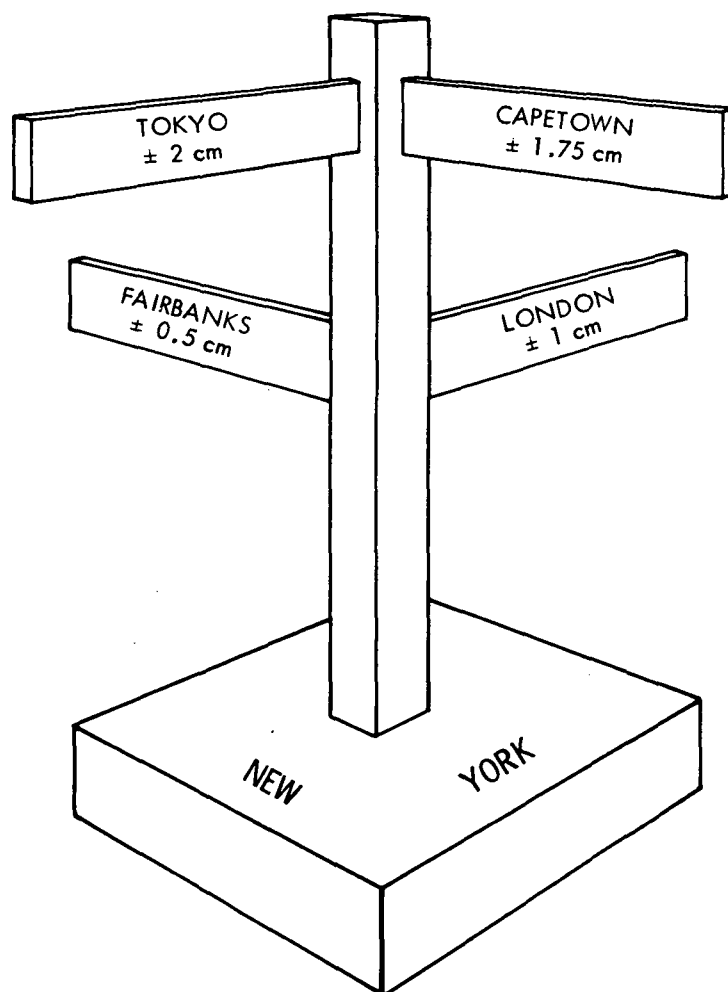
Figure 4-3. Geometric Topocentric Coordinate System.

is defined in Figure 4-3. As can be seen, the origin is placed at some geodetically known reference station, R, i. e., Station 1 whose geodetic coordinates are  $\lambda, \phi, H$ . The second station defines the X axis; the third station defines the XY plane; the Z axis is normal to the XY plane and is directed away from the Earth, and the Y axis completes a right handed system. This coordinate system will be used throughout the present report and is referred to as the adopted coordinate system.

#### 4.5 STATION COORDINATE RELATIONSHIPS

For purposes of systems analysis, specifically for actually computing sets of realistic station coordinates in the adopted geometric coordinate system from tabulations of geodetic station coordinates which are presently known, a transformation of coordinates will be required. This transformation is explicitly developed in Appendix J.

MULTILATERATION:  
A METHOD OF MEASURING INTERCONTINENTAL  
PLATE MOVEMENTS



## SECTION V

### EXPECTED SYSTEM ACCURACIES FOR REAL WORLD CONFIGURATIONS



In this Section, numerical results are presented pertaining to the system accuracy achievable by use of the geometric principles discussed in Section I.

To illustrate the versatility of the primary recommendation of this report, i. e., use of the 6-station system, four hypothetical experimental configurations using six stations are evaluated, namely:

- an intermediate distance network along the Southern California portion of the San Andreas Fault,
- a long-baseline network covering the continental United States,
- intercontinental networks of stations,
- a very short baseline network within the Los Angeles metropolitan area.

As will be seen, each of these configurations yields accurate solutions for the station coordinates which, subject to the recommendations of Paragraph 6.4, will ultimately approach accuracy levels of one centimeter.

The accuracies of the four-station, intercontinental baseline system and the three-station, short baseline system also are discussed briefly.

It should be noted that the choice of stations and satellite (or airplane) trajectory points to be used in the following applications is rather arbitrary, although in a few cases selection has been guided by preliminary geophysical considerations. No attempt has been made to achieve optimal configurations; however, care has been taken to avoid certain degenerate configurations (see Section VII). It is believed that with suitable optimization techniques (a task which is proposed in Section X for future study), and with the use of more

trajectory points than those employed in these calculations, even more dramatic accuracies than presently reported will be achieved. In all tabulations to follow, the average errors,  $\epsilon$ , in each station coordinate and the standard deviation,  $\sigma$ , have been computed on the basis of simulation results for 10 different sets of random range errors, where each set consists of 100 points drawn from a Gaussian distribution with zero mean and standard deviation of 1 cm.\* Such a procedure may be interpreted in the following manner: assume that 100 strikes of the satellite(s) per pass are possible; then the average errors quoted are what would be expected to be obtained by averaging the results over 10 identical passes; furthermore the standard deviations are the standard errors of the calculated station locations from one typical pass of data.

The procedures for calculating the various quantities used in the following subsections are outlined in Section VII, and detailed computational algorithms are given in Appendix A and Appendix C.

#### 5.1 SIX-STATION CONFIGURATION: A SYSTEM FOR ALL BASELINES

The use of six stations is the primary recommendation of this report (see Section X). A workable six-station system conceivably can be set up in any global or local region of geodetic interest. In contrast, the four-station and the collinear three-station configurations (as discussed before) will yield accurate station locations only for extremely wide and short baselines, respectively. Examples of the kind of accuracies that can be obtained in a six-station configuration are given in the following subsections.

##### 5.1.1 Local Experimental Network

Figure 5-1 shows the locations of six hypothetical stations placed along a region of great interest to geophysicists and seismologists, i. e., the Southern

---

\*Precise definitions of the quantities  $\epsilon$  and  $\sigma$  are given in Paragraph 7.3. System Bias errors are discussed in Appendix K.

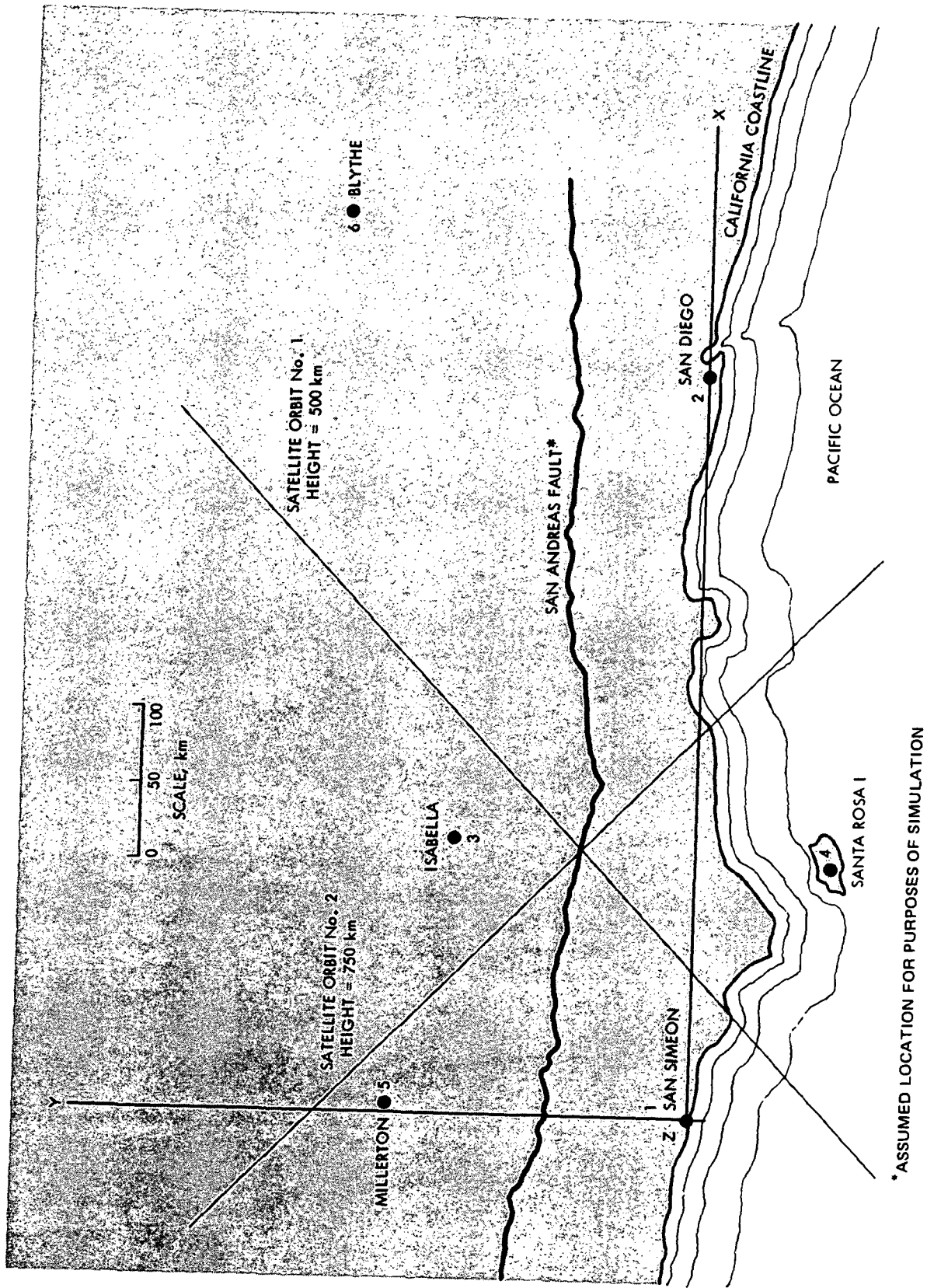


Figure 5-1. The Adopted Coordinate System for 6 Stations Along the San Andreas Fault

California portion of the San Andreas Fault. The coordinates of these stations\* in the adopted coordinate system (see Paragraph 4.4) with San Simeon as the origin are displayed in Table 5-1 and Figure 5-1.

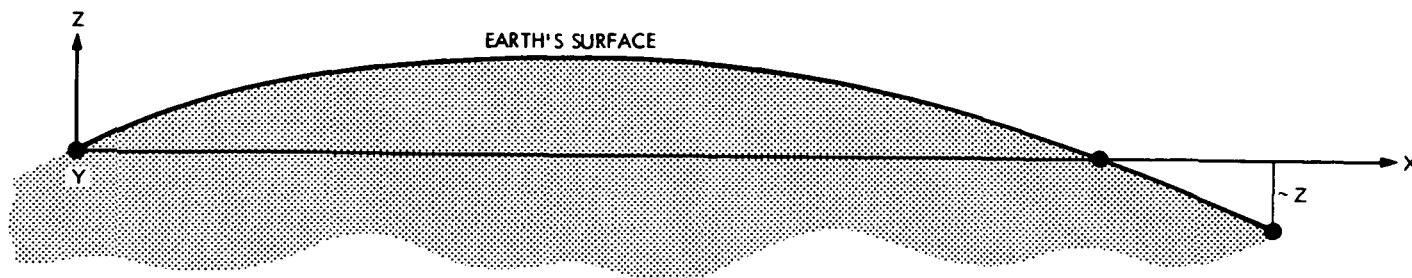
Table 5-1.

Adopted Coordinates in Kilometers of the San Andreas Fault Stations\*\*

Station	X	Y	Z
1. San Simeon	0	0	0
2. San Diego	495	0	0
3. Isabella	186	160	0
4. Santa Rosa Island	172	89	+ 5.1
5. Millerton	6.2	200	- 6.1
6. Blythe	599	235	-12.9

\*These coordinates have been obtained from a simple computer program accepting as input the geographic longitudes and latitudes of the stations. A spherical Earth was assumed.

\*\*The Z coordinates are apparently large due to the adopted coordinate system, wherein stations 1 and 2 define a chord cutting the globe; this has the effect of placing, e. g., station 6 at a sizeable distance from the X-Y plane. Note that the scale in the sketch has been exaggerated.



Two circular orbit satellite passes, whose projections on the XY plane of the adopted coordinate system are indicated in Figure 5-1, were used in the simulation. The heights of the two satellites are 500 km and 750 km for orbits 1 and 2, respectively. Fifty points from each orbital arc (a total of 100 points) were generated with the X-coordinates ranging from San Simeon to Blythe. The accuracy simulation procedure as outlined in Paragraph 7.3 was then performed. Table 5-2 summarizes the results of the simulation for this system configuration.

Table 5-2.

The Average Errors,  $\epsilon$ , and the Standard Deviations,  $\sigma$ , of the Coordinates of the San Andreas Fault Stations in Centimeters Assuming 1 cm Normal Random Errors in Ranging

Station	$\epsilon_X$	$\sigma_X$	$\epsilon_Y$	$\sigma_Y$	$\epsilon_Z$	$\sigma_Z$
2. San Diego	0.15	2.06				
3. Isabella	-0.15	1.11	0.84	3.56		
4. Santa Rosa Is.	-0.20	1.31	-0.05	1.76	0.10	0.99
5. Millerton	0.09	1.14	0.91	4.16	0.03	0.71
6. Blythe	0.26	2.64	1.41	4.74	0.24	1.18

### 5.1.2 Continental Network

A hypothetical six-station configuration spanning the continental United States is shown in Figure 5-2, with the adopted station coordinates displayed in Table 5-3. The assumed satellite trajectory data is also shown on the figure.

The numerical simulation resulting for this configuration is summarized in Table 5-4.

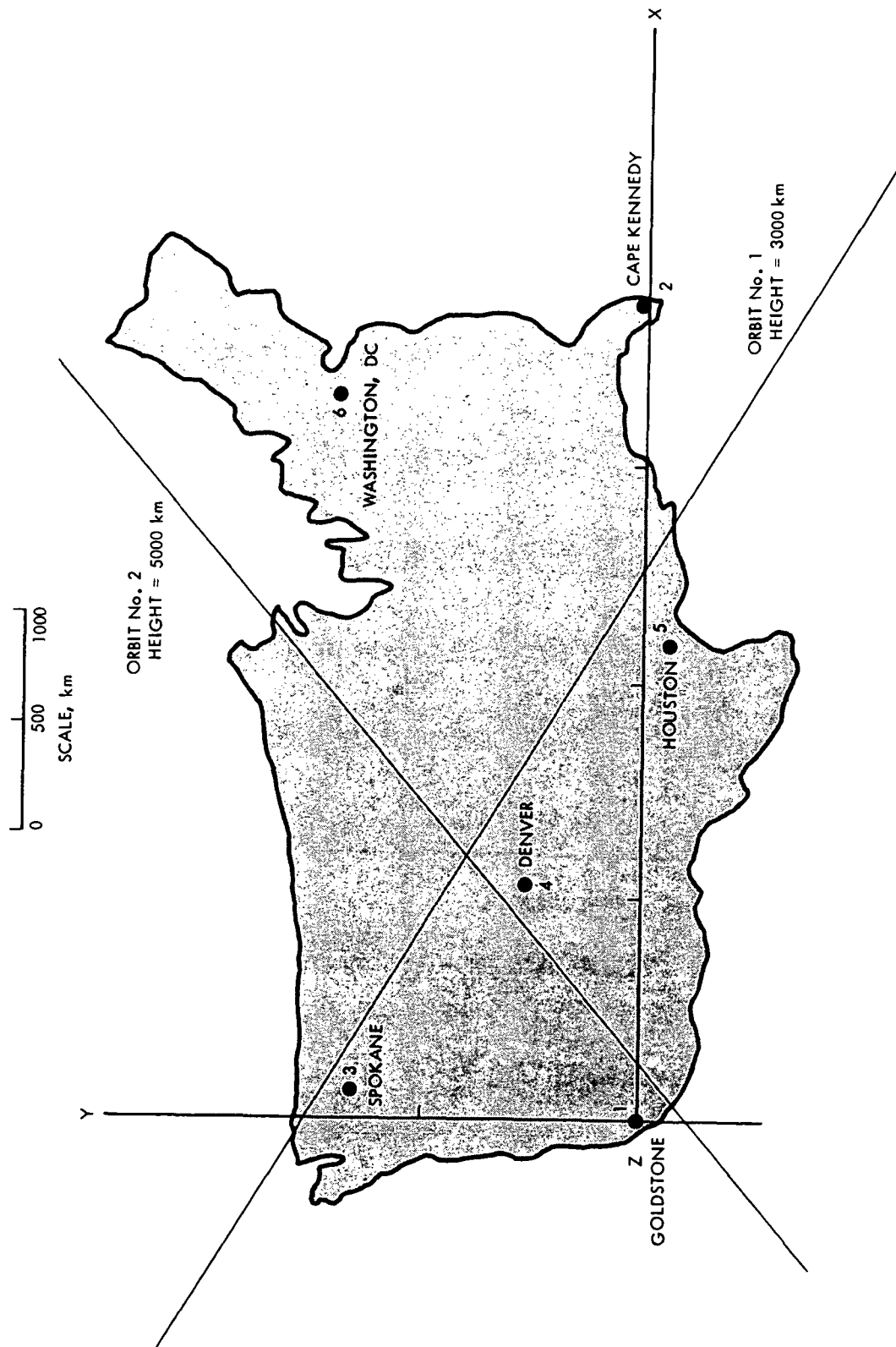


Figure 5-2. The Continental Station Network

Table 5-3.

Adopted Coordinates in Kilometers  
of the Continental Stations

	X	Y	Z
1. Goldstone, Cal.	0	0	0
2. Cape Kennedy, Fla.	3740	0	0
3. Spokane, Wash.	120	1350	0
4. Denver, Col.	1060	510	250
5. Houston, Tex.	2190	-82	270
6. Washington, D. C.	3310	1400	75

Table 5-4.

The Average,  $\epsilon$ , and the Standard Deviation,  $\sigma$ ,  
of Station Coordinate Errors in Centimeters  
for the Continental Stations, Assuming 1 cm  
Normal Random Error in Ranging

Station	$\epsilon_X$	$\sigma_X$	$\epsilon_Y$	$\sigma_Y$	$\epsilon_Z$	$\sigma_Z$
2. Cape Kennedy	-0.85	3.02				
3. Spokane	0.21	1.70	0.54	3.81		
4. Denver	-0.37	1.32	-0.09	1.22	0.25	0.52
5. Houston	-0.39	1.59	-0.28	1.02	0.32	1.00
6. Washington	-0.25	3.84	0.39	3.90	0.32	1.35

### 5.1.3 Intercontinental Networks

The determination of the coordinates of the stations located on different continents to centimeter accuracy is of great interest to geologists, tectonic physicists and astronomers.\*

It should be remarked that less-than-10 cm accuracy station location can be achieved with only four intercontinental stations, provided that the four stations are favorably located. With six stations, however, computational experience indicates that obtaining accurate solutions seems to be the rule rather than the exception. Further analysis will explicitly define this rule.

As an illustration, consider Figure 5-3 where a hypothetical configuration is adopted at the following cities: New York (U.S.A.), London (England), Mexico City (Mexico), Caracas (Venezuela), Freetown, Sierra Leone (Africa), and Reykjavik (Iceland). A total of 100 trajectory points from two satellites at altitudes 6,000 and 10,000 kilometers, respectively, were employed in the calculation. The accuracy corresponding to this configuration is displayed in Table 5-5.

As a second illustration, the following choice of sites were selected: Kaneohe, Hawaii (U.S.A.), Tarara (Peru), Calgary (Canada), Mexico City (Mexico), San Bernardino (U.S.A.), and Clipperton I. Two circular-orbit satellites of 6,000 and 10,000 km altitudes also were employed. Table 5-6 summarizes the results of the accuracy simulation.

---

\*With this kind of accuracy, the hypothesis of continental drift will be subject to direct scrutiny.

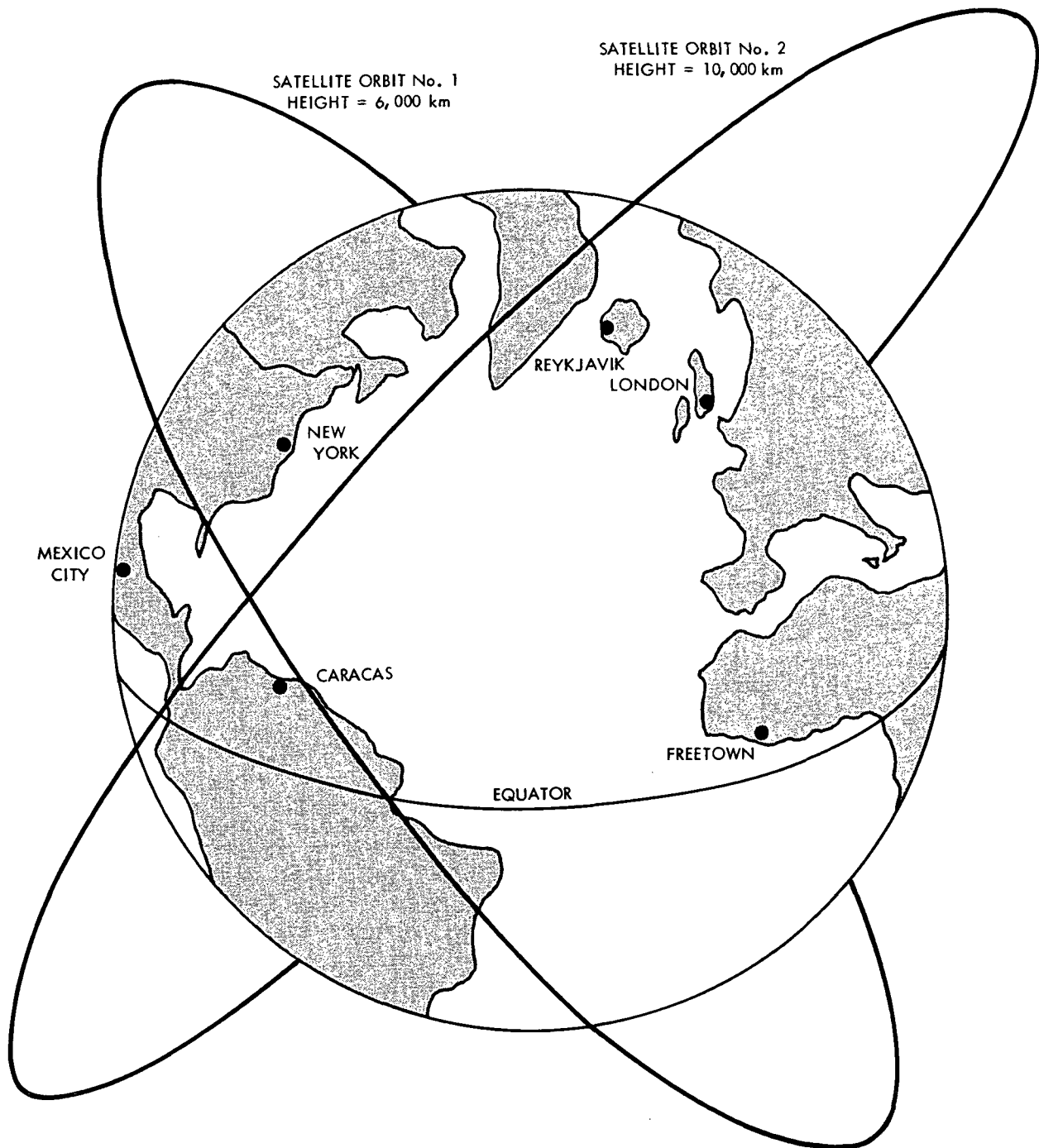


Figure 5-3. An Intercontinental Network

Table 5-5.

The Average,  $\epsilon$ , and the Standard Deviation,  $\sigma$ ,  
in Centimeters of the Errors in the  
Station Coordinates of the  
Intercontinental Configuration  
(Origin Assumed to be  
at Mexico City)

Station	$\epsilon_X$	$\sigma_X$	$\epsilon_Y$	$\sigma_Y$	$\epsilon_Z$	$\sigma_Z$
London	-0.94	4.06				
New York	-0.82	2.39	-0.83	2.07		
Freetown	-0.38	4.10	0.34	2.83	0.45	1.66
Reykjavik	-0.77	3.60	-0.50	0.89	0.02	0.41
Caracas	-0.17	1.64	-0.26	2.35	0.18	0.94

Table 5-6.

The Average,  $\epsilon$ , and the Standard Deviation,  $\sigma$ ,  
in Centimeters of the Errors in the  
Station Coordinates of the Second  
Intercontinental Configuration  
(Origin Assumed to be  
at Kaneohe)

Station	$\epsilon_X$	$\sigma_X$	$\epsilon_Y$	$\sigma_Y$	$\epsilon_Z$	$\sigma_Z$
Talara	1.06	3.84				
Calgary	2.12	4.41	-.37	4.16		
Mexico City	1.09	3.20	-.60	1.16	.19	.34
San Bernardino	1.41	2.63	-.40	2.08	-.00	.54
Clipperton I.	0.49	2.25	-.60	.93	-.02	.73

#### 5.1.4 Airplane Experiment

In extreme contrast to the previous experiment, consider a small scale experiment that can be performed within the Los Angeles basin with the stations depicted in Figure 5-4. An airplane was used in lieu of satellites. Because of the short baselines, the stations are located almost on a plane with vanishing Z-components; however, this does not affect the accuracy of the six-station system. The usual assumption about the ranging accuracy (1 cm) has been imposed. Two airplane trajectories, as indicated in Figure 5-4, were used in the simulation. The resulting accuracies of various station coordinates are shown in Table 5-7.

Table 5-7.

Average,  $\epsilon$ , and Standard Deviation,  $\sigma$ , in Station Locations  
for the Airplane System in Los Angeles  
(Origin Assumed to be at San Fernando)

Station	$\epsilon_X$	$\sigma_X$	$\epsilon_Y$	$\sigma_Y$	$\epsilon_Z$	$\sigma_Z$
Pasadena	-1.28	1.57				
Santa Monica	4.05	3.87	0.39	2.24		
Burbank	-0.13	0.48	0.38	0.32	0.49	0.91
Mt. Wilson	-0.70	1.67	0.39	0.47	0.38	1.25
Van Nuys	1.37	1.33	0.30	0.75	-0.20	0.77

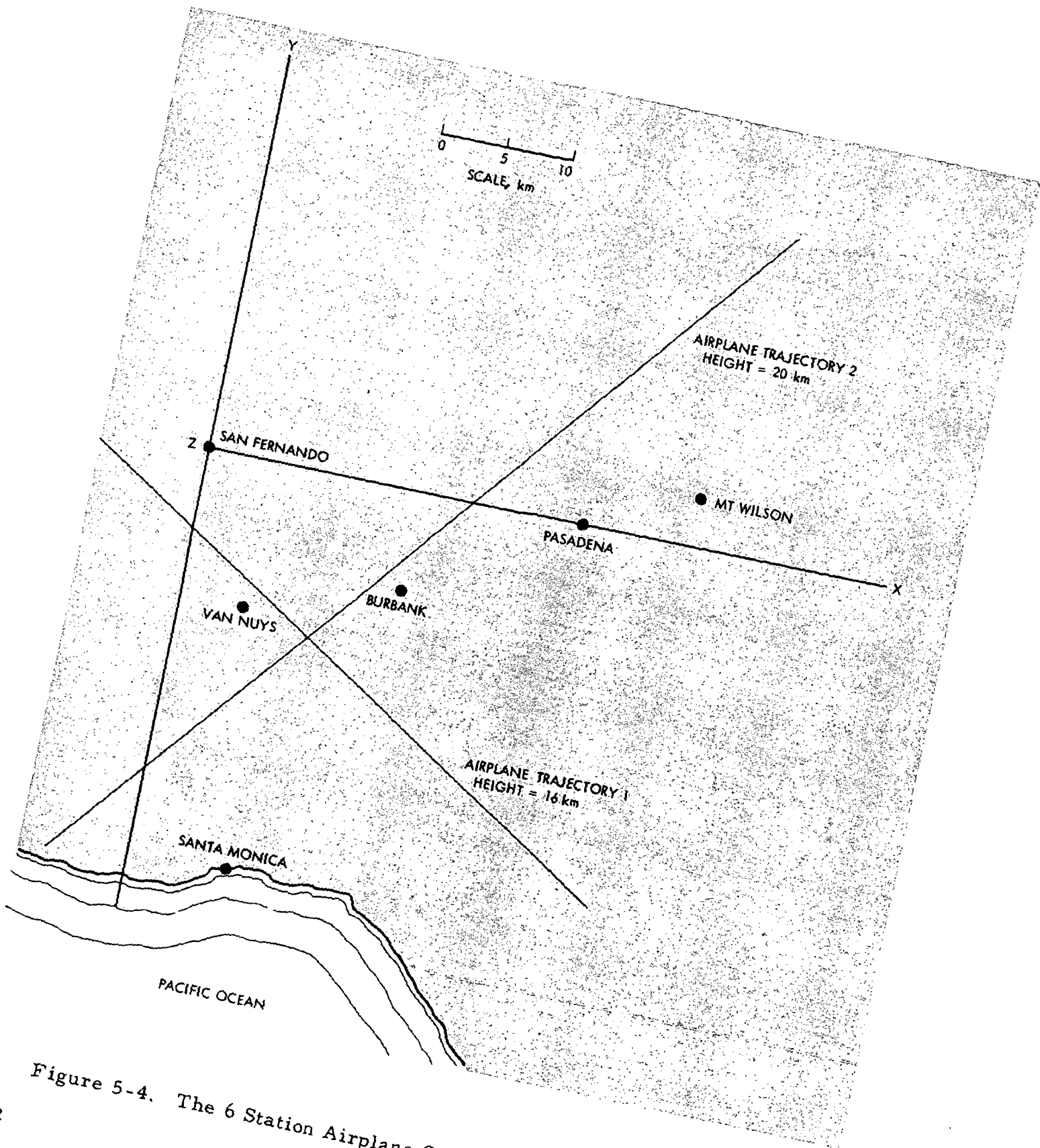


Figure 5-4. The 6 Station Airplane System in the Los Angeles Area

## 5.2 FOUR STATION CONFIGURATION: INTERCONTINENTAL BASELINES

As mentioned in the summary (Section I) and will be discussed in Section VII, a system of four stations, each ranging to at least six trajectory points in principle is a workable configuration provided that the four stations do not lie on a common plane. (Certain orbital degeneracies must also be ruled out; see Appendix B.) However, owing to the Earth's flatness over small distances, the four-station system can be utilized only if baselines are of intercontinental scale and if one of the stations is separated by a sizable amount from the plane containing the other three stations. Even if these two conditions are satisfied, there is no guarantee that the system will yield coordinates accurate to the centimeter level. However, there do exist four-station configurations that give acceptable accuracies. An example of this is the following choice of sites:

- Station 1: Mexico City
- Station 2: London
- Station 3: New York
- Station 4: Freetown

Note that the above configuration is a subset of the six-station intercontinental network discussed in Paragraph 5.1.3. The same satellite trajectories as indicated in Figure 5-3 are also used in this analysis. The results of the accuracy analysis for this configuration are shown in Table 5-8.

Table 5-8.

Average,  $\epsilon$ , and Standard Deviation,  $\sigma$ , in Centimeters of Station Coordinate Errors for the Four-Station Intercontinental System  
(Origin Assumed to be at Mexico City)

Station	$\epsilon_X$	$\sigma_X$	$\epsilon_Y$	$\sigma_Y$	$\epsilon_Z$	$\sigma_Z$
London	-3.93	7.78				
New York	-1.77	2.22	0.51	5.91		
Freetown	-4.02	13.49	1.83	2.25	1.28	1.63

A 4-station simulation was also carried out with stations situated at Kaneohe, Tarara, Calgary and Mexico City. Comparable results to the 4-station intercontinental simulation were obtained but are omitted here.

As can be seen by comparing Table 5-8 with Table 5-5, the accuracy of the four-station system is inferior to the corresponding six-station system.

### 5.3 COLLINEAR THREE-STATION CONFIGURATION: VERY SHORT BASELINES

If three stations are aligned in a straight line, then there exists a simple technique for surveying the baselines between the stations using only two simultaneous range measurements to an aircraft. Obviously, such a technique can be applied only to short baselines, since it is impossible to align widely separated stations in a straight line due to the curvature of Earth's surface. A discussion of the collinear three-station technique is presented in Paragraph 7.5 and in Appendix C.

The accuracy of the collinear three-station system depends on how well the stations can be aligned in a straight line and how the trajectory points are actually chosen. Let  $Y_3$  be the amount of misalignment of station 3 with respect to the straight line (X-axis) joining stations 1 and 2, as illustrated in Figure 5-5.

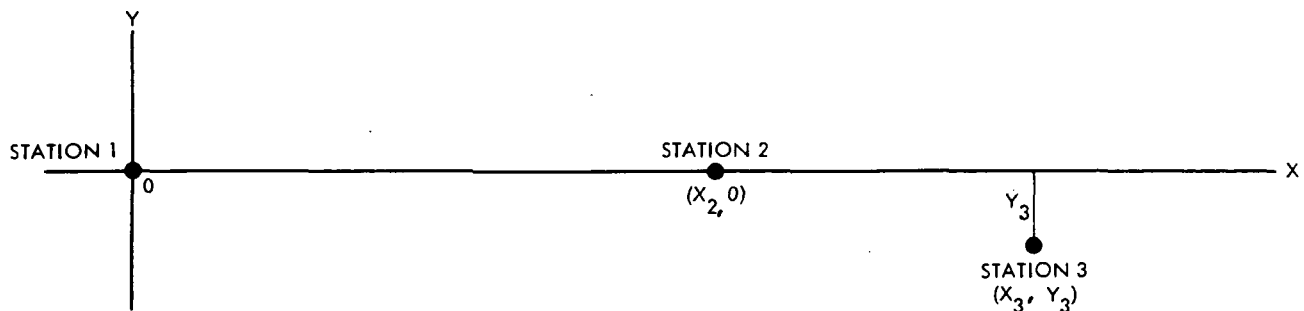


Figure 5-5. Misalignment of Station 3 in the Collinear Three-Station System

It can be shown that the trajectory points can be chosen in such a way that the induced errors in one of the station coordinates ( $X_2$  or  $X_3$ ) due to the misalignment error  $Y_3$  can be minimized. However, the corresponding errors in the other station coordinate ( $X_3$  or  $X_2$ ) will remain large.\* This implies that each of the two baseline  $X_2$  and  $X_3$  should be determined separately with suitably-chosen trajectory points.

For illustration purposes, the following nominal baselines are adopted:

$$X_2 = 40 \text{ km}$$

$$X_3 = 60 \text{ km}$$

Let the retroreflector-bearing vehicle fly a planar trajectory given by the equation

$$y = 0.5(x - X_3)$$

For various degrees of misalignment  $Y_3$ , the induced errors in  $X_2$  and  $X_3$  are computed, with the usual assumption of normally distributed ranging errors having zero mean and 1 cm standard deviation. The use of 100 trajectory points is also assumed. Results of this calculation are summarized in Table 5-8.

As can be seen from this Table, the errors in  $X_2$ , with misalignment error  $Y_3$  as large as 100 meters, remain well within the centimeter level even though errors in  $X_3$  become progressively larger as  $Y_3$  increases.

---

\*See Appendix C for more details of the error minimizing technique.

Table 5-9.

Accuracy of the 3-Station System as a Function of the Misalignment  $Y_3$  from the X-axis. Trajectory points have been chosen to minimize the induced error in  $X_2$ . Ranging errors are Normally Distributed with Zero Mean and 1 cm Standard Deviation. The Average Values for 10 Calculations each using 100 Trajectory Points are Quoted. All quantities are in Centimeters.

Misalignment $Y_3$	Error in $X_2$	Error in $X_3$
1	0.287	0.683
10	0.101	5.10
100	0.231	50.2
1,000	0.020	500.
10,000	0.350	5000.

Similarly, the errors in  $X_3$  can be minimized by flying the retroreflector on a planar course satisfying, e. g.,

$$y = -0.5(x - X_2).$$

In such a case, the errors in  $X_3$  would remain small while the  $X_2$  error increases with increasing misalignment.

#### 5.4 ULTIMATE SYSTEM ACCURACY

It must be understood that the results quoted in this section are preliminary and can be improved. In the historical development of this project (see Section II) it was pointed out that the six-station configuration was a recently developed concept. Due to this fact and lack of time, it has not been possible to determine the ultimate system accuracy. This accuracy depends on two factors, namely, the manner in which orbital orientations are adopted and upon station

location. The first factor is flexible and upon proper orbital design, accuracy improvements will be noted. The second factor is less flexible due to geographic constraints, but certain optimization can still be performed. These two factors coupled with:

- the use of more data, since only 100 measurements were utilized in most of the simulations, and
- the use of additional stations,

will result in station coordinate determination whose accuracy is only limited by the accuracy of the laser measurements, i. e., the mapping of errors from the measurements to the station coordinates will be better than one-to-one. Therefore, since laser measurements accurate to approximately 1 cm can be obtained presently (see Section X), the following conclusion can be drawn: A laser ranging system accurate to the sub-centimeter level can be constructed within the next five years.

## SECTION VI

### GEOLOGICAL APPLICATIONS OF MULTILATERATION: STATION LOCATION SELECTION

 A major geophysical objective of accurately locating widely spaced points as a function of time is to monitor the strain buildup in the Earth's crust. Then, comparing the strain buildup with the strain release resulting from earthquakes and from nonseismic slippage or creep, a model of elastic deformation and its variation from place to place can be constructed. In more detail there are three essential components in the determination of earthquake hazard to be anticipated in the major earthquake zones of the world. These three features include:

- (1) The strain field (see Glossary) of the crust of the Earth, which describes the state of deformation at any given time and how this field changes with time;
- (2) the stress field (see Glossary) in the Earth's crust and how this field changes with time, and
- (3) the critical states for rupture and tearing along earthquake faults.

In this section the critical components required for earthquake estimation will be identified. This will be followed by a brief discussion of plate tectonic theory. These discussions will naturally lead to a number of pertinent questions. Some of these questions, specifically those relative to the strain field in the Earth's crust will no doubt be answered by means of the proposed multilateration techniques.

The analysis in this Section is intended to be of a general nature and depicts the process of earthquake prediction as a complex process invoking many factors. For another viewpoint to this problem the reader is directed to Appendix L.

## 6.1 CRITICAL COMPONENTS OF EARTHQUAKE ESTIMATION

The problems of earthquake prediction can be most simply discussed by reference to Figure 6-1. Imagine that a sample of rock or other material is being loaded under a constant load stress,  $\sigma$ . Let it be assumed for the moment that a critical stress, say, the yield stress, exists and that the load stress is greater than the critical stress. Then after an almost instantaneous elastic yielding to the applied stress, the material will continue to deform in plastic deformation. Sketched schematically, in Figure 6-1, is the nonelastic or creep strain as a function of time. The creep strain is divided into three episodes, called the primary, the secondary, and the tertiary regimes. The tertiary part of the response is followed by brittle fracture (indicated by F in Figure 6-1). In the Earth this part of the strain history would be called an earthquake. Much of the present activity in the search for earthquake premonitors is connected with the local instrumentation of earthquake faults. A good example is the

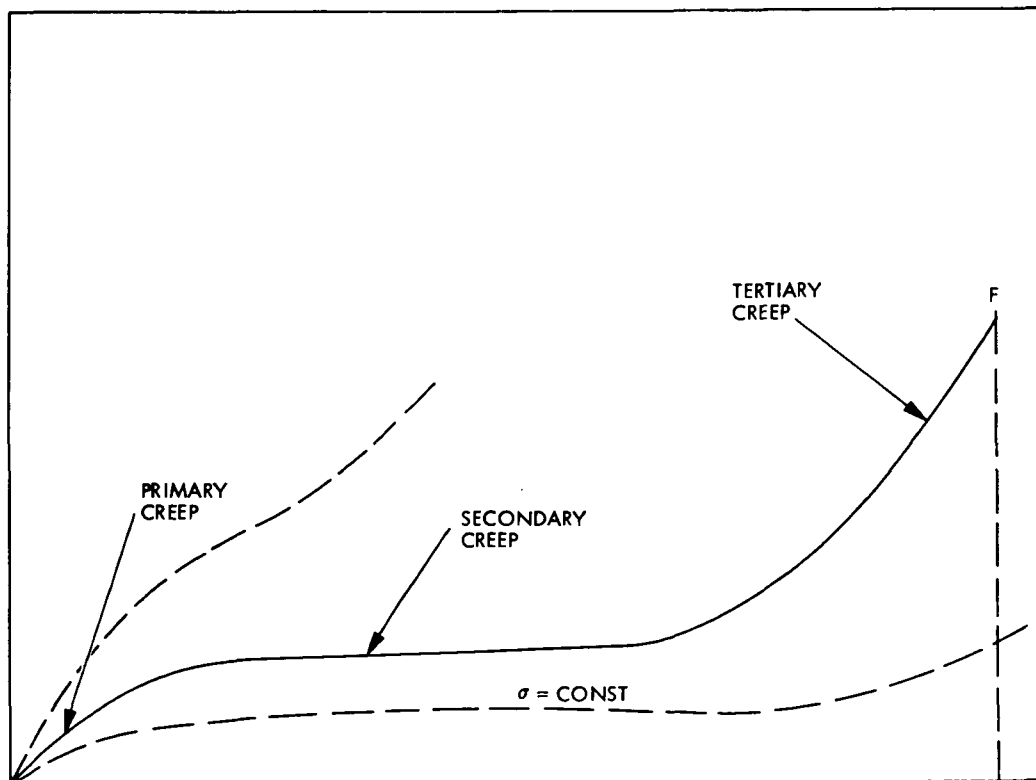


Figure 6-1. Strain as a Function of Time

San Andreas Fault where measurements of strain are being taken at this time to see if any accelerated creep is observable. If this is the case, then presumably, a region which is undergoing tertiary creep has been found; and brittle fracture, i. e., an earthquake, is expected to be imminent on some undetermined time scale.

But the problem, as it occurs frequently in nature, is hardly consistent with the simple explanation previously outlined, i. e., with the premise that the observation of tertiary creep is the solution to the problem of earthquake prediction. The more detailed problem is rather simply illustrated by the fact that along some parts of the San Andreas Fault some creep is presently being observed while other parts of the fault are "locked," i. e., at present no relative motion is currently being observed.

Some questions present themselves. Why should one part of the San Andreas Fault be locked and not another? Is the locking due to the presence of stresses that are below the yield stress of the respective materials? Or is the material in the locked sections of the fault so durable that it does not deform significantly under even relatively large stresses? The problem then becomes one of determination of the shape of the response curve sketched in Figure 6-1. At the present time it is not known where a given region of the Earth is in the strain-stress-time space depicted in Figure 6-1. Further, the shape of the creep response curve itself, namely how long the various episodes of creep should last, is not known.

The three curves of Figure 6-2 are intended to be schematic curves of creep response under constant load stress for a given material undergoing brittle fracture. For higher load stresses, the creep rates are higher, the time to fracture is shorter, and the strain at fracture is probably lower.

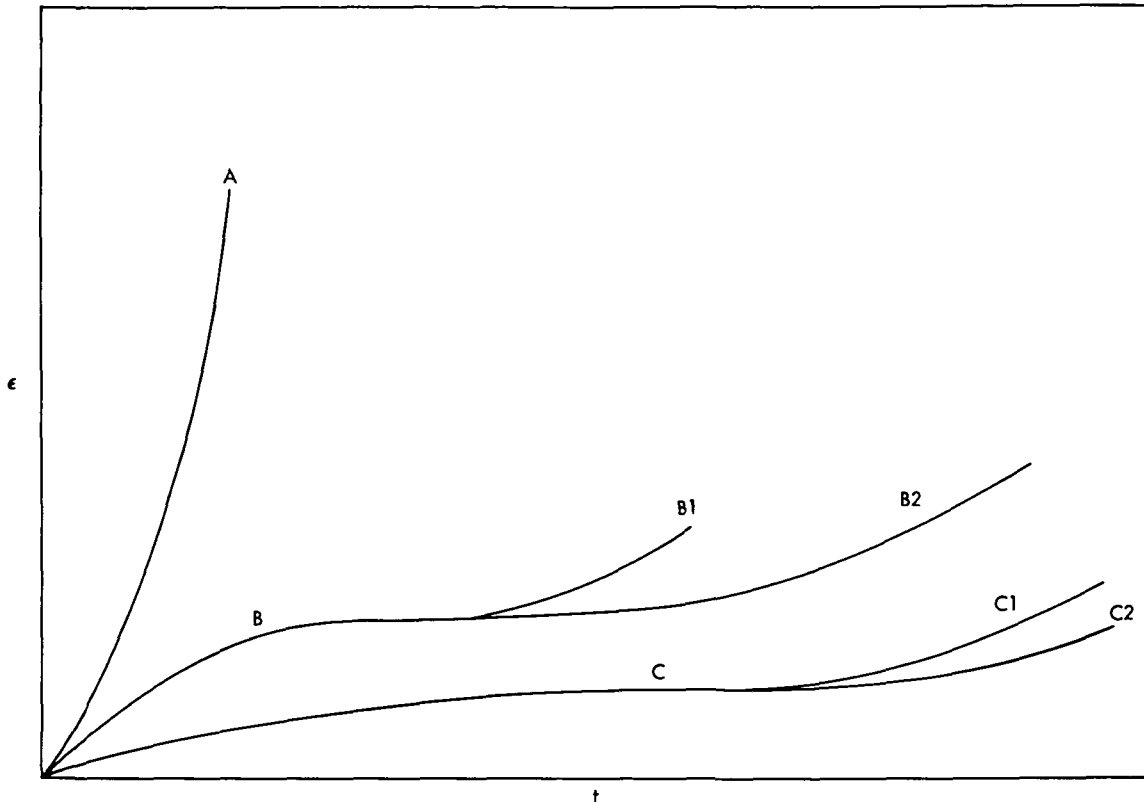


Figure 6-2. Strain Versus Time

The situation is even more complicated when different materials are considered. For example, consider a given supercritical load stress applied to a material such as chewing gum or silly putty. The creep strains become large in short time, and fracture occurs relatively quickly when compared with geological situations (see Curve A of Figure 6-2). In the seismic case, for the same load stress discussed before, the response may depend seriously on frictional forces within the fault. For lower friction, as depicted by B in Figure 6-2, there may be some creep slippage, but as indicated before, it is not known whether this implies a short time to rupture as illustrated at point B1, or a longer time as at B2. On the other hand, for a fault with high friction as illustrated in Figure 6-2, the material may not deform significantly for

a long time until an episode of accelerated creep sets in, which may be very brief, as at C1, or of a longer duration, as at C2.

Curves such as those of Figure 6-2 also apply to parts of the Earth which are not on earthquake faults. The fact of the state of occurrence of an earthfracture, i. e., do not have earthquakes, implies that the critical stress is not reached. This may be due to the fact of occurrence of an earthquake nearby. Apparently knowledge of the state of strain in regions adjacent to earthquake faults is important in understanding the state of strain in the faults themselves.

Despite this rather bleak picture, some positive remarks can be made and tests can be proposed to ascertain the validity of various conjectures, and to clarify some confusing features of this problem. Multilateration techniques cannot be expected to provide all the answers to earthquake problems, but crucial questions can be raised which multilateration, by virtue of its unique capability to obtain three dimensional station coordinates with precision, will no doubt be able to provide necessary inputs.

## 6.2 PLATE TECTONICS

According to the modern notions of plate tectonics, the surface of the Earth is covered by a relatively small number of rather rigid plates, on the order of 100 km thick. These plates\* are presumed to be in relatively uniform motion with respect to one another, at least at places remote from their common boundaries. They are being created at the great mid-oceanic rises, by virtue of the efflux of mantle material at the rises; this material is cooled and attached to the edges of the plates as they recede from the rises. The plates

---

\*The Pacific plate, which is the largest of the plates, covers about 22% of the Earth's surface.

return matter to the mantle where the oceanic plates are in collision with continental plates or with other oceanic plates. At other plate boundaries, such as the San Andreas Fault which is the boundary between the Pacific and the North American Plates, the plates slide past one another. Here the mode of earthquake motion is consistent with strike-slip or horizontal motions of slip between two plates. At the trenches the earthquake motions have components consistent with compressional stresses.

Although the plates are presumed to be in rather constant relative motion in regions remote from the plate boundaries, this is not the case at the boundaries themselves. Here the plates may be imagined to be held together by friction, and motions take place abruptly at irregular intervals. These abrupt events are earthquakes and indeed a map of earthquake epicenters delineates the boundaries of the plates. According to the model of plate tectonics, the interiors of the plates are undoubtedly in a state of stress but these stresses are subcritical for fracture except in certain rare instances. Such an event, occurring in the interior of a plate, was the earthquake at Charleston, S. C. in 1888. The earthquakes which occurred in Denver, Colorado, in 1962-1967 are testimony to the fact that the interior of the North American Plate is not stress free and indeed that the stress is subcritical at Denver; it was only when the critical stress for rupture was lowered by fluid injection at one point, that the series of earthquakes was initiated. It is further evident that the stresses in the interiors of plates are necessarily present in order that the plates can move relative to one another.

Consider that the stress field in the neighborhood of a major fault can be represented by a model of a uniform block of the Earth's crust with a uniform strain-rate or stress field applied at infinity; the block has a fault within it and

sliding at the fault is prevented from occurring by frictional forces. Unfortunately the past history of earthquakes on the fault seriously creates an inhomogeneous stress, and hence strain field, in the vicinity of the fault. When a segment of the fault ruptures, stresses on the ruptured segment are lowered while stresses outside the torn segment are raised. The material in the neighborhood of a fault break probably undergoes some post-shock creep strain due to the change in the stress conditions; such post-shock creep has been observed. Hence astride a feature such as the San Andreas Fault, the stresses can hardly be considered to be uniform. As a crude simplification, there exists the probability that following a great earthquake, there is a "waiting time" before another great shock will occur simply because the stresses and hence the strains in this region have been dropped. On this basis, a great earthquake should be expected to occur on that part of the fault which tore more recently in the past.

From the above, it might be expected that a great earthquake might occur sooner along the San Andreas Fault of Southern California near its closest approach to Los Angeles instead of in the San Francisco area, since the last great earthquake in the former segment was in 1857 while in the latter case the most recent event was in 1906. However, these two regions are not in similar seismological settings. These dissimilarities in seismological settings have implications for differences in the frictional configurations as well, and hence for the respective creep histories.

In reality, the contact between two plates such as the Pacific and North American plates in California is not a simple linear one-dimensional feature. The San Andreas Fault itself undergoes major changes in direction especially in Southern California. The Western United States and especially the seismic zones of California and Nevada are a rather complicated network of earthquake

faults, probably in some sense related with the plate boundary itself, or perhaps the network is the plate boundary. Many of the great earthquakes of California and Nevada history did not occur on the San Andreas Fault (Figure 6-3). A crucial question concerning the potential hazard on the locked (no observed creep) and the unlocked (proven or suspected creep) segments of faults concerns the sites at which the strains are being built up at this time. Estimates of the rates of motion of the Pacific and North American plates at places remote from their boundaries are of the order of 5 cm/year. In the neighborhood of the locked segments of the great faults, where is the strain rate of the order of 5 cm/year if it is zero on the faults? In central California, on the "unlocked" segment of the San Andreas Fault, what is the significance of the fact that the slip rate is only about 1 cm/year and where is the remainder of the strain field being absorbed? Does this imply strain build up on other important fault features of the Western U.S.? The fundamental question to be answered is the extent to which the fields in the interiors of plates, and to the proximity of the plate boundaries, can be considered to be uniform.

### 6.3 QUESTIONS OF PRIMARY INTEREST

A number of important questions have been raised in the discussion presented in the previous sections. These include the following:

1. Is the rate of relative motion of plate interiors truly uniform? Estimates of these rates are in the main derived from evidence which represent averages over several millions of years, although the recent JOIDES\* deep-drilling results seem to imply that these averages may hold for even longer periods; as long as 75 million years

---

\*Joint Oceanographic Institutions for Deep Earth Sampling

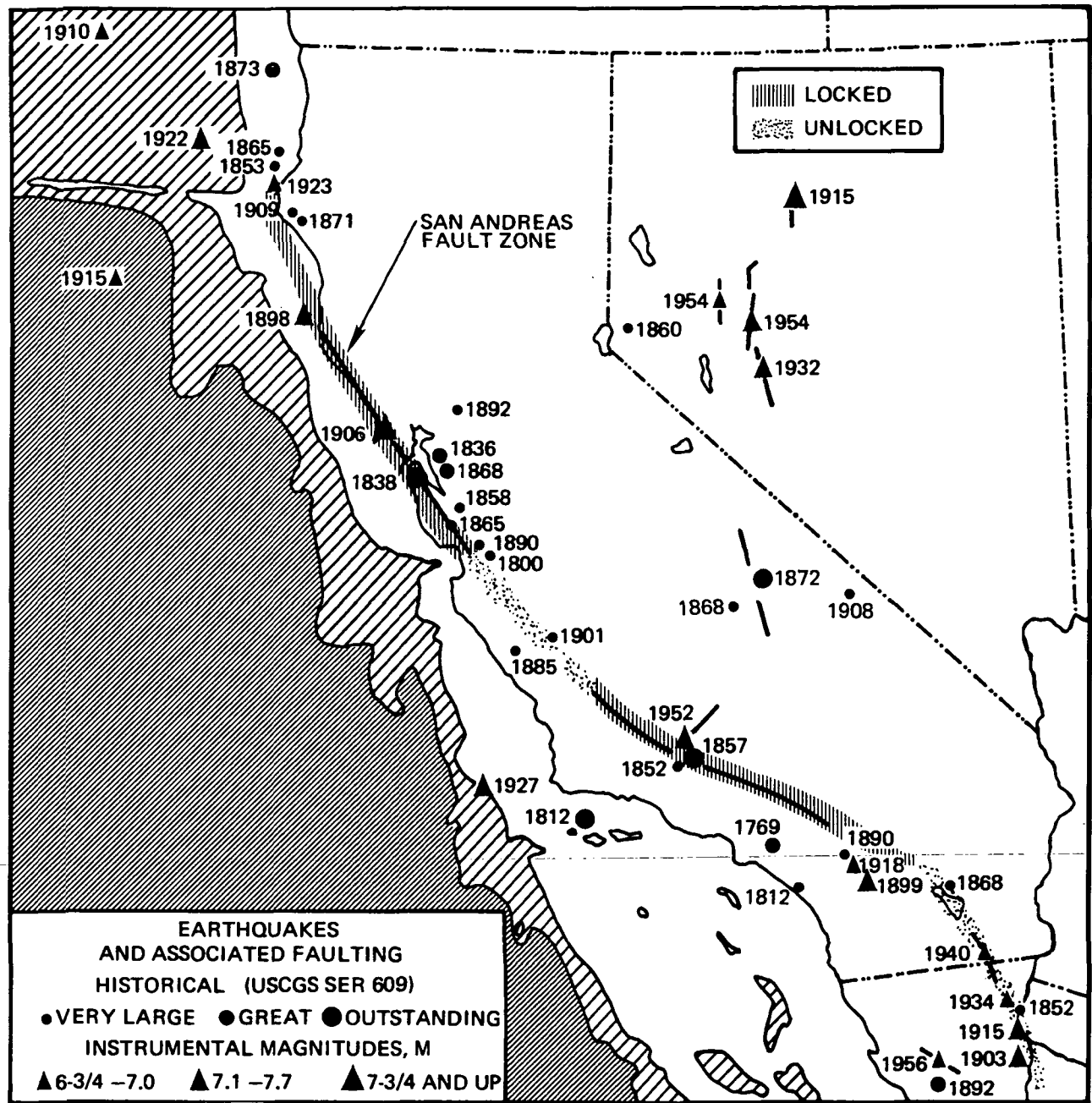


Figure 6-3. Large Earthquakes and Associated Faulting in the California and Nevada Region. The Locked and Unlocked Portions of the San Andreas Fault Zone are Delineated by the Shaded and Stippled Zones Respectively.

or more. But can these averages be applied to estimates of plate strain rates on a time scale of a few years? Measurements should be made of the relative motion of points on opposite sides of a plate boundary at points remote from the contact. It is suggested that measurement be made of the relative motion of the North American and European plates for this purpose. The Mid-Atlantic Ridge, which is the boundary in this case, appears to be less complicated than the Pacific-North American Boundary. Stations suggested for implementation of a six-station experiment might include: New Orleans, Chicago and Halifax in the North American Plate and Rome, Greenwich and Stockholm on the European Plate.

2. Are the motions of a given plate-interior relatively uniform, i. e., does a plate-interior move as a relatively rigid body? Or are the stresses subcritical for fracture but still able to produce local creep in consonance with irregularities in the stress fields at the edges of the plates. In this case an experiment is proposed to see if there is any relative motion in the interior of the "stable" North American Plate. Station locations might include: Dallas, Kansas City, Minneapolis, Atlanta, Ottawa and Halifax.
3. If motions are relatively uniform in plate interiors, how close can a plate boundary be approached before these fields show a gradient? Here it is proposed to study the Pacific-North American Plate boundary. Proposed stations might include: Oahu, Farallon Islands, San Diego, Reno, Salt Lake City and Minneapolis.

4. What ground motions take place 100 to 200 km from a given fault zone? In this case local placement of six or more stations should satisfy all experiment objectives. Knowledge of the movements of distant points is a basic requirement in constructing a strain model of a major fault zone to be used as the basis of the understanding of earthquakes. Current geodetic-net techniques, while very accurate at short distances, are line-of-sight limited and are impractical beyond distances of about 100 km for the high accuracies needed. Multilateration, however, is not hindered in this respect.

As an example consider how strain builds up along the San Andreas Fault zone as a function of whether the fault is locked or unlocked. Examination of Figure 6-3 shows four separate areas along the San Andreas Fault zone. These include: Northern California (site of the 1906 earthquake), the unlocked segment to the south, the locked segment farther south, and finally the Imperial Valley to the Gulf of California. Each of these segments will require different experiments due to the distinct geology peculiar to the respective areas. It is now believed that the type of slip that relieves strain in the San Andreas fault zone varies along the length of the fault. In certain areas, some of the slip takes place as creep, that is, slow motion with little or no radiated seismic energy (earthquakes). In other areas, almost all of the slip occurs rapidly in large but infrequent earthquakes. The former areas are considered locked inasmuch as most of accumulated strain is being elastically stored for sudden release in further large earthquakes. The regional strain field along the San Andreas is strongly affected by whether the fault is locally locked or unlocked,

and any strain measurement program should take this into account. For example, in areas of fault creep, it is important to know if the input strain, measured by the displacement of points distant from the fault (100 to 200 km), is relieved by creep along or near the fault, which is relatively easy to measure. If the strain is relieved mainly by creep, then the likelihood of a large earthquake along that part of the fault is small. However, if only a small portion of the input strain is relieved by creep, then unlocked portions of the fault are also susceptible to large earthquakes. The San Andreas and associated fault zones in California and Mexico represent one of the most studied potentially destructive seismic zones in the world. Therefore, this region provides a truly unique location for getting relative station motions and, thus, regional strain data which are scientifically pertinent.

5. What is the rate of strain build-up on other major fault zones? A number of catastrophic events have occurred in the Western United States other than on the San Andreas Fault. Note can be taken of the disastrous Owens Valley earthquake of 1872, which has been classified as having a magnitude greater than the 1906 or 1857 earthquakes that occurred on the San Andreas fault. The rate of strain build-up on other major fault zones in the Western U.S. can and should be studied via the methodology of Multilateration. It is highly likely that the network of earthquake faults in the western U.S. will have to be considered interactively instead of individually. Here, the relatively low cost of Multilateration is a distinct advantage since instrumentation of each of these faults for creep measurements may be extraordinarily complex.

6. What is the driving mechanism for plate tectonic motions? It has been suggested that the failure of the Earth to have the equilibrium shape for a fluid rotating with the present angular velocity of the Earth is evidence for the presence of stresses within the mantle of the Earth. The estimates of the flattening of the Earth are  $1/298.3$  while the equilibrium flattening is  $1/299.7$ . This discrepancy of about one part in 200 is thought to be significant.

The flattening is obtained from studies of perturbations in the orbits of satellites. A direct observation of the figure of the Earth may lead to better estimates of the stresses in the Earth. However, this information alone cannot indicate whether these stresses are caused by convection in the mantle or by finite strength of the mantle material. A direct observation of the figure of the Earth is possible by measuring the shape of the Earth at a geoid, or equipotential surface. Such an equipotential surface is provided by the surface of the ocean. Coastal stations at known heights above mean sea level could be used to determine the geoid. Suggested stations include: Halifax, Washington, Puerto Rico, London, etc.

#### 6.4 EARTH/OCEAN TIDE CALIBRATION

As mentioned in the previous sections, the prediction of earthquakes involves a succinct number of factors. One of these factors is the ability to make precision measurements across faults and between adjacent plates. These measurements are related to the plastic deformation of local ground areas. However, the Earth also experiences elastic deformation due to the perturbative effect of the Sun and Moon. Specifically, the acceleration of the

Sun and Moon on two points separated by a sizeable distance 1000-10000 km will have unequal components and thus will cause residual movements between the two points. Hence, as a function of time two points on the surface of the Earth will have a cyclic motion with amplitudes ranging from 1 to 30 cm. relative to some mean datum. Furthermore, ocean tides will also cause differential ground movements.

It therefore follows that to obtain precise station coordinates the magnitude of the Earth/ocean tides must be calibrated at each station. This calibration, i. e., the determination of curves of the sort displayed in Figure 6-4, does not present any serious problem with respect to obtaining precision plastic ground movements. The required calibration can be performed with the aid of a moveable gravimeter (placed at each station for a suitable period of time) or

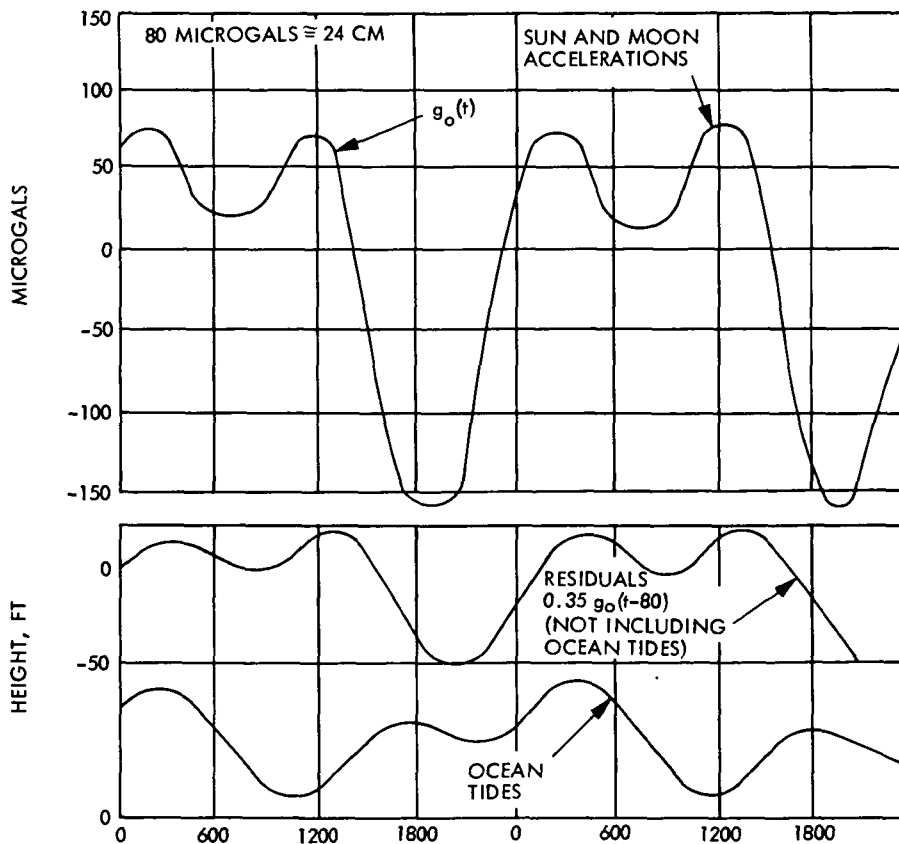


Figure 6-4. Earth/Moon Tides

perhaps directly by analytic calibration. It is estimated that the elastic deformations in the crust of the Earth can be determined to the millimeter level.

## 6.5 CONCLUDING REMARKS

This section has indicated the obvious: namely, that the prediction of earthquakes is a difficult task. It has been pointed out that Multilateration, along with carefully planned experiments will be a unique advantage to the process of earthquake prediction. Some preliminary station locations fundamental in answering the questions posed have been selected. Further analysis will permit the exact viability of these station locations to be established.

It can be concluded, at least on a preliminary basis, that use of multilateration techniques will lead to a better understanding of earthquake mechanisms. Even if the consequences of the multilateration systems discussed herein lead to the ability of only roughly estimating the epoch of major earthquakes, this will result in the development of long range planning to aid in preparing for such events. This long range planning, i. e., setting in motion the political and financial plan for the predicted event will result in great financial savings because manpower levels need only be increased when the probability of an earthquake is high. Furthermore state officials could easily budget funds for use in future reconstruction. Short range planning, i. e., the development of strategy for an earthquake predicted to occur within a week or perhaps days needs no explanation.

## SECTION VII

### GENERAL THEORY OF MULTILATERATION



This Section is primarily concerned with the mathematical theory of multilateration, i. e. , the determination of three-dimensional station locations and orbital ephemeris by the use of geometric principles only.

The first portion of this Section discusses the necessary conditions for the existence of a solution to the ranging problem. It is indicated that the sufficient conditions are not established but a preview of what will occur when systems comprised of 4, 5 and 6 stations are used is outlined with the aid of a schematic block diagram.

In Paragraph 7.2 a derivation of the actual geometric equations is undertaken. It is shown that the solution to the ranging problem consists in the simultaneous determination of the intersection of a set of spheres each centered at the location of a station. These equations can be reduced at a fixed time to yield a single nonlinear equation which describes the overall geometric relationships. The repeated application of the reduced or fundamental equation at a repeated number of times subsequently will yield the solution of the multilateration problem.

The third portion of this Section discusses the sensitivity of the solutions, i. e. , for fixed stations and orbital configurations, the manner in which errors in the observed range measurements map into the actual station positions is outlined.

Paragraph 7.4 introduces the reader to the degeneracies peculiar to the type of geometric schemes proposed herein. It is in this Section that the reasons for the degeneration of the 4 or 5 station configurations are explained in sufficient detail such that the interested reader can proceed to Appendix B for the complete theory, if it is so desired. The reason for the non-degeneracy

of the 6 station configuration also is stated. Finally, Paragraph 7.5 explains why a solution to the multilateration problem is possible using three collinear stations.

### 7.1 NECESSARY CONDITIONS FOR THE SOLUTION OF RANGE-ONLY SYSTEMS

As will be discussed presently, the mathematical relationships utilized in geometric ranging techniques give rise to one equation per station per strike of the satellite, which contains as parameters, the unknown position of the satellite  $[x, y, z]$  along with the unknown position of the station  $[X, Y, Z]$ , and as known quantities, the ranges. Owing to the adopted coordinate system (see Section 4), in which the coordinates of the first three stations are given respectively by  $[0, 0, 0]$ ,  $[X_2, 0, 0]$ , and  $[X_3, Y_3, 0]$ , the number of unknown station coordinates is reduced by 6. Hence, in the first three equations, only three unknown station coordinates are introduced.

These facts are tabulated in Table 7-1.

Table 7-1.  
Summary of Conditions

Station Number	Number of Satellite Coordinates Per Strike	Number of Station Coordinates
1	3	0
2	3	1
3	3	2
4	3	3
5	3	3
6	3	3

In the previous table, the dashed line indicates that, after the third station, the number of station unknowns is always increased by three for each new station added to the system. These statements can be expressed mathematically as:

$$\text{UNKNOWN STATION COORDINATES} = 3(I-3) + 3, \quad I \geq 3, \quad (7.1.1)$$

where  $I$  is the number of stations in the station net.

The remaining unknowns, i. e., the satellite coordinates, are simply given by three times the number of strikes (See Table 7-1) so that:

$$\text{UNKNOWN SATELLITE COORDINATES} = 3N \quad (7.1.2)$$

where  $N$  is the total number of strikes. The total unknowns are therefore given by

$$\text{UNKNOWNNS} = 3(I-3) + 3 + 3N. \quad (7.1.3)$$

Now consider the number of measurements which are made at each strike of the system. At any given time each station makes one measurement of the slant range,  $\rho$ ; therefore the measurements define a sequence equal to (See Table 7-1):

$$1, 2I, 3I, \dots, NI.$$

Therefore, the total number of knowns is

$$\text{KNOWNNS} = NI, \quad I \geq 3, \quad N = 1, 2, 3, \dots \quad (7.1.4)$$

The knowns must be at least as many as the unknowns in order to yield a theoretically deterministic system, therefore:

$$NI \geq 3(I-3) + 3 + 3N. \quad (7.1.5)$$

Satisfaction of inequality (7.1.5) is a necessary condition for the mathematic solution of a system of equations determining the satellite coordinates at any given time together with the station coordinates. The solution of the inequality is given parametrically in Table 7-2 using I, the total number of stations, as the independent parameter.

Table 7-2  
Parametric Solution of Inequality

$N \geq \frac{3I-6}{I-3}$	
Total Number of Stations (I)	Minimum Total Number of Strikes ( $N_{\min}$ )
3	$\infty$
4	6
5	5
6, 7, 8 . . . . .	4
$\infty$	3

It should be emphasized that satisfaction of inequality (7.1.5) is only a necessary condition that the system under study be solvable\*. It is only through detailed analysis, such as will be described in the following Sections and in Appendix 2 that the sufficient conditions peculiar to the ranging problem can be established.

To provide the reader with a preview of the complex logic contained in geometric ranging schemes Figure 7-1 is introduced at this point. The figure outlines the fundamental degeneracies of the laser ranging problem and is divided into two branches depicting four/five, and six station ranging systems.

\*The previously introduced three station system is not strictly a range only system (See Paragraph 7.5).

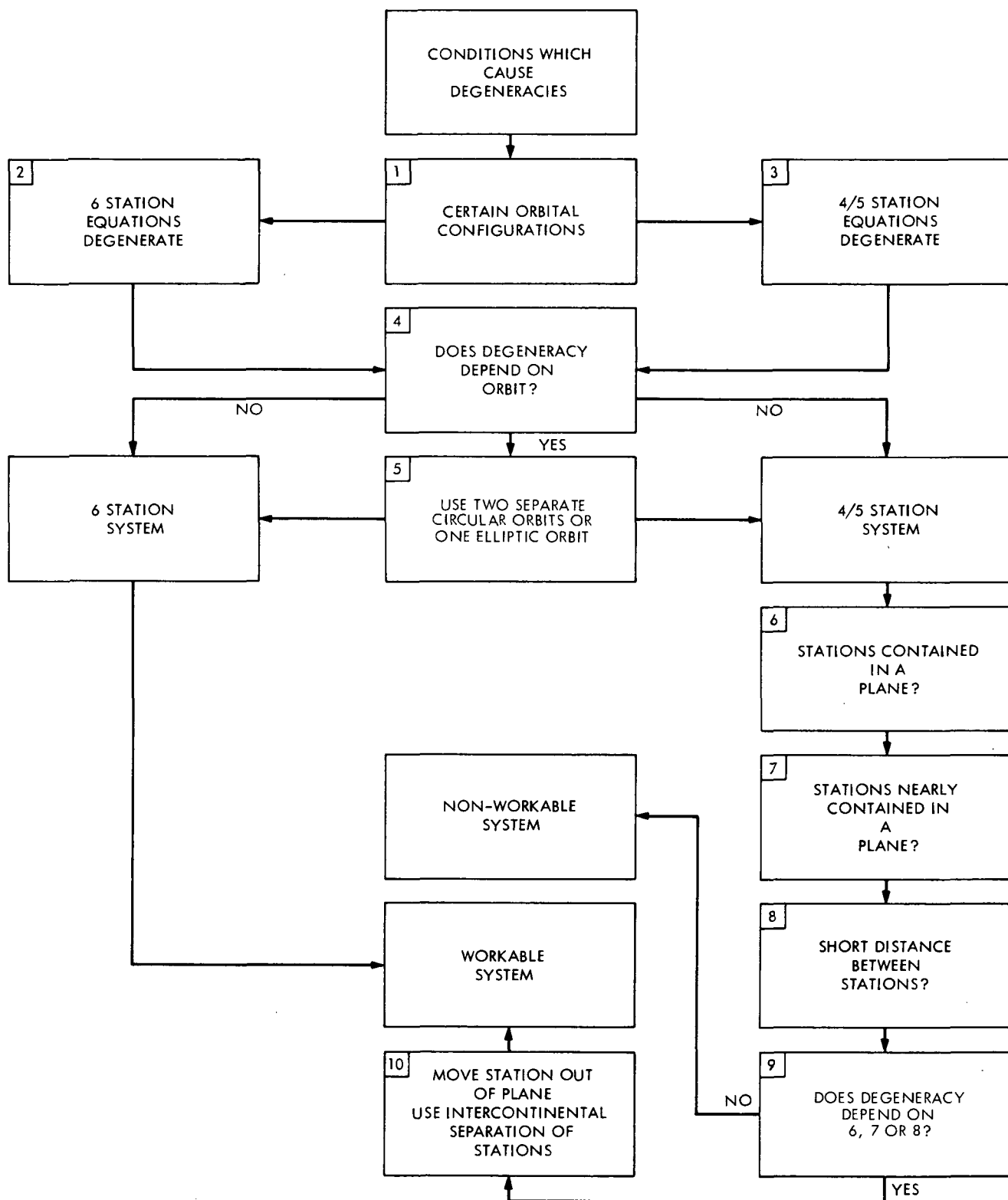


Figure 7-1. Degeneracies Causing System Malfunction

Block 1 indicates that there are certain orbital configurations in which the measured ranges do not change sufficiently and therefore whether the 6 station (Block 2) or 4/5 station (Block 3) system is utilized - the mathematical equations will become degenerate and no solution will be possible. If the degeneracy does depend on the orbit (Block 4), then by using two circular orbits of different altitude or an elliptic orbit (Block 5) the degeneracy can be removed. The six station system, whether or not the conditions outlined in Blocks 6, 7 and 8 exist will now yield a well defined numerical solution.

On the other hand, the 4 or 5 station case requires that the question in Block 9 be answered. If the stations are nearly contained in a plane, then perhaps a new station sufficiently removed from the plane of the other three can be used in the station net. Similarly, if the distance between the stations is too short then intercontinental positioning of the stations will be required (Block 10). Satisfaction of these two conditions will also yield a workable system; otherwise the system using 4 or 5 stations becomes unworkable regardless of the number of measurements which are taken.

The previous rules of geometric ranging techniques are not obvious and the proof of the previous statements is involved. Instead of discussing these details at this point, it will be better for the reader to understand the basic fundamentals (Paragraph 7.2, 7.3) first and then, after reading the introduction in Paragraph 7.4, proceed to Appendix B, if further details are desired.

## 7.2 DERIVATION AND METHOD OF SOLUTION OF MULTILATERATION EQUATIONS

As will be seen presently, the derivation of the fundamental equations of the geometric method is very simple; however as explained in Appendix B, understanding the connection between the pertinent variables is a much more complicated matter.

As illustrated in Figure 7-2 consider a station which makes a strike, i. e., a measurement of the distance between itself and an orbiting satellite\*, what geometry is described? Of course, the range distance

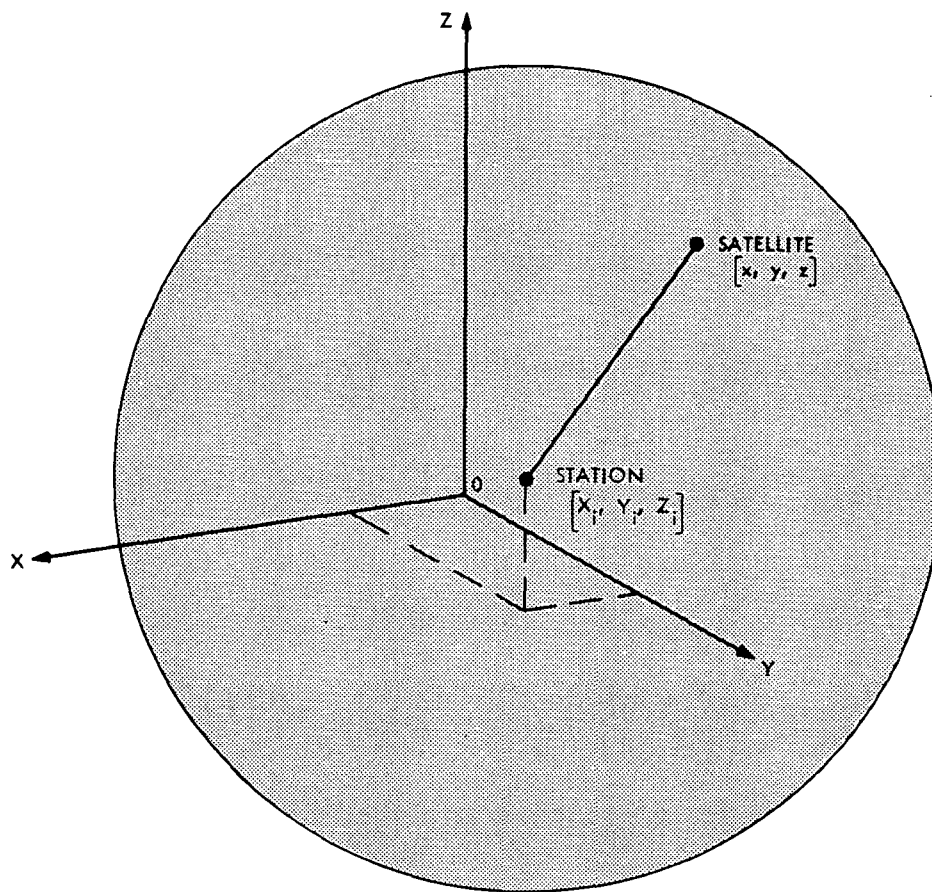


Figure 7-2. A Station Measuring the Range Between Itself and an Orbiting Satellite

\*The word satellite is used throughout for simplicity; however, for certain configurations it should be remembered that an airplane would work equally as well as a satellite.

can be pictured as the radius of a sphere centered on the station and touching the satellite. Hence the fundamental equation peculiar to all geometric techniques, as depicted graphically in Figure 1-3, is that of a sphere which has been translated to a station located at coordinates X, Y, Z relative to the adopted origin at 0. Mathematically this relationship can be stated from the principles of analytic geometry as

$$(x - X)^2 + (y - Y)^2 + (z - Z)^2 = \rho^2,$$

where x, y, z are the coordinates of the satellite.

More specifically, let there be a total of I stations on the ground all of which range simultaneously to a total of N satellite trajectory points at different times, t. Then the following equations are self-evident, i. e. ,

$$(x_n - X_i)^2 + (y_n - Y_i)^2 + (z_n - Z_i)^2 = \rho_{in}^2, \quad \left\{ \begin{array}{l} i = 1, 2, \dots, I \\ n = 1, 2, \dots, N \end{array} \right\}, \quad (7.2.1)$$

where

- $(X_i, Y_i, Z_i)$  = the coordinates of the  $i^{\text{th}}$  station,
- $(x_n, y_n, z_n)$  = the coordinates of the  $n^{\text{th}}$  trajectory point,
- $(\rho_{in})$  = the slant range from the  $i^{\text{th}}$  station to the  $n^{\text{th}}$  trajectory point.

It is convenient to work in the adopted geometric coordinate system introduced in Paragraph 4.4. In this coordinate system, the locations of stations 1, 2 and 3 are used specifically to define the coordinate axes. Thus, by definition,

$$X_1 \equiv Y_1 \equiv Z_1 \equiv X_2 \equiv Y_2 \equiv Z_2 \equiv X_3 \equiv Y_3 \equiv Z_3 \equiv 0. \quad (7.2.2)$$

The unknown station coordinates to be determined are  $X_2, X_3, Y_3, X_4, Y_4, Z_4, \dots, X_I, Y_I, Z_I$ , a total of  $(3I-6)$  parameters.

For purposes of convenience and algebraic manipulation range square difference equations will be formed by subtracting Eq. (7.2.1) written for  $i = 1$  and for  $i = 2, 3, 4, \dots, I$ , namely,

$$-2x_n X_2 + X_2^2 = \delta_{2n} \quad (7.2.3)$$

$$-2x_n X_3 - 2y_n Y_3 + X_3^2 + Y_3^2 = \delta_{3n} \quad (7.2.4)$$

$$-2x_n X_j - 2y_n Y_j - 2z_n Z_j + X_j^2 + Y_j^2 + Z_j^2 = \delta_{jn}, \quad j = 4, 5, \dots, I, \quad (7.2.5)$$

where the quantities  $\delta_{in}$ , ( $i = 2, 3, \dots, I$ ,  $n = 1, 2, \dots, N$ ), are defined by

$$\delta_{in} \equiv \rho_{in}^2 - \rho_{1n}^2 \quad (7.2.6)$$

The differenced set of equations (7.2.3) through (7.2.5), together with the equation

$$x_n^2 + y_n^2 + z_n^2 = \rho_{1n}^2, \quad n = 1, 2, 3, \dots, N \quad (7.2.7)$$

is completely equivalent to the original set of ranging equations (7.2.1).

As mentioned previously, the advantage of using the range square difference equations is that the satellite variables can be eliminated conveniently. Thus, from Eq. (7.2.3),  $x_n$  can be obtained as

$$x_n = (X_2^2 - \delta_{2n}) / (2X_2). \quad (7.2.8)$$

Substitution of (7.2.8) into (7.2.4) allows  $y_n$  also to be expressed as a function of the station coordinates and range data, i. e.,

$$y_n = \left[ X_3^2 + Y_3^2 - \delta_{3n} - \frac{X_3}{X_2} (X_2^2 - \delta_{2n}) \right] / (2Y_3). \quad (7.2.9)$$

Equations (7.2.7) can now be used to express  $z_n$  as a function of the station coordinates  $X_2$ ,  $X_3$  and  $Y_3$ :

$$z_n = \left[ \rho_{1n}^2 - x_n^2(X_2) - y_n^2(X_2, X_3, Y_3) \right]^{1/2} \quad (7.2.10)$$

Note that  $z_n$  must be positive. A negative  $z_n$  would correspond to a satellite trajectory point below the horizon from which a range measurement would not be possible.

The expressions (7.2.8) through (7.2.10) can then be substituted into (7.2.5), giving a system of  $(I - 3) \times N$  nonlinear equations in all the station coordinate variables:

$$F_m(\underline{S}) \equiv X_j^2 + Y_j^2 + Z_j^2 - 2x_n(X_2)X_j - 2y_n(X_2, X_3, Y_3)Y_j - 2z_n(X_2, X_3, Y_3)Z_j - \delta_{jn} = 0, \quad (7.2.11)$$

where the index  $j$  runs from 4 to  $I$ , the index  $n$  from 1 to  $N$ , the index  $m$  from 1 to  $(I - 3)N$ , and the vector  $\underline{S}$  denotes the collection of all the unknown station coordinates  $(X_2, X_3, Y_3, \dots, X_I, Y_I, Z_I)$ .

The system of equations (7.2.11) can be solved easily by the Newton-Raphson method [7.2]. More specifically, denoting a first estimate of any station parameter  $S_k$  to be determined by  $S_k^0$ , then an improved value of  $S_k$  is given by correcting  $S_k^0$  by the amount  $\Delta S_k$  obtained by solving the following system of linear equations:

$$\sum_{k=1}^{3I-6} \frac{\partial F_m}{\partial S_k}(\underline{S}^0) \Delta S_k = -F_m(\underline{S}^0), \quad m = 1, 2, \dots, (I - 3)N. \quad (7.2.11)$$

The appropriate algorithm for this purpose is given in Appendix A. Numerical simulation has shown that the algorithm is extremely efficient, yielding accurate solutions in 1 or 2 iterations even from starting values which are 1 kilometer in error. The equations peculiar to these parametric schemes are simple, at

least from a conceptual point of view. The reader, however, is cautioned that the singularities inherent to these systems should be well understood prior to attempting to extract meaningful information. These singularities are discussed in Paragraph 7.4 and in Appendix B.

### 7.3 SENSITIVITY ANALYSIS OF THE MULTISTATION SOLUTION

In Paragraph 7.2 it was shown that accurate solutions to the multilateration equations can be obtained in a straightforward manner. It now remains to analyze whether the solution is sensitive to small changes in the range measurements. This analysis is important because the measurements are subject to random and systematic errors which are unknown system variables. Specifically, if slight errors in these measurements produce large changes in the calculated station locations, then the mathematical method of solution and the overall system would not be useful in meeting the objectives of the present study, i.e., in the determination of station locations accurate to the centimeter level.

Numerical studies have shown that different configurations of the stations and the satellite trajectory points will in general result in different magnification factors (sensitivity numbers) in the error mapping from the measured data to the values of the station coordinates whose values are to be determined. In fact, there exist certain configurations which have infinite error factors, i.e., geometric instabilities such that a unique solution of the multilateration equations is not possible, even if a system of as many equations as unknown is formulated. Such cases are defined herein to be degenerate cases. Configurations of stations and trajectories that are close to being degenerate consequently will produce very large sensitivity numbers. Both degenerate and near-degenerate configurations should be avoided in order for

the system to yield reasonable sensitivities, i. e., small error magnifications and thus small errors in the station coordinates.

In order to decide whether or not a given configuration is geometrically stable, a sensitivity analysis must be performed. In principle, this type of analysis is simple although the algebraic details can become complex. Only the basic formulation of the analysis will be discussed herein. The details of the computational algorithm are discussed in Appendix A.

Suppose each of the measured slant ranges,  $\rho_{in}$ , is subject to an unknown range error,  $d\rho_{in}$ . The resulting solution vector of the station coordinates, namely,

$$\underline{S} = (X_2, X_3, Y_3, \dots, X_I, Y_I, Z_I), \quad (7.3.1)$$

will then differ from the true solution by the amount

$$\underline{dS} = (dX_2, dX_3, dY_3, \dots, dX_I, dY_I, dZ_I). \quad (7.3.2)$$

The purpose of performing a sensitivity analysis is to express  $\underline{dS}$  as a function of  $d\rho_{in}$  and of the fixed geometry peculiar to a given geometric configuration. Since only small changes in range are to be mapped into relatively small changes in the station coordinates (for nondegenerate cases), analysis via differentials will be adequate. To start the error mapping process, Eq. (7.2.11) is differentiated yielding

$$\begin{aligned} (2X_j - 2x_n)dX_j + (2Y_j - 2y_n)dY_j + (2Z_j - 2z_n)dZ_j - 2X_j dx_n - 2Y_j dy_n \\ - 2Z_j dz_n - d\delta_{jn} = 0, \quad j = 4, 5, \dots, I; n = 1, 2, \dots, N. \end{aligned} \quad (7.3.3)$$

The quantities  $dx_n$ ,  $dy_n$ , and  $dz_n$  can be obtained from Eqs. (7.2.8) through (7.2.10) by direct differentiation. Then by substitution into Eq. (7.3.3), an equation of the following form is obtained:

$$A_n^{(j)} dX_2 + B_n^{(j)} dX_3 + C_n^{(j)} dY_3 + a_n^{(j)} dX_j + b_n^{(j)} dY_j + c_n^{(j)} dZ_j = d\sigma_n^{(j)},$$

$$j = 4, 5, \dots, I; n = 1, 2, \dots, N, \quad (7.3.4)$$

where

$$A_n^{(j)} = (X_2 - x_n) \left( \frac{X_j Y_3 - X_3 Y_j}{X_2 Y_3} \right) + \left( \frac{X_2 - x_n}{X_2} \right) \left( \frac{-x_n}{z_n} + \frac{y_n}{z_n} \frac{X_3}{Y_3} \right) Z_j \quad (7.3.5)$$

$$B_n^{(j)} = \left( \frac{X_3 - x_n}{Y_3} \right) Y_j - \frac{y_n}{z_n} \left( \frac{X_3 - x_n}{Y_3} \right) Z_j \quad (7.3.6)$$

$$C_n^{(j)} = \left( \frac{Y_3 - y_n}{Y_3} \right) Y_j - \frac{y_n}{z_n} \left( 1 - \frac{y_n}{Y_3} \right) Z_j \quad (7.3.7)$$

$$a_n^{(j)} = x_n - X_j \quad (7.3.8)$$

$$b_n^{(j)} = y_n - Y_j \quad (7.3.9)$$

$$c_n^{(j)} = z_n - Z_j \quad (7.3.10)$$

$$d\sigma_n^{(j)} = \frac{1}{2} d\delta_{2n} \left( \frac{X_j}{X_2} - \frac{Y_j X_3}{X_2 Y_3} - \frac{x_n}{z_n} \frac{Z_j}{X_2} + \frac{y_n}{z_n} \frac{X_3 Z_j}{X_2 Y_3} \right)$$

$$+ \frac{1}{2} d\delta_{3n} \left( \frac{Y_j}{Y_3} - \frac{y_n}{z_n} \frac{Z_j}{Y_3} \right) - \frac{Z_j}{z_n} \rho_{1n} d\rho_{1n} - \frac{1}{2} d\delta_{jn}. \quad (7.3.11)$$

For the purpose of simulation,  $d\rho_{in}$  can be assumed to be a random variable with a Gaussian distribution having mean 0 and standard deviation of 1 cm. The combined error vector  $d\sigma_n^{(j)}$  is evaluated according to Eq. (7.3.11) and the linear system, Eq. (7.3.4), is solved to yield the corresponding station coordinate error vector  $\underline{dS}$ . The components of  $\underline{dS}$  divided by 1 cm are defined herein to be error-magnification coefficients. These coefficients will vary for

different sets of range errors even though the range errors are taken from the same distribution, i. e., they are themselves random variables. The probability distributions for these coefficients, which are virtually impossible to derive analytically, except for normal random errors and stationary configurations, may be studied numerically by simulating a large number of identical configurations, i. e., by repeated trails, with different sets of random range errors. A geometric configuration can then be shown to be stable only if both the mean,  $\epsilon$ , and the standard deviation,  $\sigma$ , of each error magnification coefficient are small numbers consistent with the accuracy requirements of the present study\*. Typical study results have been presented in Section V.

It should be noted that the above procedure is possible only if the particular system configuration under study is nondegenerate. For degenerate situations, the coefficient matrix corresponding to the linear system, i. e., Eqs. (7.3.4), will be rank-deficient. This means it will not be possible to solve for the station error vector  $\underline{dS}$  uniquely. A number of degeneracies have been discovered in the present study. These cases (see Paragraph 7.1) are discussed further in Paragraph 7.4. However, the most important degeneracy deserves to be mentioned in this Section. This is the coplanar degeneracy associated with the 4 station configuration.

As discussed in Paragraph 7.1, four stations with a minimum of six range measurements provide, at least in principle, enough equations for all the unknowns (station as well as satellite coordinates) to be determined. However,

---

\*Specifically, if the indicated calculations are performed M times using different sets of random range errors (drawn from the same distribution), with the mth calculation producing a set of sensitivity coefficients  $dS_i^{(m)}$  then

$$\epsilon_i \equiv \frac{1}{M} \sum_{m=1}^M dS_i^{(m)}, \quad \sigma_i \equiv \left[ \frac{1}{M} \sum_{m=1}^M \left( dS_i^{(m)} - \epsilon_i \right)^2 \right]^{1/2}$$

if all the stations are in a plane, then the system is degenerate no matter how many measurements are utilized for the solution. In fact, this degeneracy has forced the originally proposed 4-station case to be abandoned as a system for short baselines because stations are nearly in a plane unless they are separated by intercontinental distances. Only if at least 6 stations are used can this degeneracy be overcome. It should be mentioned that the 4-station system is still adequate if used intercontinentally. The next Section is intended to present a more detailed discussion of the problem.

#### 7.4 FUNDAMENTAL CAUSE AND REMOVAL OF SYSTEM DEGENERACIES

In this section the fundamental causes for some of the degeneracies previewed in Paragraph 7.1 are discussed in greater detail; i. e., the main reason for the degeneracy due to the number of stations is isolated. The detailed discussion of this problem will be found in Appendix B. The reader should consider this section as an outline which will serve to aid in the further understanding of this problem.

It will be demonstrated herein that the 4 and 5 station systems are always degenerate for geometries wherein the stations are contained in a plane, whereas the 6 station system is generally well defined.

Consider the resolvent equation of the multilateration process, i. e., Eq. (7.2.11) written for a system of 4 stations. For purposes of clarity the equation will be written out explicitly for one given time point or strike. The result is displayed in Figure 7-3.

Examination of Figure 7-3 immediately yields the Second Solution (Section I) of geometric ranging, that is, repeating the resolvent equation at 6 or more different time points will result in an algebraic system of six or more

$$\begin{aligned}
 & X_4^2 + Y_4^2 + Z_4^2 - (X_2^2 - \delta_2) X_4/X_2 - [X_3^2 + Y_3^2 - \delta_3 - X_3 (X_2^2 - \delta_2)/X_2] Y_4/Y_3 \\
 & - 2 \left\{ \delta_1 - (X_2^2 - \delta_2)^2 / 4X_2^2 - [X_3^2 + Y_3^2 - \delta_3 - X_3 (X_2^2 - \delta_2)/X_2]^2 / 4Y_3^2 \right\}^{1/2} Z_4 - \delta_4 = 0
 \end{aligned}$$

EXPLICIT NON-LINEAR EQUATION OF THE FOUR STATION GEOMETRY INVOLVING  
 THE COORDINATES OF THE FIRST 4 STATIONS AND THE MEASUREMENTS (RANGES)  
 TAKEN FROM EACH OF THE STATIONS AT ONE POINT IN TIME

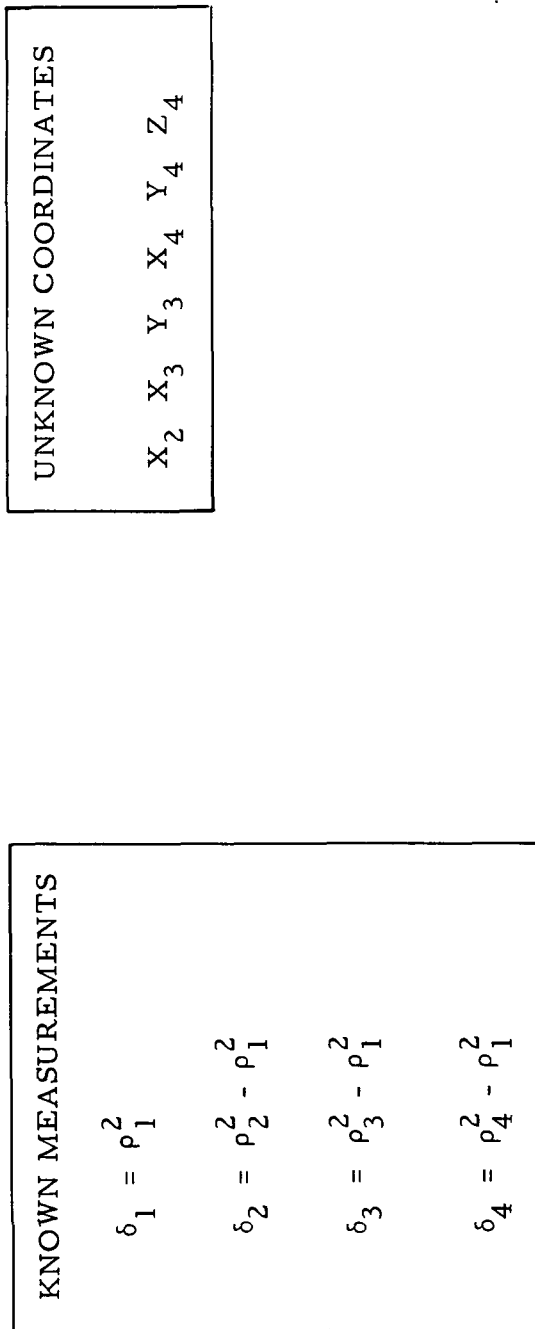


Figure 7-3. Fundamental Equation

equations in the six unknown station coordinates. Theoretically, it is evident that a solution to this problem exists.

A cursory examination of the fundamental equation displayed in Figure 7.4.1 shows that if  $Z_4 = 0$ , the equation collapses to the following form:

$$\alpha + \delta_2\beta + \delta_3\gamma = \delta_4, \quad (7.4.1)$$

where  $\alpha$ ,  $\beta$ , and  $\gamma$  are strict functions of the station coordinates. (The explicit formulas for these quantities are given in Appendix B.) Equation (7.4.1) is obviously a linear equation with known coefficients  $\delta_2$ ,  $\delta_3$ , and unknown parameters  $\alpha$ ,  $\beta$ , and  $\gamma$ . Let three strikes of the satellite be taken, i. e., let Equation (7.4.1) be written at three separate time points. The result is

$$\alpha + \delta_{2n}\beta + \delta_{3n}\gamma = \delta_{4n}, \quad n = 1, 2, 3, \quad (7.4.2)$$

a system of three equations in three unknowns which always has a unique solution unless the determinant of the system vanishes. The determinant of the system, i. e.,

$$D = \begin{vmatrix} 1 & \delta_{21} & \delta_{31} \\ 1 & \delta_{22} & \delta_{32} \\ 1 & \delta_{23} & \delta_{33} \end{vmatrix} \quad (7.4.3)$$

is a pure function of the range data and could conceivably vanish for certain combinations of the data but this occurrence would be coincidental, i. e., due to peculiar combinations of station and satellite coordinates\* and can be ignored

---

\*A discussion of this kind of degeneracy will be found in Appendix B.

herein. Hence under the assumption that  $D \neq 0$ , system (7.4.2) can always be solved but only three quantities can be obtained, namely, the parameters  $\alpha$ ,  $\beta$  and  $\gamma$ . Taking a new strike on the satellite only yields a new equation of the same form as (7.4.2) and results in an overdetermined system of linear equations. Obviously a least squares solution can then be obtained to the system but only for the three unknowns. Hence, no matter how many data points (strikes) are processed only three quantities can be obtained. However, when  $Z_4 = 0$ , there are five unknown station coordinates and therefore a unique solution for the explicit coordinates is not possible.

Consider the addition of a fifth station; obviously, the equation displayed in Figure 7.4.1 can be written with  $X_4$ ,  $Y_4$ ,  $Z_4$  replaced by  $X_5$ ,  $Y_5$ ,  $Z_5$  and in the planar case if  $Z_5 = 0$  another independent linear system such as Eq. (7.4.2) can be obtained. This independent linear system upon solution will determine another three unknowns distinct from the parameters previously determined using the first four stations. But in a system of five stations (planar) there are seven station coordinates, and as discussed above only six independent unknowns can be obtained. Obviously a solution is not possible.

However, when the sixth station is introduced into the system, then by the previous reasoning another three unknowns distinct from the first two sets of unknowns will be determined, and since in the planar geometry only the two additional unknowns  $[X_6, Y_6]$  are introduced, it follows that: nine independent coefficients of the coordinates have been specified for the nine unknown coordinates so that unless coincidental degeneracies of the kind discussed in Appendix B are present, a unique solution for the station coordinates now exists.

If the  $Z_4$  coordinates are not exactly zero, then the equation displayed in Figure 7-3, written at six different times will permit a unique solution for all the coordinates; however unless the  $Z_4$  component is large enough a nearly

singular numerical system will be obtained. This should be evident since if  $Z_4 = 0$  the preceding results show that the analytic solution degenerates absolutely. In the five station case the same result can be inferred since the mathematical degeneracy is still present in the equations. However when the sixth station is added the degeneracy is removed generally and then, even for small  $Z_4$ ,  $Z_5$ ,  $Z_6$ , a well conditioned solution exists.

The coplanar degeneracy and other forms of degeneracy which can be readily overcome are discussed further in Appendix B.

#### 7.5 THREE-STATION SOLUTION: A DEGENERATE BUT SOLVABLE CONFIGURATION

In Paragraph 7.1 it was proven that at least four stations are necessary for a mathematically deterministic solution to a truly range-only system. However, if additional information is available about station configurations, then less than four stations conceivably may be adequate to form a workable system. Indeed, it will be shown presently that the fundamental multilateration equation (see Fig. 7-3), written for three of the four stations aligned in a straight line, degenerates into a form such that the baselines between the collinear stations can be uniquely determined.

To obtain the three-station solution from the general multilateration equation displayed in Fig. 7-3, consider the following substitutions:

$$Y_4 = Z_4 = 0 \quad (7.5.1)$$

Physically, this means that Station 4 is placed on the X-axis of the adopted coordinate system, i. e., Stations 1, 2, and 4 are now collinear. The result of this substitution at any fixed time is

$$X_4^2 - \left( X_2^2 - \delta_2^2 \right) \frac{X_4}{X_2} - \delta_4^2 = 0, \quad (7.5.2)$$

which can be written as

$$X_4 \delta_2 - X_2 \delta_4 + X_2 X_4 (X_4 - X_2) = 0. \quad (7.5.3)$$

Equation (7.5.3), written at two separate times, will provide two independent equations for the two unknown baselines  $X_2$  and  $X_4$ . Hence, a unique solution can be obtained by taking two strikes. Note that the coordinates,  $X_3$  and  $Y_3$ , as well as the pseudo measurement  $\delta_3$  associated with Station 3, do not enter into Eq. (7.5.3). This in effect means that only three stations (1, 2, and 4) need be employed for the solution. Furthermore, it should be noted that only baselines are determined by this solution.

An alternate approach to the three-station solution independent of general multilateration theory will be discussed in Appendix C, where more mathematical details are given.

## SECTION VIII

### OPERATIONAL CONSIDERATIONS



This Section primarily deals with the topics which impose constraints on system operation when the basic principles of the multilateration technique are implemented in real time.

Some of the highlights of this Section include: the manner in which orbital configurations must be selected in order to achieve a numerically stable solution to the multilateration equations; the method of smoothing the data by use of a reference orbit; an examination of the accuracy to which station clocks must be synchronized; and the discussion of how the trajectory information required for aiming of the laser unit can be extracted as a by-product of the solution of the multilateration equations. The methods for selecting the mutual viewing windows of the system stations, correcting for the effects of atmospheric attenuation on the laser beam, and the examination of laser safety considerations relative to humans, are analyzed, and pertinent recommendations are given.

## 8.1 ORBIT ELEMENT SELECTION

Any experiment utilizing a satellite whose fundamental objective will be to map the relative station locations of a set of ground stations via three-dimensional laser fixes, will be fundamentally linked to the dynamic and orientation elements of the adopted satellite orbit.

### 8.1.1 Dynamic Element Selection

The shape, or dynamic orbital parameters, such as eccentricity and semi-major axis, are important parameters to select because of the geometry constraints peculiar to any scheme which intends to invoke geometric principles to aid in the process of station location estimation.

Numerical studies have indicated that for purposes of multilateration the selection of the orbit containing the satellite/retroreflector is of paramount importance. Even though the mathematical process of solution does not depend explicitly on the assumed orbit, it has been observed that the actual measurements taken over a viewing arc, must have a suitable dispersion in their respective magnitudes, i. e., the slant ranges must undergo substantial change within the common viewing window (see Paragraph 8.2) available to the station net. In fact, it has been observed that if a circular orbit is assumed, the multilateration equations yield ill defined estimates for the station coordinates. However, if a system of two circular orbits with well separated radii is used this problem is overcome and subsequently the system of equations becomes strongly non-singular. Hence, one solution to the orbit selection process is to adopt a system of two circular orbits, e. g., with altitudes of 500 and 750 km, and range over discrete segments of the viewing arc to these satellites. It should be noted that the satellites need not be visible to the stations simultaneously. Operationally this implies that a batch of data would be processed

from one satellite first and subsequently the data taken by ranging to the second satellite would be processed and combined with the first batch of data.

A second solution to avoid ill conditioning of the equations due to selection of a single circular orbit is to use an elliptic orbit having effective altitudes ranging from 500 to 750 km. This type of orbit, due to the combined rotation of the Earth and orbital perturbations acting on the orientation plane of the orbit (See Paragraph 8.1.2), will have the same stabilizing effect upon the system equations as the use of two circular orbits.

For purposes of yielding well defined geometries, it is also beneficial to select orbital altitudes which are commensurate with the baseline separations between stations.

In summary, an operational system requirement will be the use of:

- two circular orbits, or
- an elliptic orbit, both with
- altitudes commensurate with the relative station baseline separations.

These operational constraints can be attained with relative ease.

### 8.1.2 Orientation Element Selection

The orientation elements, namely, the inclination of the orbit to the equator,  $i$ , the longitude of the ascending node,  $\Omega$ , and the argument of perigee,  $\omega$ , will now be briefly discussed (see Figure 8-1).

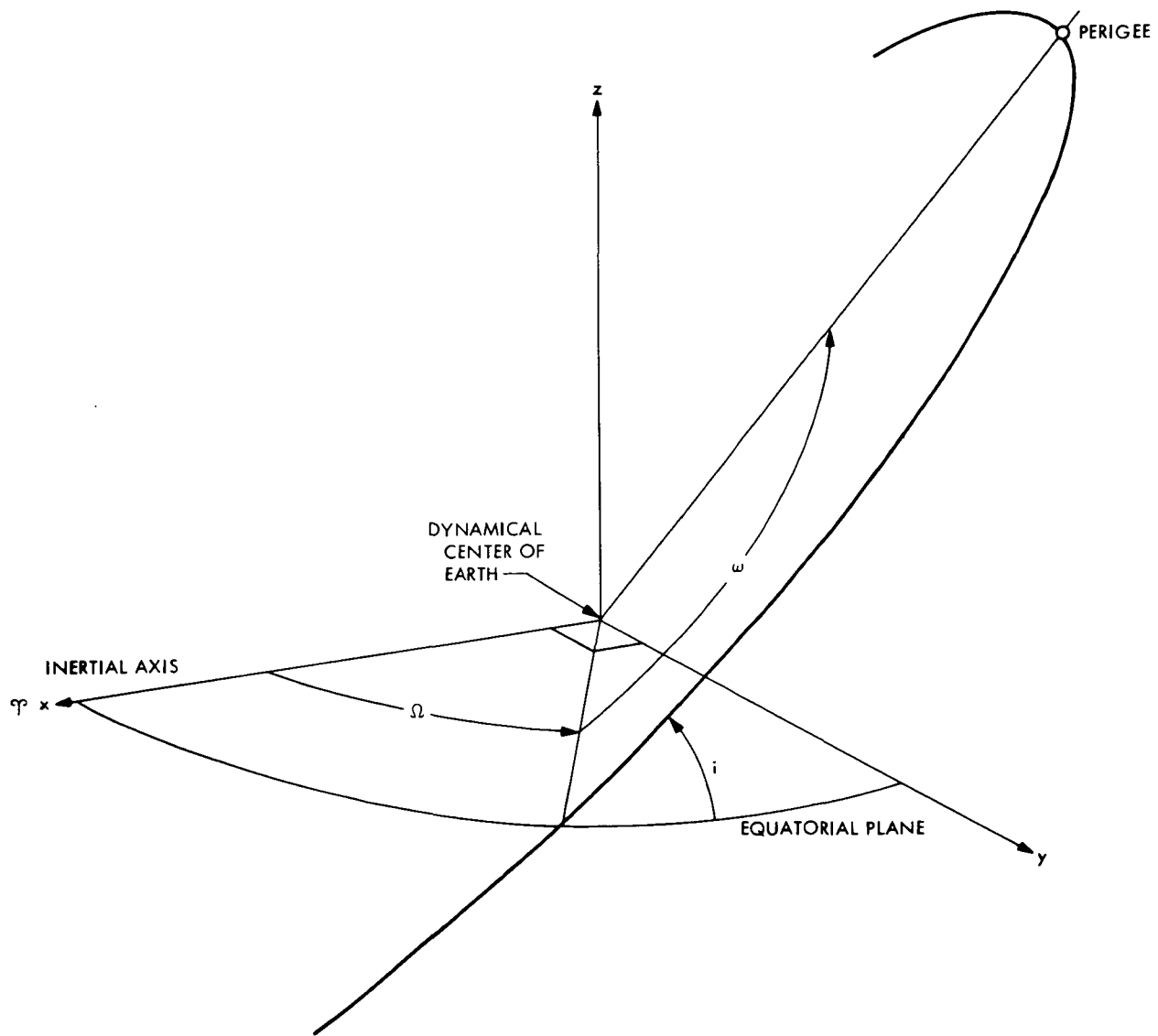


Figure 8-1. Orientation Elements

Since, the second zonal harmonic,  $J_2$ , causes the elements  $\Omega$  and  $\omega$  to have time rates of change defined by the following relationships\* [4.5]

$$\omega = \omega_0 + \left( \frac{3}{2} \frac{J_2}{a^2(1-e^2)^2} \left[ 2 - \frac{5}{2} \sin^2 i \right] \right) \bar{n} (t - t_0)$$

$$\Omega = \Omega_0 - \left( \frac{3}{2} \frac{J_2}{a^2(1-e^2)^2} \cos i \right) \bar{n}(t - t_0),$$

where  $\omega_0$  and  $\Omega_0$  are the injection values of  $\omega$  and  $\Omega$ , respectively, and the anomalistic mean motion  $\bar{n}$  is defined as

$$\bar{n} = k \sqrt{\mu} a^{-3/2} \left[ 1 + \frac{3}{2} \frac{J_2}{a^2(1-e^2)^2} \left( 1 - \frac{3}{2} \sin^2 i \right) \right]$$

with

$k$  = Gaussian planetary constant  $\equiv .07436574$  (earth radii)<sup>3/2</sup>/min,

$\mu$  = Sum of masses of satellite and Earth in terms of most ponderous mass,

$t_0$  = Adopted epoch time,

a systematic study of the desired injection values of  $\Omega_0$  must be performed.

Therefore by selecting the proper value of  $\Omega_0$  for a specified value of  $i$ , it will be possible to make certain that: first, the orbital track will pass directly over the optimum satellite/station geometric configuration, and second, that a convenient time duration between satellite injection and experiment initiation will be available to meet ground operation constraints.

---

\*The effect of  $J_2$  on the orbital parameters, although small, is not negligible in orbital operations.

It must be remembered that the satellite track will only pass in exactly the optimum position over the stations one time per satellite/station repeat period. These synodic repeat periods are of the order of years. Assuming that  $\Omega_0$  was chosen such that the optimum geometric configuration would occur on revolution N, then, the geometric accuracy picture for multilateration improves as the satellite approaches revolution N, is a maximum at revolution N and slowly degrades to zero (no visibility) on a revolution by revolution basis after revolution N. When the rise/set geometry again becomes common to all stations, the same cyclic behavior of the accuracy will occur, however due to the resulting phase difference between the satellite and Earth the accuracy of the geometry will be decreased until, as mentioned previously, the ground track precisely passes over the geometrically optimum station configuration, i. e., until satisfaction of the synodic period is achieved.

The final parameter, the inclination, must be selected such that

$$i > \phi,$$

specifically, such that the orbital inclination exceeds the most northerly or southerly station latitude,  $\phi$ , by a sufficient amount to ensure geometric stability. Intuitively it would seem that a near polar orbital system would offer the advantage of covering all available ground areas whose location might want to be surveyed. Furthermore, the polar orbit causes the rate of change of the longitude of the ascending node to vanish ( $\dot{\Omega} = 0$ ) and thus simplifies the orbital injection process.

## 8.2 VIEWING WINDOWS

From an operational point of view, the supporting software to any multilateration experiment must have the ability to define the appropriate viewing window within which the measured data, in this case time pulse or range data, will be common to the system stations and the satellite at any given time.

Figure 8-2 illustrates, in cartoon fashion, the rise/set histories of a satellite which can be expected from a net of four stations; obviously, a similar diagram can be displayed for a six station system.

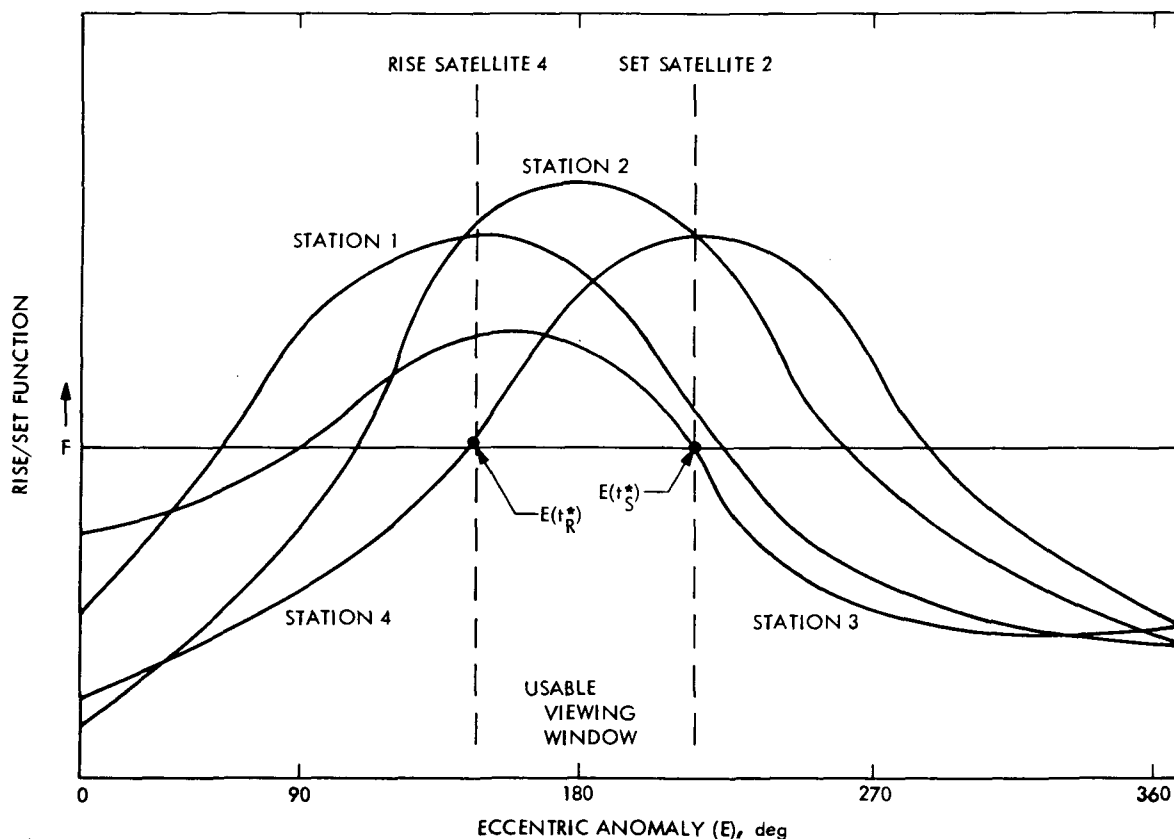


Figure 8-2. Superposition of Rise/Set Functions

The Figure is a graph of the rise/set function,  $F$ , developed in [4.5] as a function of satellite eccentric anomaly, \*  $E$ , i. e.,

$$F \equiv a(\cos E - e) \underline{P} \cdot \underline{Z} + a\sqrt{1 - e^2} \sin E \underline{Q} \cdot \underline{Z} - G = 0, \quad (8.2.1)$$

where

$$Z_x \equiv \cos \phi \cos \left( \theta_0 + \frac{d\theta}{dt} \left[ \frac{E - e \sin E}{\bar{n}} + T - t_0 \right] \right)$$

$$Z_y \equiv \cos \phi \sin \left( \theta_0 + \frac{d\theta}{dt} \left[ \frac{E - e \sin E}{\bar{n}} + T - t_0 \right] \right)$$

$$Z_z \equiv \sin \phi$$

$$G \equiv G_1 \cos^2 \phi + G_2 \sin^2 \phi$$

with  $G_1$  and  $G_2$  defined in Appendix J, and where for convenience the notation is repeated:

$\phi$  = geodetic latitude of station,

$H$  = station elevation above and normal to adopted ellipsoid,

$\theta_0$  = epoch sidereal time at injection,

$\bar{n}$  = anomalistic mean motion,

$T$  = time of perifocal passage or nodal crossing,

$d\theta/dt$  = sidereal rate of change,

$f$  = geometrical flattening of Earth

$a_e$  = equatorial radius of Earth,

---

\*Note that the eccentric anomaly and time are simply related by Kepler's equation.

$\underline{P}$  = unit vector pointing from dynamical center to orbital perigee or nodal crossing,

$\underline{Q}$  = unit vector in orbital plane advanced to  $\underline{P}$  by a right angle in direction of motion.

As can be seen from the figure the rise/set function is a smoothly varying analytic function that achieves different maximums and minimums at different times for each station of the station net. The first zero of  $F_i$  represents the rise of the satellite with respect to station  $i$ . From Figure 8-2 it is simple to extract the rule for the limiting view period wherein all stations can see the satellite, namely,

$$\Delta t = t_S^* - t_R^*, \quad (8.2.2)$$

where, if  $I$  is the total number of stations,

$$t_S^* = \text{MIN} (t_{S1}, t_{S2}, \dots, t_{SI})$$

$$t_R^* = \text{MAX} (t_{R1}, t_{R2}, \dots, t_{RI}),$$

that is,  $t_R^*$  is the critical time at which the ranging experiment must start, and  $t_S^*$  denotes the time at which the ground equipment can cease operation on a per revolution basis.

The difference  $\Delta t$  is the duration of common visibility or system up-time on a given orbital pass. Obviously, due to the rotation of the Earth and the previously discussed orbital perturbations, the value of  $\Delta t$  will vary from zero to a maximum and then back to zero. The maximum value of  $\Delta t$  will

correspond approximately to the satellite overpassing the centroid of the station net. The time  $t_R^*$  corresponding to  $\Delta t_{MAX}$  will define the optimum viewing window available for laser ranging experiments.

Future predictions of these times present no difficulty and can be handled directly in the operational software package.

### 8.3 DATA SMOOTHING

During actual operation of the laser ranging system a continuous stream of simultaneous fixes will be obtained from the set of ground stations. The laser measurement rate will be of the order of one measurement every six seconds. As is common in any measurement technique a given pulse will be corrupted with random noise and therefore occasionally bad measurements will be obtained. Since the hardware or measurement equipment will be calibrated as to expected accuracy, i. e. , a standard deviation of the time pulse or range data peculiar to the equipment will be available, it will be a simple task to reject all obviously bad points by culling out any measurements whose residual is a factor of three greater than the standard deviation associated with the equipment accuracy\*. Once this gross filtering process has been accomplished smoothing of the data can be undertaken.

Two basic requirements must be satisfied when smoothing is to be performed. First, an analytically smooth function which represents the physical behavior of the data must be adopted. Second, an analytic function which represents the data over a suitable duration with respect to the independent variable should also be assumed.

The independent variable in three dimensional laser ranging will be the time,  $t$ , in minutes after some conveniently adopted epoch,  $t_0$ , say, midnight of the day when the experiment is to be performed. The accuracy to which  $t_0$  must be known, i. e. , to which the epoch clock synchronization must be specified is discussed in Paragraph 8.4.

---

\*This is known in statistics as the " $3\sigma$  criterion," and for a normal dispersion corresponds to a confidence level of 99.9 percent.

The first analytic function for data representation (it will be assumed that the time pulse data has been converted to actual range,  $\rho$ , or extension parameters) which comes to mind is of the form:

$$\rho_i = a_i + b_i(t - t_R^*) + c_i(t - t_R^*)^2 + \dots, \quad (8.3.1)$$

where as discussed in Paragraph 8.2,  $t_R^*$  is the maximum rise time associated with the four observing stations, and  $a_i$ ,  $b_i$ ,  $c_i$  are suitable least squares coefficients obtained, probably, with equal weights for all stations. This type of representation of the data is nothing more than a Taylor expansion about  $t_R^*$  and for an assumed number of terms will obviously degrade as a function of time. The previous function is excellent for synchronous satellites but is of limited use for low Earth satellites.

To circumvent the previous problem and obtain greater accuracy in the number of significant digits consider the following scheme.

Let a two-body or Keplerian orbit including secular perturbations (see Section 8.1) be adopted as a baseline reference. To determine the elements of the baseline orbit to fair approximation, a very short arc of data can be fit as previously described via a Taylor expansion at three stations such that

$$\rho_i = a_i + b_i(t - t_R^*) + c_i(t - t_R^*)^2, \quad i = 1, 2, 3, \quad (8.3.2)$$

and by differentiation

$$\dot{\rho}_i = b_i + 2c_i(t - t_R^*). \quad (8.3.3)$$

For purposes of discussion only quadratic terms are retained.

Using a trilateration technique [1.1] , [4.7] , it now follows that the six data measurements, i. e.,  $\rho_i$ ,  $\dot{\rho}_i$  at the middle of the short arc can be mapped into the elements  $a$ ,  $e$ ,  $i$ ,  $\Omega$ ,  $\omega$ ,  $T$ , and thus the elements of the

baseline orbit become determined. These elements are now adopted as a base or reference. Being in possession of these elements permits the orbital evolution on a secularly perturbed Keplerian orbit [4.5] to be performed and the range data to be computed from the reference orbit over the duration wherein the true range data is to be measured by each observing station. The accuracy of the Keplerian reference orbit is not of any importance for the scheme to be discussed because the reference orbit ephemeris will be added in and then removed without corrupting the actual data.

For all measurement times,  $n$ , at each station it follows that the following residuals can be computed

$$\Delta \rho_{in} = \rho_{in} - \rho_{in}^K \quad \begin{array}{l} i = 1, 2, \dots, I, \\ n = 1, 2, \dots, N, \end{array} \quad (8.3.4)$$

i. e., the difference between the true measurement  $\rho$  and the computed Keplerian approximation  $\rho^K$  is formed on a point basis (sequentially).

The recommended procedure is to fit the residuals  $\Delta \rho_{in}$  as a function of time via least squares as\*

$$\Delta \rho_i(t) = \bar{a}_i + \bar{b}_i(t - t_R^*) + \bar{c}_i(t - t_R^*)^2, \quad i = 1, 2, \dots, I, \quad (8.3.5)$$

where all calculations are carried throughout to 18 digit accuracy. Once the residuals are known as a function of time, the actual model for the range history as a function of time from each station can therefore be represented as

$$\rho_i(t) = \rho_i^K(t) + \Delta \rho_i(t) = \bar{A}_i(t) + \bar{b}_i(t - t_R^*) + \bar{c}_i(t - t_R^*)^2, \quad (8.3.6)$$

---

\*The use of a second order polynomial in the fit has been found to be adequate. See also the discussion at the end of the Section.

where

$$\overline{A}_i(t) \equiv \rho_i^K(t) + \overline{a}_i . \quad (8.3.7)$$

It should be noted that in Equation (8.3.6),  $\rho_i(t)$  is calculated by adding the previously derived Keplerian range to the fitted residual and thus the actual measurement is not corrupted by the reference orbit.

An even stronger representation can be obtained by letting the curvature of all arcs be modeled simultaneously by least squares fitting of the data to the more generalized form

$$\Delta\rho_i = A_i + B_i(t - t_R^*)^\alpha + C_i(t - t_R^*)^\beta \quad (8.3.8)$$

where  $\alpha$  and  $\beta$  are exponents determined via the fitting process (see Appendix G).

#### 8.4 SIMULTANEOUS DATA DETERMINATION

It has been shown in Section VII that the relative position of stations located on the surface of the Earth can be determined accurately if a sequence of slant ranges from a satellite is known accurately and simultaneously. For purposes of multilateration, it is important that the ranges from all stations to the satellite be known at the same time. But the distances between the satellite and any two stations differ at any given time, and since the satellite is moving during the transit time of a ranging pulse, it might seem difficult to achieve the necessary simultaneity of the range measurements. To overcome this difficulty one must use an interpolation scheme. Roughly speaking, if the range history as a function of time can be modeled, then slant range histories such as those displayed in Figure 8-3 can be generated.

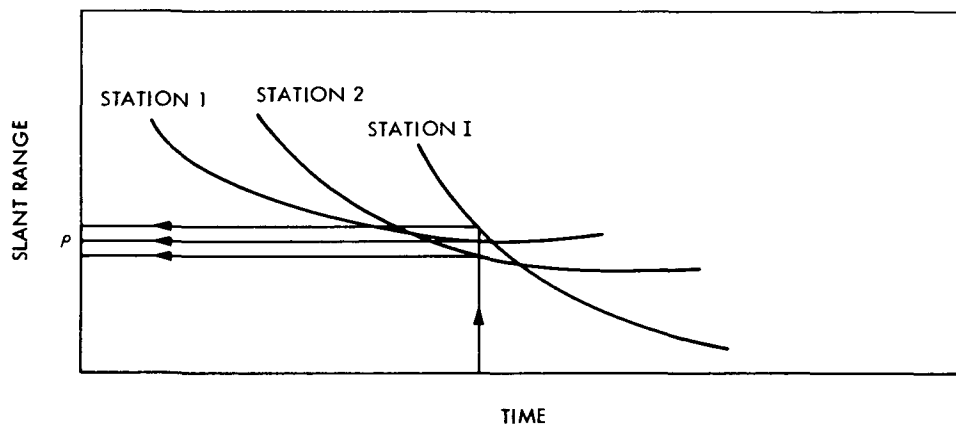


Figure 8-3. Range History as a Function of Time

Therefore, by adopting some time  $t$  and entering the curves as in Fig. 8-3, a set of pseudo observations can be obtained which must be synchronized. In this section the relative accuracy of the curves which are required to obtain the pseudo observations will be discussed, i. e., the accuracy of the epoch time peculiar to each station and therefore to the data will be specified. It will be shown that these requirements are not stringent.

Many transit times  $T(t_j)$  of a pulse emitted at times  $t_j$  are measured from each station independently during a pass, i. e. , during the viewing period common to all stations. Typically, for a pass lasting 15 minutes, a pulse can be fired every 6 seconds with existing equipment, giving 150 values for  $T(t_j)$ .

Let the range  $\rho$  be known to within 10 and 100 m from an a priori knowledge of station location and simple trilateration. From the nominal range  $\rho_N(t)$ , it is possible to obtain the residuals\* :

$$\Delta(t_j) = \frac{c}{2} T(t_j) - \rho_N(t_j). \quad (8.4.1)$$

Now, with the data available it is possible to perform a least squares analysis to smooth the measurements (8.4.1). Accordingly, having selected a set of polynomials, i. e. , Chebychev, powers of  $t$ , or the like, for modeling the data, it is possible to write

$$\Delta(t_j) = \sum a_n p_n(t_j) = P(t_j), \quad (8.4.2)$$

and to determine the coefficients  $a_n$  by the method of least squares. In this manner a smooth time function  $P(t)$  is found which represents the residuals  $\Delta(t_j)$ . Naturally,  $P(t)$  is determined in this manner for each station separately. The determination of the range  $\rho(t)$  as a function of time from  $P(t)$  for each station then proceeds as follows. First, the relationship between the range  $\rho(t)$  and the total observed transit time  $T(t)$  must be known. It can be shown (Appendix E) that within the accuracy of a centimeter this connection is given by:

$$T(t) = \frac{2}{c} \rho(t) \left[ 1 + c^{-1} \dot{\rho}(t) \right]. \quad (8.4.3)$$

---

\*The use of the nominal range is not essential but is convenient for data processing.

In Eq. (8.4.3),  $c$  is the velocity of light and  $\dot{\rho}$  the range rate. It must be emphasized that  $t$  in Eq. (8.4.3) is the time of emission of the pulse possessing the transit time  $T$ .

It is now an easy matter to extract the range information from  $P(t)$ . In fact, having substituted (8.4.3) and (8.4.1) into (8.4.2), differentiation of (8.4.2) reveals that

$$\dot{P}(t) = \dot{\rho}(t) + c^{-1} \dot{\rho}(t)^2 + c^{-1} \rho(t)\ddot{\rho}(t) - \dot{\rho}_N(t) \quad (8.4.4)$$

so that

$$\dot{\rho}(t) = \dot{P}(t) + \dot{\rho}_N(t) - \frac{1}{c} (\dot{\rho}^2 + \rho\ddot{\rho}). \quad (8.4.5)$$

Expression (8.4.5) is inserted into Eq. (8.4.3) to obtain the actual range from the measurements. Further analysis (Appendix E) will show that the last term on the right hand side of Eq. (8.4.5) is totally negligible. From Eqs. (8.4.3), (8.4.1) and (8.4.5) the range at time  $t$  is then given by:

$$\rho(t) = \left[ P(t) + \rho_N(t) \right] \left[ 1 + c^{-1} [\dot{P}(t) + \dot{\rho}_N(t)] \right]^{-1}. \quad (8.4.6)$$

The above expression contains only known quantities, namely, the nominal orbit range, and its time derivative, and the least squares fit  $P(t)$  of the data and its time derivative. If the transit time  $T$  is measured to an accuracy of 0.06 nsec, Eq. (8.4.6) gives the range between a station and the satellite within an accuracy of 1 cm.

The procedure outlined so far is applicable to any one station. What is needed is a knowledge of the ranges from different stations simultaneously. This is tantamount to demanding that the station clocks be synchronized, i. e., if the epoch times measured at different stations are the same, simultaneity is assured.

Suppose that two unsynchronized stations (1 and 2) measure the range to the same satellite. Let the clock at station 2 read the time  $t_2 = t_1 + \delta + \alpha t_1$ , where  $t_1$  is the time at station 1 and where  $\delta$  is the time difference (clock offset), and  $\alpha$  the difference in rate of clock 2 from clock 1. The parameters  $\delta$  and  $\alpha$  are usually unknown, so that a comparison between  $\rho_1(t_1)$  and  $\rho_2(t_2)$ , which is needed for achieving simultaneity, is difficult. However, as an approximation

$$\rho_2(t_2) = \rho_2(t_1) + (\delta + \alpha t_1)\dot{\rho}(t_1), \quad (8.4.7)$$

for small time differences  $t_2 - t_1$ . In Appendix E it is shown that  $\dot{\rho}$  is at most about  $1.5 \text{ km sec}^{-1}$ . Therefore, if

$$(\delta + \alpha t) \times 1.5 (\text{km sec}^{-1}) < 0.5 \text{ cm} \quad (8.4.8)$$

or if

$$\delta + \alpha t < 3 \text{ } \mu\text{sec}, \quad (8.4.9)$$

sufficient synchronization is assured. Quartz oscillators in conjunction with a ground wave LORAN system (See Glossary) are sufficient to achieve the desired synchronization, particularly since synchronization is only needed during an individual pass of comparatively short duration. Subsequent passes may be synchronized independently.

In cases where a ground wave LORAN system is unavailable because of the long distance between a laser station and the nearest LORAN station, a satellite equipped with a radio beacon may be used. An S-band pulse transmitted to, for instance, two different stations will be received with a time lag given by:

$$\Delta t = \frac{\rho_1 - \rho_2}{c}. \quad (8.4.10)$$

In the above equation  $\Delta t$  is an exact measurement but the ranges are known only approximately due to errors in station location, errors in satellite orbit, and errors in the transmission medium. In order to stay within the allowed  $3 \text{ } \mu\text{sec}$

synchronization error, the errors previously listed must total no more than 0.9 km in equivalent range. The uncalibrated transmission medium errors (troposphere and ionosphere) amount to less than 20 m for elevation angles greater than 10 degrees. The errors in station location amount to no more than 30 m. This leaves an allowable 850 m for the indeterminateness of the satellite position, and it is not difficult to have knowledge of the satellite's position to that accuracy.

Therefore, it has been shown that a data smoothing procedure together with synchronization of station clocks within several  $\mu$ sec ensures the necessary range simultaneity.

## 8.5 ATMOSPHERIC LASER CORRECTIONS

This section discusses the method of correcting laser measurements due to atmospheric attenuation. These corrections are important when station positions are to be determined to centimeter accuracy.

Laser beams are different from radio waves and are refracted in the atmosphere strictly due to dry air effects. This important fact is due to relative frequency levels, i. e., the frequency of laser light is  $10^5$  times that of microwaves used for radio tracking and ranging. In this case the dipole moments of the water molecules respond negligibly to the radiation and hence may be ignored. There are no other spectral lines in the neighborhood of  $10^{14}$  Hz (ruby laser light). As will be shown herein it will be possible to obtain accurate range calibration [8.1] , [8.2] in actual system operation.

The dry zenith range correction,  $\Delta\rho_z$ , can be computed from either surface measurement or radiosonde balloon data (See Glossary). For a static equilibrium atmosphere, the zenith range correction can be derived analytically as a function of surface pressure only, as [8.1] :

$$\Delta\rho_z = \frac{77.6 R}{g} P_0 , \quad (8.5.1)$$

where  $\Delta\rho_z$  is in meters, R is the gas constant,  $P_0$  is the surface pressure in millibars, and in these units:

$$\frac{g}{R} = 34.1 \frac{^\circ\text{K}}{\text{km}} .$$

Equation (8.5.1) is obtained under the assumptions of static equilibrium, perfect gas, and constant gravitation acceleration, g. If these assumptions are

adopted, the zenith range can be predicted with an uncertainty of  $\pm 2$  mm for a precision of  $\pm 1$  millibar in pressure measurement. Hopfield (after comparisons with observed data) [8.1] claims 2 mm as the uncertainty of the zenith range measurement from Eq. (8.5.1). It seems however, that the 2 mm uncertainty is too optimistic. First, the air convection or vertical current which is common especially near a lake or in the hot desert, may appreciably violate the assumption of static equilibrium. Second, there is no observed zenith range data to the above accuracy with which to perform a comparison to some standard. Observed data used by Hopfield must be computed from radiosonde balloon measurements which have a 3 cm uncertainty in zenith range correction.

It has been shown [8.6] that tropospheric range corrections can be expressed conveniently by the following equation:

$$\Delta \rho = \alpha \int_R^{\infty} F(r, \theta_o(r, \gamma)) \left(1 - \frac{R^2 \cos^2 \gamma}{r^2}\right)^{-1/2} dr, \quad (8.5.2)$$

where:

$R$  = radius of Earth,

$\gamma$  = elevation angle of the ray path between the laser station and the satellite,

$1 + \alpha F$  = refractive index of the troposphere,

$\theta_o(r, \gamma) = -\gamma + \cos^{-1} \left( \frac{R \cos \gamma}{r} \right)$  = raypath expressed in spherical coordinates,

$\alpha = 3 \cdot 10^{-4}$  (typically).

$F$  = scale factor depending on the modeling of the troposphere.

Expression (8.5.2) has been used to obtain simplified but accurate formulas for the atmospheric range corrections.

The range correction,  $\Delta\rho$ , for a spherically symmetric atmosphere in static equilibrium, assuming no bending of the raypath, is related to the zenith value by 8.3 :

$$\Delta\rho = \frac{\Delta\rho_z}{\sin \gamma} , \quad (8.5.3)$$

where  $\gamma$  is the elevation angle, i. e. , the angle between the horizon and the line of sight to the satellite.

However, bending effects should not be neglected for deviations from angles lower than 45 degrees. Equation (8.5.3) has an error of 1.5 cm at  $\gamma = 30^\circ$ , and 5.3 cm at  $\gamma = 20^\circ$ . For more accurate mapping valid to lower elevation angles, the following modified formula is recommended [8.3]:

$$\Delta\rho = \frac{\Delta\rho_z}{\sin \gamma + \frac{A}{\tan \gamma + B}} , \quad (8.5.4)$$

where A and B are constants obtained from fitting to Eq. (8.5.2) for dry air. For  $A = 0.00095$ ,  $B = 0$ , the error is reduced to 3 mm at  $20^\circ$ , and 1.2 cm at  $15^\circ$ .

The most accurate mapping for every path can be obtained by a ray trace program, but as long as low elevation angles ( $\gamma \leq 15^\circ$ ) are not of interest, the above semi-empirical formula is adequate to the accuracy of about 0.3 cm.

It should be noted that the dry refractivity profile used in ray trace programs is carefully determined from fitting to the radiosonde balloon data (see Glossary) [8.2]. The fluctuations of the dry profile are small, and should not cause significant mapping errors for elevations higher than  $15^\circ$  [8.3], [8.4].

In conclusion, it should be mentioned that ionospheric calibration is not required when laser ranging hardware is utilized in the proposed multilateration ranging schemes.

In conclusion, it should be mentioned that ionospheric calibration is not required when laser ranging hardware is utilized in the proposed multilateration ranging schemes.

## 8.6 TRAJECTORY GENERATION USING GEOMETRIC PRINCIPLES

During the operational phase of performing the type of multilateration experiments discussed in this report a rough knowledge of the orbital ephemeris (See Glossary) will be required. It is emphasized that the ephemeris of the orbit is not required for the determination of the station locations; it is only required for the purposes of predicting suitable viewing windows (Paragraph 8.2) and for purposes of aiming the laser beams in the approximate direction of the satellite.

A rather unique side benefit of the multilateration scheme is that a very precise ephemeris of the satellite can be generated as long as the satellite is visible to at least three stations. Specifically, if the latitude, longitude and elevation of three stations are assumed to be known\*, then the satellite ephemeris can be determined [1.1] [4.7] (See also Appendix D). The process of trilateration can be used to determine the position and velocity of the spacecraft to a high degree of accuracy over a short time span (5-10 minutes); conventional orbit determination methods would require a much longer duration to achieve the same accuracy (1-2 days).

### 8.6.1 Difference Between Trilaterated and Dynamically Determined Orbit

Usually, the objective of orbit determination is to obtain the fundamental constants of the orbit. Hence, a solution is sought for the six constants or elements, say, the position and velocity vectors at some specified time, which then can be used in conjunction with the second order differential equations of

---

\*This assumption obviously is made also when conventional orbit determination schemes are used.

motion and, upon integration, yield the future position and velocity of the satellite. To accomplish this, a model must be assumed; i. e., the potential field of the primary (See Glossary) must be specified, the perturbations due to Sun, Moon and planets must be included, and various other factors, e. g., radiation pressure, drag perturbations, etc. need to be represented.

On the other hand, when an orbit is trilaterated, the model is defined by only a set of equations which describe the intersection of spheres. (See Section 7). There are however a set of parameters common to both techniques which will be discussed presently.

The difference between the orbit determination scheme and the trilateration scheme can be discussed further by means of Figure 8-4.

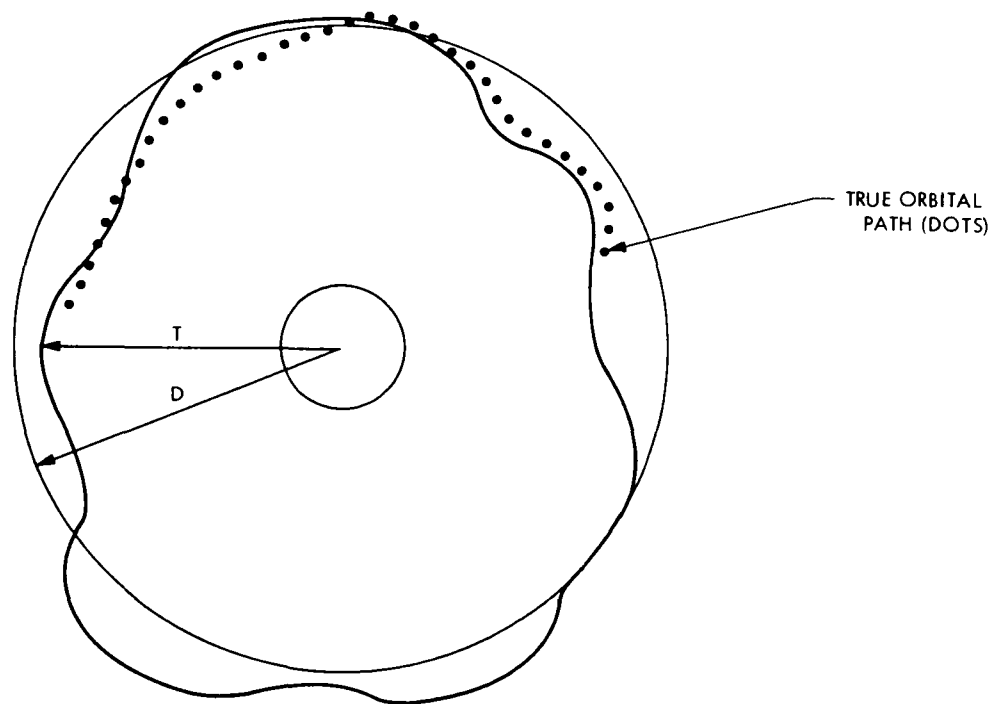


Figure 8-4. Polar View of the Orbital Path of a Trilaterated Satellite, T, and a Dynamically Determined Satellite, D

This Figure illustrates the paths that would be predicted if the orbit determination method is trilateration, T or, dynamic determination, D. The dynamic method gives rise to a mean or smooth curve which is a best fit to the assumed model discussed above. The trilaterated path yields what is called an osculating curve, i. e., a tangent curve as close as possible to the actual conditions existing at that instant of time. It is obvious that since fewer error sources exist, the ephemeris generated by trilateration techniques will be closer representation of the instantaneous positions and velocities at a given time.

This statement is best explained with the aid of Figure 8-5.

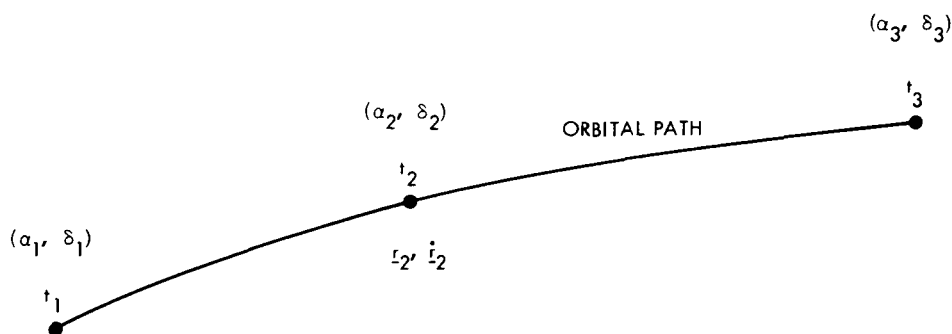


Figure 8-5. Schematic Orbit Determination Process

Standard orbit determination procedures will use many observations  $\alpha_i, \delta_i$  taken over a pass of the satellite, and by means of the assumed model reduce all of the observations to a set of initial elements at some adopted epoch. Schematically, if six observations  $\alpha_1, \delta_1, \alpha_2, \delta_2, \alpha_3, \delta_3$  are obtained, then using standard techniques the observations which are separated in time by  $(t_2 - t_1)$ , and  $(t_3 - t_2)$  can be mapped into the elements at  $t_2$ , i. e., the positions and velocities  $(\underline{r}, \underline{\dot{r}})_{t_2}$  can be determined. But these elements are a function of the model for the potential field, perturbations, etc., and are thus only defined

---

\* For example,  $\alpha$ , the right ascension, and,  $\delta$ , the declination.

with respect to the assumed model. These elements are therefore mean elements in some sense which is not easily defined; however the error sources peculiar to the model are contained in the determined elements. When the orbit is trilaterated, many of these error sources and the process of obtaining a mean fit to the dynamic model are circumvented. Hence, when the position and velocity  $(\underline{r}, \underline{\dot{r}})_{t_2}^T$ , where T denotes trilateration, are obtained via trilateration the computed elements will certainly be closer to the true values of position and velocity. This is important because, as illustrated in Figure 8-6, when a prediction to a future state of the satellite is desired the initial conditions which will be assigned to the predictor equations are closer to the true values and therefore the predicted path should follow the true path more closely.

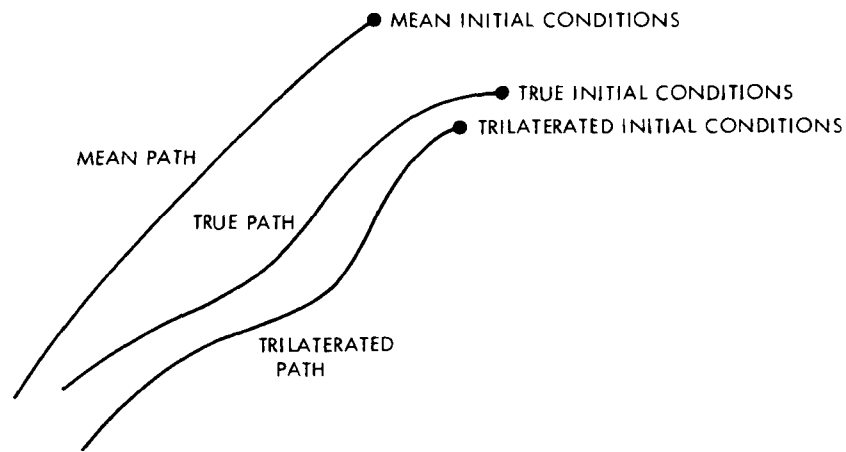


Figure 8-6. Orbital paths as a Function of Initial Conditions

### 8.6.2 Listing of Error Sources

Table 8-1 lists the error sources peculiar to each scheme and those sources common to both methods.

Table 8-1  
Error Sources

Dynamic Method	Geometric Method	Common
<ul style="list-style-type: none"> <li>● Gravitational Potential Effects</li> <li>● Sun, Moon, Planet Perturbations</li> <li>● Drag/Lift Perturbations</li> <li>● Radiation Pressure Effects</li> <li>● Magnetic Effects</li> <li>● Other Small Effects (known and unknown)</li> </ul>	<ul style="list-style-type: none"> <li>● Simultaneous ranging</li> </ul>	<ul style="list-style-type: none"> <li>● Measurement of Data</li> <li>● Station Coordinate Locations</li> <li>● Constant of Precession/Nutation</li> <li>● Sidereal Time Determination</li> <li>● Smoothing of Data</li> </ul>

The error sources common to both methods are listed under the assumption that the trilaterated orbit will be transformed from the geometric coordinate system to the standard inertial coordinate system (See Section IV). For purposes of orbit evolution this is a necessity because an inertial coordinate system wherein the equation of motion are usually evaluated must be used for purposes of determining the future orbital position and velocity. If the equations of motion are written in an Earth fixed, i. e., rotating system, no advantage is gained because the Coriolis components would have to be added to the equations.

### 8.6.3 Outline of Trilateration Technique

From an operational point of view, after a relatively short duration, the following smoothed range polynomial (Paragraph 8.3) will be available:

$$\rho_i = a_i + b_i (t - t_R^*) + c_i (t - t_R^*)^2, \quad i=1, 2, 3, \quad (8.6.1)$$

where  $i=1, 2, 3$  represents each station, and  $t_R^*$  is the maximum rise time for the three stations. A direct differentiation yields the range - rate as:

$$\dot{\rho}_i = b_i + 2c_i (t - t_R^*), \quad i=1, 2, 3,$$

so that six constants, i. e.,  $\rho_i$  and  $\dot{\rho}_i$  are available at time  $t$  (the time at which the satellite position and velocity are desired).

From the known values of the station locations, namely, the latitude, longitude and elevation, and the other parameters displayed in the Common column of Table 8-1, the inertial position of the stations is determined by the methods of Appendix J. Then utilizing the standard trilateration technique [1.1], the position and velocity components are determined in the inertial system defined in Section IV, i. e., in symbolic terms:

$$\rho_i, \dot{\rho}_i, \tilde{X}_i, \tilde{Y}_i, \tilde{Z}_i, t \longrightarrow x, y, z, \dot{x}, \dot{y}, \dot{z}, t,$$

where  $x, y, z, \dot{x}, \dot{y}, \dot{z}$  are the satellite coordinates. The process can be repeated as often as desired over the time duration of common visibility to all three stations. This is accomplished by rejecting the data associated with the earliest strike of the satellite, accepting data from the latest strike and obtaining new values of  $a, b, c$  in Eq. (8.6.1) and (8.6.2) via the process of least squares.

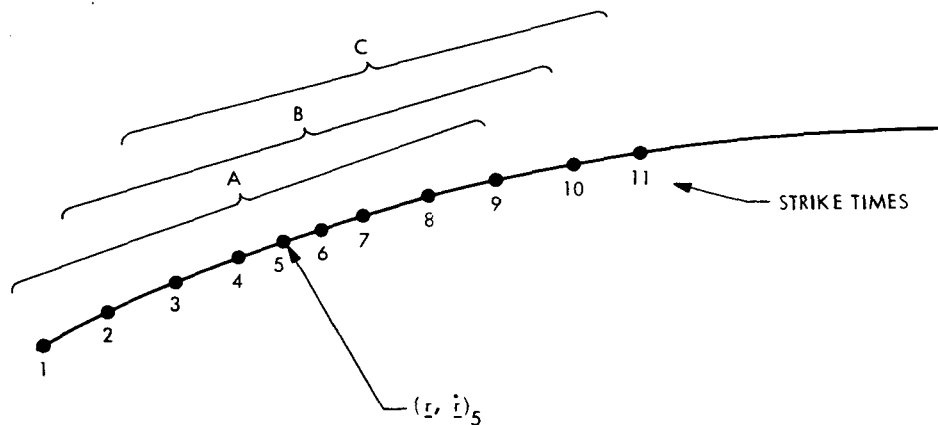


Figure 8-7. Sequential Processing of Data

Figure 8-7 is provided to clarify this technique. Suppose that data has been fit via least squares over an interval of duration A. As the illustration shows, nine data points would then be used to yield the values a, b, c of the curve fitting procedure. By means of trilateration it follows that the pseudo observations  $(\rho, \dot{\rho})$  at strike 5 can be obtained from the fit and subsequently  $(\underline{r}, \underline{\dot{i}})_5$  can be computed. Suppose that the satellite state is desired at strike 6. Since the curve fit interval or duration will be restricted, the best procedure to follow is to reject the data at strike one, pick up the data at strike 10, i. e., use an interval of duration  $B = A$ , and refit (process sequentially). The computation with a, b, c now corresponding to the data in interval B will now yield  $(\underline{r}, \underline{\dot{i}})_6$ ; etc. By this method the curve fit polynomial will be of an osculating nature and thus provide the maximum accuracy.

If a prediction of the satellite position and velocity at a time of non-visibility is desired then the position and velocity at some adopted epoch can be used along with the equations of motion and by numerical integration the desired state can be determined.

#### 8.6.4 Relative Data Accuracies

It is shown in Appendix F that the standard deviation of the data, i. e., range, can be obtained as:

$$\sigma_{\rho} = \frac{3}{2\sqrt{N}} \sigma_{\rho f}, \quad (8.6.3)$$

where N is the total number of data points and  $\sigma_{\rho f}$  is the standard deviation of the actual data from the assumed model (curve fit). It is a simple extension to show that [1.1]:

$$\sigma_{\dot{\rho}} = \frac{2\sqrt{3}}{\sqrt{N}T} \sigma_{\rho f}, \quad (8.6.3)$$

where  $\sigma_{\dot{\rho}}$  is the standard deviation of the range-rate as obtained via differentiation and T is the total duration over which measurements are taken.

With these errors, a standard mapping can be performed and the errors in the satellite positions and velocities can be obtained.

#### 8.6.5 Conclusion

The discussion of this Section demonstrates that a highly accurate method of predicting the future state of a satellite is a natural by-product of the multilateration technique. In brief, this makes the direct dependence on large software orbit determination programs a circumventable problem.

## 8.7 WEATHER CONSTRAINTS

One of the important constraints limiting the reliability with which a station can successfully range to a satellite during a given pass is weather. Fortunately, an area of exceptional interest to geophysicists involved in earthquake hazard estimation is the American Southwest, including northern Mexico. In this region the weather is often clear, and obeys predictable patterns. There, the strategy of laser satellite geodesy suggests that the establishment of benchmarks be avoided in a given area during its season of unfavorable weather. Bad weather is discussed herein under the following headings: Nimbus (raincloud), and Stratus and Cumulus clouds, associated with the two types of rainy season in the Southwest. Then cirrus (icecloud); fog, both as mist and as icefog; and dust are discussed.

### 8.7.1 Nimbus, Stratus, and Cumulus

The rainy seasons in the American Southwest are determined by the presence or absence of a tropical continental (cT) air mass which forms in summer over northern interior Mexico and adjacent parts of the U. S. , and which dissipates in winter. It appears on weather maps as an oval area of very low pressure with the axis running typically NW-SE through Yuma, Arizona. In summer and fall, when this air mass is present, Pacific storms are diverted to near the U. S. -Canadian border. In this season, tropical maritime air (mT) from the Gulf of Mexico brings storms to New Mexico, to Arizona, and occasionally as far as Salt Lake City. In winter and spring, when this air mass disappears, some storms from the stable polar maritime air mass of the north Pacific pass over the American deserts, bringing rain across the California coast and to the Mojave, Chihuahuan, and Magdalena Deserts as far south as La Paz, Mexico. Thus, this stable summer low pressure area

divides the American Southwest broadly into three regions. In California west of the Sierra Front, and in Baja California north of 30° N, rain and clouds are frequent from December to April. Such cloud formations persist for several days and nights. In Arizona, New Mexico, and northern interior Mexico, brief thunderstorms are frequent from June through September. The storms themselves last several hours at most, but they are accompanied by cumulus clouds by day and various kinds of broken clouds by night which persist over long periods. Between these two regions, in a long corridor stretching from Death Valley across Baja California below 30° N to the Pacific Ocean, rainfall averages less than 12 cm. per year. Actually, the averages are misleading because some years have no rainfall, while in wet years the precipitation comes for the most part in sudden cloudbursts. In this third region, there is no rainy season.

#### 8.7.2 Cirrus

High, feathery cirrus would impair laser ranging observations even in dry weather. They are characteristic of the passing of storm fronts, and therefore are most frequent in the rainy seasons described above.

#### 8.7.3 Fog

The west coastal deserts of Baja California are visited frequently by fog during spring and summer, as far south as 28°N. Fog is frequent on the California coast during fall and winter. A stable high pressure area often forms over eastern California and Nevada in winter, bringing fog to the San Joaquin Valley and icefog to central Nevada which persists for days, even in nominally clear weather.

#### 8.7.4 Dust

Storms of sand and dust can be expected in the American Southwest wherever there is loose, dry soil. April is the windiest month and therefore the dustiest. Winter brings comparative atmospheric calm and freedom from dust storms throughout the Southwest.

#### 8.7.5 A Model of System Reliability

Atmospheric transparency, then, is not typically limited by extensive weather systems, such as are so common east of the Rocky Mountains, which cloud out the whole Southwest. Instead, it is probable that an event which closes down one station will leave the others unaffected. In this case, a fair model of the reliability of the laser ranging system is given by the statistics of the binomial distribution. Given  $n$  stations, each of which has probability  $p$  of acquiring useful ranges on a given pass of a satellite\*, the probability that exactly  $k$  stations will acquire useful ranges is

$$B(k, n; p) = \frac{n!}{k! (n-k)!} p^k (1-p)^{n-k}. \quad (8.7.1)$$

Then the probability that at least  $k$  stations will obtain useful ranges is obtained by summing  $B(k, n; p)$  from  $k$  to  $n$ :

$$P(k, n; p) = \sum_{j=k}^n \frac{n!}{j! (n-j)!} p^j (1-p)^{n-j}. \quad (8.7.2)$$

The function  $P(k, n; p)$  is tabulated in Tables 8-2 and 8-3 for the 6- and the 4-station cases, respectively. One obvious advantage of the 4-station method (using intercontinental stations; Section I) is that the probability of

---

\*Strictly speaking each station should be assigned a different probability

success for the whole system is higher, given stations each of a certain reliability. The most cost-effective strategy, however, may be to use 8 or 9 stations, giving high probability that every satellite pass will give sufficient data for a 6-station solution.

In conclusion, weather offers no serious problem to laser satellite geodesy, at least in the American Southwest. Further study would be needed to state system constraints for other areas.

Table 8-2

The probability, given  $n$  stations, each of which has probability  $p$  of acquiring useful ranges on a given pass of the satellite, that at least 6 stations will acquire useful ranges.

n	p				
	.750	.800	.850	.900	.950
6	.178	.262	.377	.531	.735
7	.445	.577	.717	.850	.956
8	.679	.797	.895	.962	.994
9	.834	.914	.966	.992	.999
10	.922	.967	.990	.998	1.000

Table 8-3

The probability, given  $n$  stations each of which has probability  $p$  of acquiring useful ranges on a given pass of the satellite, that at least 4 stations will acquire useful ranges.

$n \backslash p$	.750	.800	.850	.900	.950
4	.316	.410	.522	.656	.815
5	.633	.737	.935	.919	.977
6	.831	.901	.953	.984	.998
7	.929	.967	.988	.997	$\dot{=}1.000$
8	.973	.990	.997	$\dot{=}1.000$	$\dot{=}1.000$

## 8.8 SAFETY CONSIDERATIONS

The use of powerful laser beams for the multilateration system contemplated herein presents some minor problems with respect to possible accidental injury. Although the energy levels preclude the possibility of damage to objects inadvertently crossing the laser beam, such as: birds, helicopters, airplanes, etc., there is still the distinct possibility of injury to the human eye; specifically, to the retina.

According to Laser Focus [8.5] a panel of the American National Standards Institute has come up with the following tentative figure for the maximum exposure of laser light permissible that does no harm to the eye. Specifically, for visible light the maximum permissible exposure (MPE) is  $5 \times 10^{-7}$  Joule/cm<sup>2</sup> for an exposure time of  $10^{-9}$  to  $2 \times 10^{-5}$  seconds. This means, that for an anticipated 0.5 Joule laser beam spread into a cone of  $10^{-3}$  rad it is only safe to look into the beam at the minimum distance of about 6 km. The previous statement can be verified by the following simple relationships:

$$\text{MPE} = 5 \times 10^{-7} \frac{\text{Joule}}{\text{cm}^2} = \frac{\text{Laser pulse energy}}{\text{beam area}} = \frac{0.5 \text{ Joule}}{\pi \theta^2 r^2}, \quad (8.8.1)$$

where  $r$  is the critical distance from the laser and  $\theta = 10^{-3}$  rad is the beam divergence. Obviously special precautions for low flying airplanes have to be taken.

Accordingly the most important and rather obvious safety measures are listed below. The implementation of these safety measures is necessary but not difficult to achieve. They are as follows:

- Operation of the laser devices should be in a controlled area.
- Operations should be restricted to authorized personnel.
- A ban on spectators in the controlled area without "appropriate supervisory approval" and protective measures, should be imposed.

- Accurate control of the beam's path must be achieved.
- "Special care" must be taken in the use of such viewing aids as telescopes, which may increase the hazard. An interlock or filter must be provided.
- Eye-protection devices "should be used as supplements to engineering controls whenever the beam path is not completely enclosed." Devices should be "specifically designed for protection against radiation from the laser system being used."

## SECTION IX

### LASER RANGING HARDWARE STUDY



The requirements on a satellite ranging system that would be suitable for use with the overall concepts presented in this report are stringent, i. e., it must determine the slant range to an Earth orbiting satellite to an accuracy of at least  $\pm 1$  cm. Present laser ranging systems have uncertainties at least a factor of 10 larger than this. There is, however, a general concensus that the accuracy stated above is presently attainable [9. 1].

This section presents a discussion of laser ranging systems, and the requirements necessary to upgrade their performance in order to attain  $\pm 3$  cm or better accuracy.

#### 9.1 PRESENT SYSTEMS

##### 9.1.1 Present Approach to Precision Laser Ranging

Techniques and apparatus have been developed to determine the range to an object by measuring of the time-of-flight of a pulse of an optical wavelength [9.2]. The availability of high brightness pulsed lasers, capable of producing short duration optical pulses, has provided the basis for high precision ranging systems. These systems closely resemble microwave radar in their mode of operation, i. e., they operate on the principle of taking a simple measurement of the time required for a pulse to travel to and from the transmitter and a selected target. Laser transmitters have three distinct advantages over microwave ranging devices, namely, higher peak power, shorter wavelength, and shorter pulse duration.

Many time-of-flight laser ranging systems have been constructed, mostly for field use by the military. The application being considered here, i. e., ranging to near Earth satellites, has not seen any commercial manufacturing

activity as of this date. Several government research centers such as Goddard Space Flight Center and Smithsonian Astrophysical Observatory and the Air Force Cambridge Research Laboratory have constructed laser systems for ranging to near Earth satellites [9.3], [9.4]. The University of Maryland, under contract to NASA, [9.5] has assembled a system for ranging to the Moon. Research organizations in France and Russia also have satellite and lunar tracking stations using lasers.

A general description of these present laser ranging systems will be given, along with a summary of their performance parameters. This will be followed by a discussion of the sources of errors and finally by some comments on the possibility of reducing these errors.

#### 9.1.2 Present Laser Satellite Ranging Systems

The laser satellite ranging systems currently in existence all operate in basically the same manner. A general description will be presented first, followed by a summary of significant differences in the systems. Frequent reference will be made to Figure 9-1, which shows a block diagram of a laser satellite ranging system. Only the salient features are presented; the description of ancillary equipment used to provide automatic operation is omitted.

The laser used for all existing systems discussed in Paragraph 9.1.1 is of the ruby type, and has been designed to make the device emit short intense pulses of light. These Q-spoiled, or giant pulse, ruby lasers typically produce pulses that are 10-30 ns in duration. Each pulse contains a few Joules of energy. After the laser fires, a small portion of the transmitted pulse is picked off by a detector which produces a pulse to start the timing electronics. The outgoing laser pulse goes through appropriate optics to give it the desired beam divergence angle, and to aim it in the proper direction. The object

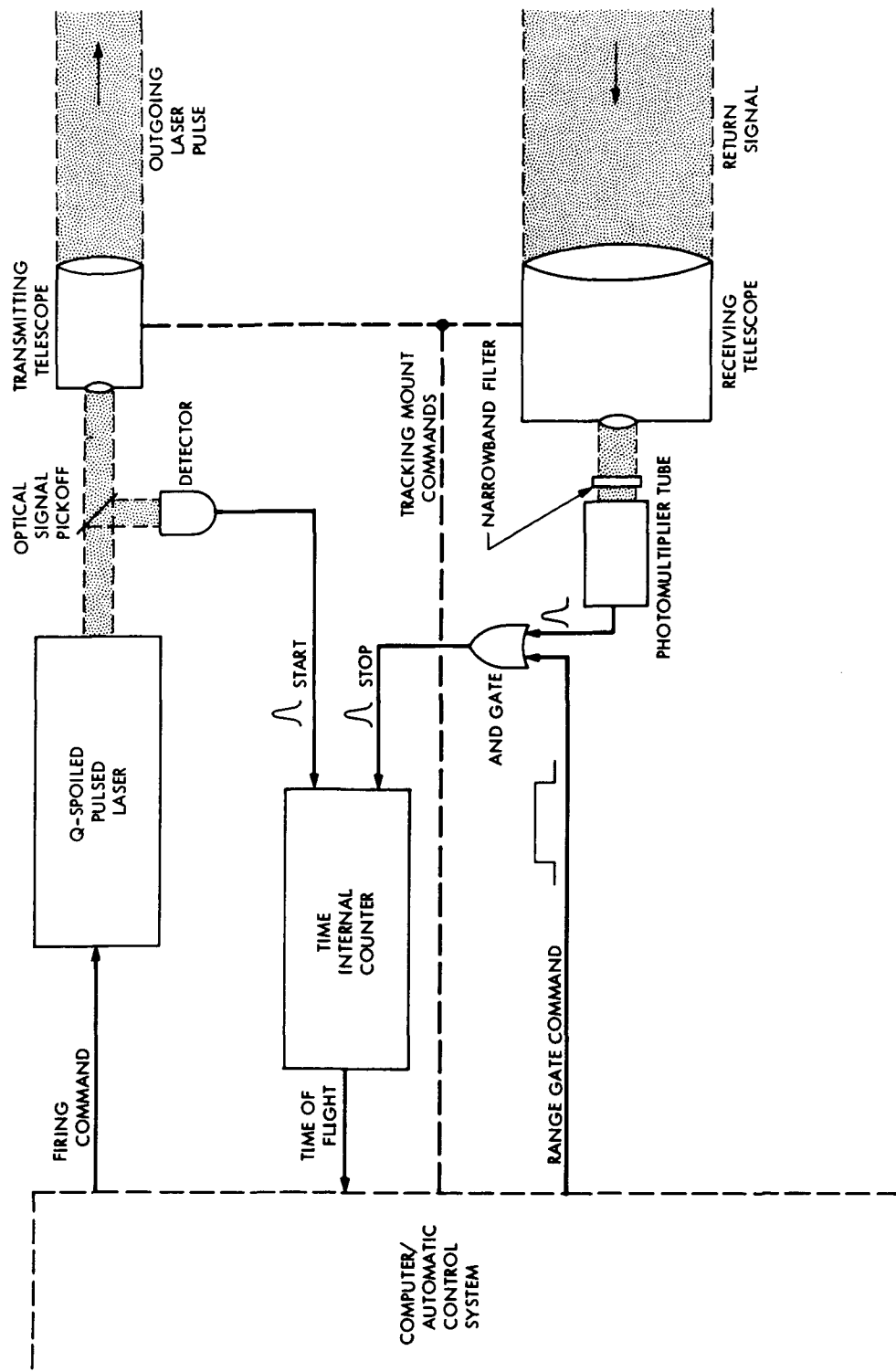


Figure 9-1 Block Diagram of a Typical Laser Satellite Ranging System Current in Use

being tracked usually carries optical cube-corner retroreflectors in order to enhance the intensity of the return signal. The return pulse is collected by the receiving telescope and is focussed through a filter upon a photomultiplier tube (PMT) (see Glossary). The electrical pulse from the PMT furnishes the stop pulse to the timing electronics. A range gate is included in this signal path, in order to prevent unwanted signals from prematurely stopping the timer. The measured time delay is then read out, and the system is reset for the next event.

The performance parameters of several existing laser tracking systems are summarized in Table 9-1. Two of the stations, GSFC and SAO, are used to track Earth satellites for geodetic purposes. The other two are used primarily for tracking the retroreflectors left on the Moon by the Apollo astronauts.

### 9.1.3 Sources of Errors in Present Systems

Present satellite laser ranging systems are limited in the accuracy they can attain by several factors. The major cause of uncertainty is produced by the duration of the transmitted pulse and the resolution of the timing electronics. Minor uncertainties are the result of uncalibrated delays in the station electronics and in the atmosphere. The laser ranging systems mentioned in Table 1 generally have overall accuracies that are in the 15-30 cm range.

Clearly, the minimum resolution of the timing system will limit the overall accuracy. With a resolution of 1 ns, the range uncertainty would be  $\pm 15$  cm on a single measurement. This error can be reduced by performing repeated measurements and averaging the results. This technique is complicated by the rapid rate-of-change of the satellite's range, particularly for low Earth orbiting satellites.

Table 9-1. Performance Parameters of Several Laser Ranging Systems

System	GSFC	SAO	AFCRL	LLRS
Pulse Energy, Joules	1	7.5	1	3
Pulse Duration, nsec	15	15	30	3
Repetition Rate, shots/min	60	1	20	20
Transmitted Beamwidth, mrad	1	0.6	2	0.008
Receiver Aperture, cm	40	51	22	270
Receiver Beamwidth, mrad	1.5-5	0.6-6	--	0.029
Receiver Bandwidth, nm	1	0.6	1	0.07
Counter Resolution, nsec	1	1	1	1
Tracking Method	Programmed Continuous	Manually Positioned	Programmed Stepwise	Programmed Continuous + Manual Guiding
<p>GSFC - Goddard Space Flight Center</p> <p>SAO - Smithsonian Astrophysical Observatory</p> <p>AFCRL - Air Force Cambridge Research Lab</p> <p>LLRS - Lunar Laser Ranging Station</p>				

The duration of the transmitted pulse can produce timing errors on the order of the pulse duration if the amplitude of the received pulse is small (a few photons). However, errors due to this effect will be relatively small ( $\approx 1$  ns) if the return pulse amplitude is large enough to permit "leading edge" detection in receiver electronics.

Uncalibrated delays in the station electronics can produce errors on the order of one nanosecond. The major contribution to this error is the transit time delay variations in the receiver photomultiplier tube. As mentioned above, the start and stop pulses for the timing electronics are derived from two different photodetectors. The start pulse typically comes from an avalanche photodiode or phototransistor while the stop pulse comes from a PMT. The transit time of the PMT usually is 40 ns, and must remain constant during the course of a tracking pass. Small temperature changes or PMT power supply changes can produce changes in this delay, and hence cause a change in the internal station delay.

The extant cube corner bearing satellites are all equipped with arrays of retro-reflectors. The physical extent of these arrays produces a smearing of the return signal, leading to errors of the order of the size of the array. In addition, the array of reflectors causes extensive amplitude fluctuations in the return signal due to interference effects (see Appendix I). This can lead to range errors even if the receiver electronics does compensate for the signal level fluctuations, since the return pulse shape may be severely distorted.

The Earth's atmosphere produces an additional delay of its own, in addition to refracting the laser beam for non-zero zenith angles. The effects of this delay and refraction are for the most part well understood (see Paragraph 8.5). Small variations exist due to the normal thermal turbulence

prevalent in the atmosphere. These variations will lead to errors generally significantly less than a nanosecond in magnitude.

## 9.2 IMPROVED APPROACH TO LASER RANGING

The utility of a satellite laser ranging system which has significantly smaller overall error performance characteristics has been clearly established in the earlier Sections of this report. There is a real need for laser ranging systems with accuracies approaching a few parts in  $10^8$ . This corresponds to a timing accuracy of 0.2 ns for typical Earth satellite ranges. The question can certainly be asked: Is it possible, using present technology, to produce a laser ranging system which is nearly a factor of 10 better than existing systems? The answer, as JPL envisions the present systems, is "yes". The components required to upgrade the system accuracy presently exist, and such a system can be constructed.

The sources of error previously mentioned, i. e., pulse duration, timing resolution, and uncalibrated station delays can all be reduced significantly, thus leading to improvements in ranging accuracy. Two recent developments have led to the availability of equipment which will aid significantly in reducing the first two error sources; these are the mode locked laser and the high resolution interpolating time interval meter. The third error source can be virtually eliminated by arranging the optics so that both start and stop pulses originate in the same PMT. These improvements are discussed further in the following Subsections.

### 9.2.1 Laser

The most significant advance toward eliminating a source of error is the development of the "mode locked", Q-spoiled laser. These devices are capable

of producing a single pulse of light of duration shorter than 0.1 ns, which has a total energy in the pulse of more than 0.5 Joule (5 gigawatt peak power).

These lasers can be either of the ruby (0.694  $\mu\text{m}$ ) or neodymium (1.06  $\mu\text{m}$ ) type, with the appropriate Q-spoiling modifications to effect a giant pulse mode of operation. The addition of a mode locking device, usually a saturable absorber which modulates the laser cavity loss at its fundamental longitudinal mode frequency, produces a phase locking of all the oscillating longitudinal modes. This results in the production of several (usually 5 - 10) very narrow pulses during a period of 30 ns. It is necessary to include an electro-optic shutter outside the laser cavity in order to provide a means for releasing only one of the several mode locked pulses.

Such a mode locked laser can produce pulses of 20 millijoules energy. The addition of two or three stages of amplification raises this energy to 0.5 joule or more. There are some differences between the ruby and neodymium lasers, the most notable being that the neodymium units are more powerful. A summary of performance parameters of one commercial laser is presented in Table 9-2.

### 9.2.2 Timing Electronics

Devices to measure the time interval between two pulses have existed for a long time. The typical unit counts the number of clock pulses which occur between the start/stop pulse pair in question. Of course, the clock pulse generator is well stabilized to minimize the effects of clock frequency errors. The timing error is at least  $\pm$  one clock period. Such units typically have a 10 MHz clock, which leads to a  $\pm 100$  ns timing error corresponding to a range error of 15 m.

Table 9-2. Mode Locked Ruby Laser Characteristics

Manufacturer	KORAD Department Union Carbide Corporation 2520 Colorado Avenue Santa Monica, CA 90406
Laser Type	Q-switched, mode locked Ruby plus three-stage amplifier
Pulse Energy	0.6 joules/pulse
Pulse Width	100 - 200 picoseconds
Repetition Rate	10 pulses per minute
Beam Divergence	2 milliradians full angle, 1/2 energy
Cost	\$55,000
<p>The single stage oscillator is Q-switched by a flowing dye cell, which also produces the mode locking action. A single pulse from the series of mode locked pulses is extracted using an electro-optic shutter, and amplified by a three-stage amplifier. The oscillator and amplifiers are operated from two separate power supplies, and cooled with a closed cycle heat exchanger.</p>	

Recently, timing devices have been built which have much higher resolution than previous units. They still operate on the same basic idea, counting pulses with the aid of a relatively low frequency clock, but they are able to determine the time of occurrence of the start and stop pulses by interpolation between clock pulses.

Three different commercial manufacturers are currently producing time interval counters which operate on this principle. All of these have minimum resolutions of about 0.1 ns. A more detailed investigation of these counters was undertaken; the results are reported in Paragraph 9.3.2.

### 9.2.3 Timing Pulse Pickoff

A description of how timing errors produced by the manner in which the start and stop pulses for the timing electronics are derived has been presented previously. Since the goal of this section is to outline a system that is capable of timing accuracies of 0.1 ns, it will be necessary to discuss a method for minimizing the errors caused by the drifting of station internal delays.

By far the best approach toward solving this problem is to arrange for the same photomultiplier to serve as the detector for both the start and stop pulses [9.6]. The procedure would be to arrange for a small amount of the transmitted pulse, only a few hundred photons, to reach the receiving PMT. This will produce a pulse at the output of the PMT which is used to initiate the timing sequence. The optical signal from the satellite received by the PMT will produce another pulse at the PMT output, which will serve to stop the timer. Since both the start and stop pulses have to traverse the same electron multiplier chain, cables, etc., only a few milliseconds apart, the effect of variations in the internal delays of all these devices will be minimized.

The use of the receiver PMT as the source of the start pulse is beset with two complications: electromagnetic interference (EMI) from the laser, and backscattered signal from the transmitted pulse. The EMI produced by the firing of the laser, electro-optic shutter, and amplifiers may cause a false or premature signal at the PMT output. An additional signal may be produced by atmospheric backscatter and stray, off-axis radiation reaching the PMT during the first few nanoseconds after the transmitted pulse leaves the system.

Control of the EMI problem may be difficult. Suitable shielding, careful attention to eliminate ground loops, and application of microwave absorbing material such as Eccosorb will be required. The backscatter can be eliminated by the use of a mechanical shutter in front of the PMT. The shutter would open one millisecond after the transmitter fires, and remain open until after the return pulse is received.

#### 9.2.4 New Design for a Retroreflector

The extant retroreflector bearing satellites, a total of six, all have large arrays of small diameter retroreflectors. A short duration laser pulse will be smeared out in time when reflected from such an array, unless the array happens to be oriented perpendicular to the line of sight. For precision ranging with short duration pulses, a different retroreflector arrangement would be necessary in order to reduce the smearing effects.

A single aperture cube-corner type retroreflector would be the best. However, the relatively narrow effective field-of-view of a cube-corner would prevent ranging from several stations simultaneously [9.11]. A special array of 4 or 8 cube-corners could be constructed, with the apexes of all cubes positioned so that they are nearly coincident with each other. This device would produce reflections from almost any angle of incidence. The individual cube-corners would be required to have a relatively large aperture, 5 cm diameter or more, and would have to be accurately constructed with the three faces mutually orthogonal to high accuracy. The return beam diameter at a receiving station site would be small enough so that the velocity aberration caused by the satellite's motion will shift the return beam completely off the

receiving telescope aperture. It will thus be necessary to somehow spread the return beam slightly. Further research would be required to develop a suitable cube-corner retroreflector array with the properties suitable for simultaneous use with several stations.

#### 9.2.5 Performance Potential

The discussion presented in the previous sections has indicated that several of the major sources of errors in laser ranging systems may be eliminated or materially reduced. If a system were built utilizing these improvements, what would be the remaining sources of error, and what would be its expected absolute accuracy? With the major error sources eliminated, some of the lesser error sources can be discussed.

There are several clearly defined sources of small errors, and probably many that we have not yet identified. Four of the more predominant effects are:

- photomultiplier tube response time,
- pulse height variation from shot-to-shot (see Appendix I)
- calibration of atmospheric delay and refraction (see Section 8.5)
- atmospheric turbulence effects.

The first two items listed are likely to be the more important of the lesser errors. They have been the subject of an extensive experimental investigation; the results are reported in Paragraph 9.3.1. The general conclusion is that: commercially available photomultiplier tubes and pulse height compensation apparatus exist, but need to be improved.

The problem of calibration of atmospheric delay has been extensively treated by several groups. The most detailed of these was performed by Hopfield [8.1]. The conclusion reached was that: with good knowledge of the

atmospheric temperature and pressure at the laser station site, it is possible to estimate the atmospheric delay to within a few millimeters at the local zenith, and to within 2 centimeters at an elevation angle of  $20^\circ$ . Clearly, experimental verification of these conclusions is necessary, but the results are encouraging since the resultant errors are small (See Paragraph 8.5 for a more detailed discussion of the problem of atmospheric calibration).

Atmospheric turbulence effects on the overall system accuracy should be small, since their time average will be zero. However, scintillation and multipath effects may deteriorate the performance by producing confusing signals in the PMT, and by causing the PMT output pulses to vary in amplitude.

The deleterious effects of all these lesser sources of errors will be small. However, in order to provide a simple system with the highest possible accuracy potential, it is necessary that these effects be understood. No attempt has been made to experimentally investigate the atmospheric effects during the course of this one year study. Any follow-on program should include a detailed study of atmospheric effects, in the hope of further improving system accuracy.

### 9.3 EXPERIMENTAL PROGRAM

Two major areas were investigated experimentally in this study, namely: the effect of photomultiplier response time on the ranging accuracy was studied, and the accuracy and resolution of the commercially available high resolution time interval meters was accessed. As part of this study a small demonstration laser ranging system was constructed in order to verify all the features necessary to achieve high accuracy range determination.

### 9.3.1 Photomultiplier Tube Response

If an optical ranging system based upon time-of-flight techniques is to have fractional nanosecond accuracy, it is clear that the majority of the components in the timing portion of the system must have response characteristics that are consistent with such a time requirement. In the discussions of equipment it has been shown that two of the critical components, the laser and the time interval electronics, have potentially adequate response times.\* The same cannot be said of the photomultiplier tube.

A typical PMT has a response time on the order of a few nanoseconds, with the duration of the entire transient lasting tens of nanoseconds. The transit time required from the reception of an optical pulse at the PMT photocathode to the detection of an electrical signal out of the anode terminal (at the base of the PMT) is usually 20 - 40 ns. The nature of the trajectories of the electrons as they travel from the photocathode through the electron optics (if any) to the first dynode, the subsequent trajectories through the electron multiplier section, the collection efficiency of the anode, and the way that the anode is connected to the world outside the PMT envelope, all contribute to deterioration of the response time of the PMT. Of all these effects, the first has the most predominant effect, accounting for about 80 percent of the time smearing [9.6].

Photomultiplier tube manufacturers are presently becoming aware of the need for improved transient response of their products. Their efforts have

---

\*The phrase response time in this report is defined to be the time required to reach a preset trigger level. The response time is related to, but not the same as, the rise time. After an event has passed a trigger level, the shape itself, or how faithfully it reproduces the initiating pulse shape is of no basic importance.

extended in many different directions, from development of radically new types of PMT's\*, to the addition of coaxial feedthroughs for the anode signal leads.\*\*

An extensive amount of research into the transient response properties of PMT's has been done by various organizations in the nuclear instrumentation field [9.7]. Their experience has led to a choice of a photomultiplier tube which is for the most part conventional in its construction, except that the large photocathode-first dynode drift space has been greatly reduced. Furthermore, the photocathode material used in this tube: gallium arsenide, is by far the best choice for use with a ruby wavelength laser.

The photomultiplier tube chosen is a "Quanticon" type C31034, manufactured by RCA. Table 9-3 presents a summary of its salient characteristics. The tube has a quantum efficiency that is 12 percent at the ruby wavelength; this is the highest efficiency of any current tube at that wavelength. It has an internal multiplication gain of  $10^7$  at 2000 V, and an exceptionally low dark current. Figure 9-2 is a photograph of a sampling scope display of the single photo output pulse shape. The rise time is approximately 3 ns, with a width at half maximum of 5 ns. This response is exceptionally fast for a PMT of this type, that is, of more or less conventional construction.

The more exotic types of PMT's mentioned previously, the crossed-field type and the channeltron type, both have some undesirable features in their performance characteristics. The crossed-field PMT has an excellent transient response ( $<0.5$  ns) but it has a low multiplication gain. The channeltron PMT's transient response is no better than a conventional PMT. They both have

---

\*The Sylvania crossed field PMT and the Bendix channeltron are examples of this type.

\*\*Both Amperex and RCA tubes use this feature.

Table 9-3. Characteristics of RCA C31034 Photomultiplier Tube

Photocathode	
Material	- Gallium Arsenide
Spectral response curve no.	- 128
Wavelength of maximum response	- 830 nm
Typical quantum efficiency	
550 nm	- 14%
694.3 nm	- 12%
860 nm	- 9%
Electron Multiplier	
Dynode material	- Beryllium-Copper
Number of stages	- 11
Structure	- In line, electrostatic focus
Dark Current Pulse Summation	
1/8 to 16 photoelectrons at 20°C	- 10,000

the more conventional types of photocathodes, with the correspondingly low efficiency at the 0.694  $\mu\text{m}$  ruby laser wavelength. These factors make the utility of these tubes questionable. In addition, the experimental set up used to test the PMT response utilized an infrared diode laser whose output wavelength is beyond the cutoff of these tubes.

The characteristics of the gallium arsenide photocathode are so superior that a program should be considered to incorporate it into the more exotic photomultipliers mentioned. Another more conventional PMT, the C31024 developed by RCA, has potential as a fast response time tube. It has a

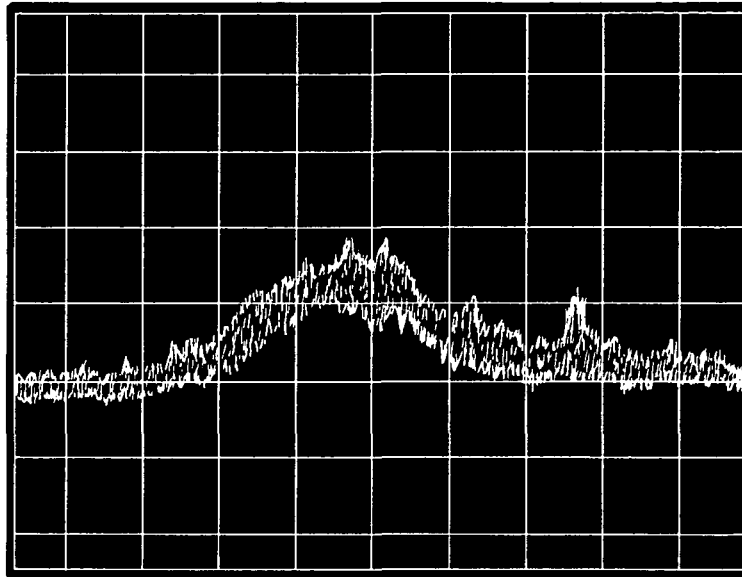


Figure 9-2. Sampling oscilloscope display of the average shape of the dark current pulse from an RCA C31034 photomultiplier tube. The abscissa is 2 ns/major division, and the ordinate is 10 mv/major division.

conventional photocathode, but only five dynodes instead of the eleven in the C31034. Each of these dynodes is fabricated from gallium phosphide, and has a single stage gain of more than 10. The five stage GaP multiplier has as much gain as the eleven stage conventional multiplier. The characteristics of a photomultiplier tube with a gallium arsenide photocathode and gallium phosphide dynodes would probably make it extremely useful as a sensitive, fast response detector for laser ranging applications.

An improved version of the RCA C31034 already exists, and is designated C31034A. This PMT has a slightly different photocathode, with enhanced quantum efficiency in the red part of the spectrum.

### 9.3.2 High Resolution Time Interval Meters

One major requirement for a centimeter accuracy ranging system is a device that will determine the time-of-flight of the laser pulse to an accuracy of 0.1 nanoseconds. A conventional time interval meter, which measures time by counting clock pulses between the start and stop signals, would require a 10 GHz clock frequency in order to have a resolution of 0.1 ns. Such devices presently do not exist, although they may in the near future due to micro-integrated circuit technology.

Electronic timers with resolutions of 0.1 ns have been developed recently, and are available from three different commercial manufacturers. These devices all operate on the same principle: utilizing a basic clock frequency of only a few megahertz; the time between start and stop signals is determined by counting the clock pulses, with the added ability to determine the time of occurrence of the start and stop signals between the clock pulses. This is accomplished by the use of electronic interpolators that are able to effectively resolve the basic clock period into 0.1 ns intervals.

Figure 9-3 shows a block diagram of an interpolating time interval meter. The pulse counter commences counting the first clock pulse after reception of the start trigger signal, and ceases counting with the next clock pulse after reception of the stop trigger signal. The start (stop) interpolators measure the time between the reception of the start (stop) signal and the next clock pulse. The special purpose processor performs the mathematical addition and

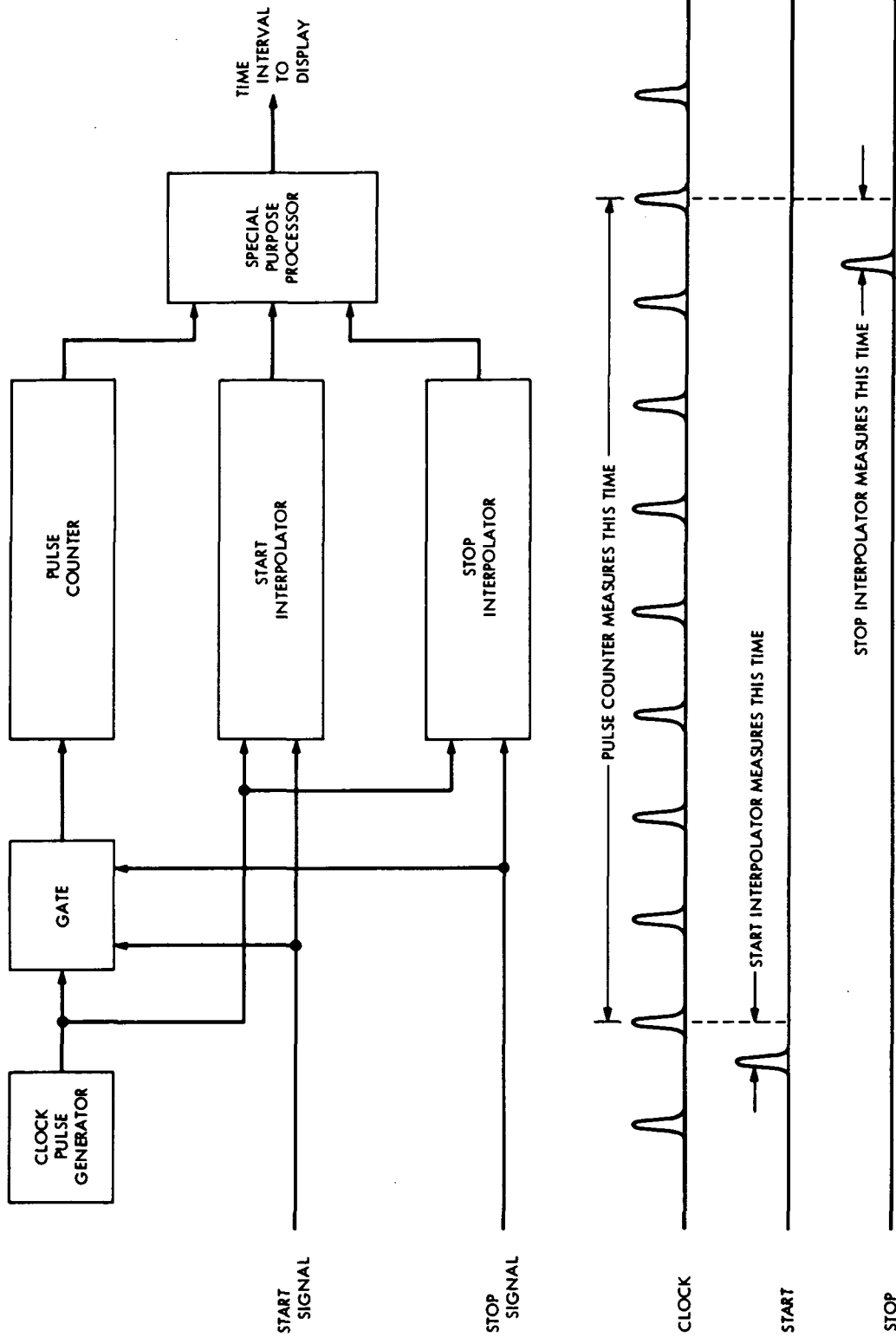


Figure 9-3. Block Diagram of a High Resolution Time Interval Meter

subtraction necessary to produce the time reading for the display and/or output. A typical time interval meter utilizes a clock pulse generator with a 100 ns period (10 MHz), and interpolators capable of resolving the clock period into 1000 parts, each of 0.1 ns duration.

The accuracy of these devices is limited by the usual problem of clock generator frequency stability, interpolator linearity, and input pulse shapes. For purposes of the present program, the frequency stability does not represent a problem since the total time duration being measured will only be a few milliseconds. The interpolator nonlinearity may be a source of error, but as reported below the effects of linearity can be measured. Errors due to input pulse shapes can be minimized by providing fast risetime, constant shaped pulses to the input of the timing circuitry.

Three commercial units are available that have the 0.1 ns resolution required for this program. The salient features of these high resolution counters are summarized in Table 9-4.

The procedure for testing the accuracy of these counters is based upon the following assumption: the major source of error will be in the start and stop interpolators, with systematic errors in measurement of long time intervals being attributed to a clock frequency error. A test procedure was developed to determine the variation in measured delay caused by interpolator errors. No attempt was made to measure clock frequency errors.\*

Figure 9-4 shows a diagram of the experimental apparatus used to generate the start and stop pulses that are used as inputs to the time-interval-meters under test. The pulse generator is set to deliver a so-called NIM Standard fast pulse. The pulse has a duration of 10 ns, an amplitude of

---

\*Clock frequency stability will not be a problem, since it is always possible to provide an external clock source with the required stability.

Table 9-4. High Resolution Time Interval Meters

Manufacturer	Hewlett-Packard Co. Palo Alto, Calif.	EG & G, Inc. Nuclear Instrumentation Division Oak Ridge, Tenn.	Nanofast, Inc. Chicago, Ill.
Model No.	5360A with H01-5379A plugin	TDC 100	536B with M/2 plugin
Input Type	Start and Stop or Common	Start and Stop	Start and Stop
Trigger Level	Adjustable	Fixed	Automatically set to half pulse height
Range Gate	Yes	Yes	Yes
Clock Frequency, MHz	10	62.5	10 MHz
Interpolator Resolution, ns	0.1	0.125	0.0125
Display	Decimal	Binary	Decimal
Display Resolution, ns	0.1	0.125	0.050
Additional Features	Small minicomputer capable of some data processing	Multiple Stop; built in range gate	Built in range gate
Price	\$7325 + ≈1000 for computer interface	\$7500 + ≈1000 for computer interface	\$7950

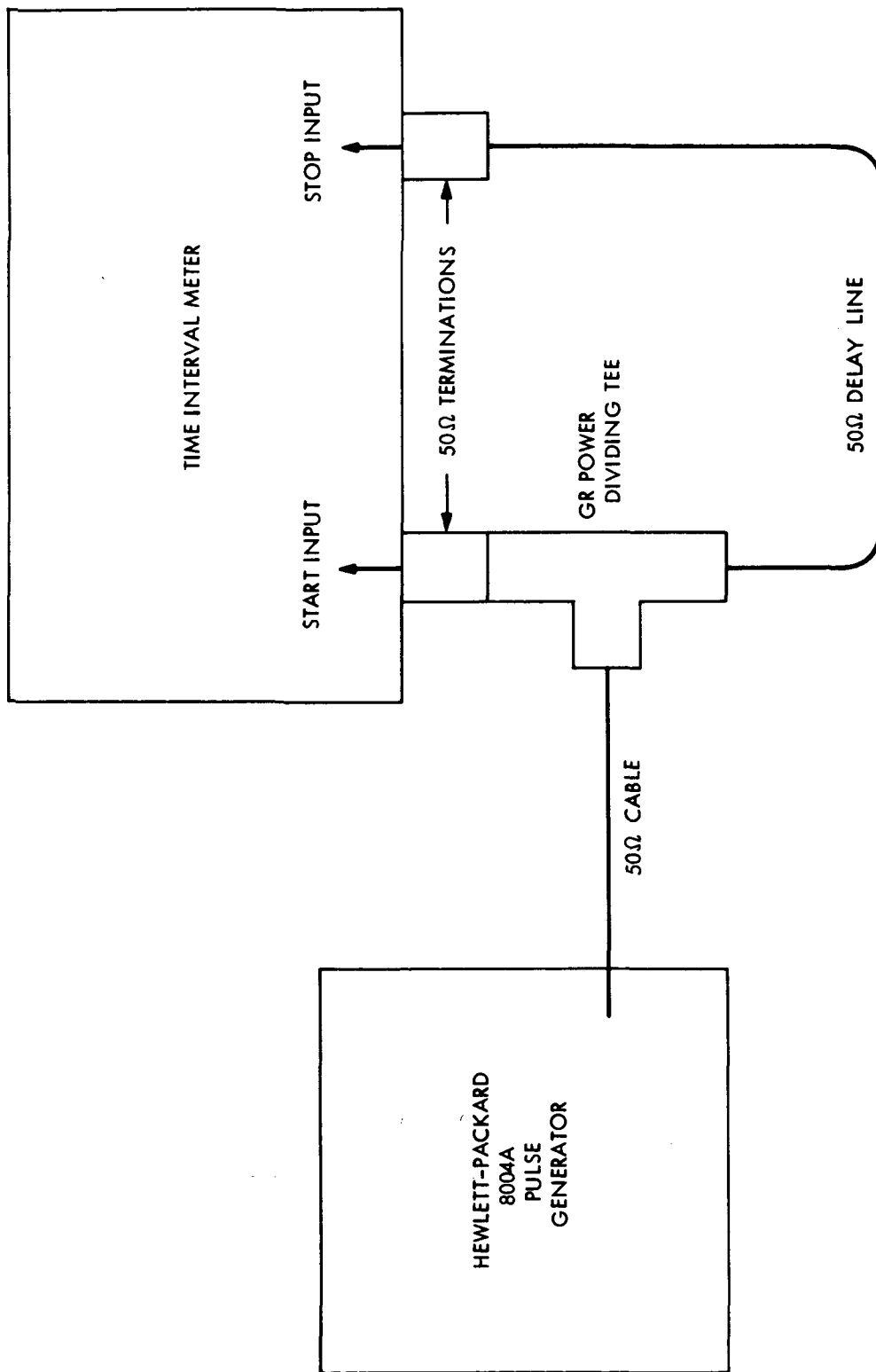


Figure 9-4. Diagram of Experimental Apparatus for Testing for Time Interval Meter Interpolator Errors.

-1 volt, and a risetime of 1 ns. It is split by a power dividing tee. One of the split pair is terminated in  $50\Omega$  and serves as the start pulse; the other is introduced into a delay line which is terminated in  $50\Omega$  and serves as the stop pulse. The pulse generator is set to run at a frequency which is not harmonically related to the internal clock of the time-interval-meter under test. This provides essentially a random time of occurrence of the start pulse with respect to the internal clock pulses.

Repeated single measurements of the time delay between the pulses was made, and a record of each occurrence kept. The average value of the measurements will be a reasonable indication of the delay between the pulses, and the standard deviation will be an indication of the errors introduced by the interpolators.\*

The results of the measurements are summarized in Table 9-5. The standard deviation of the measurement of each of the three timers indicates that each one was performing within manufacturer specification. That is, all three units had a resolution of about 0.1 ns, and the data are in agreement. If an interpolator was not performing in a linear fashion, the random time of occurrence of the timing pulses would produce a larger spread of the measured events, and hence a larger standard deviation.

The conclusion of this test of commercial time-interval-meters is that they have adequate accuracy performance to satisfy our timing requirements. The present implementation calls for a unit that has a common input, due to the fact that the start and stop pulses originate within the same PMT, and will travel along the same transmission line. The Hewlett-Packard unit is the only

---

\*No corrections were made for the effects of transmission line loss on the shape of the stop pulse. This effect is a constant, and will not alter the conclusions about interpolator errors.

Table 9-5. Measurement of Time-Interval Meter Interpolator Error

Unit Tested	HP 5360A + 5379A	EG & G TDC 100	Nanofast 536B + A-3 plugin
Measured Times and Number of Occurrences	28.6 - 2	17.25 - 8	5.9 - 1
	28.8 - 58	17.375 - 72	6.0 - 10
	28.9 - 223	17.50 - 15	6.1 - 69
	29.0 - 196	17.625 - 5	6.2 - 20
	29.1 - 18		
	29.2 - 2		
	29.7 - 1		
Number of Events	500	100	100
Mean Value, ns	28.936	17.397	6.108
Standard Deviation, ns	0.085	0.079	0.058

one presently that has a common input. The other manufacturers indicate that they can provide such an option on their units.

At the present time, our recommendation would be to use the Hewlett-Packard H12-5360A plus the H01-5379 plugin. This recommendation is based solely on cost. The H12 option eliminates unneeded features, and is priced at \$5445.00.

#### 9.4 DEMONSTRATION LASER RANGING SYSTEM

An experimental apparatus was devised to demonstrate the response of a photomultiplier tube to short duration light pulses, and to demonstrate the concept of ranging with only a single photodetector. The apparatus utilizes a

pulsed injection diode laser as a source of light, a sampling oscilloscope to display the signals, and a high resolution time-interval-meter to measure the transit time of the light pulses. Figure 9-5 is a photograph of the apparatus.

#### 9.4.1 General Description

Figure 9-6 presents a diagram of the apparatus, showing the general layout of the various optical components. The light from the diode laser is collimated into a 20 mm diameter beam by a lens.\* This beam is then split into two beams of approximately equal intensity. One beam goes to a nearby mirror and the other travels to a cube-corner retro-reflector (CCRR) located some distance away. The light from each reflector returns to the beam splitter, half of each beam being directed toward the photomultiplier tube. A narrow band interference filter is placed in front of the PMT to cut down on the stray light that reaches the photocathode. An aperture of 8 mm diameter limits the PMT field of view. Photographs of the optical component arrangements are presented in Figure 9-7.

The duration of the light pulse that the laser emits is very short, only 3 ns. Thus, two distinct light pulses reach the PMT, with the time difference between them being related directly to the difference between the optical path lengths of the paths the two beams traverse. The nearby mirror produces the start pulse for time interval meter, and the distant CCRR produces the stop

---

\*The lens, a 30 mm focal length Hastings triplet, had no astigmatic correction to accommodate the effective shape of the diode laser's output aperture. Consequently, the beam had an approximately elliptical shape in the far field.

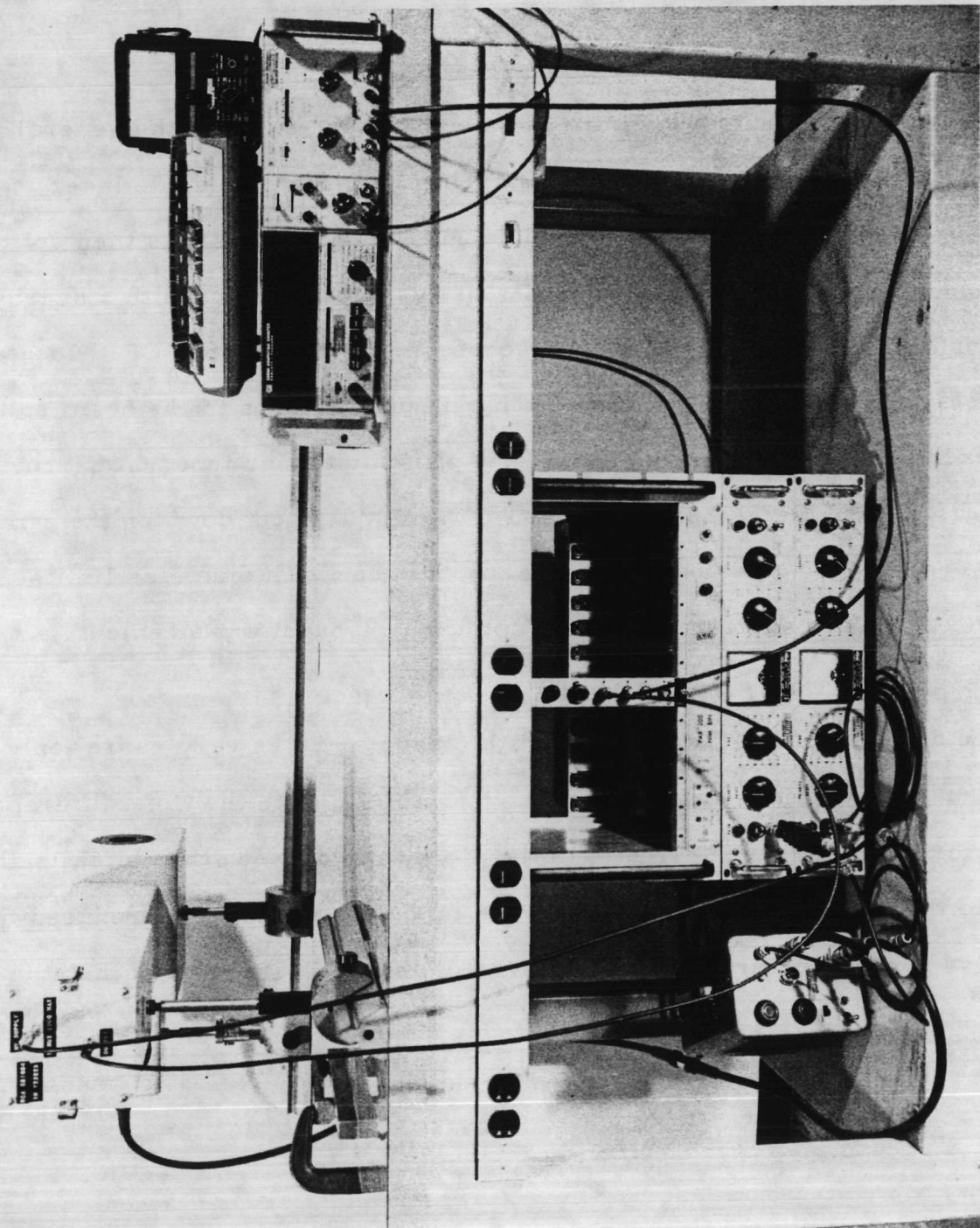


Figure 9-5. Photograph of the Demonstration Laser Ranging System, Showing the Optical Assembly, Laser Pulse Generator, Power Supplies, Constant Fraction Timing Discriminator, and Time Interval Meter.

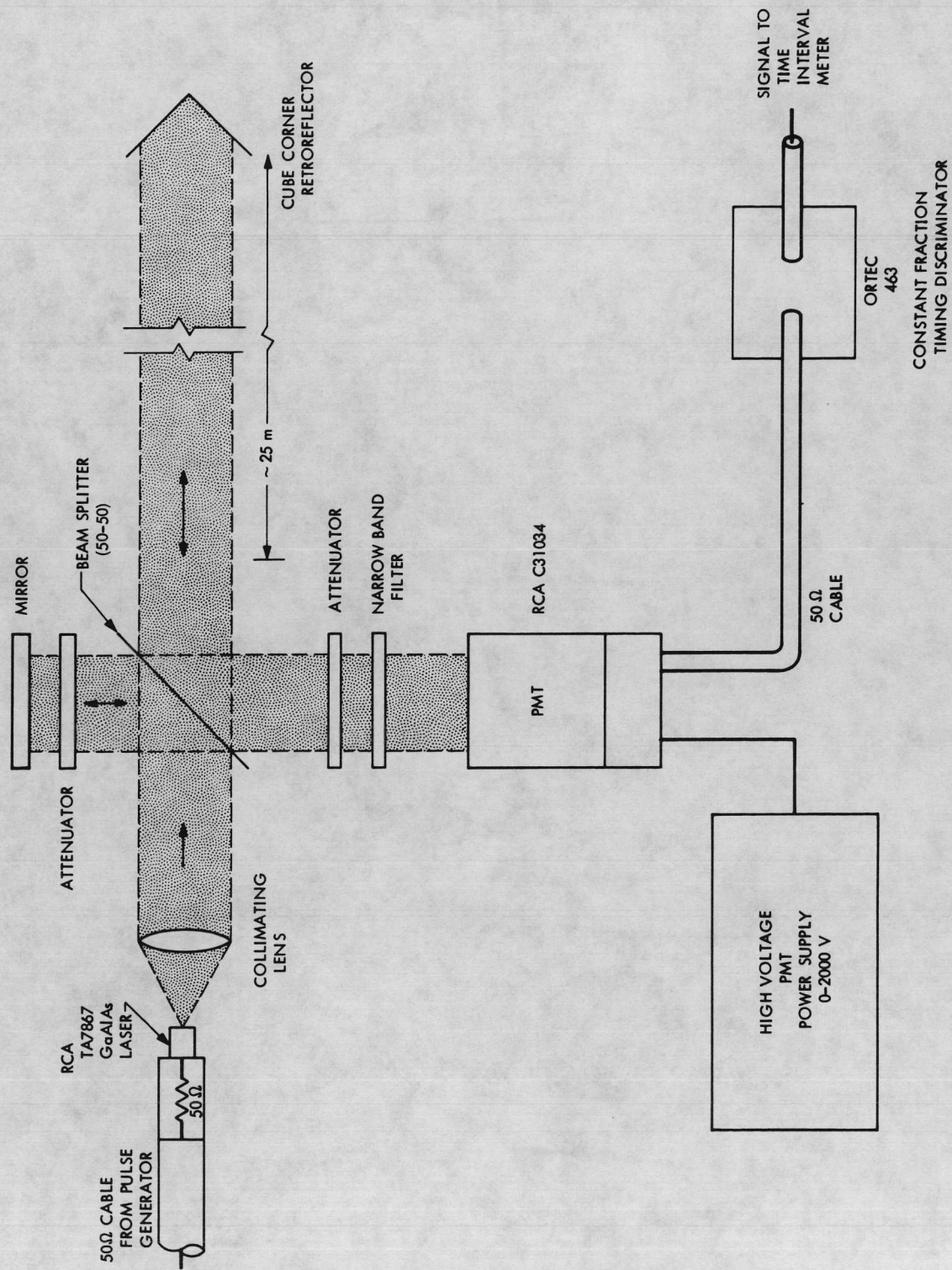


Figure 9-6. Block Diagram of the Demonstration Laser Ranging System.

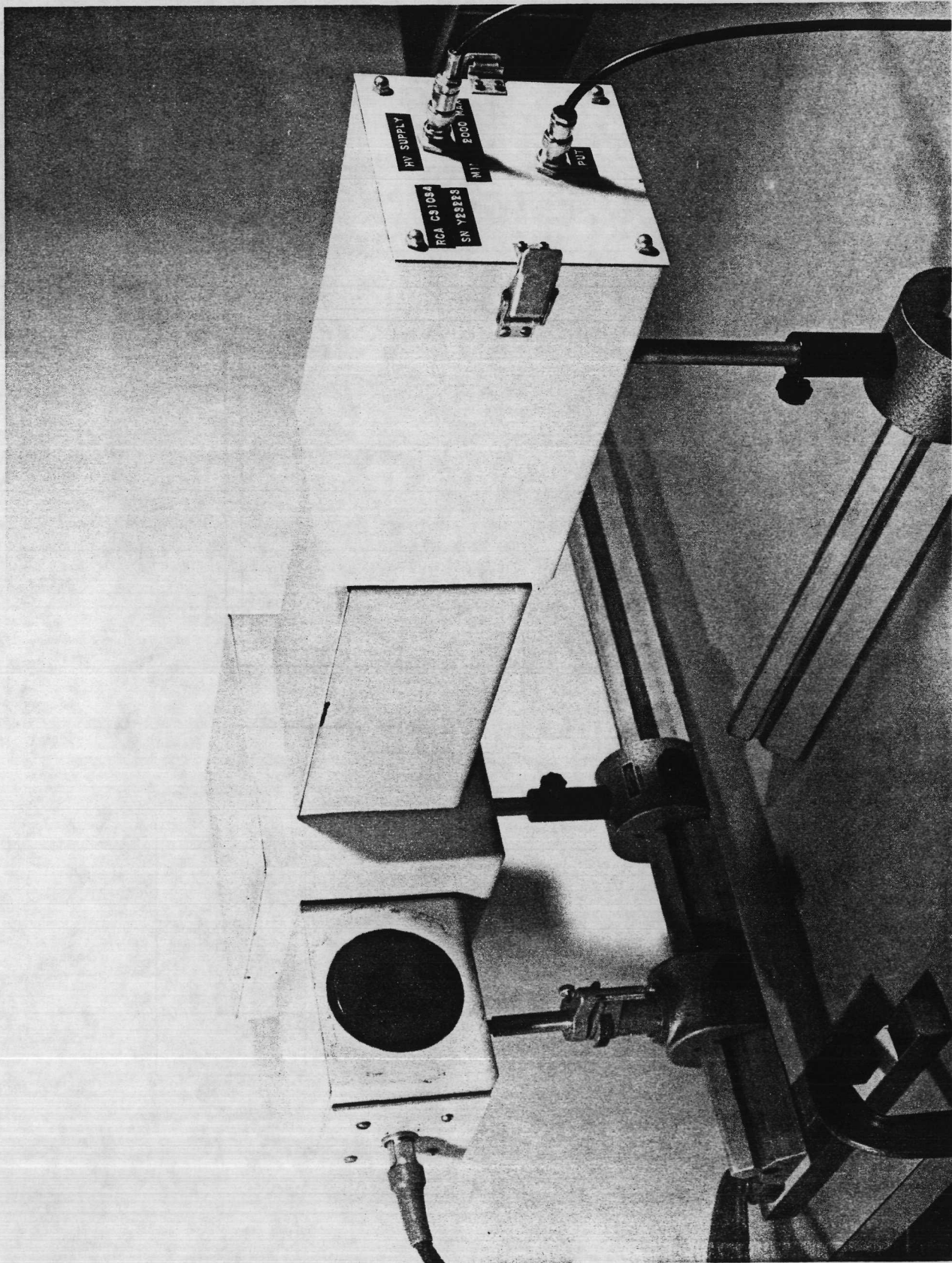


Figure 9-7 (a). Optical Assembly with Covers in Place

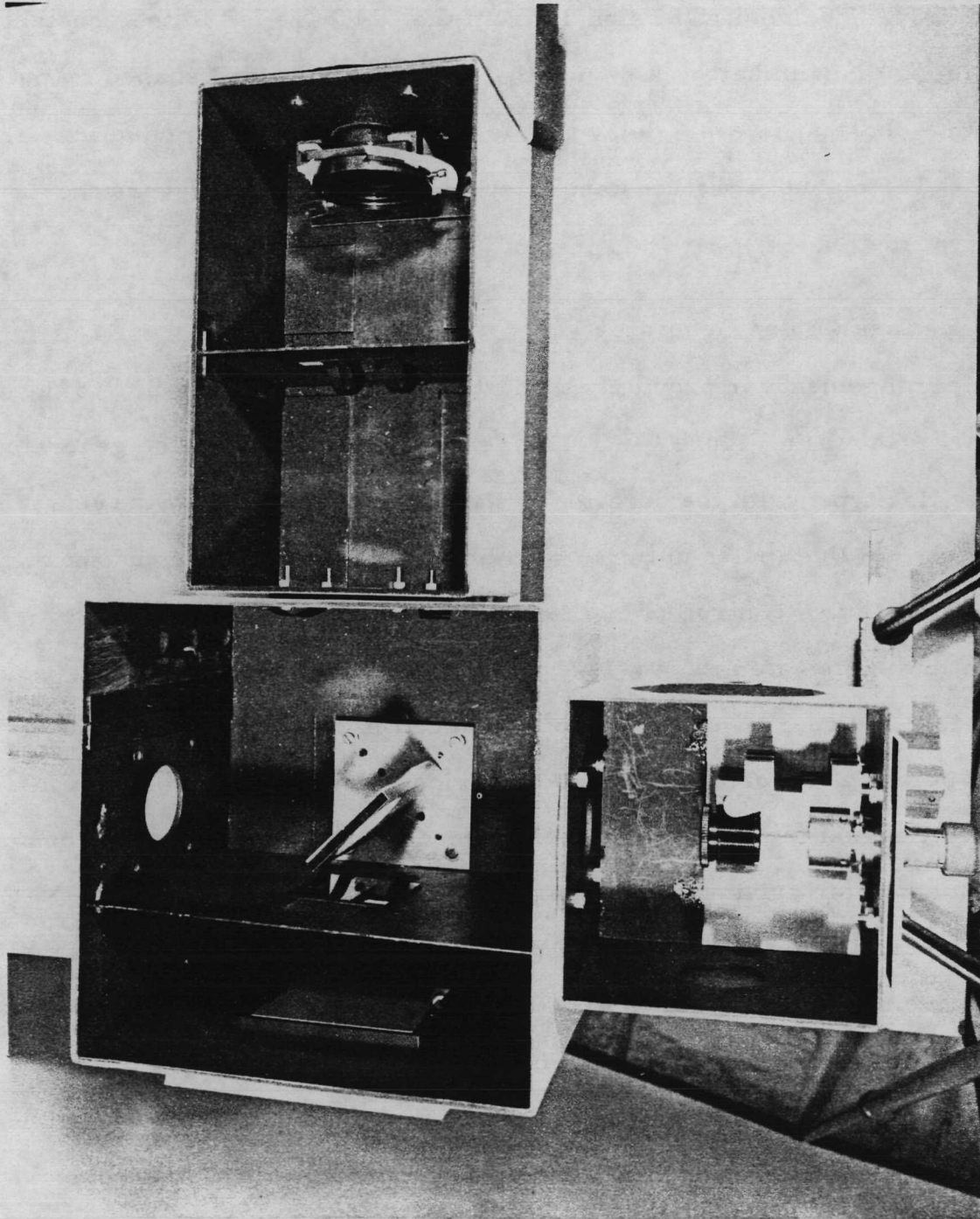


Figure 9-7(b). Optical Assembly with Covers Removed. The laser and collimating lens are in the box at the bottom. The large box at left-center contains the beam splitter, mirror, and start pulse attenuator. The box at right-center contains another attenuator and a narrow band interference filter. The photomultiplier tube is in the closed box on the extreme right.

pulse. An optical attenuator\* placed in front of the nearby mirror allows control over the intensity of the start pulse, and another optical attenuator placed in front of the PMT allows the intensity of both pulses to be adjusted simultaneously. The electrical signals from the PMT are fed to the constant fraction timing discriminator, a device that produces standard shaped output pulses with a constant internal delay that is independent of input pulse amplitude. The output of the constant fraction discriminator triggers the time interval meter.

#### 9.4.2 Laser Pulse Generator

The arrangement for providing a short duration electrical pulse to the diode laser is shown in Figure 9-8. The Tektronix Model 109 pulse generator is a charge line type, with the duration of the pulse determined by the length of the  $50\Omega$  charge line (pulse duration =  $2x$  electrical line length), and the amplitude of the pulse controlled by the amplitude of the voltage stored on the charge line (pulse amplitude =  $1/2$  stored voltage). The repetition rate is approximately 250 pps. A signal pickoff is placed in the output line of the device, to permit monitoring of the laser driving pulse, and to provide a synchronizing signal for a sampling oscilloscope. (Fischer [9.8] describes a similar method for driving diode lasers.)

The laser diode, an RCA TA7867 gallium aluminum arsenide type, emits light at a wavelength of 850 nm. This type of diode used has a threshold current of 10 amp, a maximum current of 25 amp, and a peak power output of 5 watts. The laser is mounted on a copper heat sink, with a  $49.8\Omega$  resistor connected in series with the center conductor to provide proper termination for the

---

\*All attenuators used in this experiment are of the Schott glass neutral density filter type.

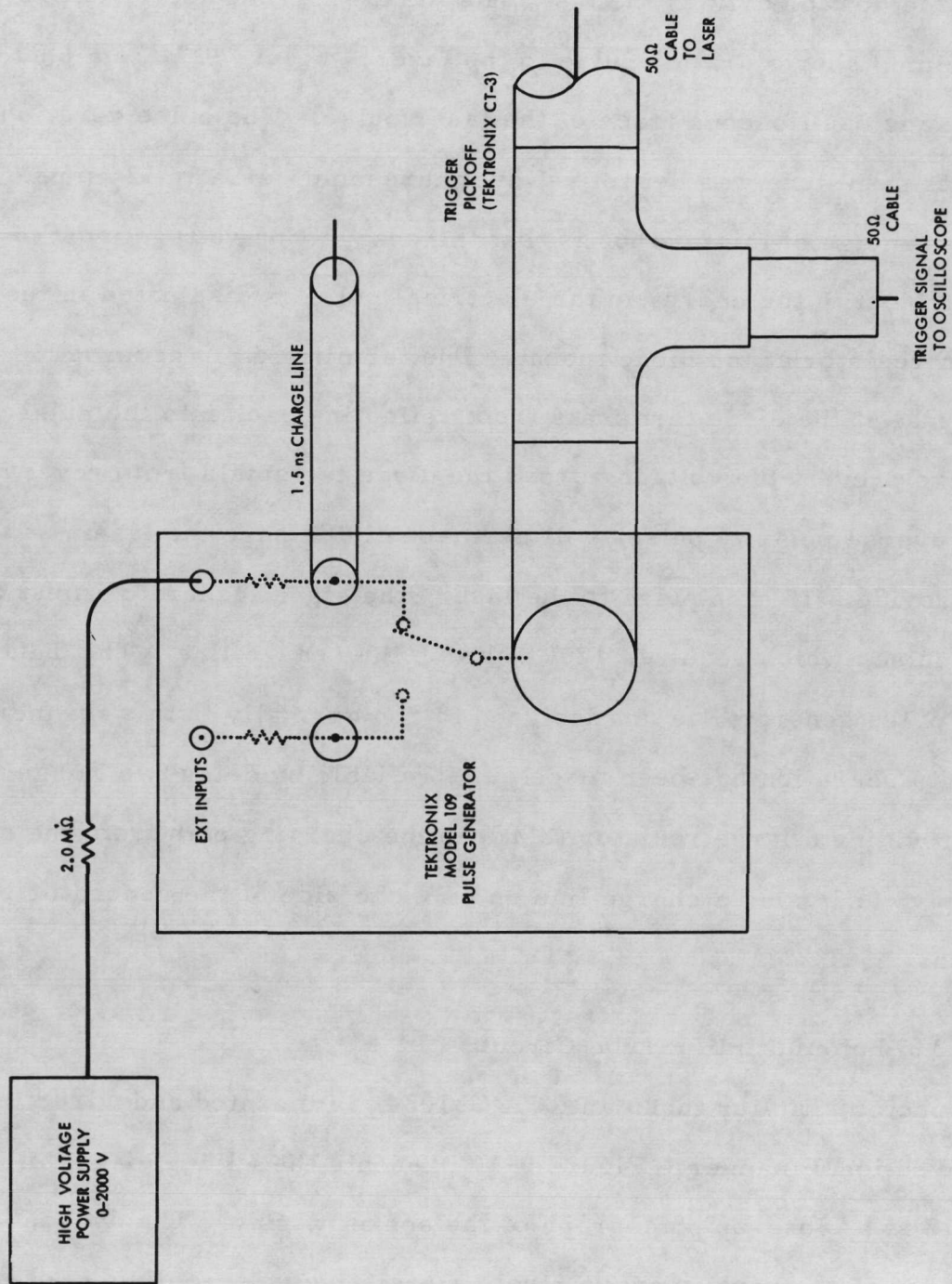


Figure 9-8. Pulse Generator Circuit for Providing Short Duration, Fast Rise Time Pulses to a Gallium-Aluminum-Arsenide Diode Laser.

electrical drive pulse. A photograph of the laser in its mount is shown in Figure 9-9.

This method for driving the laser has the distinct advantage of providing a fast risetime, short duration pulse to the laser. Figure 9-10 is a photograph of the sampling oscilloscope trace of the laser pulse. The pulse duration was 3 ns, and its amplitude was set to just over threshold, usually 12 amps. The major disadvantage of this method is that the charge line voltage must be excessive. Most of the energy in the electrical pulse is dissipated in the termination resistor at the diode mount. The termination is necessary to prevent the signal at the diode terminals from reflecting back into the pulse generator and to prevent the voltage across the diode terminals from reversing. Note that reverse polarity pulses will permanently damage the laser.

To provide a 12 amp pulse to the laser, the signal generator must deliver a 600 volt pulse, which requires 1200 volts on the charge line. The Tektronix Model 109 pulse generator is not designed to run normally in this manner. However, its operation has been made quite reliable by doing two things: namely, providing a large resistor ( $2M\Omega$ ) in the charging path from the external power supply, and using a charge line on only one side of the generator's SPDT reed switch.

#### 9.4.3 Photomultiplier Tube Circuit

The photomultiplier tube, an RCA C31034, is mounted and wired in a nearly conventional manner. Figure 9-11 presents the wiring diagram. Figure 9-12 is a close-up photograph of the socket wiring. The dynode voltages were provided in the usual manner, from a resistive voltage divider chain, as recommended for this tube by RCA. The last four dynodes were bypassed with appropriate capacitors, to prevent saturation from large pulses.

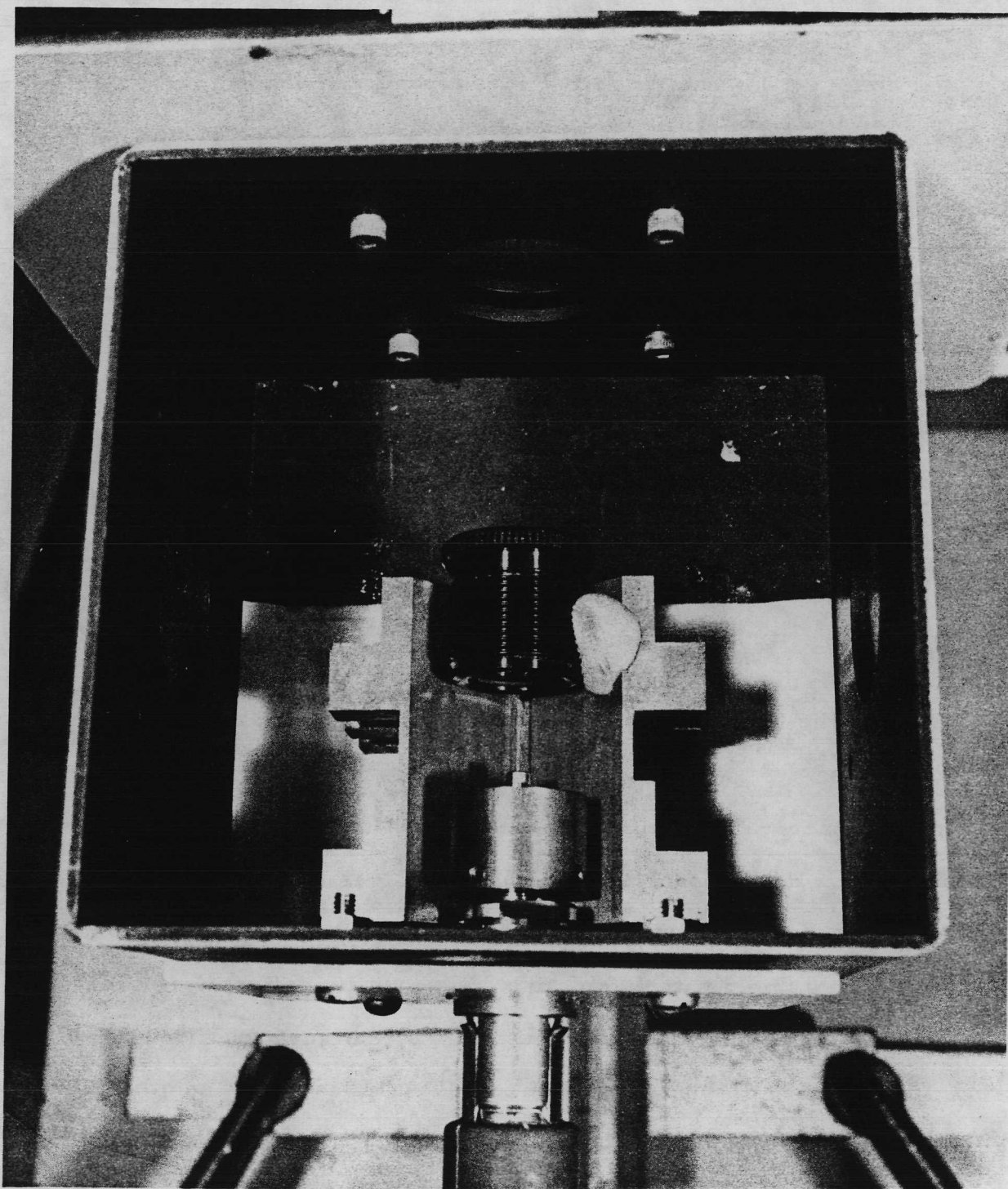


Figure 9-9. Gallium-Aluminum-Arsenide Diode Laser Mount. The Laser, an RCA TA7867, is Mounted in a Cylindrical Copper Block. A  $49.8\ \Omega$  Terminating Resistor is Installed Inside the Center Hole of the Block, in Series With the Center Conductor of the Diode.

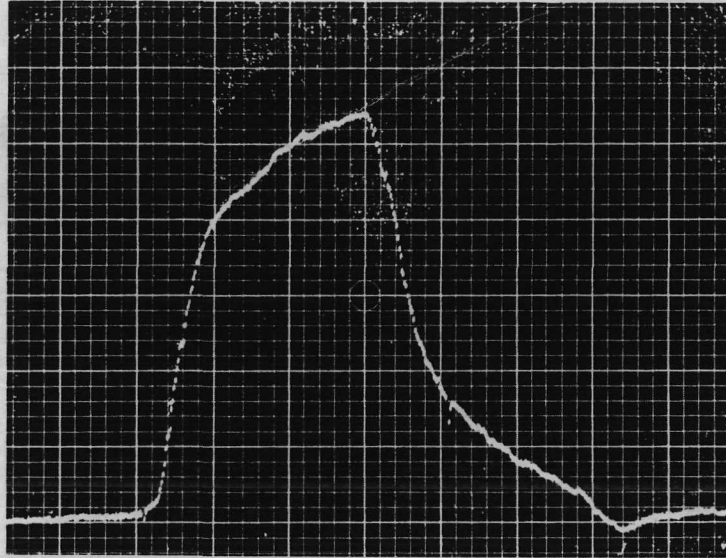


Figure 9-10. Sampling Oscilloscope Trace of the Electrical Pulse Driving the Diode Laser. The abscissa is 1 ns/major division, and the ordinate is 100 volts/major division.

Extreme care was taken in the connection of the output signal cable to the PMT socket. Hard copper shielded  $50\Omega$  coax was used, with the shield ending 3 mm from the pins on the tube socket. The last two dynodes were connected to the coax shield with 100 pf high frequency capacitors\*, in order to maintain some semblance of a transmission line configuration through the tube socket. (The C31034 is supplied with internal strip leads between the anode/last dynodes assembly and the tube socket pins. This arrangement improves

---

\*Microwave ceramic capacitors with metal strip leads supplied by the American Technical Ceramics Co., Huntington Station, New York.

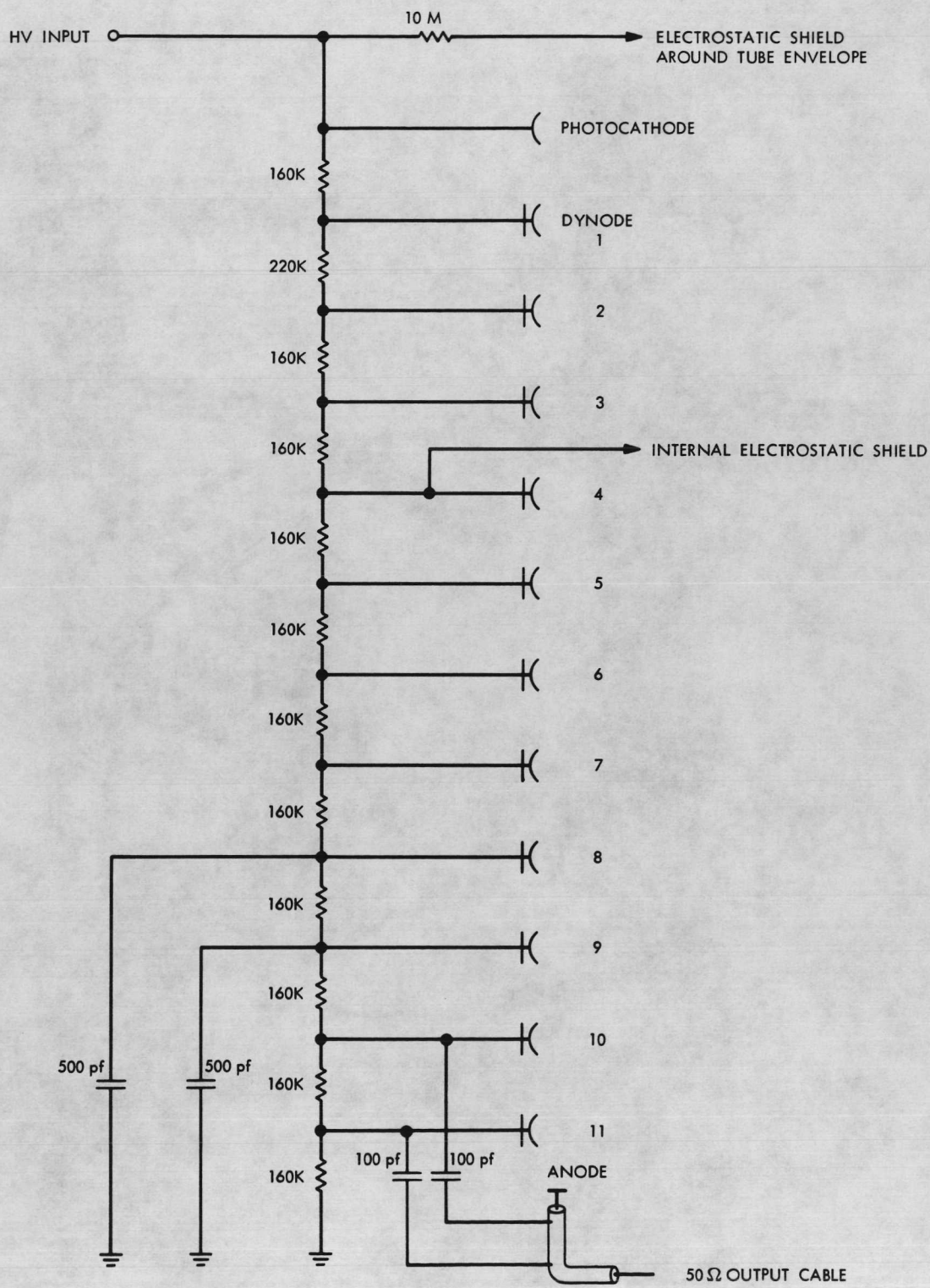


Figure 9-11. Photomultiplier Tube Socket Wiring Schematic.  
The tube is an RCA C31034.

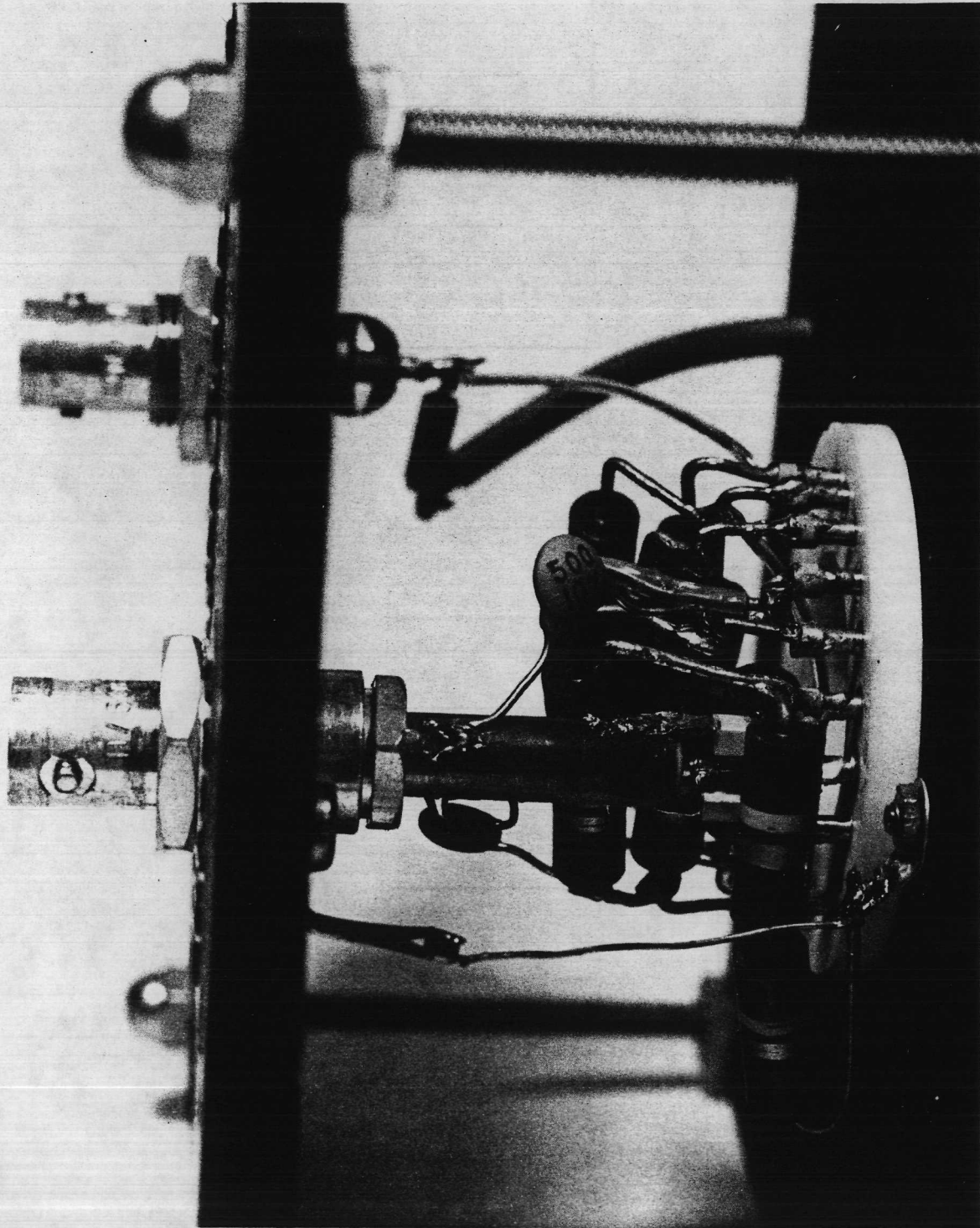


Figure 9-12. Close-Up Photograph of the Photomultiplier Tube Socket Wiring, Showing Details of the Output Cable Connection to the Tube Socket Pins.

the high frequency characteristics of the tube.) Electromagnetic interference from the pulse generator was minimized by placing a block of Eccosorb in the PMT housing.

A time domain reflectometer was used to check the tube/socket assembly for mismatches on the signal output cable. The result is displayed in Figure 9-13. The strip line inside the PMT appears to have a  $75\Omega$  characteristic impedance.

Improvements could be made in the PMT wiring. RCA suggests that the dynode voltages can be modified to provide improvement in the saturation characteristics at large pulse amplitudes. A matching network could be placed between the tube socket and the  $50\Omega$  output cable, to provide a better match to the internal strip line, or the external cabling and circuitry could be changed to a  $75\Omega$  characteristic impedance. No serious problems in the operation of this demonstration laser ranging system were encountered, therefore no attempt was made to include these improvements into the system.

#### 9.4.4 Constant Fraction Timing Discriminator

The constant fraction timing discriminator is basically an active pulse shaping network. It produces a constant shaped output pulse, independent of the shape of the input. The discriminator is intended for use with scintillation and other particle detectors in timing systems for nuclear instrumentation, but is ideally suited for this present application. Its main function is to prevent the stray, low amplitude PMT output pulses caused by background and dark current from triggering the timing electronics. The discriminator must do so in such a manner that it does not introduce any undesirable delay variations of its own. The device has the built in ability to correct for input pulse height variations, greatly reducing the "walk" error.

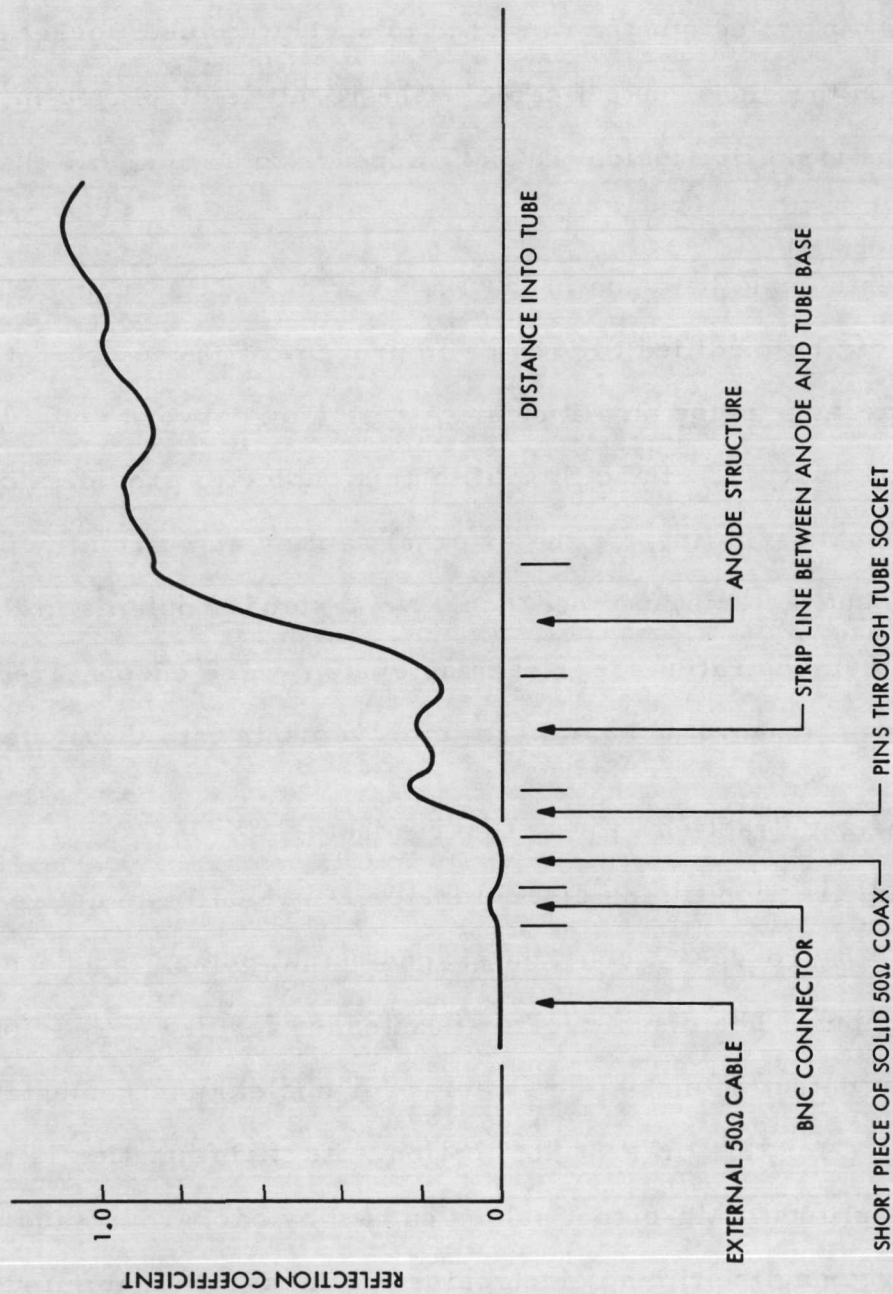


Figure 9-13. Time Domain Reflectometer Display of the PMT Output Circuit. The various sections of the trace are identified by the part designation. The abscissa is distance along the structure (scale undefined), and the ordinate is the reflection coefficient, 0.2/division.

The constant fraction timing discriminator used for this series of experiments was the ORTEC model 463. Its salient characteristics are summarized in Table 9-6.

Table 9-6. Constant Fraction Discriminator Characteristics

Manufacturer:	ORTEC, Inc. 100 Midland Road Oak Ridge, Tenn. 37830
Model No.:	463 - Constant Fraction Discriminator
Input:	Accepts negative pulses to 10 V without saturation
Dynamic Range:	Walk error less than $\pm 150$ psec for a range of 100 mv to 10 v
Output:	NIM Standard fast negative output signal
Cost:	\$550.00

#### 9.4.5 Experimental Results

The demonstration laser ranging system was used to study the performance of the photomultiplier tube and timing system with signal levels similar to those expected in an operational laser ranging system. The response of the photomultiplier tube to pulses of different amplitude was studied, and the absolute accuracy and random errors of a complete ranging system were investigated.

##### 9.4.5.1 Photomultiplier Tube Response

The shape and time of arrival fluctuations of the electrical pulses out of the RCA C31034 PMT were studied by recording the pulse shapes on a sampling oscilloscope as a function of the intensity of the optical pulse reaching the photocathode. Figure 9-14 is a photograph of a typical sampling oscilloscope trace of signal from an RCA C31034 PMT. The particular PMT used, serial number Y07716, produces a 10 millivolt output pulse from one photoelectron when the operating potential is 2000 volts. The trace in Figure 9-14 is 1.4 volts at the peak and has a duration that is similar to the single photoelectron response shown in Figure 9-2. The assumption is made that the peak of the transient scales linearly as the number of photoelectrons in the signal.\* The signal was produced by 140 photoelectrons, or assuming 10% quantum efficiency, 1400 photons. This number checks with the calibration data of the laser and the filters used to attenuate the signal.

Figure 9-14 can also be used to estimate the transit time dispersion. Since a sampling oscilloscope was used to obtain the photograph, the resultant

---

\*The justification for this assumption is based upon the fact that the duration of the laser pulse, 3 ns, is less than the impulse response of the PMT, including transit time dispersion. Thus almost all the photoelectrons and their secondaries reach the PMT anode in a time that is less than the single photoelectron impulse response time.

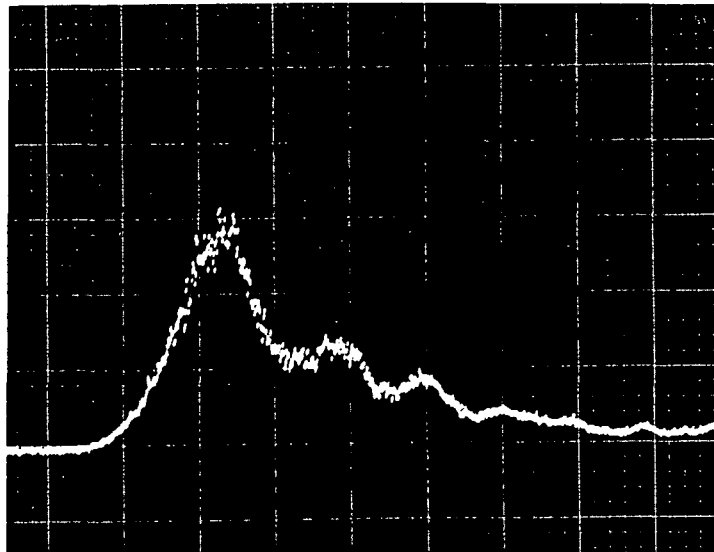


Figure 9-14 Sampling oscilloscope trace of the electrical signal from an RCA C31034 PMT. The optical pulse from the laser was 3 ns long, and approximately 1400 photons reached the photocathode. The abscissa is 2 ns/major division, and the ordinate is 0.5 v/major division.

trace is effectively an average of many pulses, 140 per major division. The time spread in the leading edge of the pulse at the half peak value is approximately 0.2 ns. The transit time dispersion has a Poisson distribution, and if the 0.2 ns is assumed to be a  $3\sigma$  limit, then the standard deviation of the transit time is approximately 0.068 ns.

Similar data was taken for several different signal levels, with the result plotted in Figure 9-15. The standard deviation of the response time dispersion is 0.1 ns at a signal level of 100 photoelectrons. This is an acceptably small response time variation, and will not contribute significant errors to a range measurement. The minimum acceptable signal should produce at least 100 photoelectrons at the PMT photocathode.

#### 9.4.5.2 Experimental Ranging System Accuracy

The entire experimental apparatus, as shown in Figure 9-6, was used in conjunction with a Hewlett-Packard (HP) 5360A/5379A high resolution time interval meter to determine the overall system accuracy. The optical signal levels were adjusted to correspond to those expected in an operational system, with 100 photoelectrons/pulse being the standard acceptable signal level.

The HP 5360A/5379A time interval meter was used in conjunction with another HP accessory, the HP 5375A keyboard, which gives the time interval meter the capability to perform some computations from an internally stored program. The unit was programmed to calculate the mean value and standard deviation of a successive series of time interval measurements from the ranging experiment. The number of samples in the ensemble could be set to any of the following numbers: 1, 10, 100, 1000, or 10,000.

The program presents the result in distance, rather than time. The value for the speed of light that is used,  $2.997141 \times 10^8$  m/sec, is for dry air at

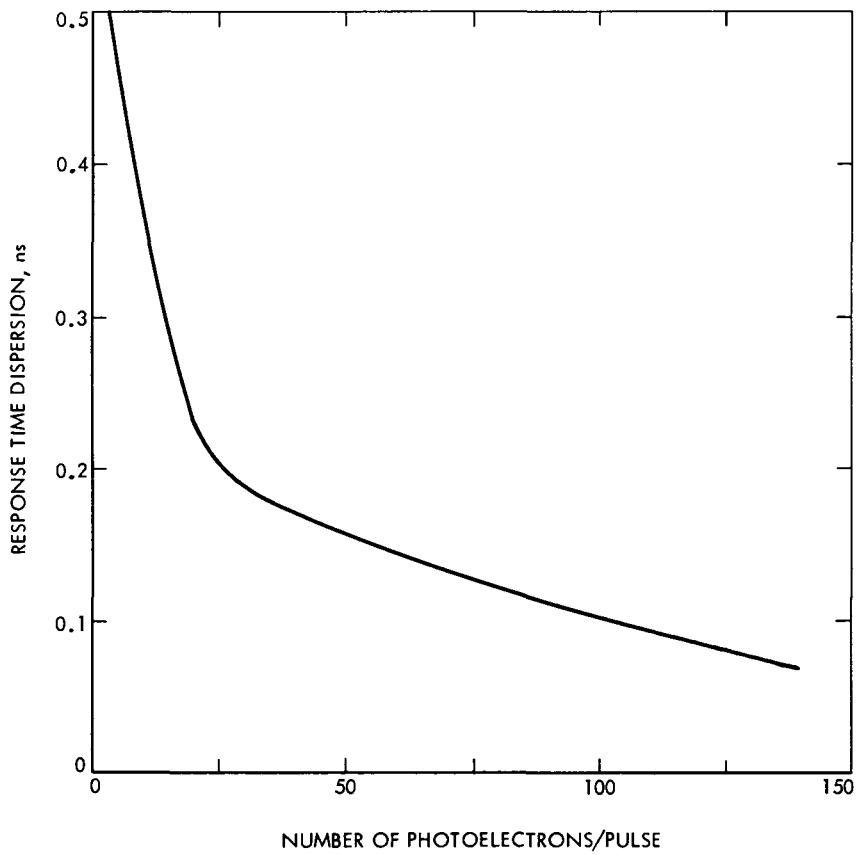


Figure 9-15. Variation of the Response Time of an RCA C31034 PMT with Signal Level. The PMT was Operated with a Divider Network Shown in Figure 9.11, and a Supply of 2000 Volts.

mean temperature and pressure that exists at the test range used for these measurements. The correction for changes in atmospheric conditions is negligible because of the short ranges used, typically less than 50 meters.

The measured values of mean range and standard deviation are presented in Table 9-7, for various values of range and for different signal levels. The range was adjusted by placing the cube-corner-retroreflector at three different distances from the apparatus. Each distance was carefully measured with a tape measure. The signal levels were adjusted by inserting neutral density filters in front of the PMT and/or in front of the nearby mirror. The amplitude of the start and stop pulses could thereby be adjusted independently.

The results indicate that the system was capable of measuring the range to within an accuracy of 20 mm, provided the start and stop signals were the same size and contain at least 100 photoelectrons. The standard deviation of the measurements indicates that random errors in the system are no larger than expected. The data for the longer ranges shows an increase in the standard deviation above the 20 mm level. This is due to severe atmospheric turbulence effects, caused by the optical path being too close to the ground surface, and was further complicated by the small diameter receiving aperture. A larger diameter receiving aperture would materially reduce this effect. It is pointed out in Paragraph 8.5 that atmospheric turbulence effects for reasonable elevation angles are of the order of 10 mm or less.

There is an error which occurs when the start and stop pulses are not the same size. This error has been traced to the ORTEC Constant Fraction Discriminator in our experimental setup. Subsequent tests of it indicate that it does in fact make such errors, which were reduced further by performing the so-called "walk" adjustment. Further research will be required with constant

Table 9-7 Experimental Ranging System Accuracy

Actual Distance m	Measured Distance m	Standard Deviation mm	Number of Data Points	Signal Levels No. of Photoelectrons	
				Start	Stop
23.695	23.691	16	3000	200	200
23.695	23.692	23	4000	100	100
23.695	23.696	25	400	60	60
23.695	23.668	25	4000	200	100
23.695	23.637	50	400	100	50
23.695	23.658	70	500	60	30
44.600	44.580	20	400	120	100
44.600	44.526	30	400	120	40
59.684	59.646	40	400	120	100
59.684	59.623	30	400	170	130
74.314	74.283	30	400	150	50-200*
74.314	74.261	50	400	70	50-80*

\*Return signal levels variable due to atmospheric turbulence effects.

fraction discriminators in order to verify that such devices can function properly without introducing appreciable errors.

## 9.5 Transportable Laser Tracking Station

The basis for the entire concept of precision determination of interstation distances and coordinates is a transportable laser station capable of accurately measuring the range to a cube corner bearing Earth satellite. This section discusses the requirements that a suitable station must meet, and describes a station in moderate detail. A cost estimate for development and procurement of a network of these stations is presented.

### 9.5.1 System Range Equation

Utilizing the standard communication range equation [9.4], with appropriate corrections for the laser beam angle [9.10], the useful energy at the photomultiplier photocathode is defined by Eq. (9.5.1), as

$$N = \left(\frac{\pi}{4}\right)^4 \frac{\lambda D_d^2 D_r^2}{hc\theta_t^2 \theta_r^2 R^4} \eta_t \eta_a^2 \eta_r \eta_d \eta_q P_t \quad , \quad (9.5.1)$$

where the various terms and their units are presented in Table 9-8, and suitable values for these various terms are also listed. Substitution of the typical values into Eq. (9.5.1) yields

$$N = 814 \text{ photoelectrons.}$$

This is a sizable signal. Note that one of the design criteria is that the return pulse should contain at least 100 photoelectrons. The system could operate at a range of 1.7 Mm and still have a suitable return.

Table 9-8 Description of Terms and Typical Values for Equation (9.5.1)

Term	Description and Units	Typical Value
N	Number of photoelectrons liberated from the PMT photocathods	--
$D_d$	Receiving aperture diameter (meters)	0.5
$D_r$	Retroreflector diameter (meters)	0.05
R	Slant range (meters)	$10^6$
$\lambda$	Laser operating wavelength (meters)	$0.694 \times 10^{-6}$
hc	Product of Plank's constant and the speed of light (meter-joules)	$1.986 \times 10^{-25}$
$\theta_t$	Transmitted beam divergence angle at the half power points (radians)	$\frac{10^{-3}}{\sqrt{2}}$
$\theta_r$	Retroreflector return beam divergence angle at the half power points (radians)	$\frac{10^{-4}}{\sqrt{2}}$
$\eta_t$	Transmitter optics efficiency	0.8
$\eta_a$	Atmospheric transmission efficiency	0.7
$\eta_r$	Retroreflector efficiency	0.5
$\eta_d$	Receiving optics efficiency (including filter)	0.25
$\eta_q$	Detector quantum efficiency	0.10
$P_t$	Energy of transmitted pulse (Joules)	0.5

It is thus clearly feasible to obtain reasonable signal returns with a modest system (1/2 joule pulses, 50 cm collecting aperture).

#### 9.5.2 Tracking Mount Description

The basic specifications for this assembly are that it be capable of tracking an Earth orbiting satellite in a 500 km or higher orbit, with full sky coverage to 20° elevation angle and an accuracy of  $\pm 0.5$  milliradian. The optical package includes 50 cm diameter receiving optics and a 4 cm diameter transmitting optics. Special requirements include the need to be fully automated for unmanned operations and the need to be transportable to remote stations with a minimum setup time and installation crew.

The ground station that best meets the above requirements as well as the criteria of minimum cost is described as follows. An X-Y mount will be placed on air ride shock absorbers in a specially built trailer. The trailer will also contain all of the laser equipment and control electronics required to operate in remote locations. The basic concept is that special pads would be prelocated and aligned at remote sites; the trailer would then be brought to the location and lowered onto the special pads, thus requiring only minimum alignment prior to operation. The basic power source would be commercial power or independent generators.

The tracking mount will be an X-Y configuration with the X axis aligned with the trailer. Several types of mount configurations were studied, AZ-EL and polar mounts have gimbal-lock problems to get the required sky coverage and fork type X-Y mount has no advantages since bearing errors are not a severe problem.

The basic structural element for this mount will be standard 20 inch thin wall, seamless steel pipe. Major assemblies will be welded and stress relieved. Axis bearings will be ABEC class 5 which are available at a reasonable cost. The major assemblies will be insulated to minimize the thermal deflection errors.

The axis of the mount will be driven directly with DC torque motors of 50 lb-ft capacity ( $6.8 \times 10^8$  dyne-cm). Axis rates are low because of the X-Y configuration, only  $1^\circ/\text{sec}$  velocity and  $0.02^\circ/\text{sec}^2$  acceleration. The servo electronics will consist of a control chassis which will be integrated with the station computer and a drive power amplifier. Current, rate, and position feedback loops will be closed to insure the stability of the mount and to minimize the tracking error.

To provide digital readout of axis position an encoding system will be geared to each axis. Although some angular errors are introduced by this technique, there is considerable cost savings over a direct shaft encoding system. The encoder type selected will be geared 36 to 1 with the axis, the resolution will be  $0.001^\circ$  and the accuracy equal to  $0.005^\circ$ . Gearing errors will be less than  $0.003^\circ/\text{axis}$ .

Receiving optics will utilize a 50 cm diameter f-2 reflector with a detector package mounted at the prime focus. A flip mirror will be utilized to provide a Newtonian visual system for alignment purposes. The mirror materials will be standard, there is no apparent advantage to use replica or aluminum mirrors. The laser assembly will be stationary off the X-axis and a series of four mirrors will be provided to transmit the output beam up to the Y-axis. Field alignment equipment will be provided to verify the parallelism

of the output beam and the receiver optics. Figure 9-16 shows a diagram of the optical paths in the mount. The start pulse path would be provided by a fibre-optic bundle, with appropriate attenuation to control the amplitude of the start pulse. Figure 9-17 is an artist's sketch of the optical mount assembly.

The pointing accuracy of the tracking mount is calculated by taking the root of the sum of squared peak values of the independent error sources. Table 9-9 presents the significant error sources. The  $3\sigma$  value of the peak errors listed is 42 arc sec. On the basis of engineering analysis of the proposed mount design the principal error sources will be: axis orthogonality, mount alignment and the encoders. These errors could be reduced by increasing the cost of the mount, but it is felt that the present design is a satisfactory balance between cost and performance. Some reduction can also be achieved by calibration of systematic errors and programming corrective offsets into the pointing computer. This programming complexity is not costed and the error calculation in Table 9-9 assumes no compensation.

### 9.5.3 Return Pulse Detection System

The detector assembly mounted at the focus of the 50 cm collecting optics must incorporate a shutter, narrowband interference filter, photomultiplier tube, and pulse discriminating electronics.

The shutter is provided to prevent scatter light from the transmitted pulse from reaching the PMT. It must be a fast acting, electromechanical unit which opens a millisecond or so after the transmitter has fired.

The narrowband interference filter is provided to permit day time operation of the system. The bandwidth should be less than 1 nm, and it should have a peak transmission of at least 50% (such filters are readily available).

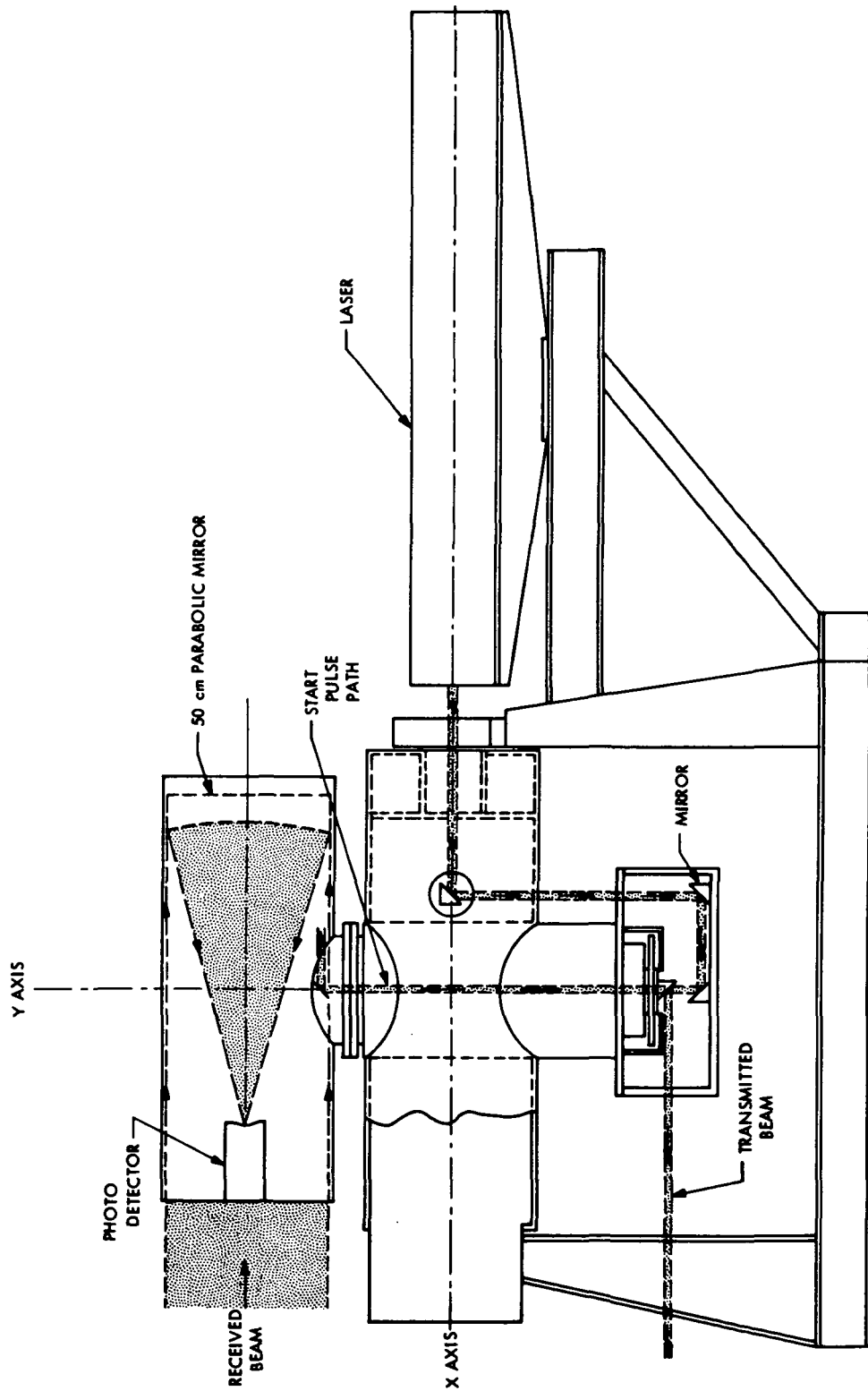


Figure 9-16 Diagram of the major optical components in a proposed transportable laser ranging system. The mount is an X-Y type.

C3

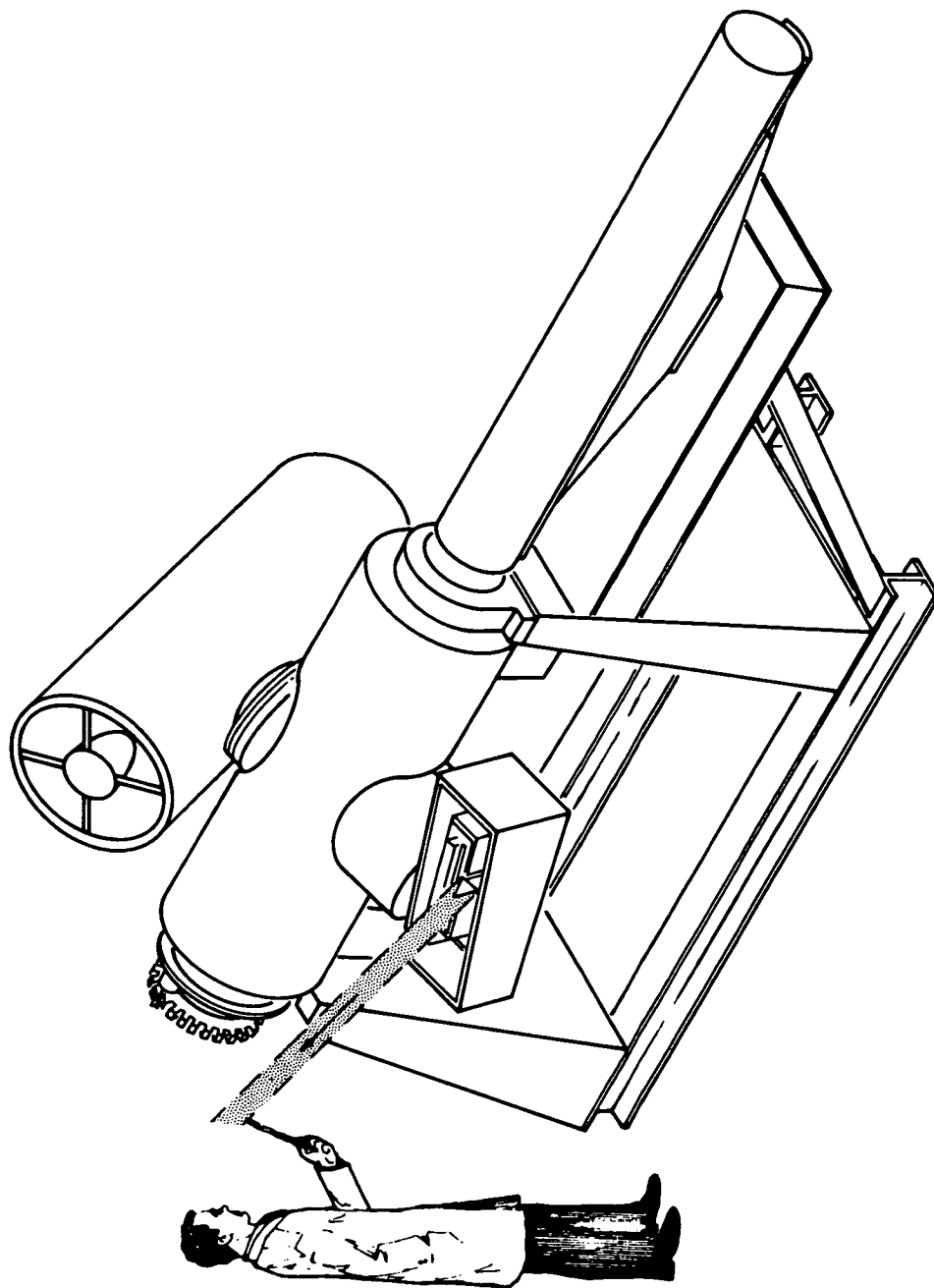


Figure 9-17 Artist's sketch of the optical mount assembly  
diagrammed in Figure 9-16.

Table 9-9. Tracking Mount Errors

Error Source	Type	Peak Value (Arc Sec)
1. Telescope Tube def.	Systematic	0.9
2. Y-Axis bending	Systematic	3.0
3. Y-Axis bearing def.	Systematic	1.0
4. X-Axis Torsion	Systematic	0.9
5. Y-Axis Bearing Runout	Random	7.7
6. X-Axis Bearing Runout	Random	3.3
7. Orthogonality	Systematic	20.0
8. Temp. Gradient in Telescope Tube	Random	6.0
9. Temp. Gradient in Base Legs	Random	2.0
10. Y-Axis Encoders	Systematic	18.0
11. Y-Axis Encoder Gearing	Random	10.0
12. X-Axis Encoders	Systematic	18.0
13. X-Axis Encoder Gearing	Random	10.0
14. Mount Alignment	Random	20.0

The photomultiplier tube should be one of the new Quanticon type (see Paragraph 9.3.1), in order to utilize their enhanced sensitivity at the ruby laser wavelength. Special care must be taken with the design of the PMT circuit, in order to provide an optimum match between the output of the tube and the external electronics. The circuit design also must prevent gain saturation in the PMT for large amplitude pulses.

The last component of the detection system is the pulse height discriminator. This device is used primarily to discriminate between PMT output pulses that are caused by the return signal, and pulses caused by dark current and background radiation. The unit's output is a standard NIM fast negative

pulse, and occurs only when the input pulse has exceeded a preset height, presumably determined by the background and dark current levels.

As discussed in Paragraph 9.4.4, this unit must introduce no variable delay of its own. The so-called constant fraction pulse height discriminator is designed to prevent the most common such variable delay, that caused by different amplitude signals. Although the constant fraction discriminator used in the experimental part of this program did not perform entirely satisfactorily, it is felt that such units can be constructed.

#### 9.5.4 Laser

The type of laser to be used in this ranging system is clearly very necessary to the operation of the system. The laser must emit optical pulses that are of very short duration: 100-200 picoseconds. The mode-locked, Q-spoiled ruby laser discussed in Paragraph 9.2.1 fulfills this requirement, and has enough energy in each pulse to permit the use of modest size cube-corner retroreflectors and receiving apertures.

At the present time, the KORAD Department of Union Carbide Corporation is the only laser manufacturer that claims to have such lasers "off the shelf". There are many other manufacturers of pulsed ruby lasers, and these should be contacted if there is an interest in pursuing this multilateration concept.

#### 9.5.5 Laser Ranging System Transporter

A special purpose trailer is included as part of the ground station. Although transportability was not a prime requirement of this preliminary design, it was felt that the most cost effective solution to the various problems of transport, on-site set-up, electronic equipment housing, and protective covers could be solved with this special trailer. An artist's sketch of the assembly is shown in Figure 9-18.

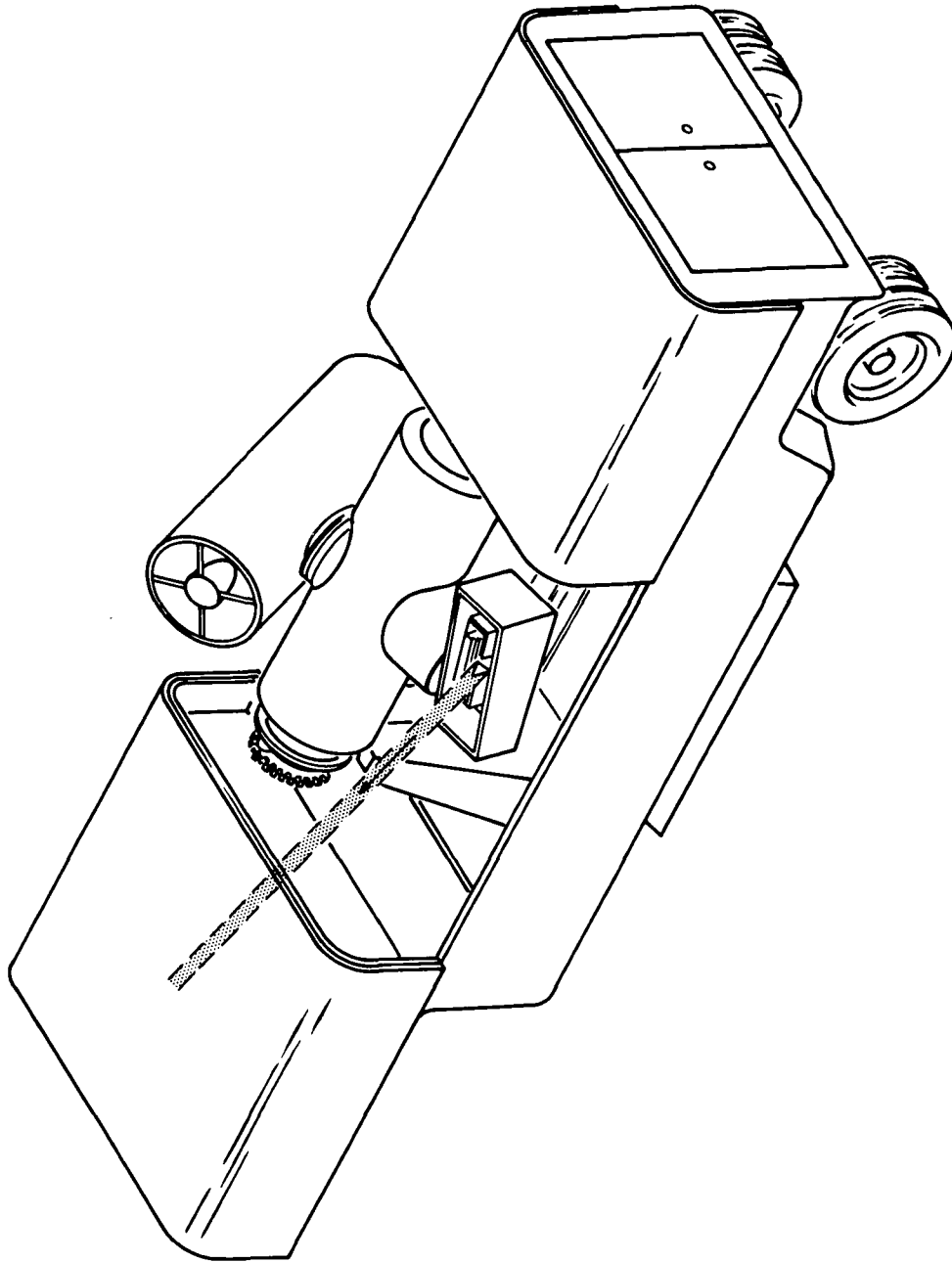


Figure 9-18 Artist's sketch of a complete transportable laser ranging system, showing the optical mount in its transporter. The transporter is positioned over a concrete pad and the mount is lowered onto alignment pins. The transporter contains all the necessary station electronics, but does require an external power source.

The mount and laser assembly will be carried in the trailer on air ride shock absorbers to minimize the shock of highway transport. On arrival at a ground station the trailer will be positioned over a specially designed concrete foundation. The foundation will have 3 pre-aligned register pins which mate with the base of the X-Y mount. The mount is lowered onto the register pin by deflating the air ride shocks. After the mount is set on the pins only a small amount of alignment verification tests will be required.

The trailer will be equipped with a roll-back type of cover which is removed when the mount is in use. This type of cover is not as effective a thermal shield as a telescope type astrodome, but is a much more practical solution to this problem.

The trailer also contains the space for the electronics and the laser power supplies. Also provided is the equipment air conditioning for the four racks of equipment.

#### 9.5.6 Laser Ranging System Block Diagram

A block diagram of the ground station is included as Figure 9-19. A small general purpose computer is used to run the station; including angle pointing, laser control, station monitor, data storage, range gating and many other requirements.

It is planned that with an absolute minimum of information, such as the orbit parameters and laser firing times, the station could complete a mission automatically. The minimal input/output data is necessary because of the assumed poor quality of land communications to remote sites.

The final sizing and configuration of the computer and its peripheral equipment will depend on the monitor and control requirements, which in turn

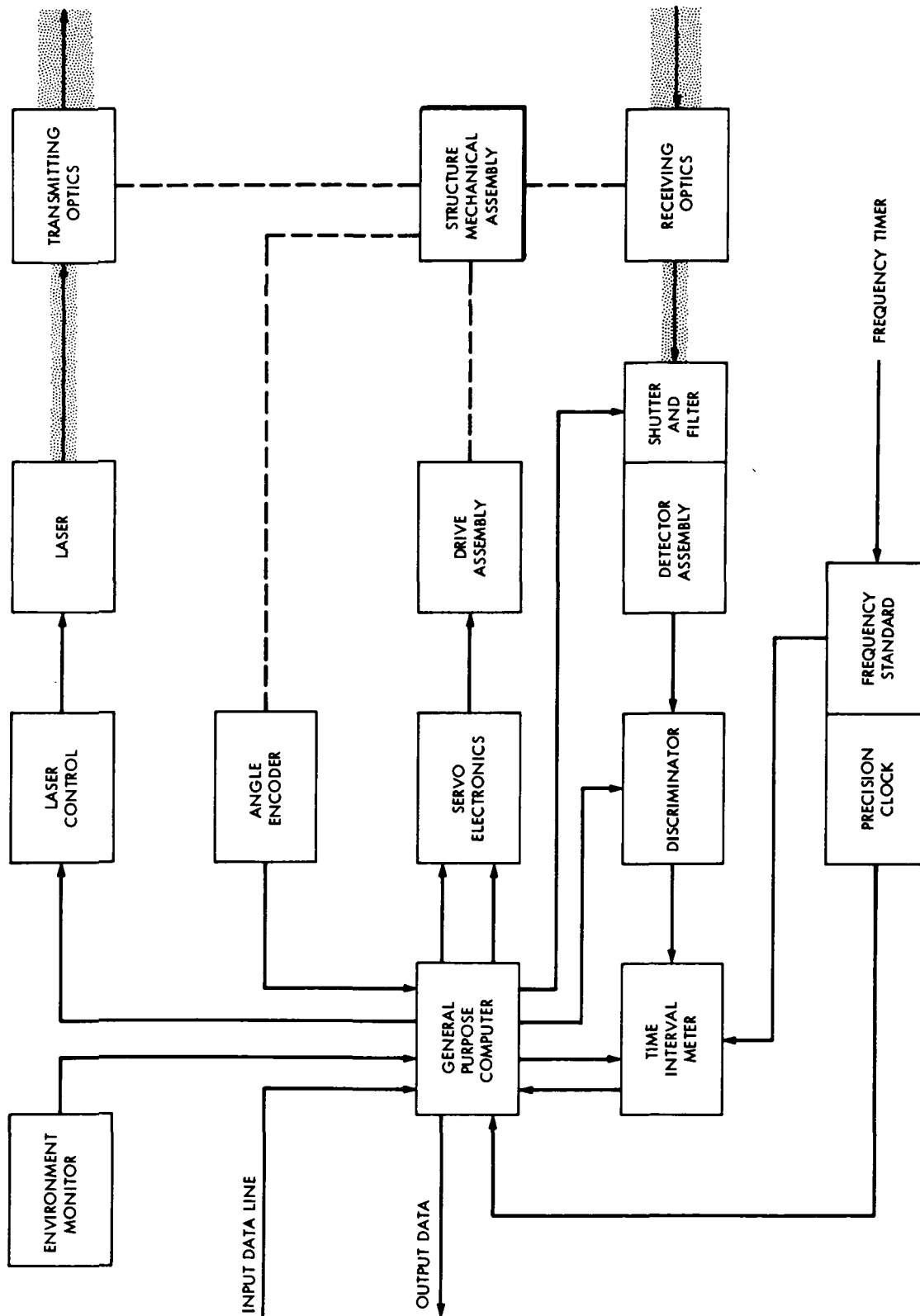


Figure 9-19 Block diagram of a transportable laser ranging station.

are dependent on the requirements and desirability of unmanned operations. For the purpose of this estimate a small computer with 10K of memory was used as a baseline.

The frequency and timing equipment is dependent on where the stations will be used. The network requirements are that the four station clocks of a network be synchronized within 10 microseconds and the network be synchronized to Universal Time within a few milliseconds.

Two clock synchronization systems are available. The first is the best and the least expensive, it depends on being within range of a commercial television station. Currently the NBS is broadcasting on the west coast for 4 hours/day; a 1 megahertz signal and a time code as part of an experimental program called the TV line-10 system. This system will provide a clock synchronization of 1 to 2 microseconds as well as a digital time code. By using this system crystal oscillators can be used at the sites.

If the sites are not within range of a TV station then a rubidium frequency standard should be provided at each site. Also a master clock will have to be circulated among the sites on a weekly basis to maintain the 10 microseconds synchronization; the drift rate of a rubidium being about 1 microsecond/day.

As part of the station equipment a remote weather station is included to monitor wind velocity and direction, ambient temperature, atmospheric pressure, and humidity. These parameters will be digitized and stored in the computer for remote readout.

#### 9.5.7 Cost Summary

A cost summary for construction of a six station network of transportable laser ranging stations was prepared. The costs are broken down into three

areas: design, station equipment, and network support. The design cost presumes that commercial drawing and documentation practices are adequate, rather than the more elaborate JPL/NASA standards. The mount, laser, and equipment costs make no assumptions about quantity discounts. It is felt that the cost estimates are reasonable and possibly conservative.

A network of six stations could be designed and constructed for a total cost of \$1.85 million. This figure does not include site preparation costs. No attempt has been made to estimate the yearly cost associated with the operation of this network. This figure is very subjective at this time, depending upon the total number of sites necessary for geophysical significance, the ease of remote automatic operation, etc.

Table 9-10 presents the design cost estimate, broken down into the man-months required. Table 9-11 summarizes the cost of equipment and assembly for one complete station. Table 9-12 is an estimate of the equipment costs associated with support of the six station network.

Table 9-10 Design Cost

Item	Engineering	Drafting
Mount	3 mm	6 mm
Optics	1 mm	
Servo	4 mm	4 mm
Encoders	1 mm	1 mm
Trailer	1 mm	1 mm
Foundation	1 mm	2 mm
Alignment	2 mm	
Programming	3 mm	
Total Man months	<u>16</u>	<u>14</u>
Total Cost	\$100K	

Table 9-11 Equipment Cost

Item	Cost
Mount	\$50K
Optics	\$15K
Servo	\$13K
Encoders	\$ 7K
Trailer	\$25K
Foundations	\$10K
Assembly	\$25K
Freq and Time	\$20K
Computer	\$20K
RCVR etc.	\$10K
Laser	\$55K
	<hr/>
	\$250K
Contingency 10%	\$25K
	<hr/>
	\$275K/Station
Total for 6 stations	\$1.65M

Table 9-12 Network Support Equipment

Item	Cost
Transportable Primary Time Standard	25K
Alignment Equip.	10K
Test Equip. and Special Tools	15K
Spare Parts	50K
	<hr/>
Total	100K

## SECTION X

### RECOMMENDATIONS AND FUTURE ACTIVITIES

! In the final Section of this report, four areas are discussed; i. e. , the recommended multilateration system is outlined, a tentative future plan of operations is presented, a detailed but brief listing of the future areas of investigation is listed, and some pertinent recommendations are listed. No detailed attempt to plan the future of this project is presented herein; only sufficient information to focus on future activity is detailed. It is felt that the final program plan development is of sufficient magnitude to warrant analysis and is, therefore, more properly included in the advanced systems planning phase (See Paragraph 10.2).

#### 10.1 RECOMMENDED SYSTEM CONFIGURATION

Analysis performed within this report has treated the multilateration problem in a general context. The techniques developed herein can be applied to an arbitrary number of stations ( $\geq 4$ ) and trajectory points. In this section, the practical "minimum" system configurations are examined.

As has been demonstrated in Section VII, in a range-only system, the 4-station/6-trajectory point configuration is a theoretical minimum with respect to the number of stations. On the other hand, no matter how many stations are used, at least 4 trajectory points are still required, with the 6-station/4-trajectory point configuration being the minimum system in this class.

Evidently, the cost of stations is an important consideration in designing a prototype system, whereas, the cost of additional measurements is not. Therefore, the 4-station system would have been the preferred configuration except for the very important fact that the 4-station problem is degenerate when the stations all lie on a plane (the coplanar degeneracy). As a result of this degeneracy, the 4-station system yields very poor sensitivities when stations

are nearly coplanar; this is inevitable if the stations are to be placed on the surface of the Earth over relatively short distances (1000-km or less).

As discussed in Paragraph 7.4 and Appendix B the coplanar degeneracy persists even with 5 stations. Only when 6 stations are used can this degeneracy be removed. Hence, the analysis has dictated the following recommendations.

- Primary Recommendation:—————→6-Station System

This is a general-purpose system which can be made to work with short as well as long baselines. No satellite ephemeris information, beyond that required for aiming the laser beam, need be employed. Excellent sensitivities can be obtained for favorably located stations even if the stations are nearly coplanar. Hence, a 6-station configuration is recommended as the foundation of a workable system.

- Secondary Recommendation:—————→4-Station System

This system works only if stations are separated by large intercontinental distances, with one station located out of the plane defined by the other three by a large distance. Satellite ephemeris information is not required, but the altitude of the satellite must be high enough; i. e., the altitude should be equal (approximately) to the Earth's radius. This will ensure that a sizable portion of the trajectory will be simultaneously visible from all four intercontinentally separated stations. In turn this requires a high-power laser, and ranging at large zenith angles. Good sensitivities are possible if the above requirements are satisfied.

Hence, if the cost of two additional stations is prohibitive, the four-station system is recommended.

- Third Recommendation: —————→ 3-Station, Collinear System

This is a baseline-determination system utilizing three laser ranging stations approximately aligned in a straightline configuration. Due to the alignment requirement, only short baselines, less than 200 km, can be determined. An approximate knowledge of the satellite ephemeris (with an accuracy of about a meter) is needed to calibrate the misalignment error (see Appendix C). Accurate solutions are obtainable for at least one of the baselines.

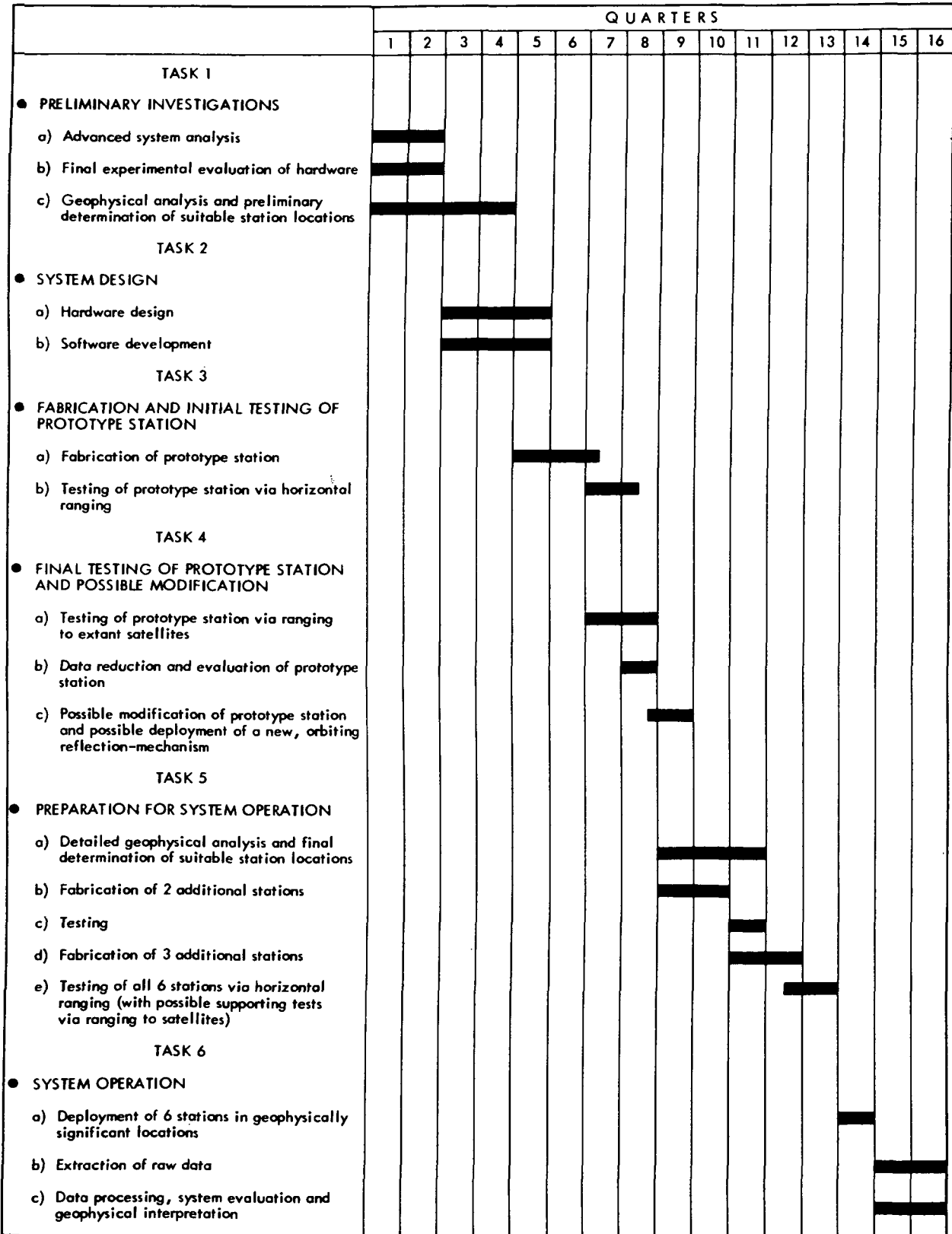
This is a minimum-cost system and is recommended (See Paragraph 10.2) as an interim step in the overall project plan. Certainly, if this system is implemented, the construction of an additional station would be a trivial expense. The fourth station would then permit the 4-Station System to be exercised, etc.

## 10.2 PROGRAM PLAN

A schedule for the development of the proposed laser ranging system is shown on the next page. The schedule indicates the estimated time period (in quarters of a year, starting from the initiation of funding) during which various tasks will be performed.

The first phase of the program will be devoted to advanced investigations. During the first six months, an intensive system analysis will be performed. This analysis will make considerable use of computer simulation, and will resolve all the questions raised in Paragraph 10.3 except those specifically related to hardware. Laboratory tests to evaluate the critical hardware components, e. g., lasers, PM tubes and time-interval meters, will be performed concurrently with the systems analysis. Certain geophysical questions (such as the required

# Project Plan



frequency and accuracy of data measurements, and the selection of suitable station locations\*) will be examined in detail in a sustained, moderate-level effort.

System design will commence in the third quarter and extend through the fifth quarter. Detailed specifications for the hardware complement of a ground station will be developed. Considerable effort will be expended in order to achieve a hardware design which utilizes commercially available components and is of maximum cost-efficiency. A complete software package for the system will be evolved, debugged and finalized. Program efficiency will be emphasized due to the fact that an extremely large amount of data will have to be processed during the operational life of the system.

Fabrication of a prototype station will begin during the latter part of the system-design phase. Any overlap between the fabrication and system design phases will be primarily devoted to procuring those long-lead items already predicated by the system-design study. Fabrication will be completed twelve quarters after the consummation of the system design. The prototype station will then be intensively tested by horizontally ranging to a ground-based retroreflector. Although these tests will suffer from the deleterious atmospheric effects common to all horizontal-ranging systems, they will provide a convenient and inexpensive means for identifying hardware imperfections and estimating overall performance.

---

\*Initial investigations of suitable station locations have already been made, and are described in Section VI.

Final testing of the prototype station will commence in the seventh quarter. The prototype station will be used to track the extant, retroreflecting satellites; these tests will not only provide a considerable amount of extremely-significant performance data, but will also discover possible operational problems (such as difficulties in achieving proper satellite tracking). The data obtained from these tests will then be analyzed in detail so as to determine the statistics of the received-signal power, the severity of atmospheric effects, and -- most importantly -- the fluctuations in measured range due to different pulses being reflected from different corner reflectors on the satellite. An evaluation of system performance will then be made, and, if necessary, appropriate modifications to the system will be specified and implemented. If acceptable system performance is precluded because of the multiplicity of corner reflectors on the satellites, a new orbiting reflection-mechanism will be designed and launched.

Once satisfactory results have been achieved from the prototype station, project effort will be focused on developing a complete operating system. An interesting system test can be performed as soon as three of the stations have been built, i. e., in the twelfth quarter a test of the three station system will be undertaken (possibly with an airplane).

A detailed geophysical analysis to select optimal station locations and the construction of three additional ground stations (identical to the prototype station) will dominate the final quarters of this project. All six ground stations will be tested via horizontal ranging to Earth-based retroreflectors; also, if further evaluation of station performance appears necessary, each station will be tested via ranging to satellites.

The six stations will be deployed in their specified locations during the 14th quarter, and the complete system will be operated for a period of a year. The considerable amount of data resulting from this operation will be processed and examined for geological significance, and a new program plan will be developed to schedule possible modifications and future deployments of the total system.

### 10.3 FUTURE STUDY AREAS

Paragraph 10.2 indicates that the future program plan will commence with an advanced systems study. This study will be necessary to answer some of the details not considered under the present study phase and also to provide a second indenture analysis of some of the topics which were considered only superficially herein. Certainly, the main objective of this study, i. e., to prove the feasibility of the geometric technique, has been accomplished. However prior to implementing the multilateration scheme some further analysis will be required. These areas of investigation are briefly outlined in this Section as study tasks. From the length of the list it is obvious that a sizeable effort will be required to codify the remaining details.

#### Task A-Systems Planning

This will be a planning phase to develop a detailed milestone schedule and to set priorities on the remaining tasks which are defined herein.

#### Task B-Solution Degeneracies

A detailed study of degeneracies which occur when certain station and orbital configurations are assumed will be undertaken. This task which is a logical continuation of Appendix B of the present report, will identify potentially unstable configurations and explicitly define operational rules to circum-

vent these problems. It should be noted that these degeneracies are not fundamental in the prevention of system operation; however, the attainment of maximum system accuracy demands a more detailed understanding of these effects.

#### Task C-Number of Stations and Optimal Deployment

This report has answered the question relative to the number of stations which are theoretically required in order to ensure nominal system operation. The advantages of using more than the minimum number of stations are not however understood. There is a possibility that use of more than the minimum number of stations will result in even more dramatic accuracy improvements than are displayed in Section V. This task will perform the analysis required to answer the question of what additional coordinate accuracies are achievable via the use of more stations. The selection of stations for performing multilateration experiments will also be analyzed on a firm geophysical foundation with much more detail than in Section VI. Once the theoretical configurations yielding optimum accuracy station locations are understood, a proper compromise with the geodetic constraints will be undertaken and an optimum realistic system configuration will be defined.

#### Task D-Error Analysis

Due to pressing project schedules the detailed error mapping of sources affecting station coordinate accuracies was undertaken using Monte Carlo techniques. In this task the explicit covariance mapping of the random error sources, and the effect of system bias errors will be performed.

#### Task E-Use of Range-Rate Data

The use of range-rate data was not considered in this study. A possibility exists that use of this type of data will result in further accuracy

gains. Task 4 would perform this type of analysis and incorporate any resulting advantages into the overall system.

#### Task F-Closed Form Solution

There is theoretical justification to believe that the multilateration equations can be solved in closed form. A solution to these equations in closed form would result in further understanding of the geometric process and in possible system simplification during real time operations. Analysis will be performed in this Task to verify the possibility of obtaining a closed solution to the fundamental equations of the process.

#### Task G-Curve Fit Accuracies

The detailed analysis to determine the maximum duration over which data can be fit to the adopted models will be undertaken in this task. This is a prerequisite to any operational system.

#### Task H-Data Displays

Useful displays of the parameters obtained from the multilateration process will be defined. These displays will aid in the efficient transfer of information and in simplifying system operation.

#### Task I-Pulse Shape Degradation

A detailed study and verification of pulse shape degradation due to multiple reflections will be performed in this Task.

#### Task J-Atmospheric Calibration

An in-depth analysis of the best manner in which atmospheric calibration can be performed in order to minimize measurement errors will be performed (see Paragraph 8.5). This task is central to lowering the total system error budget.

#### Task K-Tracking Analysis

Task K will deal primarily with defining the accuracy which will be required in satellite state estimation for purposes of pointing the laser assemblies. As a function of these accuracies the suitable azimuth/elevation slaving equations will be derived and the respective hardware accuracies will be specified.

#### Task L-Launch Vehicle Analysis

The total retroreflector system weight budget will be specified in this task and a systematic search of possible satellite/launch vehicles which can accommodate the retroreflector package (as an additional mission objective) will be specified.

#### Task M-Airplane Vehicle Analysis

For purposes of interim experiments, the requirements imposed for implementation of Principle 3 (3 station system, Section I) upon suitable aircraft will be outlined. This will include hardware constraints and operational flight path maneuvers to ensure proper system operation.

#### Task N-Three Station Calibration

A detailed analysis of the effect of misalignment in the 3 station system will be performed. This error source was briefly analyzed in the present study. A better understanding of these effects is required.

#### Task O-Inverse Trilateration

The use of the method of inverse trilateration (Appendix D) for determination of new station locations as a function of previously defined station locations will be investigated for possible singularities and the best accuracies attainable in the solutions. The proper recommendations for operational implementation of this technique will be specified.

#### Task P-Generalized Coordinate Systems

An investigation of the use of more generalized coordinate systems (See Section IV) will be performed. This task will be of fundamental importance if comparisons of parameters estimated via geometric and dynamic principles are to be undertaken.

#### Task Q-Comparison of Geometric and Dynamic Techniques

This task will concern itself with the information that can be extracted when residuals in the parameters obtained by means of geometric principles and dynamic principles are computed. There is theoretical justification which shows that certain astrodynamical constants can be calibrated using such methods. These constants would be identified and appropriate conclusions as to their accuracy would be drawn.

#### Task R-Comparison With Other Systems

The final task of the advanced study phase will concern itself with a detailed comparison of the final multilateration system configuration with other competitive systems. Items such as accuracy, cost, ease of implementation, etc. will be tabulated (See Section III).

#### Task S-Software Development

Throughout the duration of the advanced study phase, the development of the software tools required to analyze the measured data will be undertaken.

#### Task T-Documentation

The results of the advanced study phase will be documented in a continuing effort such that at completion of this phase, detailed and final documentation of the multilateration technique will be available. This documentation will include the operational description of the non-real time software developed during this period.

#### 10.4 PROJECT RECOMMENDATIONS

In light of the previous discussion, it is recommended herein that the study phase of this project be continued on a moderate level; i. e. , a funding level of approximately \$80,000 to \$100,000 should be expended during the next study period for continued systems analysis. An equal amount should be utilized to answer hardware-oriented problems. About \$50,000 should be utilized to integrate the hardware and software subsystems, to provide future planning, and to develop appropriate system test plans.

In summary, an effort with funding equal to approximately \$250,000 would ensure continued effort on a system whose ultimate accuracy in the location of station coordinates can be measured in subcentimeter units.

SECTION XI  
REFERENCES

- [1.1] Escobal, P. R., et al., Trilateration Measurement and Position Prediction, Hughes Aircraft Company Data Bank Report No. 1-3883-2, December 1971.
- [3.1] Journal of Geophysics Research, pp. 1493-1505, 1970.
- [3.2] von Roos, O. H., Analysis of Dual Frequency Calibration for Spacecraft VLBI, JPL TR 32-1526, Vol. VI, 1971.
- [4.1] Explanatory Supplement to the Astronomical Ephemeris and the American, Her Majesty's Stationery Office, London, 1960.
- [4.2] Ephemeris and Nautical Almanac, Her Majesty's Stationery Office, London, 1961.
- [4.3] Woolard, E. W., A.P.A.E., 15, Part 1, 1953.
- [4.4] Melbourne, W. G., et al., Constants and Related Information for Astrodynamics Calculations, 1968, JPL Technical Report 32-1306, July 1968.
- [4.5] Escobal, P. R., Methods of Astrodynamics, John Wiley and Sons, 1958, Chapter 8.
- [4.6] Markowitz, W., and Guinot, B., Continental Drift, Secular Motion of the Pole, and Rotation of the Earth, IAU Symposium No. 32, Streso, Italy, 1967, pp. 5-6.
- [4.7] Escobal, P. R., Methods of Orbit Determination, John Wiley and Sons, New York 1965.
- [5.2] Pipes, L. A., Matrix Methods for Engineering, Prentice Hall, Englewood Cliffs, N. J., 1963.

- [5.3] Golub, G. H., Reinsch, C. Handbook Series Linear Algebra, Singular Value Decomposition and Least Squares Solutions, Technical Report CS-133 Computer Sciences Department, Stanford University, May 1969.
- [6.1] Whitcomb, J. H., Placement of 3-D Laser Stations for the Purpose of Strain Monitoring and Earthquake Prediction, Seismological Laboratory, California Institute of Technology.
- [6.2] Pettit, J. T., Slichter, L. B. and LaCoste L., Earth Tides, Transactions American Geophysics Union, Vol. 34, No. 2, April 1953, p. 174.
- [6.3] Griggs, D., Experimental Flow of Rocks Under Conditions Favoring Recrystallization. Bull. of the Geological Society of America, Vol. 51, 1940, pp. 1001-1002.
- [6.4] Earthquake Prediction, A Proposal for a Ten Year Program of Research, Ad Hoc Panel on Earthquake Prediction, Prepared for the Office of Science and Technology, Washington, D. C., Sept 1965.
- [8.1] Hopfield, H. S., "Tropospheric Range Error at the Zenith", Preprint for 14th Plenary Meeting, June 1971, Applied Physics Laboratory, The Johns Hopkins University.
- [8.2] Ondrasik, V. J. and Thuleen, K. L., "Variations in the Zenith Tropospheric Range Effect Computed from Radiosonde Balloon Data", SPS 37-65, Vol. II.
- [8.3] Chao, C. C., "Seasonal Variations in the Tropospheric Refraction Profiles", TM 391-216, 21 July 1971.
- [8.4] Miller, L. F., Ondrasik, V. J. and Chao, C. C., "A Cursory Examination of the Sensitivity of the Tropospheric Range and Doppler Effects to the Shape of the Refractivity Profile", JPL TR 32-1526, Vol. I.

- [8.5] Laser Focus, Vol. 8, No. 5, May 1972, pp. 22-27.
- [8.6] von Roos, O. H., Tropospheric and Ionospheric Range Corrections for an Arbitrary Inhomogeneous Atmosphere, JPL TR 32-1526, Vol. VI, p. 99.
- [9.1] Bender, P. L., private communication.
- [9.2] Fiocco, G., "A Summary of Research with Optical Radars", 20th Annual ISA Conference, Los Angeles, California, October 4-7, 1965, preprint No. 40.1-3-65.
- [9.3] Premo, D. A., "Goddard Mobile Laser System Description", Proc. of the GEOS-2 Program Review Meeting, V. III, pp. 101-114, June 22-24, 1970, NASA Goddard Space Flight Center, Greenbelt, Maryland.
- Lehr, C. G., Pearlman, M. R., Scott, J. L., and Wohn, J., "Laser Satellite Ranging", in Laser Applications in the Geosciences, ed. by J. Gauger and F. F. Mall, Jr., pp. 111-130, Western Periodicals Co., No. Hollywood, California.
- [9.4] Iliff, R. L., "A Laser System for Satellite Geodesy", Report No. AFCRL-70-0614, November 10, 1970, Air Force Cambridge Research Lab, L. G. Manscom Field, Bedford, Massachusetts.
- [9.5] Silverberg, E. C., and Currie, D. G., "A Description of the Lunar Laser Ranging Station at McDonald Observatory", Proc. COSPAR, June 1971, Seattle, Washington.
- [9.6] Nutt, R., private communication.
- [9.7] ORTEC, Inc., Oak Ridge, Tennessee, publication no. AN-35, 1971.

- [9.8] Fischer, E., "Laser Diode Sub-Nanosecond Risetime Source of Radiant Flux for Photodetector Testing", RCA Application Note AN-4553, Radio Corp. of America, Solid State Div., Somerville, New Jersey, February 1971.
- [9.9] Potter, P. D., Shumate, M. S., Stelzried, C. T., and Wells, W. H., "A Study of Weather-Dependent Data Links for Deep Space Applications", Technical Report 32-1392, Jet Propulsion Laboratory, Pasadena, California, October 15, 1969.
- [9.10] Pratt, W. K., Laser Communication Systems, John Wiley & Sons, New York, New York, 1969, p. 6.
- [9.11] Eckhardt, M. D., "Simple Model of Corner Reflector Phenomena", Appl. Opt., V7 No. 10, July 1971, p. 1559.
- [A. I. 1] Jaffe, Richard M., JPL TM 391-218, 28 July 1971, "Signal Strength Fluctuation in a Laser Ranging System Due to Optical Interference Between the Many Reflectors on a Satellite."
- [A. I. 2] Slack, Margaret, "The Probability Distributions of Sinusoidal Oscillations Combined in Random Phase, "Journal of the Institution of Electrical Engineers, Vol. 93, No. 22 (England), pp. 76-86.
- [A. I. 3] Magnus, A. W., Oberhettinger, F., and Soni, R. P., Formulas and Theory for the Special Functions of Mathematical Physics, Springer Verlag, New York, 1966.
- [P. 1] Blaha, G., "Investigation of Critical Configurations for Fundamental Range Networks", Ohio State University Dissertation University Microfilms, Ann Arbor, Michigan, 1971; and other references cited therein.

## SECTION XII

### GLOSSARY

Bouguer Correction: The gravity values at an elevation  $h$  above sea level must be reduced to values at sea level. A number of corrections are therefore necessary. The correction for the effect of the mass in the layer between  $h$  and sea level suggested by Bouguer equals  $-2\pi G\rho h$  and is called the Bouguer Correction. Here  $\rho$  is the mass density and  $G$  the gravitational constant.

Constant Fraction Timing Discriminator: An electronic device to measure the arrival time of a pulse accurately by integrating over its length, and taking a preset fraction of its height, so that the leading edge of the pulse can be determined.

Corner Reflector: An arrangement of mirrors in such a fashion that any light beam will be reflected back independent of the attitude of the mirror system.

Degeneracies: The process wherein the multilateration equations cannot be solved for station coordinates due to geometric or numerical instability in the equations.

Drag: A force opposite to the velocity vector induced on a satellite or airplane due to air viscosity and density.

Dynode: An electron current amplifier in a photomultiplier tube. Electrons are accelerated in an electric field, impinge on a plate (the dynode), and liberate secondary electrons. The gain of a dynode is between 2-3 and there are up to 14 dynodes in a photomultiplier tube. This makes the overall gain equal to  $2^{14} - 3^{14}$ ; a rather respectable amplification.

Eccentric Anomaly: An auxiliary angle defined in terms of the true anomaly via the relationships:

$$\cos E = \frac{\cos v + e}{1 + e \cos v}$$

$$\sin E = \frac{\sqrt{1 - e^2} \sin v}{1 + e \cos v}$$

where E is the eccentric anomaly, v is the true anomaly and e is the orbital eccentricity.

Ecliptic: The plane of the apparent motion of the Earth about the Sun.

Ephemeris: The position and velocity of a celestial body tabulated as a function of some independent variable, say, time.

Epoch: A fixed time origin, i. e. , a starting time.

Equinox: Usually called the equator and equinox, i. e. , the position of the Earth's equatorial plane and the position of some reference axis (x axis) at a given time.

Fault: The surface of fracture between two blocks of rock which have moved relative to one another.

Geodetic Datum: A surface, line, or point, and/or the measurements pertaining thereto, from which geodetic information may be calculated.

Geodolite: The trade name of a commercial laser ranging device used for surveying manufactured by Spectra-Physics.

Geometric Flattening of Earth: A measure of the difference between the polar and equatorial radius of the Earth ( $f \cong 1/298.3$ ).

Gravimeter: An instrument (usually portable) for measuring the acceleration due to gravity.

Laser: Light Amplification by Stimulated Emission of Radiation. A device to generate extremely monochromatic radiation making use of the coherence properties of stimulated emission.

Loran System: An electronic navigational system by which hyperbolic lines of position are determined by measuring the difference in the time of reception of synchronized pulse signals.

Magma Vent: The route by which magma, i. e., molten rock under pressure is extruded through the Earth's crust, e. g., into the neck of a volcano.

Magnetic Lineations: A zebra-stripe pattern of the directions of magnetization in the rock of an ocean floor, generally found to be parallel to a mid-ocean ridge. The existence of this pattern is evidence both of changes in the direction of the Earth's magnetic field and of sea-floor spreading.

Mode Locked: The internal modulation of a laser cavity leads to a radiation field which consists of many modes which are "locked" into oscillations with the same phase.

Nutation: The perturbative effect upon the pole of the Earth caused by the Moon.

Obliquity: Usually called the obliquity of the ecliptic; an angle between the planes of the Equator and Ecliptic ( $\epsilon \cong 23^\circ 5'$ ).

Perigee: Point of closest approach of a satellite to the Earth; when referred to any other planet the corresponding term would be apoapsis.

Plate Tectonics: Theory of: The hypothesis that the uppermost layer of the Earth's crust consists of a mosaic of rigid plates, and that oceanic trenches, continental drift, and at least some types of orogeny (mountain building) can be explained in terms of the relative motion of these plates.

Photodiode: A semiconductor device, i. e. , a p-n junction. Minority carriers created by absorption of light within a diffusion length of the junction may diffuse to the junction and give a photocurrent.

Photomultiplier: An extremely sensitive photon counting device which operates on the principle of the photo electric effect (release of an electron by a photon impinging on a solid state surface). Subsequent current amplification is accomplished by means of the release of secondary electrons.

Primary: The mass about which local motion is occurring, e. g. , the Earth is the Secondary of the Sun (which is Primary) or the Moon is the Secondary of the Earth (which is the Primary); etc.

Pseudo Observation: The observation obtained from raw data after performing mathematical/statistical operations on the raw data.

Q-Spoiled: The Fabry-Perot cavity of a laser ideally has a very high Q. With the help of an electro-optic shutter or passive absorbing shutter, the Q will be considerably lowered to allow a light pulse to escape. The magnitude of Q is a measure of the sharpness of a resonance.

Quartz Oscillator: A very stable electronic oscillator using a quartz crystal to define and stabilize its frequency via piezoelectricity.

Radiation Pressure: Force per unit area exerted by electromagnetic radiation on a surface of a body. Its magnitude is  $(4\pi)^{-1} |\mathbf{E} \times \mathbf{H}|$  which amounts to  $4.46 \times 10^{-5}$  dyne  $\text{cm}^{-2}$  for the Sun's radiation at the distance of the Earth.

Radiosonde: A balloon with attached measurement equipment to measure the temperature and pressure of the troposphere as a function of altitude. The information is telemetered back to ground by radio.

Range Gate: When a number of pulses are transmitted and subsequently received the possibility of confusion arises, i. e. , a pulse which is transmitted may not correspond to a pulse which is received. The range gate is electronically present to the approximate arrival time and therefore rejects all other pulses and allows for an accurate measurement of the time of transit.

Range Residual: Usually the difference between a pseudo observation and the raw data, i. e. , the difference between a nominal range and the raw range.

Range Square Differences:  $\rho_i^2 - \rho_j^2$  where  $\rho_i$  and  $\rho_j$  are slant ranges evaluated at different points (times).

Retroreflector: See corner reflector.

Strain: The process whereby a given material undergoes a change in deformation.

Stress: The forces on a given area which give rise to internal tension or compression.

True Anomaly: The angle, measured in the orbital plane of motion, between a line from the center of mass to perigee (apoapsis) and the position of a satellite.

## APPENDIX A

### COMPUTATIONAL ALGORITHMS FOR GEOMETRIC LASER RANGING

In this Appendix, the detailed computational algorithms are given for the solution of the multilateration equations and the sensitivity equations (See Paragraphs 7.2 and 7.3). For definiteness, the more general algorithms of the six-station configuration are given herein. Specialization to the four- and five-station cases or generalization to more than six-stations can be accomplished easily. The three-station collinear case is discussed in Appendix C.

The input to the solution algorithm is the set of simultaneous slant ranges  $\rho_{in}$ ,  $i = 1, 2, \dots, 6$ ;  $n = 1, 2, \dots, N$ , where  $N$  is the total number of trajectory points used, and the nominal values of the station coordinates, namely,  $(X_2^{(o)}, X_3^{(o)}, Y_3^{(o)}, X_4^{(o)}, Y_4^{(o)}, Z_4^{(o)}, X_5^{(o)}, Y_5^{(o)}, Z_5^{(o)}, X_6^{(o)}, Y_6^{(o)}, Z_6^{(o)})$ . The output will be the set of 12 relative station coordinates,  $(X_2, X_3, \dots, Z_6)$  and, as a by-product, the satellite positions  $(x_n, y_n, z_n)$ ,  $n = 1, 2, \dots, N$ . The sensitivity analysis algorithm, on the other hand, requires as input the positions of the satellite developed from an adopted orbit and the station coordinates, and calculates the magnification coefficients (sensitivity numbers) for the mapping of errors in the range measurements to the errors in each station coordinate. These algorithms are discussed below separately.

#### A.1 The Solution Algorithm

In Paragraph 7.2, the basic idea of the method of solution, namely, the Newton-Raphson method applied to the multilateration problem has been outlined. Starting with the given ranges  $\rho_{in}$  ( $i = 1, 2, \dots, 6$ ;  $n = 1, 2, \dots, N$ ),

and the nominal values of the station coordinates  $(X_2^{(o)}, X_3^{(o)}, \dots, Z_6^{(o)})$ , the computation proceeds as follows:

- a) Calculate the range-square differences:

$$\delta_{in} = \rho_{in}^2 - \rho_{1n}^2, \quad i = 2, 3, \dots, 6; \quad n = 1, 2, \dots, N.$$

- b) Calculate the nominal satellite coordinates ( $n = 1, 2, \dots, N$ ):

$$x_n^{(o)} = \left( X_2^{(o)2} - \delta_{2n} \right) / \left( 2X_2^{(o)} \right)$$

$$y_n^{(o)} = \left( X_3^{(o)2} + Y_3^{(o)2} - 2x_n X_3^{(o)} - \delta_{3n} \right) / \left( 2Y_3^{(o)} \right)$$

$$z_n^{(o)} = \left[ \rho_{1n}^2 - x_n^{(o)2} - y_n^{(o)2} \right]^{1/2}$$

- c) Calculate the following partial derivatives evaluated at the nominal values of the parameters. Note that the superscript  $(o)$  for "nominal" is heretofore suppressed:

$$\frac{\partial x_n}{\partial X_2} = \frac{X_2 - x_n}{X_2}$$

$$\frac{\partial y_n}{\partial X_2} = \frac{-X_3}{Y_3} \left( \frac{X_2 - x_n}{X_2} \right)$$

$$\frac{\partial z_n}{\partial X_2} = \left( \frac{-x_n}{z_n} + \frac{y_n}{z_n} \frac{X_3}{Y_3} \right) \left( \frac{X_2 - x_n}{X_2} \right)$$

$$\frac{\partial y_n}{\partial X_3} = \frac{X_3 - x_n}{Y_3}$$

$$\frac{\partial z_n}{\partial X_3} = -\frac{y_n}{z_n} \left( \frac{X_3 - x_n}{Y_3} \right)$$

$$\frac{\partial y_n}{\partial Y_3} = \frac{Y_3 - y_n}{Y_3}$$

$$\frac{\partial z_n}{\partial Y_3} = -\frac{y_n}{z_n} \left( \frac{Y_3 - y_n}{Y_3} \right).$$

- d) Calculate the  $3N \times 12$  matrix  $P(m, k)$  ( $m = 1, 2, 3, \dots, 3N$ ;  $k = 1, 2, \dots, 12$ .) at the nominal values of the parameters, according to the following rules:\*

$$P(m, 1) = -2X_j \frac{\partial x_n}{\partial X_2} - 2Y_j \frac{\partial y_n}{\partial X_2} - 2Z_j \frac{\partial z_n}{\partial X_2}$$

$$P(m, 2) = -2Y_j \frac{\partial y_n}{\partial X_3} - 2Z_j \frac{\partial z_n}{\partial X_3}$$

$$P(m, 3) = -2Y_j \frac{\partial y_n}{\partial Y_3} - 2Z_j \frac{\partial z_n}{\partial Y_3}$$

$$P(m, 4) = \begin{cases} 2(X_4 - x_n) & \text{if } m \leq N \\ 0 & \text{if } m > N \end{cases}$$

---

\*The rules for setting up the  $[P]$  matrix follow from Eq. (7.2.12).

$$P(m, 5) = \begin{cases} 2(Y_4 - y_n) & \text{if } m \leq N \\ 0 & \text{if } m > N \end{cases}$$

$$P(m, 6) = \begin{cases} 2(Z_4 - z_n) & \text{if } m \leq N \\ 0 & \text{if } m > N \end{cases}$$

$$P(m, 7) = \begin{cases} 2(X_5 - x_n) & \text{if } N < m \leq 2N \\ 0 & \text{otherwise} \end{cases}$$

$$P(m, 8) = \begin{cases} 2(Y_5 - y_n) & \text{if } N < m \leq 2N \\ 0 & \text{otherwise} \end{cases}$$

$$P(m, 9) = \begin{cases} 2(Z_5 - z_n) & \text{if } N < m \leq 2N \\ 0 & \text{otherwise} \end{cases}$$

$$P(m, 10) = \begin{cases} 2(X_6 - x_n) & \text{if } m > 2N \\ 0 & \text{otherwise} \end{cases}$$

$$P(m, 11) = \begin{cases} 2(Y_6 - y_n) & \text{if } m > 2N \\ 0 & \text{otherwise} \end{cases}$$

$$P(m, 12) = \begin{cases} 2(Z_6 - z_n) & \text{if } m > 2N \\ 0 & \text{otherwise.} \end{cases}$$

In the evaluation of the above matrix elements, the subscripts  $n$  and  $j$  appearing on the right-hand sides of the above equations are determined according to the value of  $m$  as follows:

- If  $m \leq N$ , then  $j = 4$ ,  $n = m$
- If  $N < m \leq 2N$ , then  $j = 5$ ,  $n = m - N$
- If  $2N < m \leq 3N$ , then  $j = 6$ ,  $n = m - 2N$ .

- e) Calculate the  $3N \times 1$  column vector  $Q(m)$  at nominal values of the parameters according to the following formula:

$$Q(m) = 2x_n X_j + 2y_n Y_j + 2z_n Z_j - X_j^2 - Y_j^2 - Z_j^2 - \delta_{jn},$$

where the subscripts  $j$  and  $n$  are determined as in d) above.

- f) Solve the linear system of equations expressed in matrix form:

$$[P]\Delta\underline{S} = \underline{Q},$$

for the  $12 \times 1$  column vector  $\Delta\underline{S}$  by any standard technique. Note that for  $N > 4$ , the above system must be treated as an overdetermined system and the solution vector  $\Delta\underline{S}$  is to be interpreted as the least-squares solution. The components of  $\Delta\underline{S}$  are the corrections to the nominal station coordinates in first iteration.

- g) The corrected station coordinates  $\underline{S}^0 + \Delta\underline{S}$  are treated as new nominal values and the algorithm returns to b) through f) for another iteration until two successive iterations agree to within

the specified accuracy. The final answer is the last-corrected solution. Note that the satellite coordinates  $(x_n, y_n, z_n)$  are computed by the formulas of b) above, except, that the newly corrected values of  $X_2$ ,  $X_3$  and  $Y_3$  are used in place of their nominal values.

The above algorithm was coded in Fortran. Computational experience indicates that the iteration converges rapidly. If the starting nominal values of the coordinates are accurate to within 10 meters, then only one iteration is required to generate a solution accurate to 1 cm. Even if the initial estimate is as poor as 1 km away from the true solution, only two iterations are needed to attain centimeter accuracy.

## A.2 THE SENSITIVITY ANALYSIS ALGORITHM

The basic ideas and the mathematical formalism of sensitivity, or error magnification analysis peculiar to the multilateration problem have been given in Paragraph 7.3, where it was shown that the error  $dS$  in the station coordinate vector,  $\underline{S} = (X_2, X_3, Y_3, X_4, Y_4, Z_4, \dots, X_6, Y_6, Z_6)$ , due to errors in the measured range  $d\rho_{in}$  is given by the solution of the linear system:

$$A_n^{(j)} dX_2 + B_n^{(j)} dX_3 + C_n^{(j)} dY_3 + a_n^{(j)} dX_j + b_n^{(j)} dY_j + c_n^{(j)} dZ_j = d\sigma_n^{(j)}$$

$$(j = 4, 5, 6; n = 1, 2, \dots, N),$$

where the coefficients  $A_n^{(j)}$ , etc., are defined by Eqs (7.3.4) through (7.3.10). The computational algorithm for the simulation study outlined in Paragraph 7.3 proceeds as follows.

- a) From the given configuration of stations and satellite trajectory points, calculate the slant ranges  $\rho_{in}$  and range square differences  $\delta_{in}$  by means of the formulas

$$\rho_{in} = \left[ (x_n - X_i)^2 + (y_n - Y_i)^2 + (z_n - Z_i)^2 \right]^{1/2}, \quad i = 1, 2, \dots, 6;$$

$$n = 1, 2, \dots, N,$$

$$\delta_{in} = \rho_{in}^2 - \rho_{1n}^2, \quad i = 2, 3, \dots, 6; \quad n = 1, 2, \dots, N.$$

- b) Obtain a set of random errors  $d\rho_{in}$  in the slant ranges from a random number generator. These errors should be drawn from a Gaussian distribution with zero mean and unit standard deviation. The physical unit need not be specified for this purpose.
- c) Compute the coefficients

$$A_n^{(j)}, B_n^{(j)}, C_n^{(j)}, a_n^{(j)}, b_n^{(j)}, c_n^{(j)} \quad j = 4, 5, 6,$$

$$n = 1, 2, \dots, N,$$

according to Eqs. (7.3.4) through (7.3.10), and the combined error vector  $d\sigma_n^{(j)}$  according to (7.3.11).

- d) Form the  $3N \times 12$  matrix  $P$  according to Eq. (7.3.4) as follows:

$$[P] = \left[ \begin{array}{ccc|cc|c|c}
 A_1^{(4)} & B_1^{(4)} & C_1^{(4)} & a_1^{(4)} & b_1^{(4)} & c_1^{(4)} & & \\
 \vdots & \vdots & \vdots & \vdots & \vdots & \vdots & 0 & 0 \\
 \vdots & \vdots & \vdots & \vdots & \vdots & \vdots & & \\
 A_N^{(4)} & B_N^{(4)} & C_N^{(4)} & a_N^{(4)} & b_N^{(4)} & c_N^{(4)} & & \\
 \hline
 A_1^{(5)} & B_1^{(5)} & C_1^{(5)} & & & & a_1^{(5)} & b_1^{(5)} & c_1^{(5)} \\
 \vdots & \vdots & \vdots & & 0 & & \vdots & \vdots & \vdots \\
 \vdots & \vdots & \vdots & & & & \vdots & \vdots & 0 \\
 A_N^{(5)} & B_N^{(5)} & C_N^{(5)} & & & & a_N^{(5)} & b_N^{(5)} & c_N^{(5)} \\
 \hline
 A_1^{(6)} & B_1^{(6)} & C_1^{(6)} & & & & & & a_1^{(6)} & b_1^{(6)} & c_1^{(6)} \\
 \vdots & \vdots & \vdots & & 0 & & & 0 & \vdots & \vdots & \vdots \\
 \vdots & \vdots & \vdots & & & & & & \vdots & \vdots & \vdots \\
 A_N^{(6)} & B_N^{(6)} & C_N^{(6)} & & & & & & a_N^{(6)} & b_N^{(6)} & c_N^{(6)}
 \end{array} \right]$$

and the  $3N \times 1$  column vector  $\underline{dQ}$ :

$$\underline{dQ} = \begin{bmatrix}
 d\sigma_1^{(4)} \\
 \vdots \\
 d\sigma_N^{(4)} \\
 \text{---} \\
 d\sigma_1^{(5)} \\
 \vdots \\
 d\sigma_N^{(5)} \\
 \text{---} \\
 d\sigma_1^{(6)} \\
 \vdots \\
 d\sigma_N^{(6)}
 \end{bmatrix} .$$

- e) Solve the linear system

$$[P] \underline{dS} = \underline{dQ}$$

by any standard technique to obtain the vector  $\underline{dS}$ . The 12 components of  $\underline{dS}$  are the sensitivity numbers corresponding to the coordinates  $X_2, X_3, Y_3, X_4, Y_4, Z_4 \dots X_6, Y_6, Z_6$  respectively.

- f) Repeat the calculations b) through e) with a different set of random range errors a sufficient number of times such that meaningful statistical information, i. e., the mean and the variance of each sensitivity number  $dS_k$ , can be extracted.

This algorithm has been coded in Fortran. Typical study results are discussed in Section V.

## APPENDIX B

### DEGENERACIES IN MULTILATERATION THEORY

It has been repeatedly mentioned in the main body of this report that there exist station-satellite configurations such that the system of mathematical equations describing the multilateration technique is degenerate, i. e., a unique solution to the station coordinates cannot be found. For example, when 4 or 5 stations lie on a plane, then the system is always degenerate. This so-called coplanar degeneracy has been discussed briefly in Paragraph 7.4. In this Appendix, the nature of this degeneracy and why removal is possible using 6 stations is examined in more detail. In so doing, an exact solution to the coplanar 6-station problem will be derived. The conditions for further station degeneracies due to peculiar station coordinate combinations also will be discussed.

Another kind of degeneracy which arises as the result of certain geometric relationships between the trajectory points and/or the stations will then be considered. Degeneracies due to inadvertent use of badly correlated data are also briefly discussed. It should be pointed out that a complete, exhaustive treatment of all conceivable degeneracies has not been performed at the present time. However, it is believed that the most important degeneracies have been isolated. Any further degeneracies that occur as the result of a peculiar interplay of configurational elements will show up as singularities in the sensitivity matrix or as nonconvergence of the Newton-Raphson iteration scheme (Paragraph 7.2). Finally, an operational technique for circumventing degeneracies will be explained.

## B.1 Resumé of the Coplanar Degeneracy

In Paragraph 7.4, it has been shown that the fundamental equation of multilateration, Eq. (7.2.11), (also displayed in Figure 7.4.1 for the first 4 stations and 1 time-point), collapses for  $Z_j(j=4, 5, \dots, I)$  equal to zero, to the following form:

$$\alpha_j + \beta_j \delta_{2n} + \gamma_j \delta_{3n} = \delta_{jn}, \quad \left\{ \begin{array}{l} n=1, 2, \dots, N \\ j=4, 5, \dots, I \end{array} \right\}, \quad \text{A(B-1)}$$

where the quantities  $\delta_{in}$  are functions of the measurement data defined by Eq. (7.2.6), and the quantities  $\alpha_j$ ,  $\beta_j$ , and  $\gamma_j$  are functions of the station coordinates given by the following expressions:\*

$$\alpha_j = X_j^2 + Y_j^2 - X_2 X_j - \frac{Y_j}{Y_3} (X_3^2 + Y_3^2 - X_2 X_3) \quad \text{A(B-2)}$$

$$\beta_j = (X_j Y_3 - X_3 Y_j) / (X_2 Y_3) \quad \text{A(B-3)}$$

$$\gamma_j = Y_j / Y_3. \quad \text{A(B-4)}$$

To recapitulate the argument presented in Paragraph 7.4 consider the following argument: suppose the system consists of only 4 stations all contained in a plane, then no matter how many measurements are taken, the system of equations A(B.1) can at best determine three quantities\*\*, namely the 3 station

---

\*Note that the values of  $X_2$  and  $Y_3$ , which occur as divisors in these equations, cannot be zero, since they define the adopted coordinate system (See Section 4).

\*\*Data point-caused degeneracies can further restrict the number of quantities determinable. See Paragraph B.4.

coordinate-parameter combinations  $\alpha_4$ ,  $\beta_4$  and  $\gamma_4$ . These three quantities are not sufficient for the unique determination of the 5 unknown station parameters  $X_2$ ,  $X_3$ ,  $Y_3$ ,  $X_4$  and  $Y_4$  characterizing the planar 4-station configuration. Likewise, in a 5-station coplanar system, at most 6 quantities are available for 7 unknowns. Only when 6 stations are used, enough quantities (9) can generally be obtained for a unique determination of all of the 9 coordinate parameters. Singular configurations, however, could still exist even if there are 6 or more stations in the system. To discover such peculiarities, it is necessary to solve the coplanar 6-station problem exactly, as is accomplished in the next section.

## B.2 EXACT SOLUTION OF THE COPLANAR SIX-STATION PROBLEM AND THE CONDITION FOR STATION DEGENERACY

The previous section shows that in general nine quantities can be determined from the planar multilateration equations for 6 stations. These are the quantities  $\alpha_j$ ,  $\beta_j$ , and  $\gamma_j$ ,  $j=4, 5, 6$  defined by Eqs. A(B-2), A(B-3) and A(B-4). These equations can be inverted easily. To proceed, consider the following operations.

Equation A(B-4) is rewritten as

$$Y_j = \gamma_j Y_3, \quad \text{A(B-5)}$$

which upon substitution into Eq. A(B-3) yields the following expression for  $X_j$ :

$$X_j = \beta_j X_2 + \gamma_j X_3. \quad \text{A(B-6)}$$

Equations A(B-5) and A(B-6) are then substituted into A(B-2), and after some algebra, the following result emerges:

$$\beta_j(\beta_j - 1) X_2 + \gamma_j(\gamma_j - 1) (X_3^2 + Y_3^2) + 2\beta_j \gamma_j X_2 X_3 = \alpha_j. \quad \text{A(B-7)}$$

Equation A(B-7), written for  $j=4, 5,$  and  $6,$  represents three linear equations in the three coordinate combinations  $X_2^2, X_3^2 + Y_3^2,$  and  $X_2 X_3.$  The condition for unique solution of these parameters to exist, which in turn determine  $X_2, X_3$  and  $Y_3$  is that the determinant

$$\Delta \equiv \begin{vmatrix} \beta_4(\beta_4 - 1) & \gamma_4(\gamma_4 - 1) & 2\beta_4\gamma_4 \\ \beta_5(\beta_5 - 1) & \gamma_5(\gamma_5 - 1) & 2\beta_5\gamma_5 \\ \beta_6(\beta_6 - 1) & \gamma_6(\gamma_6 - 1) & 2\beta_6\gamma_6 \end{vmatrix} \quad \text{A(B-8)}$$

must not vanish. Note that  $\beta_j$  and  $\gamma_j$  are pure functions of the station coordinates defined by Eqs. A(B-3) and A(B-4). The same is true of the determinant. The condition for station degeneracy\* for the 6 station planar geometry can thus be stated simply as

$$\Delta(X_2, X_3 Y_3, \dots, X_6, Y_6) = 0. \quad \text{A(B-9)}$$

Extensive numerical calculations have shown that degeneracies of this kind are infrequent. A general theory explaining the occurrence of station degeneracies has not been formulated at this time.

To complete the solution of the problem when  $\Delta \neq 0,$  i. e., when no station degeneracy exists, the quantities  $\xi=X_2^2, \eta=X_3^2 + Y_3^2,$  and  $\zeta=X_2 X_3$  are determined by solving the linear simultaneous Eqs. A(2-7) written for  $j=4, 5,$  and  $6$  with the coefficients  $\beta_j(\beta_j - 1),$  etc., determined from the solution of

---

\*Degeneracy caused by the station configuration alone, independent from trajectory points.

A(B. 1) in terms of the measurement data. The station coordinates  $X_2, X_3$  and  $Y_3$  are then given by:

$$\begin{aligned} X_2 &= \pm\sqrt{\xi} \\ X_3 &= \zeta/\sqrt{\xi} \\ Y_3 &= \pm(\eta - \zeta^2/\xi)^{1/2}. \end{aligned} \tag{A(B-10)}$$

The ambiguity in sign in the above equations can be resolved once a definite coordinate system has been adopted. Having determined  $X_2, X_3$  and  $Y_3$ , the coordinates of the fourth, fifth and the sixth stations then follow immediately from Eqs. A(B-5) and A(B-6).

### B. 3 ORBIT-DEPENDENT DEGENERACIES

There exists the possibility that certain regularly related orbital trajectory points would cause degeneracy in the system equations. At the present time, no complete theory can be given for such degeneracies. However, certain obvious singularities can be isolated and should be avoided.

The best way to discuss these orbit-dependent degeneracies is via the coefficient matrix  $P$  used in the sensitivity analysis described in Paragraph 7. 3. It was pointed out in Paragraph 7. 3 that the system is degenerate if the coefficient matrix is singular\*. Inspection of this matrix, which has been explicitly written out in Appendix A, Paragraph A. 2, shows that it is singular if any one of the following submatrices  $P^{(j)}$  is singular, where

---

\*Singularity herein of a rectangular matrix is considered in the generalized sense of it being not of full rank. Thus, when a singular-value decomposition [5.3] is performed on the rectangular matrix, less than the maximum allowable number of singular values are different from zero. (The maximum allowable number of non zero singular values for a given rectangular matrix equals the smaller of the number of rows and the number of columns).

$$P^{(j)} = \begin{bmatrix} x_1 - X_j & y_1 - Y_j & z_1 - Z_j \\ \cdot & \cdot & \cdot \\ x_N - X_j & y_N - Y_j & z_N - Z_j \end{bmatrix} \quad j=4, 5, 6. \quad A(B-11)$$

An obvious way for the matrices  $P^{(j)}$  to be singular is for one of its columns to be a linear combination of the other two, or if constants  $k_1$  and  $k_2$  exist such that

$$z_n - Z_j = k_1(x_n - X_j) + k_2(y_n - Y_j)$$

for given  $j$  and all  $n$ . In other words  $P^{(j)}$  and hence  $P$  is singular, or the system is degenerate if all satellite trajectory points lie on a plane passing through one of the stations. This also includes the case in which all trajectory points lie on a straight line. This is true because a plane containing the straight line can always be constructed to pass through a given station.

Other orbital degeneracies can conceivably occur. Computational experience has indicated that using data from one pass of a circular orbit satellite generally leads to a singular  $P$  matrix. Even if multipass data (for the same circular satellite) are used, the sensitivity numbers obtained are rather poor. This indicates the near degeneracy of such configurations. However, if two circular orbits of different altitudes are used in conjunction with 6 stations, excellent sensitivities are generally obtained. The theoretical basis for such phenomena is not presently well-understood, and is proposed in this report as part of future study areas. (See Paragraph 10.2).

#### B.4 DATA DEGENERACIES

Sometimes, due to the inadvertent use of highly correlated data, the resulting solutions to the multilateration equations become ill-defined. For example, in obtaining the exact solution of the coplanar 6-station problem in Paragraph A.2.2, it is necessary to obtain uniquely the 9 quantities  $\alpha_j, \beta_j, \gamma_j, j=4, 5, 6$ . These quantities are determined by solving the system of equations A(B.1). This process yields unique solutions only if the matrix D, where

$$D = \begin{bmatrix} 1 & \delta_{21} & \delta_{31} \\ 1 & \delta_{22} & \delta_{32} \\ 1 & \cdot & \cdot \\ \cdot & \cdot & \cdot \\ \cdot & \cdot & \cdot \\ \cdot & \delta_{2N} & \delta_{3N} \end{bmatrix} \quad \text{A(B-12)}$$

is nonsingular. Obviously, singularities of the D matrix are quite coincidental and the use of more data points (perhaps from another orbital pass) will generally remove the degeneracy.

Since each data value is determined by the geometry of the station/trajectory configuration, data degeneracies are merely different descriptions of orbit/station degeneracies discussed in the previous two sections of this Appendix. For instance, the matrix D above can be written with the aid of the multilateration equations (7.2.3) and (7.2.4), as:

$$D = \begin{bmatrix} 1 & -2x_1X_2 + X_2^2 & -2x_1X_3 - 2y_1Y_3 + X_3^2 + Y_3^2 \\ 1 & -2x_2X_2 + X_2^2 & -2x_2X_3 - 2y_2Y_3 + X_3^2 + Y_3^2 \\ \cdot & \cdot & \cdot \\ 1 & & \end{bmatrix} = D(\underline{r}_n, \underline{R}_i),$$

A(B-13)

where  $\underline{r}_n$  and  $\underline{R}_i$  are the coordinate vectors of the trajectory points and the station locations. The condition that D be singular is thus equivalent to specifying certain station/orbit geometries.

#### B.5 OPERATIONAL METHOD FOR THE REMOVAL OF DEGENERACIES

Despite the seemingly large number of degenerate possibilities which may cause system malfunctioning, there is, however, a practical method which will enable the analyst to discover these degeneracies and to avoid them. This simply consists of the combined use of the solution and sensitivity analysis algorithms detailed in Appendix A. To explain this, the reader is referred to Fig. B-1. Starting with Block 1, where the measurement data is assembled and a rough estimate of the station locating parameters in an adopted coordinate system is made, the Newton-Raphson solution algorithm is run (Block 2). If the algorithm converges to a solution, then the configuration corresponding to this solution is further checked by the sensitivity analysis algorithm (Block 3). If the analysis produces small error magnification factors, then an acceptable solution has been obtained (Block 4). Otherwise a nearly degenerate configuration is encountered (Block 5) and variation of the configurational element is

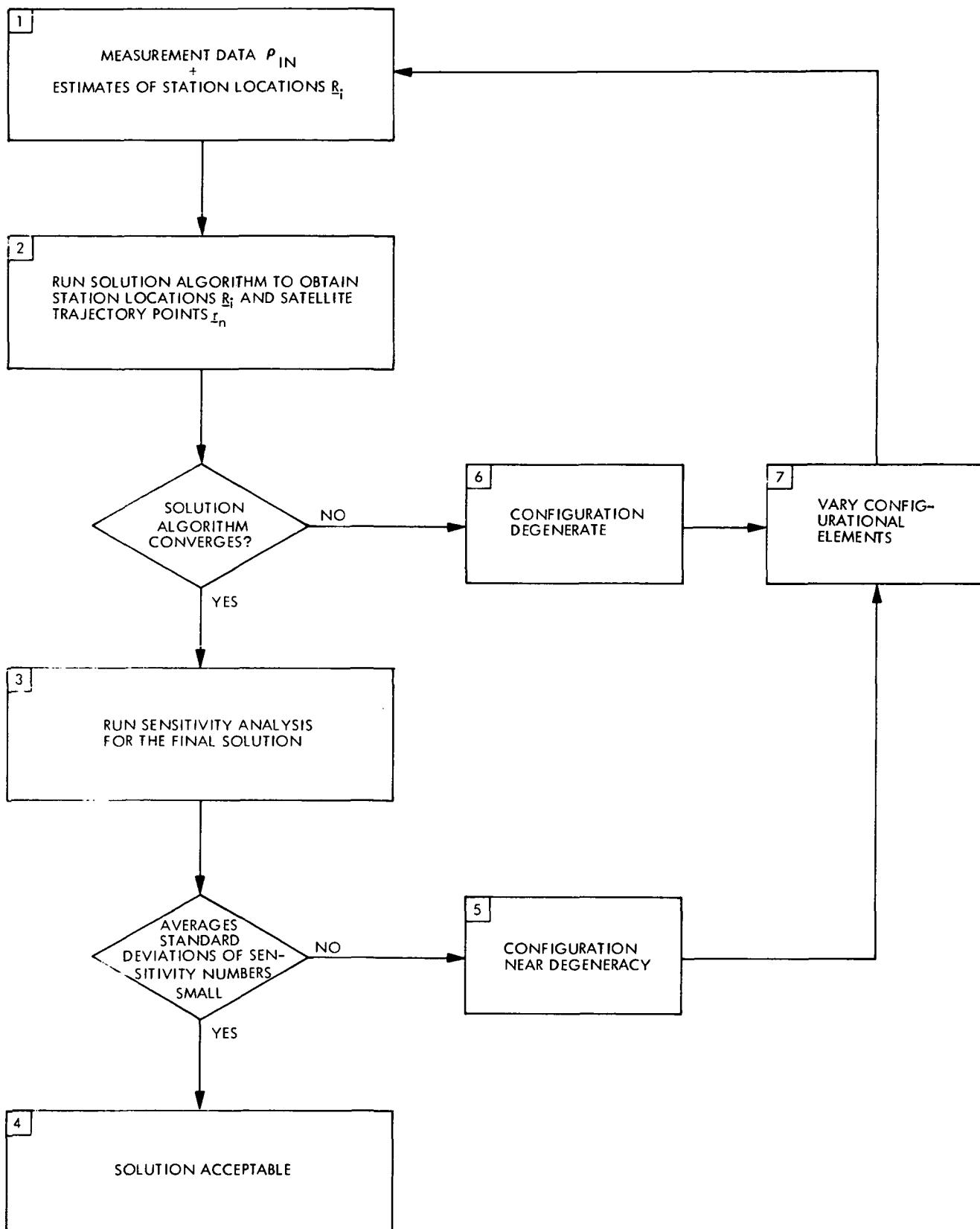


Fig. B-1. An Operational Flow Diagram for the Discovery and Avoidance of Degeneracies

indicated, ie., the system must use data from other satellite positions and/or move some of the stations to other sites (Block 7). If however, the solution algorithm of Block 2 fails to give a convergent answer, then a degenerate situation is obtained (Block 6) and the configuration should be varied (Block 7). The data and estimates associated with the new configuration are then of course reprocessed as indicated until an acceptable solution has been discovered.

## APPENDIX C

### OBTAINING BASELINES USING ONLY 3 STATIONS

In this Appendix, the following items relative to the three station solution are discussed in more detail.

First, it is shown that if 3 stations can be aligned along a straight line, then simultaneous ranging to two satellite trajectory points will enable determination of the baselines to high accuracy.

Second, analysis indicates that if the assumption of perfect alignment is relaxed, then an approximate solution to the 3 station (not perfectly aligned) problem, useful for surveying baselines up to 40 km, can be obtained.

Third, simple formulas are given for the effect of small errors in alignment of the stations on the derived distances between them. It is shown that errors in the derived distances due to horizontal and vertical misalignments vanish if the airplane or satellite flies along certain optimal paths.

Finally, it is concluded that the 3 station technique is best suited for measuring a network with mesh spacings of 10 to 40 kilometers, and for using an airplane as the retroreflector-bearing vehicle.

#### C.1 EXACT SOLUTION FOR PERFECTLY-ALIGNED STATIONS

Suppose 3 stations are aligned in a straight line, as illustrated in Figure C-1 and each of these stations ranges simultaneously to a satellite twice. Let a coordinate system with station 1 defining the origin, and the line joining the stations defining the X-axis, be adopted. The coordinates of stations 2 and 3 are  $(X_2, 0, 0)$  and  $(X_3, 0, 0)$  respectively. Let the coordinates of the two satellite trajectory points be  $(x_1, y_1, z_1)$  and  $(x_2, y_2, z_2)$ . By defining  $\rho_{in}$  to be the range from the  $i^{\text{th}}$  station to the  $n^{\text{th}}$  trajectory point, the following equations are evident:

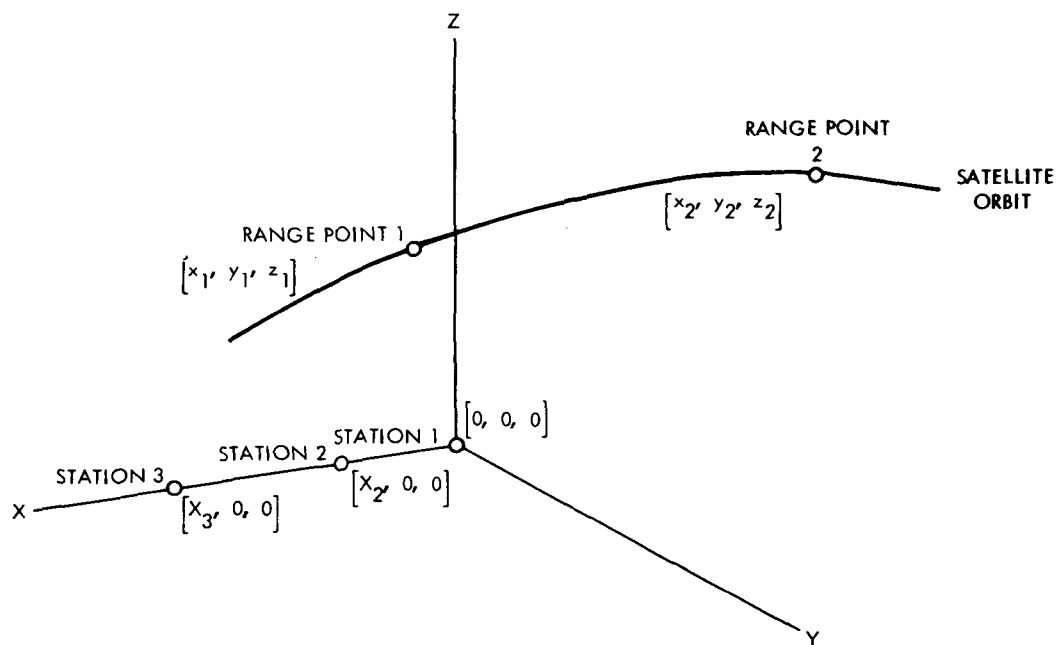


Figure C-1. Three Station Collinear System

$$\rho_{in}^2 = (x_n - X_i)^2 + y_n^2 + z_n^2, \quad n = 1, 2; i = 1, 2, 3. \quad \text{A(C-1)}$$

Note that  $X_1 \equiv 0$  in the adopted coordinate system.

At first sight, it appears that Eq. A(C-1) defines only 6 equations for 8 unknown quantities  $x_1, y_1, z_1, x_2, y_2, z_2, X_2$  and  $X_3$ . However, the important quantities  $X_2$  and  $X_3$  can nevertheless be uniquely determined. By defining the usual range square differences (See Glossary):

$$\delta_{in} \equiv \rho_{in}^2 - \rho_{1n}^2; \quad i = 2, 3, \quad n = 1, 2, \quad \text{A(C-2)}$$

it follows that

$$\delta_{in} = (x_n - X_i)^2 - x_n^2 = -2x_n X_i + X_i^2. \quad \text{A(C-3)}$$

Equation A(C-3) determines four equations in four unknowns, and can be solved easily. The solutions for  $X_2$  and  $X_3$  are:

$$X_2 = \left[ \frac{(\delta_{22} - \delta_{21})(\delta_{21}\delta_{32} - \delta_{22}\delta_{31})}{(\delta_{32} - \delta_{31})(\delta_{22} - \delta_{21} - \delta_{32} + \delta_{31})} \right]^{1/2} \quad \text{A(C-4)}$$

$$X_3 = \left[ \frac{(\delta_{32} - \delta_{31})(\delta_{21}\delta_{32} - \delta_{22}\delta_{31})}{(\delta_{22} - \delta_{21})(\delta_{22} - \delta_{21} - \delta_{32} + \delta_{31})} \right]^{1/2} \quad \text{A(C-5)}$$

These solutions are exact under the assumption of perfect station alignment. A simple sensitivity analysis also shows that the solutions are stable with respect to slight changes in the measured ranges, with very low error magnifications.

## C.2 APPROXIMATE SOLUTION FOR NONPERFECT ALIGNMENT

If Station 3 does not lie on the straight line joining Stations 1 and 2 (the X-axis), it can be assumed to be on the XY plane. Let  $Y_3$  be assigned to its Y coordinate. It will also be assumed that the values of  $Y_3$  and the Y-component,  $y_n$  of the satellite trajectory points are approximately known. The following ranging equations can be written:

$$\delta_{2n} = -2x_n X_2 + X_2^2 \quad \text{A(C-6)}$$

$$\delta_{3n} = -2x_n X_3 - 2y_n Y_3 + X_3^2 + Y_3^2 \quad n = 1, 2. \quad \text{A(C-7)}$$

Equation A(C-7) can be rewritten as follows:

$$\delta'_{3n} = -2x_n X_3 + X_3^2, \quad \text{A(C-8)}$$

where

$$\delta'_{3n} = \delta_{3n} + 2y_n Y_3 - Y_3^2 \quad \text{A(C-9)}$$

These equations are exact, whether  $Y_3$  is small or large.

The important approximation that  $\delta_{3n}$  can be replaced by  $\delta'_{3n}$  is now made. This approximation is valid if  $Y_3$  is a small quantity; that is, if the stations are approximately aligned. Equations A(C-6) and A(C-7) can now be solved exactly. The solutions are identical with Eqs. A(C-4) and A(C-5). with the quantities  $\delta_{3n}$ ,  $n = 1, 2$  in these equations replaced by the corresponding quantities  $\delta'_{3n}$  as defined by Eq. A(C-9).

### C.3 ERROR ANALYSIS

From Equations A(C-4) and A(C-5) formulas for the errors in the derived quantities  $X_2$  and  $X_3$  as functions of the alignment error  $Y_3$  can now be derived. Notice, from the symmetry of the geometry around the X-axis, that y and z are interchangeable in all equations; and therefore no generality is lost by representing the alignment error by  $Y_3$  only, since similar formulas for the effect of  $Z_3$  can be written by inspection. If station 3 is slightly displaced from the X-axis, then the appropriate values of  $\delta$  for insertion into the above formulas will be  $\delta_{2n}$  and  $\delta'_{3n}$  of Eqs. A(C-6) and A(C-8); but the use of  $\delta_{2n}$  and  $\delta_{3n}$  computed directly from the ranges will introduce an error.

To the first order,

$$\begin{aligned} \frac{\Delta X_2}{X_2} &= d \ln X_2 \\ &= -\frac{\frac{1}{2} \Delta(\delta_{22} - \delta_{21})}{(\delta_{22} - \delta_{21})} + \frac{\frac{1}{2} \Delta(\delta_{21} \delta_{32} - \delta_{22} \delta_{31})}{(\delta_{22} \delta_{32} - \delta_{22} \delta_{31})} - \frac{\frac{1}{2} \Delta(\delta_{32} - \delta_{31})}{(\delta_{32} - \delta_{31})} \\ &\quad - \frac{\frac{1}{2} \Delta(\delta_{22} - \delta_{21} - \delta_{32} + \delta_{31})}{(\delta_{22} - \delta_{21} - \delta_{32} + \delta_{31})}. \end{aligned} \tag{C-10}$$

The differentials  $\Delta\delta_{in}$  are produced by the small displacement  $Y_3$  of the third station from exact alignment on the X-axis. The values of  $\delta_{in}$ , including the effect of the displacement, become:

$$-\delta_{21} = +2x_1 X_2 - X_2^2$$

$$-\delta_{22} = +2x_2 X_2 - X_2^2$$

$$-\delta_{31} = +2x_1 X_3 + 2y_1 Y_3 - (X_3^2 + Y_3^2)$$

$$-\delta_{32} = +2x_2 X_3 + 2y_2 Y_3 - (X_3^2 + Y_3^2).$$

Hence, to the first order,

$$\frac{1}{2} \Delta \delta_{21} = \frac{1}{2} \Delta \delta_{22} = 0,$$

$$\frac{1}{2} \Delta \delta_{31} = -y_1 Y_3,$$

$$\frac{1}{2} \Delta \delta_{32} = -y_2 Y_3,$$

and also,

$$(\delta_{32} - \delta_{31}) = 2(x_1 - x_2)X_3 + 2(y_1 - y_2)Y_3$$

$$\left[ (\delta_{22} - \delta_{21}) - (\delta_{32} - \delta_{31}) \right] = 2(x_1 - x_2)(X_2 - X_3) - 2(y_1 - y_2)Y_3$$

$$(\delta_{21}\delta_{32} - \delta_{22}\delta_{31}) = 2(x_1 - x_2)(X_2^2 X_3 - X_3^2 X_2)$$

$$+ 4(x_1 y_2 - x_2 y_1)X_2 Y_3 + 2(y_1 - y_2)X_2^2 Y_3;$$

whereupon, again to the first order, the expression for  $\Delta X_2/X_2$  becomes

$$\frac{\Delta X_2}{X_2} = \left\{ \frac{2(x_1 y_2 - x_2 y_1)X_2 + (y_1 - y_2)X_2^2}{2(x_1 - x_2)(X_2^2 X_3 - X_3^2 X_2)} - \frac{y_1 - y_2}{2(x_1 - x_2)X_3} \right. \\ \left. + \frac{y_1 - y_2}{2(x_1 - x_2)(X_2 - X_3)} \right\} Y_3.$$

Putting all terms in the above expression over the common denominator

$$2(x_1 - x_2)X_3(X_2 - X_3),$$

the expression becomes

$$\frac{\Delta X_2}{X_2} = \frac{[(x_1 y_2 - x_2 y_1) + X_3(y_1 - y_2)] Y_3}{(x_1 - x_2)X_3(X_2 - X_3)}. \quad \text{A(C-11)}$$

The formula for  $\Delta X_3/X_3$  is virtually the same. Only the signs are changed in the first and fourth terms of the expression for  $d \ln X$ , giving

$$\frac{\Delta X_3}{X_3} = \frac{[(x_1 y_2 - x_2 y_1) + X_2(y_1 - y_2)] Y_3}{(x_1 - x_2)X_3(X_2 - X_3)}. \quad \text{A(C-12)}$$

#### C-4 CONFIGURATIONS THAT MINIMIZE ALIGNMENT ERRORS

It is shown in this subsection that the trajectory points can be chosen in such a way that the errors in the computed distances  $X_2$  and  $X_3$ , due to alignment errors  $Y_3$  and  $Z_3$ , can be made to vanish.

If the satellite or airplane flies a planar course defined by the equation

$$y = A + Bx ,$$

then

$$\Delta X_2 = \frac{X_2(A + BX_3)Y_3}{X_3(X_2 - X_3)}, \quad \text{A(C-13)}$$

$$\Delta X_3 = \frac{(A + BX_2)Y_3}{X_2 - X_3}. \quad \text{A(C-14)}$$

Three cases of interest may be considered:

1. If  $A = B = 0$ , then  $\Delta X_2 = \Delta X_3 = 0$ ;

physically, this implies that if the vehicle flies over the X-axis, i. e., in the XZ plane, then the effect of station misalignment on both  $X_2$  and  $X_3$  vanishes.\*

2. If  $A + BX_3 = 0$ , then  $\Delta X_2 = 0$  (but  $\Delta X_3 \neq 0$ );

this means that  $\Delta X_2 = 0$  if the vehicle flies in the plane defined by

$$y = B(x - X_3),$$

with B arbitrary.

In other words, if the trajectory plane is parallel to the Z-axis and passes through Station No. 3, then the effect of alignment error on the coordinate  $X_2$  vanishes.

3. If  $A + BX_2 = 0$ , then  $\Delta X_3 = 0$  (but  $\Delta X_2 \neq 0$ );

namely, if the trajectory plane is parallel to the Z-axis and passes through Station No. 2, then the effect of alignment error on the coordinate  $X_3$  vanishes.

Combining the above results, it is easy to prove the following:

If the vehicle flies in a straight line course, approaching to or receding from Station 3, then the error induced upon the calculated value of  $X_2$  due to any small horizontal and vertical misalignment of the stations vanishes in the first order;

---

\*The reason why the effects of the alignment errors vanish if the retroreflector lies in the XZ plane can be seen intuitively from Figure C-2. The ratio of the range which would be measured if Station No. 3 were on the X-axis to the true range from the position displaced by  $Y_3$ , is  $\cos \phi$ . The variation of  $\cos \phi$  from unity is of second order in  $Y_3$ .

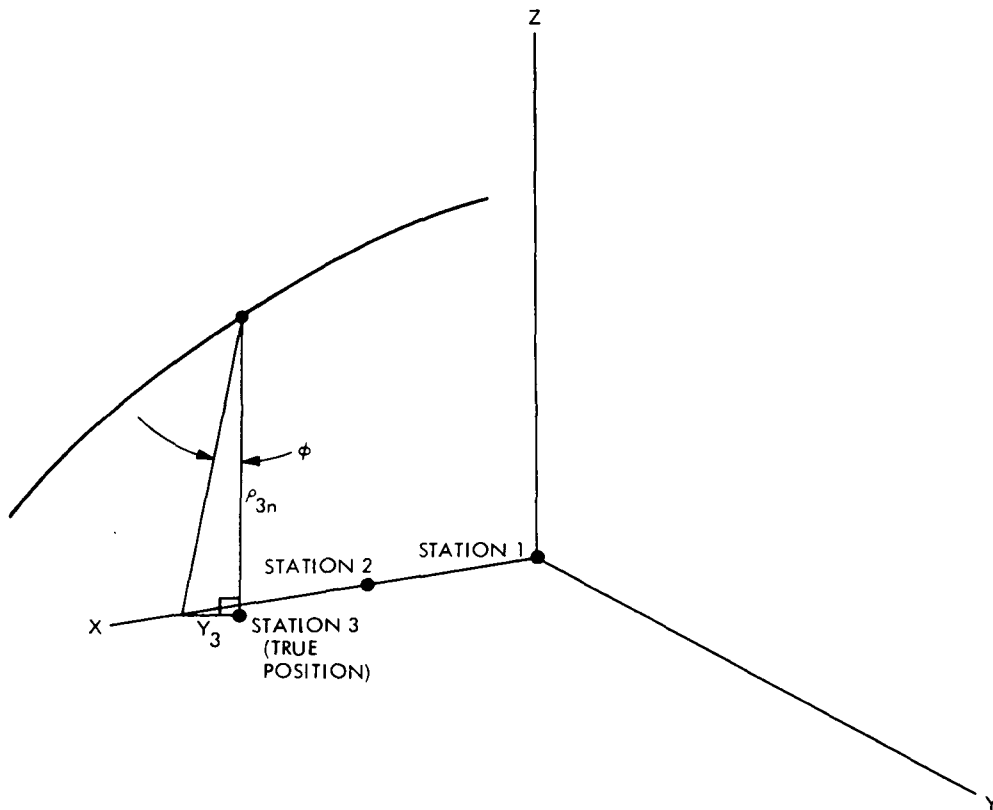


Figure C-2. Physical Interpretation of Alignment Error

likewise, if the vehicle flies in a straight line to or from Station 2, then the error in  $X_3$  vanishes.

The above theorem has been tested numerically, and has been found to yield extremely accurate results (Typical values have been quoted in Sec VI).

### C.5 CONCLUSIONS

It has been shown in this Appendix that a range-only system for measuring interstation baselines is possible with only 3 stations, provided that these stations are approximately aligned. The accuracy of the 3-station system can be greatly increased by optimally choosing the trajectories such that the effects of station alignment errors are minimized.

The requirement of approximate alignment of stations restricts the 3-station system to short baseline applications. For baselines of less than 40 km, an airplane can conveniently serve as the retroreflector-bearing vehicle. The maneuverability of the airplane can then be used to advantage for flying the optimum trajectories. Further studies should be made of this promising technique.

## APPENDIX D

### INVERSE TRILATERATION: A METHOD OF STATION LOCATION

The general technique of geometric multilateration developed in Section 7 of this report requires no prior knowledge of any station coordinates, other than a very rough initial estimate for the purpose of starting the Newton-Raphson iteration. This self-starting property of the general technique is important whenever a new geographic area is to be surveyed. However, it is usually beneficial to establish new benchmarks (landmarks) in the general area where several stations already have been precisely located. For purposes of locating a new station, it is always possible to repeat the general multilateration calculation simply by using the new station as one of a six-station or four-station configuration. However, with this procedure the coordinates of some of the established stations will be redundantly calculated, and thus waste much computational effort. In this Appendix, a simple algorithm, based on the well-known trilateration principle, is given whereby coordinates of new stations can be readily obtained once the coordinates of 3 master stations have been firmly established by using the general technique. This algorithm provides an auxiliary, efficient method for locating new benchmarks, i. e., stations.

#### D.1 THE SOLUTION TO THE GENERAL TRILATERATION PROBLEM

The trilateration principle, as will be explained below, is well-known in orbit determination. It has been successfully applied to the tracking of synchronous artificial satellites by the Goddard Space Flight Center. However, as will be seen in the following section, it is equally valuable as a technique for locating new station coordinates. In the present section, the general theory of trilateration is discussed.

Expressed geometrically, the problem is as follows: to determine the three-dimensional coordinates of a point  $\underline{R}(X, Y, Z)$  in space, given its distances  $\rho_n$  to 3 other points  $\underline{r}_n = (x_n, y_n, z_n)$ ,  $n = 1, 2, 3$ , whose coordinates are assumed to be given in an arbitrary reference frame.

The solution of the above problem is straightforward. Defining the vector slant-range  $\underline{\rho}_n$  by

$$\underline{\rho}_n = \underline{r}_n - \underline{R}, \quad \text{A(D-1)}$$

the following equations may be obtained:

$$\rho_n^2 = r_n^2 + R^2 - 2 \underline{r}_n \cdot \underline{R}, \quad n = 1, 2, 3. \quad \text{A(D-2)}$$

Equation A(D-2) represents a system of 3 equations in three unknowns, i. e., the X, Y, Z components of  $\underline{R}$ . The solution to these equations is exact and is given in algorithmic form as follows:

(i) By use of the auxiliary quantities:

$$x_{mn} = x_m - x_n, \quad y_{mn} = y_m - y_n, \quad z_{mn} = z_m - z_n$$

$$\delta_m = \rho_m^2 - \rho_1^2, \quad m = 2, 3,$$

$$\alpha_m = \frac{1}{2} \left( r_m^2 - r_1^2 - \delta_m \right), \quad m = 2, 3.$$

$$D = x_{21} y_{31} - x_{31} y_{21}$$

$$p_1 = (\alpha_2 y_{31} - \alpha_3 y_{21})/D$$

$$p_2 = (\alpha_3 x_{21} - \alpha_2 x_{31})/D$$

$$q_1 = (z_{21} y_{31} - z_{31} y_{21})/D$$

$$q_2 = (z_{31} x_{21} - z_{21} x_{31})/D$$

$$a = 1 + q_1^2 + q_2^2$$

$$b = -2(p_1 q_1 + p_2 q_2 - x_1 q_1 - y_1 q_2 + z_1)$$

$$c = p_1^2 + p_2^2 - 2x_1 p_1 - 2y_1 p_2 + r_1^2 - \rho_1^2 ,$$

(ii) the solution is given by:

$$Z = (-b \pm \sqrt{b^2 - 4ac})/(2a)$$

$$X = p_1 - q_1 Z$$

$$Y = p_2 - q_2 Z.$$

The ambiguity in sign in the Z equation above must be resolved by appealing to physical principles. As illustrated in Fig. D-1, it is evident geometrically that for a set of 3 given points in space and 3 ranges, there always exist, two trilateration solutions symmetrically located on both sides of the plane containing the 3 given points. Of these two solutions only one has physical meaning. For example, if the technique is used for orbit determination, then the physical solution is the solution that is above the plane of the stations (away from the Earth).

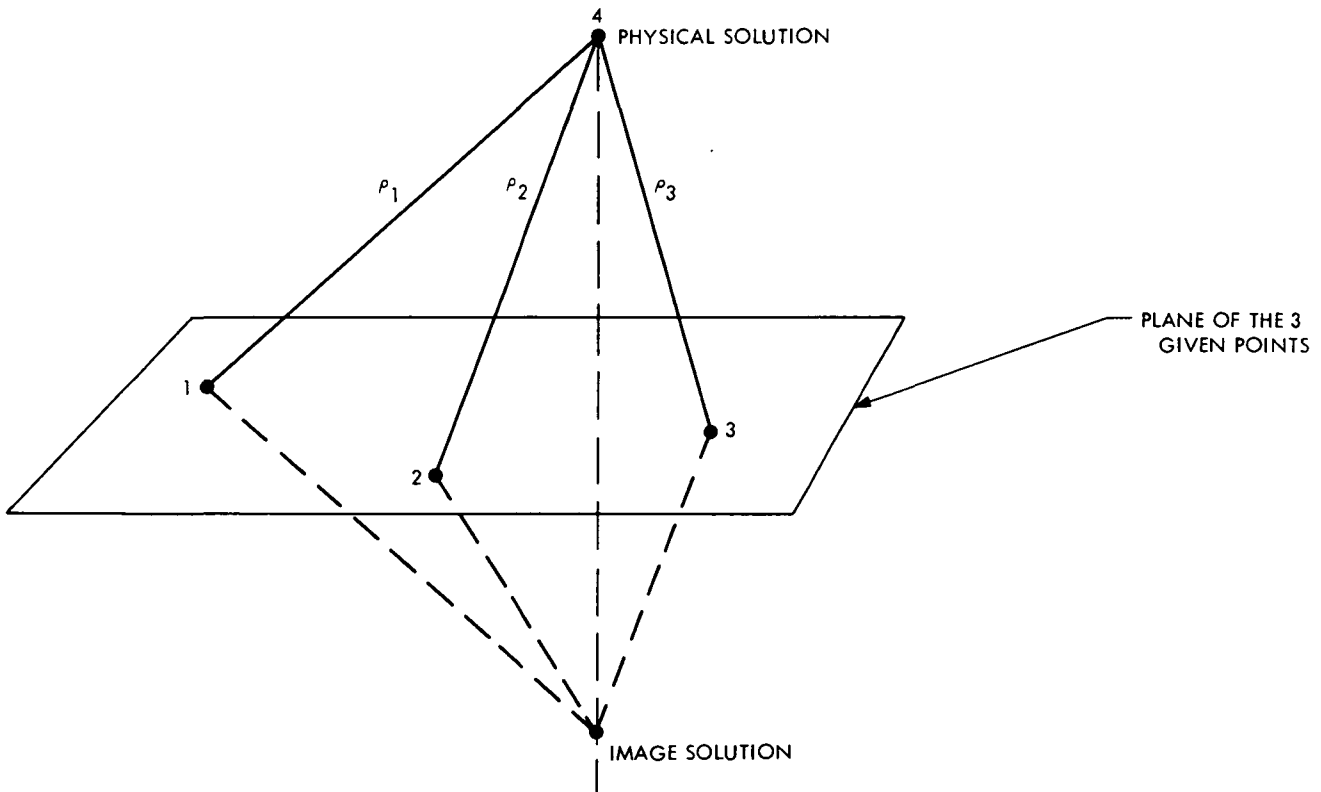


Fig. D-1. Relation between the physical and the image solutions to the trilateration problem

## D.2 INVERSE TRILATERATION FOR STATION LOCATION

It is clear that the geometric statement of the trilateration problem given in the previous section makes no inherent distinction between the 4 points (3 known and 1 unknown) in space. By treating the 3 known points as master station locations, a trilateration will yield the coordinates of the fourth point (the satellite coordinates at a given time). Inversely, if the 3 known points are considered to be satellite trajectory points, then the fourth point, the location of an unknown station, can be trilaterated.

The above trilateration scheme is especially simple when expressed in the adopted geometric coordinate system (Section 4.4), where the coordinates

of the 3 master stations are given as  $(0, 0, 0)$ ,  $(X_2, 0, 0)$ , and  $(X_3, Y_3, 0)$ . Let the unknown coordinates in the master frame of reference of a new station be  $(X, Y, Z)$ . Now since a sequence of satellite position coordinates  $(x_n, y_n, z_n)$  can be generated by direct trilateration from the master stations, then in the familiar notation of Section 7, these points can be expressed explicitly in terms of the known coordinates  $X_2$ ,  $X_3$  and  $Y_3$  and the range square differences  $\delta_{in}$  (See Section 7.2) as:

$$x_n = \left( X_2^2 - \delta_{2n} \right) / (2X_2) \quad \text{A(D-3)}$$

$$y_n = \left( X_3^2 + Y_3^2 - \delta_{3n} - 2x_n X_3 \right) / (2Y_3) \quad \text{A(D-4)}$$

$$z_n = + \left( \rho_{1n}^2 - x_n^2 - y_n^2 \right)^{1/2}, \quad \text{A(D-5)}$$

where the positive sign of the square root of the  $z_n$  equation is chosen because the range point must lie above the XY-plane. Note that this solution, i. e., Eqs. A(D-3) through A(D-5) is completely equivalent to the solution obtained by applying the trilateration algorithm given in the previous section (with the proper interpretation of symbols).

Therefore, any three of the generated trajectory points can be used as the base for trilaterating the coordinates of a fourth point in space, i. e., the new station location. As is evident, the entire algorithm of the previous section can be used for this computation.

### D.3 POSSIBLE DIFFICULTIES

The dual trilateration scheme explained in Paragraph D.2 as in other geometric approaches, may run into difficulties because certain geometric configurations may result in singular algebraic systems. Therefore, care should be

exercised in the choice of the trajectory points used as the basis of an inverse trilateration. Generally speaking, a trilateration geometry is healthy unless all 4 space points lie on the same plane. Thus a satellite trajectory passing over a station should not be used to trilaterate the station location. Another singular situation is caused if the three trajectory points are collinear. All these difficulties can usually be overcome by data manipulation. A simple sensitivity analysis can assess the accuracy of any given configuration. This analysis has been performed, but is omitted herein.

APPENDIX E  
TIMING REQUIREMENTS

The critical equation which relates the range to the total observed transit time is derived in this Appendix, i.e., Eq. (8.4.3) is explicitly obtained. In a stationary (nonrotating) geocentric coordinate system, let  $\underline{r}_s(t)$  be defined as the instantaneous vector distance (magnitude  $r_s$ ) between the center of the Earth and the position of a satellite at time  $t$ . The instantaneous topocentric vector distance from a ranging station to the satellite is denoted by  $\underline{\rho}(t)$  (magnitude  $\rho$ ). Finally,  $\underline{R}(t)$  is the instantaneous vector distance between the center of the Earth and the station on the surface of the Earth (magnitude  $R$ ).

Let a laser pulse be emitted at time  $t$ . It will arrive at the satellite at time  $t + \Delta$  such that

$$c\Delta = |\underline{r}_s(t + \Delta) - \underline{R}(t)|. \quad \text{A(E-1)}$$

The pulse will now be reflected and arrive back at the station at time  $t + \Delta + \Delta'$  such that

$$c\Delta' = |\underline{r}_s(t + \Delta) - \underline{R}(t + \Delta + \Delta')|. \quad \text{A(E-2)}$$

Before solving Eqs. A(E-1) and A(E-2) it is important to know the magnitude of various quantities which are going to be used. The range will be of the order of  $10^3 - 10^4$  km, so that the time  $\Delta$  will be of the order of  $3 \cdot 10^{-3} - 30 \cdot 10^{-3}$  sec. Hence, a Taylor series for  $\underline{r}_s$  and  $\underline{R}$  about  $t$  retaining only a very few terms will therefore be adequate. Accordingly:

$$\left. \begin{aligned} \underline{r}_s(t + t') &= \underline{r}_s(t) + t' \dot{\underline{r}}_s(t) + \frac{t'^2}{2} \ddot{\underline{r}}_s(t) + \dots \\ \underline{R}(t + t') &= \underline{R}(t) + t' \dot{\underline{R}}(t) + \frac{t'^2}{2} \ddot{\underline{R}}(t) + \dots \end{aligned} \right\} \quad \text{A(E-3)}$$

and

To obtain an estimate of the order of magnitude of the various terms in Eq. A(E-3) a realistic satellite orbit will be utilized. The radial velocity of a satellite is given by:

$$\dot{r}_s^2 = GM \left[ \frac{2}{r_s} - \frac{1}{a} - \frac{a}{r_s^2} (1 - e^2) \right], \quad \text{A(E-4)}$$

where:

$$\left. \begin{array}{l} M = \text{mass of Earth} \\ G = \text{gravitational constant} \end{array} \right\} GM = 4 \cdot 10^5 \text{ [km}^3 \text{sec}^{-2} \text{]}$$

$|\underline{r}_s| = r_s =$  radial distance from the center of the Earth,  
 $a =$  semimajor axis of the orbital ellipse,  
 $e =$  orbital eccentricity.

By choosing a representative orbit with minimum altitude above the surface of the Earth,  $H_{\min} = 900$  km, and a maximum altitude of,  $H_{\max} = 4500$  km, it follows that:

$$a = 9100 \text{ km} \qquad e = 0.1978. \qquad \text{A(E-5)}$$

From Eq. A(E-4) it follows that the maximum radial velocity (at  $r_s = a[1 - e^2]$ ) is given by  $\dot{r}_{\max} = 1.325 \text{ km sec}^{-1}$  in which case  $\ddot{r}_s = 0$  and that the maximum radial acceleration (at perigee) is given by  $\ddot{r}_{\max} = -0.726 \cdot 10^{-3} \text{ km sec}^{-2}$  in which case the velocity  $\dot{r}_s = 0$ .

On the other hand the transit time of a pulse from station to satellite, when the satellite is at perigee, is about  $15 \cdot 10^{-3}$  sec, so that the satellite has moved  $10^{-2}$  cm during this time. However, when the satellite experiences the largest radial velocity it can move during the then prevailing transit time of  $8 \cdot 10^{-3}$  sec by 100 m; a change far from negligible. In any case range changes during pulse transit times are not affected by the satellite's acceleration within the accuracy desired (1 cm).

Stations located on the surface of the Earth will also move due to rotation of the Earth. Since the angular velocity of the Earth is  $\omega \cong 7.3 \cdot 10^{-5} \text{ sec}^{-1}$  an upper limit for both the absolute velocity and absolute acceleration is:  $\dot{R} = 0.47 \text{ km sec}^{-1}$  and  $\ddot{R} = 3.4 \cdot 10^{-5} \text{ km sec}^{-2}$  respectively. As can be seen the acceleration again is totally negligible during the transit time of a pulse but due account has to be taken of the velocity. Neglecting the acceleration terms in Eq. A(E-3) it follows that

$$c\Delta = \rho(t) + \dot{\underline{r}}_s(t) \cdot \underline{\rho}(t)\rho(t)^{-1}\Delta \quad \text{A(E-6)}$$

$$c\Delta' = \rho(t) + \dot{\underline{r}}_s(t) \cdot \underline{\rho}(t)\rho(t)^{-1}\Delta - \dot{\underline{R}}(t) \cdot \underline{\rho}(t)\rho(t)^{-1}(\Delta + \Delta'), \quad \text{A(E-7)}$$

where of course

$$\underline{\rho} = \underline{r}_s - \underline{R}. \quad \text{A(E-8)}$$

It follows from Eqs. A(E-6), A(E-7), and A(E-8) that the observed total transit time  $\Delta + \Delta' = T$  is given by

$$T(t) = \frac{2}{c} \rho(t) \left[ 1 + c^{-1} \dot{\rho}(t) \right]. \quad \text{A(E-9)}$$

Equation A(E-9), the fundamental equation for the analysis of Section 8.4, shows that the total measured transit time  $T$  of a pulse emitted at time  $t$  is connected to the range at time  $t$  in the manner displayed.

## APPENDIX F

### EXPECTED DATA ACCURACY

As was discussed in Paragraphs 8.3 and 8.4 the process of obtaining synchronized range measurements will require that the range measurements or residuals be curve fit over suitable intervals by some assumed analytic function.

The question addressed in this appendix is related to the accuracy, i.e., error bound, that will be obtained from the analytic model assumed for the curve fitting procedure when the number of measurements (range points) is large.

#### F.1 STANDARD DEVIATION OF DATA

An important measure of the accuracy with which a given model, e.g., polynomial will approximate the range history as a function of time, is the standard deviation of the raw data. If the modeled value of the slant range is denoted by  $\bar{\rho}_n$  and the actual measurement is  $\rho_n$ , then the standard deviation of the model can be computed directly as:

$$\sigma_{\rho f} = \sum_{n=1}^N (\rho_n - \bar{\rho}_n)^2 / (N - 1), \quad \text{A(F-1)}$$

where N is the total number of range measurements taken in an interval of specified duration.

#### F.2 ASSUMED MODEL AND LEAST SQUARES FITTING PROCEDURE

As was discussed in Section 8.4, the data peculiar to this problem will be fit via least squares by the following function

$$\Delta \rho_n = a + b(t_n - t_0) + c(t_n - t_0)^2, \quad n = 1, 2, 3, \dots, N \quad \text{A(F-2)}$$

where  $\Delta\rho_n$  are the true minus Keplerian range residuals, (See Glossary),  $n$  refers to the  $n^{\text{th}}$  observation out of  $N$  total observations,  $t$  is the system time, and  $t_o$  is the adopted epoch time (See Para 8.4).

As is well known from the theory of least squares, the object of obtaining the so-called best fit can be stated mathematically as that of minimizing the function  $\Omega$  defined by

$$\Omega \equiv \left( \Delta\rho_1 - a - b[t_1 - t_o] - c[t_1 - t_o]^2 \right)^2 + \left( \Delta\rho_2 - a - b[t_2 - t_o] - c[t_2 - t_o]^2 \right)^2 + \dots \quad \text{A(F-3)}$$

By extracting and equating the partial derivatives of  $\Omega$  with respect to  $a$ ,  $b$  and  $c$  to zero it follows that the least squares equations become

$$\begin{bmatrix} N & \sum_1^N [t_n - t_o] & \sum_1^N [t_n - t_o]^2 \\ \sum_1^N [t_n - t_o] & \sum_1^N [t_n - t_o]^2 & \sum_1^N [t_n - t_o]^3 \\ \sum_1^N [t_n - t_o]^2 & \sum_1^N [t_n - t_o]^3 & \sum_1^N [t_n - t_o]^4 \end{bmatrix} \begin{bmatrix} a \\ b \\ c \end{bmatrix} = \begin{bmatrix} \sum_1^N \Delta\rho_n \\ \sum_1^N \Delta\rho_n [t_n - t_o] \\ \sum_1^N \Delta\rho_n [t_n - t_o]^2 \end{bmatrix} \quad \text{A(F-4)}$$

A useful simplification of these equations can be obtained by letting

$$t_n = t_1 + \Delta t(n - 1),$$

namely, by assuming that  $t$  is the laser data rate and choosing  $t_1 - t_o = 0$ , i. e., the epoch and initial times are arbitrarily taken equal to zero so that

$$t_n - t_o = \Delta t(n - 1).$$

For large N (say, N > 50), the following approximations may be used:

$$\Delta t \sum_1^N [n - 1] \cong \Delta t \frac{N^2}{2}, \quad \Delta t \sum_1^N [n - 1]^3 \cong \Delta t \frac{N^4}{4},$$

$$\Delta t \sum_1^N [n - 1]^2 \cong \Delta t \frac{N^3}{3}, \quad \Delta t \sum_1^N [n - 1]^4 \cong \Delta t \frac{N^5}{5}.$$

The system A(F-4) collapses to

$$\begin{bmatrix} N & \Delta t \frac{N^2}{2} & \Delta t^2 \frac{N^3}{3} \\ \Delta t \frac{N^2}{2} & \Delta t^2 \frac{N^3}{3} & \Delta t^3 \frac{N^4}{4} \\ \Delta t^2 \frac{N^3}{3} & \Delta t^3 \frac{N^4}{4} & \Delta t^4 \frac{N^5}{5} \end{bmatrix} \begin{bmatrix} a \\ b \\ c \end{bmatrix} = \begin{bmatrix} \sum_1^N \Delta \rho_n \\ \Delta t \sum_1^N \Delta \rho_n (n - 1) \\ \Delta t^2 \sum_1^N \Delta \rho_n (n - 1)^2 \end{bmatrix} \quad \text{A(F-5)}$$

The above matrix equation can be solved and the quantities a, b, and c obtained as functions of N,  $\Delta \rho_n$  and  $\Delta t$ , i. e.,

$$a = a(N, \Delta t, \Delta \rho),$$

with similar equations in b and c. Furthermore the partial derivatives of the least squares coefficients with respect to the  $\Delta \rho_i$ , which only appear linearly, can be obtained as

$$\frac{\partial a}{\partial \Delta \rho_n} = f(N, \Delta t), \quad \frac{\partial b}{\partial \Delta \rho_n} = g(N, \Delta t), \quad \frac{\partial c}{\partial \Delta \rho_n} = h(N, \Delta t).$$

The algebraic manipulations become rather tedious and are omitted herein. Once the partial derivatives are obtained, the resulting error in the range assuming equal random errors in the  $\Delta \rho_n$  measurements, can be written as:

$$\sigma_{\Delta\rho} = \left[ \sum_1^N \left( \frac{\partial a}{\partial \Delta\rho_n} \right)^2 + \sum_1^N \left( \frac{\partial b}{\partial \Delta\rho_n} \right)^2 + \sum_1^N \left( \frac{\partial c}{\partial \Delta\rho_n} \right)^2 \right]^{1/2} \sigma_{\Delta\rho f}, \quad \text{A(F-6)}$$

where  $\sigma_{\Delta\rho f}$ , the standard deviation of the data, is defined via Eq. A(F-1) with  $\rho_n$  and  $\bar{\rho}_n$  replaced by  $\Delta\rho_n$  and  $\Delta\bar{\rho}_n$ .

Note that the partial derivatives are summed from 1 to N with index n. Therefore using the previously stated summation formulas and after much patience

$$\sigma_{\Delta\rho} = \left[ \frac{3(3N^2 - 7)}{4N(N^2 - 4)} \right]^{1/2} \sigma_{\Delta\rho f}, \quad \text{A(F-7)}$$

which for large N reduces to

$$\sigma_{\Delta\rho} = \frac{3}{2\sqrt{N}} \sigma_{\Delta\rho f}. \quad \text{A(F-8)}$$

In summary, Eq. A(F-8) states that once the standard deviation of the actual data  $\rho_n$  from the assumed curve fit  $\bar{\rho}_n$  is computed, i.e., once  $\sigma_{\Delta\rho f}$  is determined, the actual value of the error in the range measurement can be obtained directly. It is this value,  $\sigma_{\Delta\rho}$ , that would be used in the explicit error mapping through the multilateration equations to yield the random errors in the station coordinates.

APPENDIX G  
CURVE FITTING TECHNIQUE WITH RATIONAL FUNCTIONS

As indicated in Section 8.3 there may be advantages in fitting residuals with rational functions. For purposes of outlining this technique only a truncated rational fit is discussed in this Appendix.

If it is assumed that observations are related to time by means of the relationship

$$\rho = A + Bt^k, \quad \text{A(G-1)}$$

then the values of A, B, and k which make the square of any given residual, r, where

$$r \equiv A + Bt^k - \rho, \quad \text{A(G-2)}$$

a minimum must be determined. In other words, for N observations, the function  $\Omega$ , where

$$\Omega \equiv r_1^2 + r_2^2 + r_3^2 + \dots + r_N^2. \quad \text{A(G-3)}$$

is to be minimized.

To accomplish this, the partial derivatives of  $\Omega$  with respect to A, B and k must be set to zero. Proceeding formally,

$$\frac{\partial \Omega}{\partial A} = r_1 + r_2 + \dots + r_N = 0$$

$$\frac{\partial \Omega}{\partial B} = r_1 \frac{\partial r_1}{\partial B} + r_2 \frac{\partial r_2}{\partial B} + \dots + r_N \frac{\partial r_N}{\partial B} = 0$$

$$\frac{\partial \Omega}{\partial k} = r_1 \frac{\partial r_1}{\partial k} + r_2 \frac{\partial r_2}{\partial k} + \dots + r_N \frac{\partial r_N}{\partial k} = 0.$$

The expression for  $\partial \Omega / \partial A$  implies that

$$A + Bt_1^k - \rho_1 + A + Bt_2^k - \rho_2 + \dots = 0$$

or

$$(N) A + \left( \sum_1^N t_i^k \right) B = \sum_1^N \rho_i. \quad \text{A(G-4)}$$

The expression for  $\partial \Omega / \partial B$  implies that

$$(A + Bt_1^k - \rho_1) t_1^k + (A + Bt_2^k - \rho_2) t_2^k + \dots = 0$$

or

$$\left( \sum_i^N t_i^k \right) A + \left( \sum_i^N t_i^{2k} \right) B = \sum_i^N \rho_i t_i^k. \quad \text{A(G-5)}$$

Equations A(G-4) and A(G-5) form a linear system of two equations in A and B with the solutions

$$A = \frac{\left(\sum t_i^k\right)\left(\sum \rho_i t_i^k\right) - \left(\sum t_i^{2k}\right)\left(\sum \rho_i\right)}{\left(\sum t_i^k\right)^2 - N\left(\sum t_i^{2k}\right)}$$

$$B = \frac{\sum \rho_i \sum t_i^k - N \sum \rho_i t_i^k}{\left(\sum t_i^k\right)^2 - N\left(\sum t_i^{2k}\right)} . \quad \text{A(G-6)}$$

Hence, A and B are directly calculable once the value of k is known. The expression for  $\partial\Omega/\partial k$  implies that

$$\left(A + Bt_1^k - \rho_1\right)\left(Bt_1^k \text{LOG}_e t_1\right) + \left(A + Bt_2^k - \rho_2\right)\left(Bt_2^k \text{LOG}_e t_2\right) + \dots = 0$$

or

$$\left(\sum_i^N t_i^k \text{LOG}_e t_i\right) A + \left(\sum_i^N t_i^{2k} \text{LOG}_e t_i\right) B = \sum_i^N \rho_i t_i^k \text{LOG}_e t_i . \quad \text{A(G-7)}$$

Substituting for A and B from above yields

$$\frac{\left(\sum \rho_i\right)\left(\sum t_i^k\right) - N\left(\sum \rho_i t_i^k\right)}{\left(\sum t_i^k\right)^2 - N\left(\sum t_i^{2k}\right)} \sum t_i^{2k} \text{LOG}_e t_i$$

$$+ \frac{\left(\sum t_i^k\right)\left(\sum \rho_i t_i^k\right) - \left(\sum t_i^{2k}\right)\left(\sum \rho_i\right)}{\left(\sum t_i^k\right)^2 - N\left(\sum t_i^{2k}\right)} \sum t_i^k \text{LOG}_e t_i - \sum \rho_i t_i^k \text{LOG}_e t_i = 0 .$$

A(G-8)

The preceding equation is a non-linear equation in the parameter  $k$ . A solution can be obtained in one or two iterations via a numerical Newton procedure using  $k = 1$  as an initial estimate.

## APPENDIX H

### LASER PULSE SHAPE DEGRADATION BY MULTIPLE REFLECTION FROM CORNER REFLECTORS MOUNTED ON A SATELLITE

Appendices H and I consider pulse shape degradation and pulse height degradation due to interference effects from multiple retroreflectors. It will be shown that for a large number of reflectors the interference effects will degrade the returned pulse, both in dynamic range (See Appendix I) and in pulse shape (Appendix H) to unacceptable levels. The analysis will indicate the need to use a small number of corner reflectors.

In this Appendix the change of a rectangular laser pulse upon reflection from an array of retroreflectors will be analyzed via a simplified model. A numerical calculation for a typical set of parameters will also be presented.

Suppose the corner reflectors are mounted uniformly and radially on a spherical satellite; i. e., the reflectors are positioned equidistantly along a circle facing radially outward so that the angle subtended by the two lines emerging from the center of any two adjacent reflectors joining the center of the spherical satellite is a constant angle  $\theta_0$  (See Figure H-1).

Next consider a ruby laser light pulse of frequency  $\nu = 4.3 \cdot 10^{14} \text{ sec}^{-1}$  which is conveniently expressed analytically in an arbitrary coordinate system as:

$$A(t) = [S(\underline{k} \cdot \underline{r} - \omega t) - S(\underline{k} \cdot \underline{r} - \omega t - T)] \cos(\underline{k} \cdot \underline{r} - \omega t), \quad A(H-1)$$

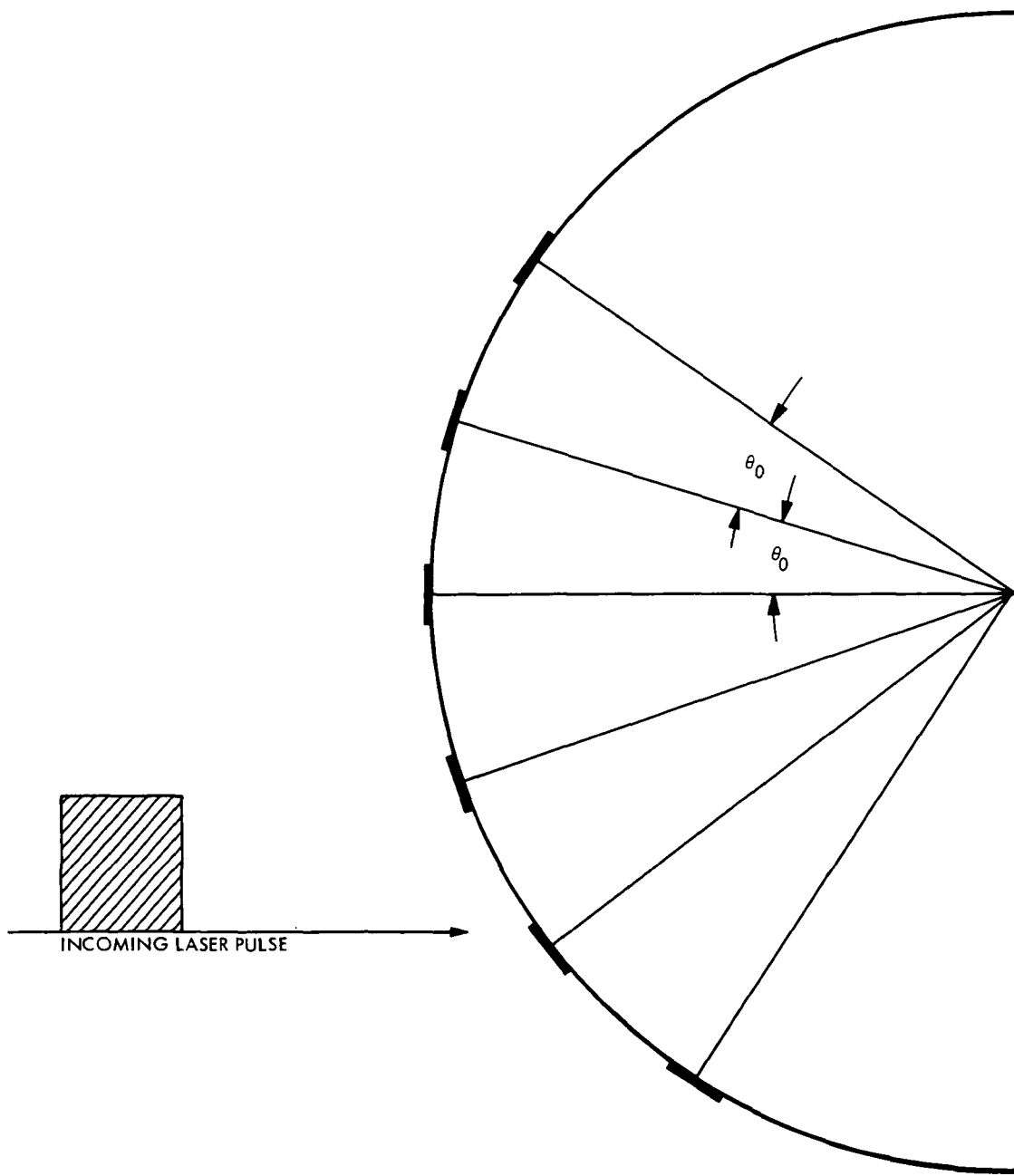


Fig. H-1. Reflectors Mounted on Spherical Satellite

where  $A$  is the amplitude of the electric field,  $\underline{k}$  is the propagation vector,  $T$  is the pulse duration (assumed equal to  $2 \cdot 10^{-9}$  sec), and  $S$  is the step function defined by:

$$S(\chi) = \begin{cases} 1 & \text{if } \chi > 0 \\ 0 & \text{if } \chi < 0 \end{cases} \quad \text{A(H-2)}$$

The light pulse A(H-1), subject to the previously described reflector model, will therefore be reflected by the arrangement of mirrors. Assuming that the incoming light strikes one reflector normally, all the other reflectors will receive the light under a slant angle governed by  $\theta_0$ . The intensity of the back scattered light is sensitive to the angle  $\theta$  between the axis of the reflector and the direction of the incoming light beam.

It can be shown that, for reflectors currently in use, the amplitude of the reflected light may be expressed by:

$$A = e^{-\frac{\theta_0}{\alpha}} \quad \text{A(H-3)}$$

with  $\alpha = 16^\circ$ . The reflected light may now be expressed easily in a coordinate system centered at the center of the spherical satellite, viz:

$$A(t) = \sum_{n=0}^N \left[ S\left(t + \frac{r}{c} \cos n\theta_0\right) - S\left(t + \frac{r}{c} \cos n\theta_0 - T\right) \right] \cdot \cos\left(\omega \frac{r}{c} \cos n\theta_0 - \omega t\right) e^{-\frac{n\theta_0}{\alpha}}, \quad \text{A(H-4)}$$

where  $r$  is the radius of the sphere and the summation index runs over all corner reflectors.

Since the receiving photo multiplier is sensitive only to power, and since the inverse frequency  $\nu^{-1}$  is much smaller than the pulse length, a time averaging can be performed over the period of the carrier wave, i.e., over the high frequency component. Hence, from Eq. A(H-4):

$$\begin{aligned}
 2P(t) = & \left\{ \sum_n \left[ S\left(t + \frac{r}{c} \cos n\theta_o\right) - S\left(t + \frac{r}{c} \cos n\theta_o - T\right) \right] \right. \\
 & \left. e^{-\frac{n\theta_o}{\alpha}} \cos\left(\omega \frac{r}{c} \cos n\theta_o\right) \right\}^2 \\
 & + \left\{ \sum_n \left[ S\left(t + \frac{r}{c} \cos n\theta_o\right) - S\left(t + \frac{r}{c} \cos n\theta_o - T\right) \right] e^{-\frac{n\theta_o}{\alpha}} \right. \\
 & \left. \cdot \sin\left(\omega \frac{r}{c} \cos n\theta_o\right) \right\}^2
 \end{aligned} \tag{A(H-5)}$$

where  $P(t)$  is the instantaneous power in the received signal.

Figure H-2 displays a graph of Eq. A(H-5) for the following set of parameters:  $T = 2 \cdot 10^{-9}$  sec,  $r = 1\text{m}$ ,  $\omega = 2.84 \cdot 10^{15}$  sec<sup>-1</sup> and  $\theta_o = 5^\circ$ . Although only one set of parameters was used, albeit a typical one, it is clearly seen that the pulse shape degradation is significant. As is seen from Fig. H-2 the leading edge of the reflected pulse is shifted somewhat in time. The constant fraction timing discriminator employed in the receiving electronics (See Section 9) integrates the pulse, determines the half width, and decides on the arrival time by selecting the particular point on the leading edge which corresponds to the half width. For the parameters chosen, it is clearly seen from

Fig. H-2 that the arrival time determined in this manner is late by  $1/8 \times 10^{-9}$  sec; this corresponds to about 4 cm.\* This of course is unacceptable for a system which purports to be accurate to the centimeter level.

On the other hand, a shortening of the pulse would eventually create a separate return from each reflector, and therefore a series of individual but weaker pulses would be obtained. Again this is unacceptable since it would confuse the receiving electronics (See Section IX). Here, as well as in Appendix I, the necessity of a small number of corner reflectors is demonstrated.

---

\*See  $\Delta$  in Fig. H-2.

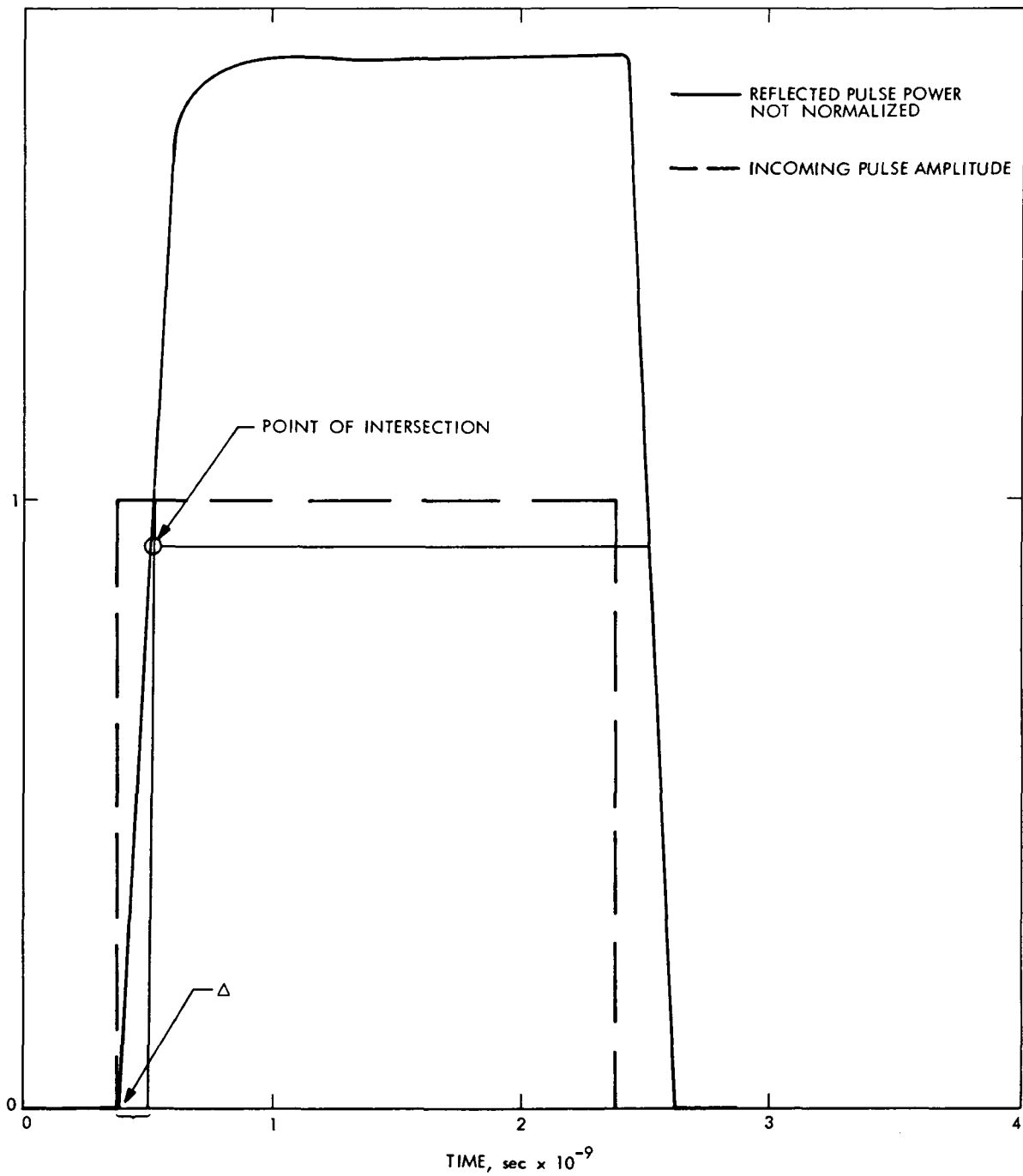


Figure H-2. Pulse Shapes

## APPENDIX I

### SIGNAL STRENGTH FLUCTUATIONS IN A LASER RANGING SYSTEM DUE TO OPTICAL INTERFERENCE BETWEEN THE MANY REFLECTORS ON A SATELLITE

#### I.1 INTRODUCTION

An important parameter used in pulsed laser ranging systems is called the dynamic range. Leaving details aside for the present, the dynamic range in a sequence of M pulses emitted by a laser and returned to the receiving system, is simply given by:

$$\text{dynamic range} = \frac{\text{power of strongest returned pulse}}{\text{power of weakest returned pulse}}. \quad \text{A(I-1)}$$

Because of interference effects, the pulses reflected from corner reflectors mounted on a satellite will vary in magnitude. In this Appendix the expected variation of pulse size will be calculated. The raison d'etre for performing this calculation is the simple fact that the receiving system, as it is conceived, consists of a photomultiplier (PMT) and a constant fraction timing discriminator (CFTD), and these components experience such variations. In this system the CFTD searches electronically for the complete pulse as generated by the PM.\* This search is performed in order to determine at which time the leading edge of the incoming pulse was received. In order to determine this time the dynamic range must be known because when the dynamic range is large, many of the received pulses cannot be handled by the receiving system, i. e., they are lost for use in the process of range determination.

In the following analysis the aim will be to determine the dynamic range for a reflecting system consisting of a large number of individual corner

---

\*The PM becomes saturated, i.e., overloads, at an input level of about 5V.

reflectors. The reason is twofold: first, the mathematical complexity is enormously simplified, and second, a large number of corner reflectors signifies a large return signal and therefore weaker laser pulses might be employed. The obvious advantages are: considerably reducing any safety hazards and also reducing the net cost per station. However it will turn out that the dynamic range is too large when the number of corner reflectors is large. Realizing that the dynamic range is just a measure of the interference effects caused by the interplay of the multitude of corner reflectors it is clear that a small number of corner reflectors will bring the dynamic range to acceptable levels.

## I.2 DERIVATION OF THE PROBABILITY DENSITY OF THE RECEIVED POWER

The net signal received at the ground station will be the sum of the signals returned from the ensemble of retroreflectors. Since each retroreflector is at a slightly different distance from the ground station, the signals returned from the ensemble of retroreflectors will all have different phases.\* Consequently, the signals from the retroreflectors will constructively and destructively interfere.

In an actual system, the laser transmitter emits a sequence of pulses at a rate of 10 pulses/minute. Since each pulse is extremely short ( $<10^{-9}$  seconds), the relative positions of the retroreflectors (and consequently, the relative phases of the reflected signals) will not vary appreciably within the duration of a single pulse. However, the satellite will move a vast number of optical wavelengths between successive pulses. Consequently, the relative phases of the reflected signals will vary drastically from pulse to pulse, and the resulting

---

\*At the light frequency (approximately  $10^{14}$  cycles/sec).

variation in interference effects will cause significant fluctuations in the net received power from pulse to pulse.

### I.3 ANALYSIS

The linearly polarized electric field,  $E$ , of the light transmitted from the ground station can be represented as\*

$$E_T(t) = k \cos(\omega t), \quad A(I-2)$$

where  $k$  is a gain constant and  $\omega$  is the light frequency. Now consider the light reflected from the  $i^{\text{th}}$  reflector on the satellite. The  $E$ -vector of the light, when received at the ground station, can be represented as

$$E_i(t) = a_i E_T \left( t - \frac{2\rho_i}{c} \right), \quad A(I-3)$$

where  $a_i$  is a gain constant,  $\rho_i$  is the range between the station and the  $i^{\text{th}}$  reflector, and  $c$  is the speed of light.\*\* Combining Eqs. A(I-2) and A(I-3) yields

$$E_i(t) = k a_i \cos \omega \left( t - \frac{2\rho_i}{c} \right). \quad A(I-4)$$

---

\*Only the magnitude (not the direction) of the  $E$ -vectors in these equations will be considered.

\*\*Throughout this analysis, the following effects are ignored: 1) atmospheric effects upon propagation, and 2) the variation of  $a_i$  with range. Since both of these effects will tend to increase the fluctuations of the received signal (as measured over a large number of pulses), the estimate of fluctuations will be conservative.

Since the argument of the cosine can be varied by any integral multiple of  $2\pi$  without changing the value of the cosine, the value of  $2\omega\rho_i/c$  can be replaced by

$$\phi_i = \left[ \frac{2\omega\rho_i}{c} \right]_{\text{mod } 2\pi} . \quad \text{A(I-5)}$$

Combining Eqs. A(I-4) and A(I-5) yields the final equation for the E-vector of the light which is reflected from the  $i^{\text{th}}$  reflector and received at the ground station:

$$E_i(t) = k a_i \cos(\omega t - \phi_i) . \quad \text{A(I-6)}$$

since all E-vectors will add algebraically\*, if there are N contributing reflectors on the satellite, the net E-vector of the light received at the ground station will be given by

$$\begin{aligned} E_R(t) &= \sum_{i=1}^N E_i(t) \\ &= k \sum_{i=1}^N a_i \cos(\omega t - \phi_i) . \end{aligned} \quad \text{A(I-7)}$$

---

\*The aperture of the ground station's receiving telescope subtends a miniscule angle as seen from the satellite. Consequently, the light rays which are received from the ensemble of reflectors must be essentially parallel in order to be received. Therefore, all of the E-vectors will lie in the same plane i. e., in the plane perpendicular to the direction of propagation, and the net received light will constitute a plane wave. If all reflected signals are linearly polarized the net received E-vector will be the algebraic sum of the individual E-vectors, and Eq. A(I-7) will be strictly valid. However, since mode-locked ruby lasers emit linearly-polarized light, and since all of the extant satellites employ metal-coated, e. g., aluminized, reflectors which do not appreciably distort the polarization of the incident light, it is reasonable to assume that all reflected signals will be linearly polarized and that Eq. A(I-7) is valid.

The assumption is now made that each reflected signal has the same amplitude (this will be essentially true if all reflectors have the same size and are mounted in the same plane), and therefore Eq. A(1-7) simplifies to

$$E_R(t) = ka \sum_{i=1}^N \cos(\omega t - \phi_i), \quad A(1-8)$$

where each of the various  $a_i$ 's have been replaced by the single parameter,  $a$ .

In order to determine the probability densities of the amplitude and power of the net received signal, it will be necessary to specify the probability densities of the  $\phi_i$ 's. First note that Eq. A(1-5) can be rewritten as:

$$\phi_i = \left[ \frac{4\pi\rho_i}{\lambda} \right]_{\text{mod}2\pi}, \quad A(1-9)$$

where  $\lambda$  is the wavelength of the light. Since  $\lambda$  will have a typical value of about  $7 \times 10^{-5}$  centimeters, i. e., about  $7000 \text{ \AA}$ , even slight changes in  $\rho_i$  (the range between the station and the  $i^{\text{th}}$  reflector) can cause large changes in  $4\pi\rho_i/\lambda$ . Since  $\phi_i$  is equal to the value of  $4\pi\rho_i/\lambda$  taken mod  $2\pi$ , the various  $\phi_i$ 's will assume essentially-random values from pulse to pulse.\* In particular:

- a) the value of  $\phi_j$  during one pulse will be independent of the value of  $\phi_j$  during all preceding pulses (where  $j$  is any integer from 1 to  $N$ ), and
- b) the values of all  $\phi_i$ 's will be independent of each other during any one pulse.

---

\*The relationship between  $\rho_i$  and  $\phi_i$  is analogous to the relationship between  $x$  and  $y$ , where  $y$  is the 10th significant figure of  $\log x$ . In general, even if a succession of  $x$  values has a definite pattern, the corresponding succession of  $y$  values will be essentially random.

Now consider the random process which consists of a large number of successive received pulses. In this process, each of the  $\phi_i$ 's will represent a random variable, i. e., each  $\phi_i$  will assume random values from pulse to pulse. Since each  $\phi_i$  is equally likely to have any value from 0 to  $2\pi$ , the probability density of each  $\phi_i$  will be:

$$p(\phi_i) = \frac{1}{2\pi} ; 0 \leq \phi_i \leq 2\pi .$$

Furthermore, since the various  $\phi_i$ 's are independent, the joint probability density of the  $\phi_i$ 's will equal the product of the individual probability densities, viz.,

$$p(\phi_1, \phi_2, \dots, \phi_N) = p(\phi_1) p(\phi_2), \dots, p(\phi_N) .$$

Equation A(I-8) shows that the net received E-vector is proportional to the sum of N sinusoids which have the same amplitude and frequency but different phases. The remaining problem consists in determining the probability distribution of the electric field Eq. A(I-8) and that of its amplitude. According to the foregoing assumptions the probability of  $E_R(t)$  having the value E is given by the phase space available to all random variables  $\phi_i$  subject to the condition:\*

$$E = \frac{1}{\sqrt{N}} \sum_{i=1}^N \cos(\omega t - \phi_i) . \quad \text{A(I-10)}$$

---

\*Equation A(I-10) is conveniently normalized by the number N of corner reflectors to ease a subsequent passage to a large number of such reflectors. Note that E is a normalized electric field.

Taking into account condition A(I-10), the probability density of  $E_R(t)$ , can then be written as

$$P(E, t) = (2\pi)^{-N} \int_0^{2\pi} \prod d\phi_n \delta \left[ E - \frac{1}{\sqrt{N}} \sum_1^N \cos(\omega t - \phi_i) \right], \quad A(I-11)$$

where  $\delta(x)$  is the Dirac  $\delta$ -function.\*

The integral A(I-11) can be evaluated with the help of the integral representations of the  $\delta$ -function and the Bessel function\*\*, yielding:

$$P(E, t) = \frac{1}{2\pi} \int_{-\infty}^{\infty} e^{iEy} \left[ J_0 \left( \frac{y}{\sqrt{N}} \right) \right]^N dy, \quad A(I-12)$$

---

\*The  $\delta$ -functions in Eq. A(I-11) may be thought of as the conditional probability density that  $E_R(t)$  will have the value of  $E$ , given the values of  $\phi_1, \phi_2, \dots, \phi_N$ . Hence, the probability that  $E_R(t)$  will have any value is given by

$$\int_{-\infty}^{\infty} \delta \left[ E - \frac{1}{\sqrt{N}} \sum \cos(\omega t - \phi_i) \right] dE = 1,$$

which is consistent with the definition of the  $\delta$ -function.

---

\*\*These integral representations are as follows:

$$\delta(y) = \frac{1}{2\pi} \int_{-\infty}^{\infty} dx e^{ixy}$$

and

$$J_0(y) = \frac{1}{2\pi} \int_0^{2\pi} d\theta e^{iy \cos \theta}$$

These formulas can be looked up, e.g., in Ref. [A.1.3.]

where  $J_0$  is the Bessel function of zero order. Equation A(I-12) determines the instantaneous probability density of expression A(I-11) and is seen to be time independent. The determination of the probability for the instantaneous electric field given in Eq. A(I-12) is not yet quite what is needed. The PM tube responds to the average power\*  $W$  rather than to the instantaneous electric field. The derivation for the probability density of the average power  $W$  is somewhat more involved but follows strictly along the same lines as the derivation given above. This is amply explained in [A. I. 2] and [A. I. 1]. For the sake of brevity and for the simple reason that essentially no additional physical insight is gained from a straightforward but tedious derivation, the result will merely be quoted, namely, the probability density for the average power  $W$  is given by:

$$P(W) = \int_0^{\infty} J_0(y\sqrt{2W}) \left[ J_0 \left( \frac{y}{\sqrt{N}} \right) \right]^N y \, dy . \quad \text{A(I-13)}$$

For a large number of corner reflectors,  $N$ , Eq. A(I-13), expanding the Bessel function, results in

$$P(W) \sim 2e^{-2W} . \quad \text{A(I-14)}$$

This equation shall be used in the subsequent analysis.

#### I. 4 PROBABILITY DISTRIBUTION OF THE DYNAMIC RANGE

The probability distribution of the dynamic range of a sequence of  $M$  pulses will now be derived.

Let the following definitions be introduced:

$v \equiv$  power of the strongest pulse in a sequence of  $M$  pulses, \*\*

---

\*Averaged over the period of the carrier wave.

\*\*Throughout this analysis, we will assume that  $M > 2$ .

$u \quad \equiv$  power of the weakest pulse in a sequence of  $M$  pulses.

$g_M(u, v) \equiv$  joint probability density of  $u$  and  $v$ .

Since the power of each pulse in the sequence has a probability density of  $P(W)$ , then:

$P(u) du =$  probability that any one pulse will have a power between  $u$  and  $u + du$ ,

$P(v) dv =$  probability that any one pulse will have a power between  $v$  and  $v + dv$ ,

$\int_u^v P(W) dW =$  probability that any one pulse will have a power between  $u$  and  $v$ .

There are  $M$  possible choices for the weakest pulse,  $M-1$  possible choices for the strongest pulse (after the weakest pulse has been chosen), and  $M-2$  pulses whose powers have to lie between  $u$  and  $v$  in order for  $u$  and  $v$  to respectively correspond to the powers of the weakest and strongest pulses. Thus:

$M P(u) du =$  probability that the weakest pulse will have a power between  $u$  and  $u + du$ ,

$(M-1)P(v) dv =$  probability that the strongest pulse will have a power between  $v$  and  $v + dv$  (after the weakest pulse has been chosen),

$\left[ \int_u^v P(W) dW \right]^{M-2} =$  probability that  $M-2$  pulses have power between  $u$  and  $v$  (assuming that the pulses are statistically independent).

Since the definition of  $g_M(u, v)$  shows that,

$g_M(u, v) \, du \, dv =$  probability that, in a sequence of  $M$  pulses, the power of the weakest pulse lies between  $u$  and  $u + du$ , while the power of the strongest pulse lies between  $v$  and  $v + dv$ ,

and since the pulses are statistically independent, it therefore follows that:

$$g_M(u, v) \, du \, dv = [MP(u) \, du] [(M-1)P(v) \, dv] \left[ \int_u^v P(W) \, dW \right]^{M-2} \quad \text{A(I-15)}$$

Combining Eqs. A(I-14) and A(I-15) shows that, when the probability density of power in a single pulse is given by A(I-14), the joint probability density described by  $g_M(u, v)$  becomes:

$$g_M(u, v) = 4M(M-1) \exp \left\{ -2[(M-1)u + v] \right\} \left\{ 1 - \exp[-2(v-u)] \right\}^{M-2} \quad \text{A(I-16)}$$

I. 5 Probability That the Dynamic Range of the Sequence of  $M$  Pulses will be  $\geq k$ .

Let  $P_M(k)$  be the probability that the dynamic range of a sequence of  $M$  pulses will be  $\geq k$ . Then, using the definition of  $g_M(u, v)$  given above:

$$P_M(k) = \text{Prob}(v \geq ku) = \int_0^\infty \int_{ku}^\infty g_M(u, v) \, dv \, du \quad ; \quad k \geq 1^* \quad \text{A(I-17)}$$

---

\*Note that  $k$  must be  $\geq 1$  since we have assumed in the derivation of  $g_M(u, v)$  that  $v$  is  $\geq u$ . Specifically, it is assumed that  $v$  is the power of the strongest pulse and  $u$  is the power of the weakest pulse.

The integral A(I-17) can be evaluated and after some admittedly tedious algebra yields the result:

$$P_M^{(k)} = 1 - \frac{1}{\underbrace{\left(1 + \frac{M}{M-1} \Delta\right) \left(1 + \frac{M}{M-2} \Delta\right) \dots (1 + M\Delta)}_{M-1 \text{ Terms}}}, \quad \text{A(I-18)}$$

where  $\Delta = (k - 1)^{-1}$ . Equation A(I-18) is displayed in Fig. I-1 with M as a parameter.

## I.6 CONCLUSIONS

The receiving system can handle a ratio  $k = 50$  efficiently. However, as seen from Fig. I-1, for a series of 100 pulses, the dynamic range  $k$  is twice as much with essentially unit probability.\* This of course means that the pulse rejection rate is high. It must be remembered however that Fig. I-1 is based on the simplifying premise of assuming a large number of corner reflectors. This assumption is tantamount to saying that interference effects are particularly severe. The use of a minimum number of corner reflectors is therefore a logical conclusion.

---

\*This is just the dynamic range of Beethoven's 5<sup>th</sup> Symphony during the transition from the second to the third movement.

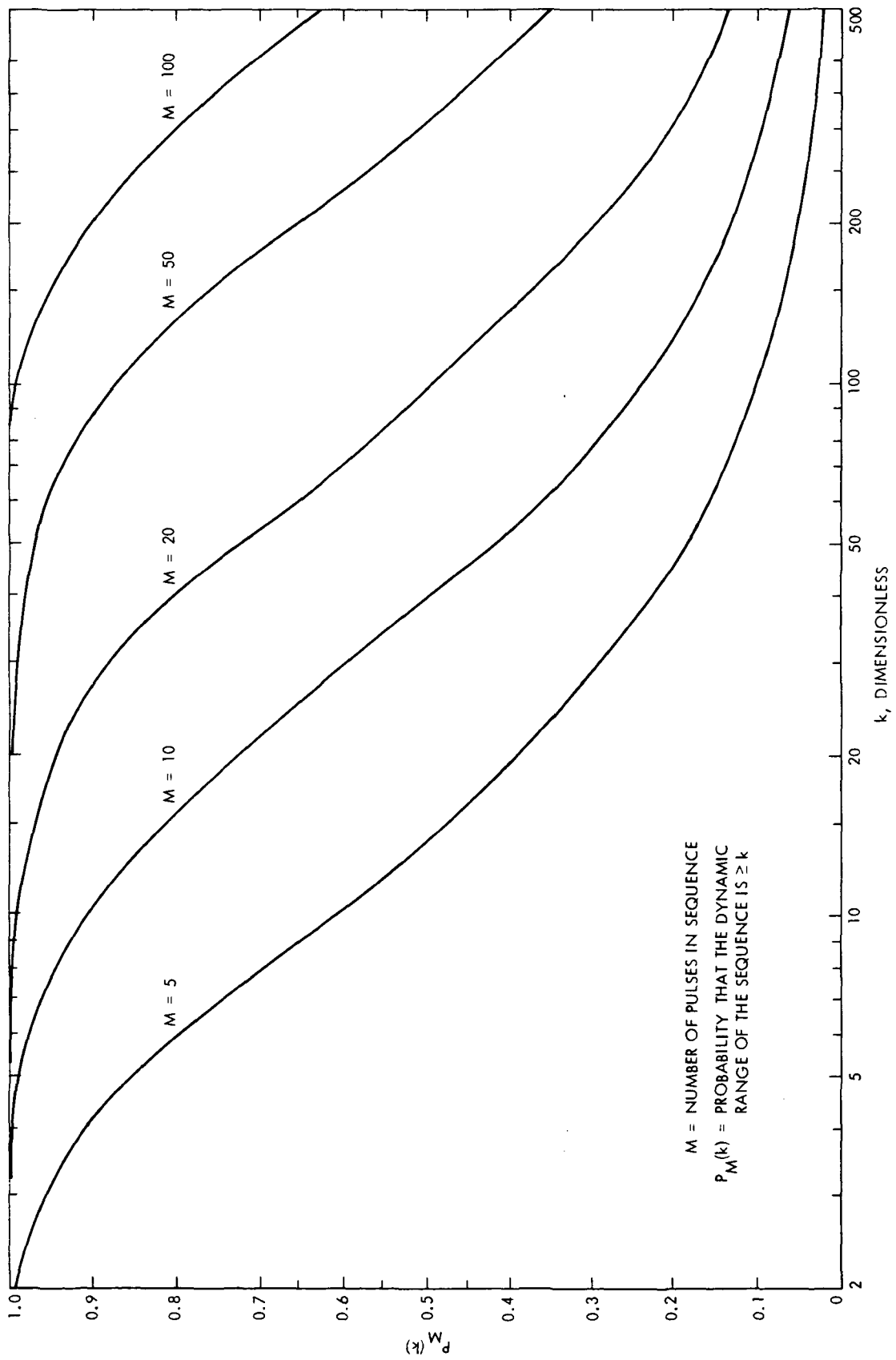


Fig. I-1. Probability distribution of dynamic range

APPENDIX J  
TRANSFORMATION OF COORDINATES

Consider Figure J-1 which illustrates the two basic coordinate systems of this study. In the Figure the numbers 1, 2 and 3 refer respectively to the three primary stations which define the geometric coordinate system.

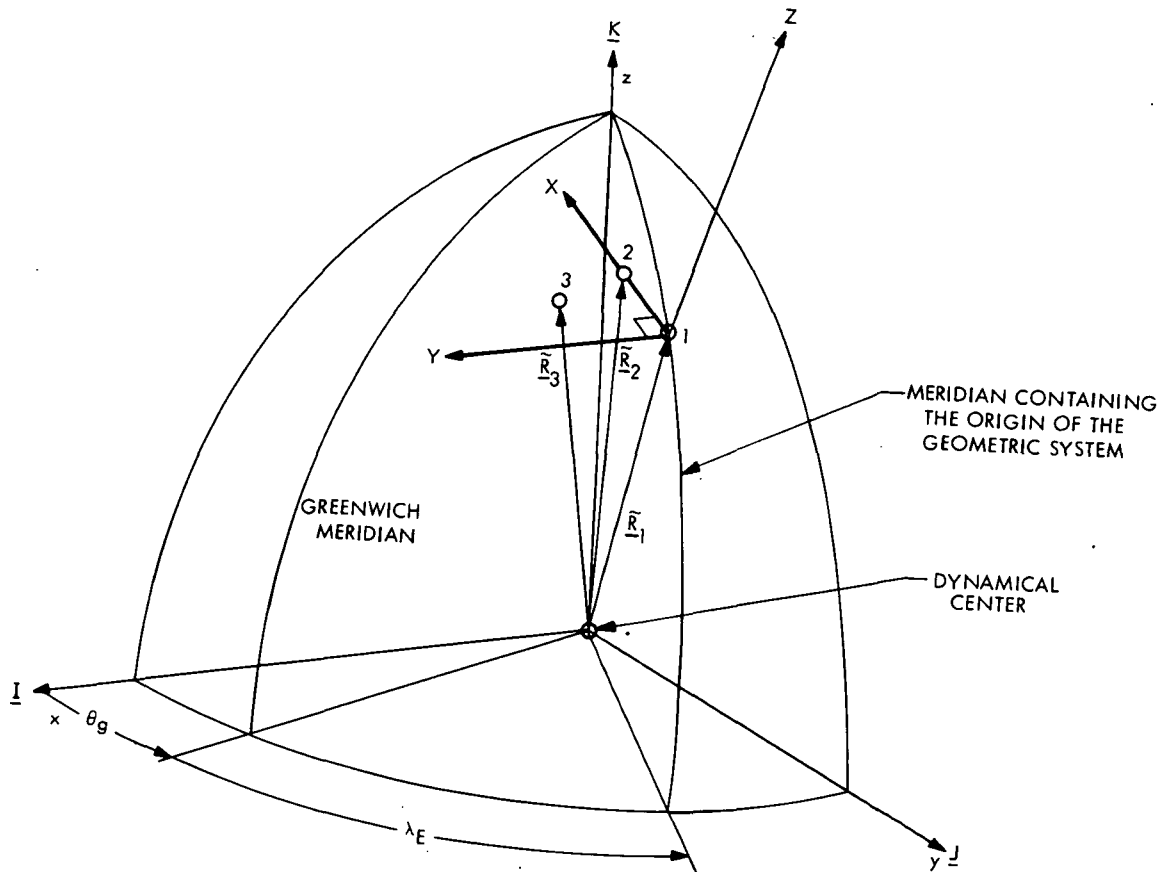


Fig. J-1. Inertial and Geometric Coordinate Systems

Figure 4.5.1 has displayed the basic relationships of the station geocentric coordinate vectors  $\underline{R}_i$ , namely [4.7].

$$\underline{\tilde{R}}_i = \begin{bmatrix} \tilde{X} \\ \tilde{Y} \\ \tilde{Z} \end{bmatrix}_i = \begin{bmatrix} G_1 \cos \phi \cos \theta \\ G_1 \cos \phi \sin \theta \\ G_2 \sin \phi \end{bmatrix}_i,$$

where  $i$  is the station number and

$$G_1 \equiv \frac{a_e}{[1 - (2f - f^2) \sin^2 \phi]^{1/2}} + H$$

$$G_2 \equiv \frac{(1 - f)^2 a_e}{[1 - (2f - f^2) \sin^2 \phi]^{1/2}} + H$$

with

$\phi \equiv$  geodetic latitude,

$\theta \equiv \lambda_E + \theta_g$

$H \equiv$  elevation of station measured normal to and relative to the adopted ellipsoid,

$\lambda_E \equiv$  east longitude of station,

$\theta_g \equiv$  Greenwich sidereal time,

$a_e \equiv$  equatorial radius of Earth,

$f \equiv$  geometric flattening of Earth.

As can be seen from Figure J-1,  $\underline{\tilde{R}}_1$  is the vector from the dynamical origin to station one, i.e., to the geometric origin. The vector from the dynamical origin to station 2 is denoted by  $\underline{\tilde{R}}_2$ . Subtracting these vectors and normalizing results in

$$\hat{X} = \frac{\underline{\tilde{R}}_2 - \underline{\tilde{R}}_1}{|\underline{\tilde{R}}_2 - \underline{\tilde{R}}_1|} = \frac{(\tilde{X}_2 - \tilde{X}_1)\underline{I} + (\tilde{Y}_2 - \tilde{Y}_1)\underline{J} + (\tilde{Z}_2 - \tilde{Z}_1)\underline{K}}{[(\tilde{X}_2 - \tilde{X}_1)^2 + (\tilde{Y}_2 - \tilde{Y}_1)^2 + (\tilde{Z}_2 - \tilde{Z}_1)^2]^{1/2}},$$

the overhead tilde denotes geocentric coordinates and where  $\underline{I}$ ,  $\underline{J}$ ,  $\underline{K}$  are the unit vectors in the geocentric coordinate system, in this case, along the x-axis of the geometric system. Similarly, the vector subtraction of the third and origin station yields

$$\hat{S} = \frac{\underline{\tilde{R}}_3 - \underline{\tilde{R}}_1}{|\underline{\tilde{R}}_3 - \underline{\tilde{R}}_1|} = \frac{(\tilde{X}_3 - \tilde{X}_1)\underline{I} + (\tilde{Y}_3 - \tilde{Y}_1)\underline{J} + (\tilde{Z}_3 - \tilde{Z}_1)\underline{K}}{\left[ (\tilde{X}_3 - \tilde{X}_1)^2 + (\tilde{Y}_3 - \tilde{Y}_1)^2 + (\tilde{Z}_3 - \tilde{Z}_1)^2 \right]^{1/2}},$$

a unit vector toward station 3 in the geometric system. Taking the cross product of these vectors produces a unit vector in the geometric Z-direction:

$$\begin{aligned} \hat{X} \times \hat{S} = & \left\{ [(\tilde{Y}_2 - \tilde{Y}_1)(\tilde{Z}_3 - \tilde{Z}_1) - (\tilde{Y}_3 - \tilde{Y}_1)(\tilde{Z}_2 - \tilde{Z}_1)]\underline{I} \right. \\ & + [(\tilde{Z}_2 - \tilde{Z}_1)(\tilde{X}_3 - \tilde{X}_1) - (\tilde{Z}_3 - \tilde{Z}_1)(\tilde{X}_2 - \tilde{X}_1)]\underline{J} \\ & \left. + [(\tilde{X}_2 - \tilde{X}_1)(\tilde{Y}_3 - \tilde{Y}_1) - (\tilde{X}_3 - \tilde{X}_1)(\tilde{Y}_2 - \tilde{Y}_1)]\underline{K} \right\} / |\hat{X} \times \hat{S}| \end{aligned}$$

Hence using the definition of the cross product

$$\hat{Z} = s \hat{X} \times \hat{S} / [1 - (\hat{X} \cdot \hat{S})^2]^{1/2},$$

where if all stations are in the northern hemisphere  $s = 1$ , if  $(\tilde{X}_2 - \tilde{X}_1)(\tilde{Y}_3 - \tilde{Y}_1) - (\tilde{X}_3 - \tilde{X}_1)(\tilde{Y}_2 - \tilde{Y}_1) \geq 0$ ; otherwise  $s = -1$ ; however if all stations are in the southern hemisphere the previous rule is reversed unless station 1 is in the equator plane in which case  $\hat{Z} = \underline{\tilde{R}}_1 / |\underline{\tilde{R}}_1|$ .

Finally taking the cross product of the two orthogonal unit vectors yields

$$\hat{Y} = \hat{Z} \times \hat{X},$$

which completes the determination of the  $\hat{X}$ ,  $\hat{Y}$ ,  $\hat{Z}$  basis.

In terms of these unit vectors, the coordinates of the stations relative to the geometric system are now given simply by

$$\begin{aligned}
 X_i &= (\underline{\tilde{R}}_i - \underline{\tilde{R}}_1) \cdot \hat{X} \\
 Y_i &= (\underline{\tilde{R}}_i - \underline{\tilde{R}}_1) \cdot \hat{Y} \\
 Z_i &= (\underline{\tilde{R}}_i - \underline{\tilde{R}}_1) \cdot \hat{Z} .
 \end{aligned}$$

The transformation is now complete and can be expressed symbolically as:

Polar Geodetic	→	Rectangular Geodetic	→	Adopted Rectangular Geometric
$\phi_i, \lambda_i, H_i$		$\tilde{X}_i, \tilde{Y}_i, \tilde{Z}_i$		$X_i, Y_i, Z_i.$

APPENDIX K  
MULTILATERATION SYSTEM BIAS STUDY

In this Appendix, the effect of possible station bias errors in range measurements on the resulting multilateration solution is discussed. For this purpose, a simple model of the bias is used. It is shown numerically that arbitrary but small bias errors in the ranges measured at each station, that are maintained fixed throughout each individual calculation (but could be varied in different calculations), act very much like random range errors (of the Gaussian "noise" type) employed in the simulation results presented in Section V. A complete study of different kinds of biases will not be attempted here, but this study is recommended as a future task (See Section 10.3, Task D).

The reader is referred to Section 7.3 for the theory of accuracy simulation used in this report. Let the error in each measured slant range  $\rho_{in}$  include a bias term  $b_i$  which is fixed for the  $i$ th station, in addition to the Gaussian-noise type of random error  $g_{in}$  which has been used in the analysis of Sec 7.3; namely;

$$d\rho_{in} = g_{in} + b_i \quad \text{A(K-1)}$$

$$i = 1, 2, \dots, I,$$

$$n = 1, 2, \dots, N.$$

The "combined error vector"  $d\sigma_n^{(j)}$  can now be separated into two terms as follows:

$$d\sigma_n^{(j)} = \gamma_n^{(j)} + \beta_n^{(j)} \quad \text{A(K-2)}$$

$$j = 4, 5, \dots I;$$

$$n = 1, 2, \dots N,$$

where

$$\gamma_n^{(j)} = \sum_{\ell=1}^3 F_{\ell}(\underline{r}, \underline{S}) \rho_{\ell n} g_{\ell n} + F_j(\underline{r}, \underline{S}) \rho_{jn} g_{jn} \quad A(K-3)$$

$$\beta_n^{(j)} = \sum_{\ell=1}^3 F_{\ell}(\underline{r}, \underline{S}) \rho_{\ell n} b_{\ell} + F_j(\underline{r}, \underline{S}) \rho_{jn} b_n \quad A(K-4)$$

and the functions  $F_{\ell}(\underline{r}, \underline{S})$  are strict functions of the station-satellite geometry.

The error  $dS_i$  induced on station coordinate  $S_i$  due to ranging errors  $d\rho_{in}$  is calculated via the matrix equation

$$P \underline{dS} = \underline{d\sigma} = \underline{\gamma} + \underline{\beta}, \quad A(K-5)$$

where the matrix  $P$  is also a function of the geometry. Since Eq. A(K-5) is a linear matrix equation, we can separate the contributions to the induced station coordinate error into two parts, i.e., "Gaussian noise contribution"  $\underline{dS}_{\gamma}$  and "bias contribution"  $\underline{dS}_{\beta}$ :

$$\underline{dS} = \underline{dS}_{\gamma} + \underline{dS}_{\beta}, \quad A(K-6)$$

where

$$P \underline{dS}_{\gamma} = \underline{\gamma} \quad A(K-7)$$

$$P \underline{dS}_{\beta} = \underline{\beta}. \quad A(K-8)$$

It has been shown in Section V that random range errors (which make up the components of  $\underline{Y}$ ) resulted in excellent sensitivities in station locations for the 6-station configurations analyzed therein. It is reasonable to expect that bias errors of the type considered in this Appendix will behave similarly, inasmuch as the forms of the equations for the two kinds of errors are very much alike [Eqs A(K-3), A(K-4), A(K-7) and A(K-8)]. This has been verified numerically. As a typical illustration, consider the 6-station configuration along the Southern California portion of the San Andreas Fault (See Paragraph 5.1.1). In addition to the 1 cm standard deviation Gaussian noise on the measured slant ranges, an arbitrary fixed bias (chosen also from a Gaussian distribution with zero mean and 1-cm standard deviation) was imposed on all the slant ranges measured from each given station. The induced errors on station coordinates are then calculated using the algorithm given in Paragraph A, Paragraph A1.2. The calculation was then repeated 10 times, each time with a different set of random noise and a new set of station biases. The results of these calculations are summarized in Table K-1.

TABLE K-1

The Average Error  $\epsilon$  and the Standard Deviation  $\sigma$  of the Coordinates of the San Andreas Fault Stations in Centimeters, Assuming 1 CM Standard Deviation Normal Random Errors in Ranging and 1 CM Standard Deviation Bias for Each Station

Station	$\epsilon_X$	$\sigma_X$	$\epsilon_Y$	$\sigma_Y$	$\epsilon_Z$	$\sigma_Z$
San Diego	-0.23	2.06				
Isabella	-0.50	1.25	0.72	3.94		
Santa Rosa I	-0.63	1.56	-0.21	1.93	-0.83	2.03
Millerton	-0.07	1.32	0.71	4.65	0.23	2.21
Blythe	-0.40	2.97	1.23	5.03	1.64	2.01

Comparing Table K-1 with Table 5-2, it is evident that the accuracies of the computed station coordinates are not significantly degraded by the introduction of small station biases. In fact, the average errors remain well within 1-2 cm, whereas the standard deviations (which measure the error for a single 100-point calculation) are only slightly larger than the corresponding quantities in the absence of the biases.

## APPENDIX L

### EARTHQUAKE HAZARD ESTIMATION ALONG THE SAN ANDREAS FAULT ZONE FROM A LONG-BASELINE STRAIN NET

Clarence R. Allen, Don L. Anderson, and James H. Whitcomb  
Seismological Laboratory  
California Institute of Technology

A major geophysical objective of accurately locating widely-spaced points as a function of time is to monitor the strain build-up in the earth's crust. Then, comparing the strain build-up with strain release resulting from earthquakes and from non-seismic slippage or creep, we can make a model of elastic deformation and its variation from place to place from which earthquake hazard can be estimated. Until now, geodetic techniques have not been able to measure relative locations over more than 100 kilometers to an accuracy of a few centimeters, the accuracy desired for geophysical relevance. However, new techniques developed in the space program promise this precision.

The San Andreas and associated fault zones in California and Mexico represent one of the most studied, least complicated (compared to other fault zones) and potentially destructive seismic zones in the world. Therefore, this region provides a truly unique location for getting relative station motions and, thus, regional strain data which are both socially and scientifically pertinent.

#### L.1 Major Questions to Answer

We must first determine the most important questions that can be answered by monitoring crustal locations in time and space. These questions should relate the California fault system to the new theories of plate tectonics and to possible earthquake prediction by strain monitoring. The questions are:

(1) What are the ground movements at large distances (100-200 km) from the San Andreas fault zone? Knowledge of distant point movements is a basic

requirement in constructing a San Andreas zone strain model to be used as the basis of earthquake understanding. Current geodetic-net techniques, while very accurate at short distances, are line-of-sight limited and are impractical beyond distances of about 100 km for the high accuracies needed.

(2) How does strain build-up along the San Andreas zone vary as a function of whether the fault is locked or unlocked; i. e., how much of the accumulated strain is relieved by creep at the unlocked portions of the fault? It is now accepted that the type of slip that relieves strain in the San Andreas zone varies along the length of the fault. In some areas, much of the slip takes place as creep, that is, slow motion with little or no radiated seismic energy (earthquakes). In other areas, almost all of the slip occurs rapidly in large but infrequent earthquakes. The former areas are considered unlocked inasmuch as the accumulating strain is being at least partially relieved as creep. The latter areas are considered locked inasmuch as most of the accumulated strain is being elastically stored for sudden release in further large earthquakes.

Common sense dictates that the regional strain field along the San Andreas is strongly affected by whether the fault is locally locked or unlocked, and any strain measurement program should take this into account. For example, in areas of fault creep it is important to know if the input strain, measured by the displacement of points distant from the fault (100-200 km), is relieved by creep along or near the fault, which is relatively easy to measure. If the strain is relieved mainly by creep, then the likelihood of a large earthquake along that part of the fault is small. However, if only a small portion of the input strain is relieved by creep, then unlocked portions of the fault are also susceptible to large earthquakes.

Figure L-1 shows a map of the San Andreas fault zone and the regions of proven or suspected creep (unlocked) and regions with no observed creep

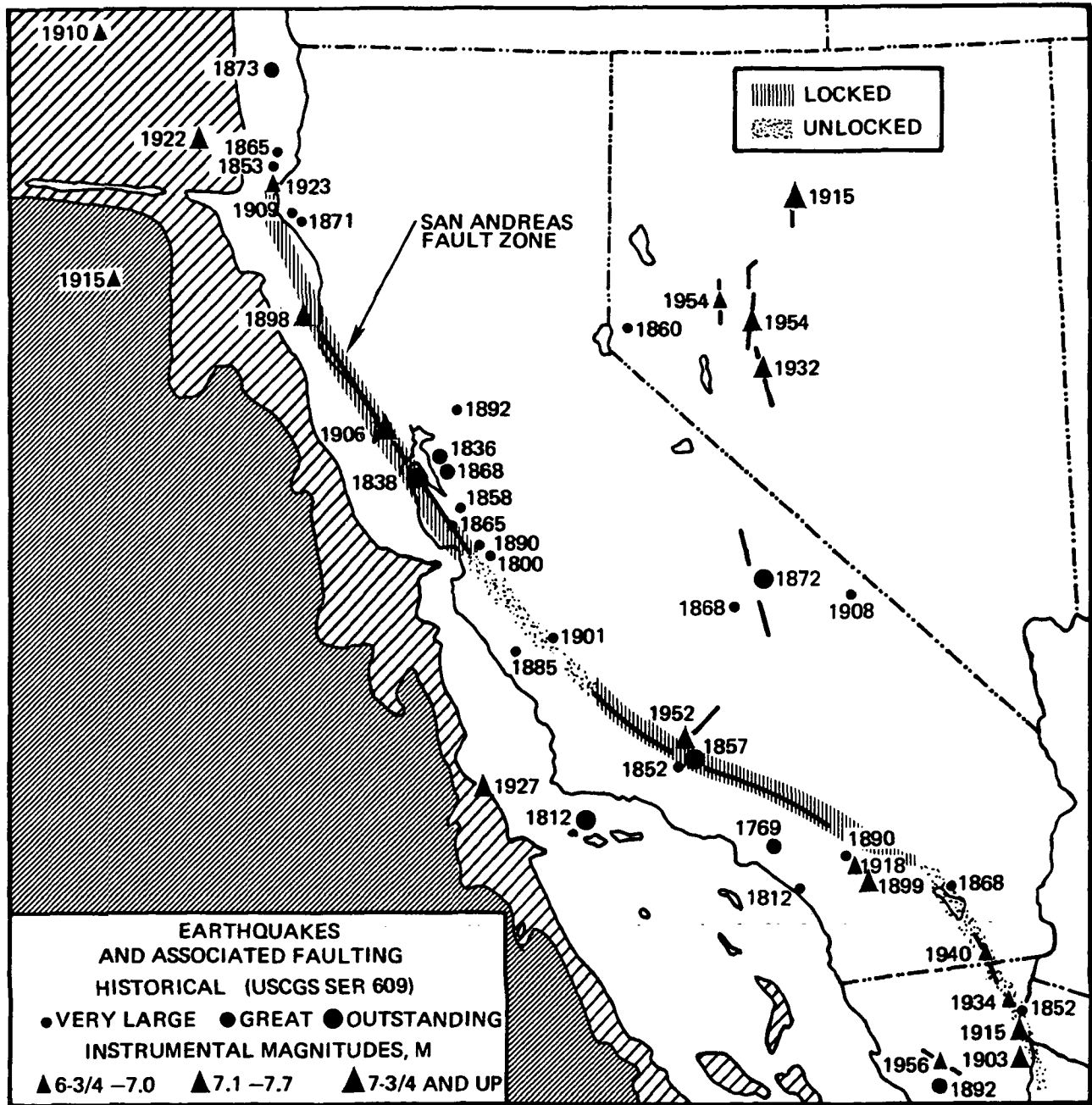


Figure L-1. Large Earthquake and Associated Faulting in the California and Nevada Region. The Locked and Unlocked Portions of the San Andreas Fault Zone are Delineated by the Shaded and Stippled Zones Respectively

(locked). Also shown are the larger earthquakes in the California region from Richter (1958, p. 472). Certainly if we take into account the fault breaks of the 1857 and 1906 earthquakes (shown as solid lines in Figure A. 12. 1) the unlocked zone between San Francisco and Los Angeles has had fewer large earthquakes than the locked parts of the zone. This may be true of the unlocked zone of the Imperial Valley, although the picture there is not as clear. Whether this lack of seismicity is mainly due to creep relief of strain can be answered only by a direct monitoring of the input strain measured at distances far from the creep areas.

(3) Is strain release occurring at places other than along the San Andreas fault zone? Two main possibilities exist. First, significant strain release may be occurring at other faults. As can be seen in Figure L-1, major earthquakes have occurred on fault systems other than the San Andreas, and one should evaluate the importance of these events in terms of the regional strain build-up and release. Second, strain release may be taking place as permanent plastic deformation of the crust. This last statement, if true, contradicts a basic axiom of new plate tectonic theory, i. e. , that the plates are rigid. This axiom is by no means proven on a local scale such as in California and is an important point to investigate when developing a strain model.

(4) What is the relationship of strain build-up along the San Andreas zone to sea-floor spreading in the Gulf of California? This question involves both the question of rigidity of the plates and the continuity of the Gulf of California's spreading rate; i. e. , is it spreading now at 6 cm/yr as calculated from magnetic lineations in the oceanic crust?

(5) What is the instantaneous velocity or displacement rate between adjacent plates? This is the most critical question that relates to earthquake frequency and hazard estimation along the plate boundaries. The displacement

rate determines how much slippage must be made up along the fault zone as creep or as earthquakes. The San Andreas fault zone forms the boundary between plates along its entire length, which explains its high seismicity. Other seismically active zones in the California-Nevada area also may be major plate boundaries, such as the fault system striking north through the Owens Valley, but data are incomplete for firm conclusions on these zones.

## L.2 What is Needed?

In order to measure a plate's horizontal movement completely, the time history of the relative locations of at least two points in the plate is needed. Thus, with four points for two plates, a direct confirmation of the movement predicted by plate tectonic theory is possible. Only one point per plate is necessary if we assume some constraint on its motion, for example, that one boundary remain parallel to a strike-slip fault.

The crustal motions that we anticipate are of the order of 6 cm/yr. Therefore, a measurement of the rate would begin to be significant if it could be made to within about 2 cm/yr. After the positions of the stations have been initially determined, the time to wait for a significant remeasurement depends on the accuracy of the measurement technique.

Figure L-2 shows a schematic graph of a real station displacement rate  $\underline{r}$  and two measurements of station position which will be within  $\pm a$  and  $\pm b$  respectively of the actual position. The time interval between measurements is  $i$ . Taking the worst cases from figure 1, we see that the rate  $\underline{r}$  could be measured between

$$r = \frac{a + b}{i}$$

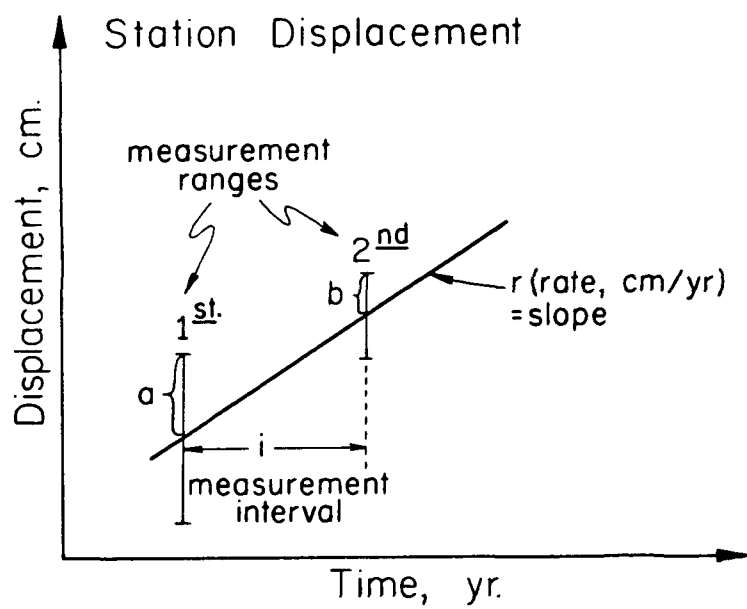


Figure L-2. Schematic Graph of a Real Station Displacement Rate  $\underline{r}$  and Two Displacement Measurements with Errors  $\pm a$  and  $\pm b$  Respectively and With Intervening Time Interval  $\underline{i}$ .

and

$$r + \frac{a + b}{i}$$

so that the error resulting from error a of the first measurement and error b of the second measurement would be

$$\pm \frac{a + b}{i}$$

Now assume that both a and b are 3 cm. The error in rate measurement is then

$$\pm 6/i$$

This means that we must wait three years before remeasurements would give an accuracy of  $\pm 2$  cm/yr, but we will have increasing accuracy with each remeasurement thereafter. If we had to accept  $\pm 10$  cm accuracy for both measurements then the waiting interval would be ten years to get the same rate accuracy of  $\pm 2$  cm/yr. Current Jet Propulsion Laboratory work shows that  $\pm 3$  cm accuracy is now realistic. Therefore, a program begun now would measure the gross plate motions of the earth's crust to an accuracy of 2 cm/yr by at least 1976, with the accuracy improving at each successive measurement.

### L. 3 Recommended Station Placements

In the framework of new plate tectonics, borders of active plates are mainly defined by zones of high seismicity, that is, high earthquake activity. This definition, when applied to the seismicity as represented by the largest earthquakes in the California-Nevada region in Figure L-1, determines three major plates in the area: the North American plate, the North Pacific Plate, and what we define as the Sierra plate as shown in Figure L-3. This figure

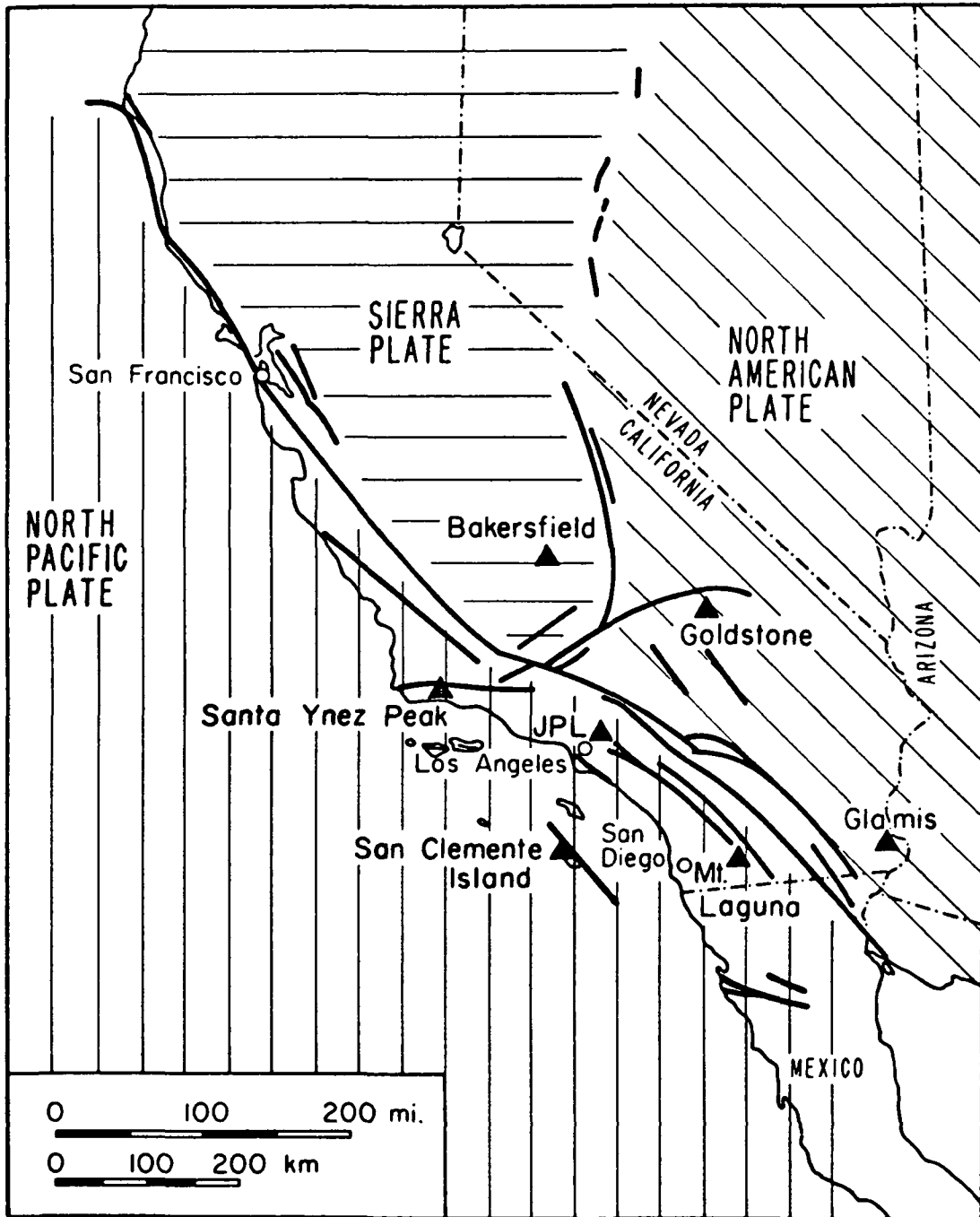


Figure L-3. Major Faults, Lithospheric Plates, and Proposed Stations for the Initial Long-Baseline Strain Net in Southern California.

also shows the major mapped faults in the area as dark lines. With this division we can readily see that a strain build up across the northern San Andreas zone, between the North Pacific and Sierra plates, can be different than that across the southern San Andreas zone, between the North Pacific and North American plates.

Because Goldstone is to be one of the first stations due to its existing antenna facilities, it is best to have the first stations in the region which includes Goldstone, the southern San Andreas zone. Thus, our attention will be focused initially between only two of the above plates, the North American and North Pacific in southern California. We feel that the initial station locations should be Goldstone, JPL, San Clemente Island, and the areas of Mount Laguna, and Glamis as shown in Figure L-3. The San Clemente-Mount Laguna-Glamis line crosses a San Andreas zone of known fault activity and suspected creep in the Imperial Valley of California. Indeed the Imperial Valley is the area of highest continuing seismic activity in the coterminous United States. Here, several parallel faults complicate the picture and the Mount Laguna-Glamis line straddles them for a measure of overall displacement across the valley. An added attraction in the Imperial Valley is that a unique history of geodetic data from government optical surveys is available as an independent check of the results. The San Clemente station to the west provides us with important data at a much greater distance from the fault zone. In addition, the relative displacements between San Clemente and Mount Laguna will shed light on current controversial questions of earthquake potential in the San Diego area.

The Goldstone-JPL-San Clemente line is across a locked portion of the San Andreas zone, the Cajon Pass area, where many seismologists feel a great

earthquake (near magnitude 8.0) is possible within about 50 years.<sup>1</sup> In addition to monitoring strain build-up across this zone, it would be extremely important for us to measure these station locations before a large earthquake happens in order to make post-earthquake comparisons with theoretical strain models.

When additional stations are possible, the next logical extension of the net would be north to the Sierra plate. Stations at Santa Ynez peak and north of Bakersfield shown in Figure L-3 measure displacements across the 1857 earthquake break (solid line on Figure L-1) of the San Andreas zone between the North American and Sierra plates. Motion of these two plates determines strain rates pertinent to the entire northern San Andreas zone including the San Francisco area. Further extension of the net with two additional pairs of stations across the northern San Andreas fault zone and two pairs south across the Gulf of California in Mexico would cover the entire San Andreas-Gulf of California plate boundary system.

It is well to keep in mind in pioneer studies of this type that new and unexpected phenomena may make desirable a more detailed net in a critical area rather than an expansion to other regions of the San Andreas zone. Therefore, we should remain flexible as to future station locations. The portability of the proposed Jet Propulsion Laboratory system should make this not difficult.

---

<sup>1</sup>For a review, see Brune, J.N., 1971, Seismic Sources, Fault Plane Studies and Tectonics, Trans. Am. Geophys. Union, v. 52, no. 5, IUGG 178.

APPENDIX M  
PHYSICAL CONSTANTS

Constant	Adopted Value
Earth Equatorial Radius, $a_e$	6378165 meters
Flattening, $f$	1/298.3
Sidereal Rate, $\dot{\theta}$	$4.37527 \times 10^{-3}$ rad/min
Speed of Light, $c$	299714.1 meters/sec
Second Harmonic, $J_2$	$1082.28 \times 10^{-6}$
Air Density (0°C, 760 mm), $\rho_a$	0.001293 gm/cm <sup>3</sup>
Earth Gaussian Constant, $k$	0.07436574 (e. r.) <sup>3/2</sup> /min
Gravity Acceleration, $g$	980.616 cm/sec <sup>2</sup>
Gas Constant, $R$	8.31 J/mole °K

APPENDIX N  
ABERRATION AND FRESNEL DIFFRACTION

The need for a compact corner reflector has been demonstrated in Appendices H and I. Accordingly, the reflected light will consist of a narrow (~5 cm) diffraction limited beam. Furthermore, it is well known that the reflected beam will also suffer an angular shift due to the motion of the satellite. This angular shift is called aberration and its value,  $\alpha$ , is:

$$\alpha = 2 \frac{v}{c} , \quad \text{A(N-1)}$$

where  $\alpha$  is in radians and  $v$  is the velocity component of the satellite perpendicular to the line of sight. The factor 2 is due to the fact that reflected light rather than emitted light is being considered.

Since satellites in circular orbits of from 500 to 1000 km have relative velocities approximately equal to 7.5 km/sec, the maximum value of angular shift when ranging to these satellites is

$$|\alpha| = \frac{2v}{c} = \frac{2 \times (7.5 \times 10^3)}{3 \times 10^8} = 50 \text{ } \mu\text{radians} = 10 \text{ arcsec} \quad \text{A(N-2)}$$

This amount of angular shift is about 5 times the diffraction-limited beamwidth of a 5 cm corner reflector at ruby-laser wavelengths. Consequently if this size corner reflector is needed (in order to obtain sufficient capture area), the beamwidth of the corner reflector must be increased in order to cause a usable amount of reflected light to return to the ground station.

One way of ameliorating the situation is to artificially widen the beam by means of a divergent lens or by rounding off appropriately the faces of the

reflector. The following analysis is a preliminary study of this problem using cylindrically symmetric apertures.

The equation governing the diffraction pattern as depicted on Fig. (N-2) is derived in Sommerfeld's lectures on theoretical physics [\*]. However, before going into a detailed analysis of the diffraction pattern corresponding to Fig. (N-2) a connection between Fig. (N-1) and (N-2) must be established. Figure (N-1) shows a corner reflector. A diverging lens has been placed in front of the corner reflector. The purpose of this lens is simply to make the reflected beam sufficiently divergent so that the receiving telescope, which incidentally is also the transmitting telescope, does not have to be aimed at a different angle upon receiving the returned pulse. To repeat, the aberration is an angular deviation of about  $5 \cdot 10^{-5}$  radians assuming a satellite velocity of about 7 km/sec. This angular deviation is sufficient so that a telescope transmitting a laser pulse will not be able to receive the pulse back unless the telescope is aimed at the new direction. This is very difficult to accomplish. Obviously, the alternative is to widen the reflected beam sufficiently to overcome the problem.

In order to analyze this problem proceed from Fig. (N-1) to Fig. (N-2). Figure (N-2) shows (in cross section) a circular aperture illuminated by a point source at position S. The object here is to determine the far field diffraction pattern [ $R \rightarrow \infty$  in Fig. (N-2)]. The light source at S (Fig. N-2) is just a replica of the virtual focal point of Fig. (N-1). The problem as stated in Fig. (N-1) can therefore be transposed to the configuration depicted in Fig. (N-2) and it is then amenable to mathematical analysis.

---

\*Sommerfeld A., Optik, Dieterich'sche Verlagsbuchhandlung, Germany, 1950.

The analysis starts with Kirchoff's Integral:

$$U(P) = -\frac{iA}{2} \iint dS \frac{e^{ik(r+s)}}{rs} [\cos(n, r) - \cos(n, s)]. \quad A(N-3)$$

Most symbols are amply explained by merely scrutinizing Fig. (N-2). The other quantities are defined as follows: A is the strength of the source [the focal point of Fig. (N-1)]. The wave length,  $\lambda$ , of the radiation is assumed to be monochromatic. The angles  $(n, r)$  and  $(n, s)$  are clearly defined in Fig. (N-2). A number of assumptions are now made: 1) the radius of the circular aperture a is 2.5 cm, 2) the distance  $r_o$  of the focal point from the aperture is large compared to its radius a, and 3) the distance R between the aperture and the observation plane is essentially infinite. Therefore it follows that to a high degree of accuracy:

$$\cos(n, r) = 1 \quad , \quad \cos(n, s) = -\cos \alpha. \quad A(N-4)$$

Since the aperture of radius a is symmetrical about the z-axis it suffices to contemplate Fig. (N-2). Let  $\xi$  and  $\eta$  be the integration variables corresponding to x and y inside the aperture ( $z = 0$ ). The location of S, the focus of the lens off the center axis, is

$$S \equiv (-x_o, 0, -r_o) \quad A(N-5)$$

The location of P is

$$P \equiv (\tan \alpha R, 0, R) \quad A(N-6)$$

Therefore:

$$r = \left[ r_0^2 + (\xi + x_0)^2 + \eta^2 \right]^{1/2} \doteq r_0 + \frac{\eta^2 + \xi^2}{2r_0} + \frac{\xi x_0}{r_0} . \quad \text{A(N-7)}$$

If  $x_0$  is not small, then:

$$r = r_0 + \frac{\delta^2}{2r_0} + \frac{\xi x_0}{r_0} - \frac{\xi x_0 \delta^2}{2r_0^3} , \quad x_0 \ll r_0$$

and

$$s = \left[ R^2 + \eta^2 + (R \tan \alpha - \xi)^2 \right]^{1/2} = R (\cos \alpha)^{-1} - \xi \sin \alpha , \quad \text{A(N-8)}$$

where  $R \rightarrow \infty$  (far field).

Let:

$$\xi^2 + \eta^2 = \delta^2 , \quad \xi = \delta \cos \phi \quad \text{A(N-9)}$$

so that upon omitting all irrelevant phase factors:

$$U(P) \sim \frac{A}{2\lambda} \frac{1 + \cos \alpha}{R r_0} \cos \alpha \int ds \exp \left\{ -ik \xi \sin \alpha + ik \frac{\delta^2}{2r_0} + i \frac{x_0 k}{r_0} \cos \phi \right\} .$$

A(N-10)

Letting

$$\lim_{R \rightarrow \infty} \frac{A}{R} \rightarrow B$$

and omitting all factors which vary slowly with  $\alpha$  in the neighborhood of  $\alpha \approx 10^{-4}$  radians, it follows that:

$$U(P) \sim \int_0^a \delta d\delta \int_0^{2\pi} d\phi \exp \left\{ ik \frac{\delta^2}{2r_o} \right\} \exp \left\{ ik \delta \cos \phi \left( \sin \alpha - \frac{x_o}{r_o} \right) \right\} \quad A(N-11)$$

Equation (N-11) can be written immediately with the use of Bessel function representations as:

$$U(P) \sim \int_0^a \delta d\delta \exp \left( i \frac{k\delta^2}{2r_o} \right) J_0 \left[ k\delta \left( \sin \alpha - \frac{x_s}{r_o} \right) \right] \quad A(N-12)$$

Equation A(N-12) is true for large values of  $r_o$  (the focal length of the lens). Hence, it is seen that the diffraction pattern is just shifted by the amount  $x_o/r_o$ . This amount is a small number considering that  $r_o$  is of the order of hundreds of meters.

For the case in point  $x_o/r_o$  therefore can be neglected.

Figure (N-3) has been computed with values of the pertinent parameters, given by

$$ka = 2 \cdot 10^5, \quad r_o = 250 \text{ m, } 500 \text{ m, } 1000 \text{ m, and } \infty.$$

The scale is normalized to the intensity  $P_o$  of the far field center line diffraction pattern without a lens ( $r_o = \infty$ ) and is plotted in db  $\left( db = 10 \log \left[ \frac{P}{P_o} \right] \right)$ .

It is usual to call the case  $r_o = \infty$  Fraunhofer diffraction since the incoming light is a plane wave. The other cases deal with spherical waves and are called Fresnel diffraction; hence the caption on Fig. (N-3). Figure (N-3)

depicts the four cases just mentioned. Because of the rapid fluctuations and the wide spacing of the computed values, at least for the case  $r_0 = \infty$ , it was not possible to actually draw a curve through the black dots representing the Fraunhofer case of Fig. (N-3). Indicated on the abscissa of Fig. (N-3) are the first three zeros of the  $r_0 = \infty$  pattern. It is seen that (at least for the aperture and wave length used here) the third zero appears in the neighborhood of  $50\mu$  radius. This is the critical angle for aberration, so that the beam cannot be seen by the receiving telescope. The other cases shown, although there are no nulls, are down in power by at least two orders of magnitude in the critical region around  $50 \mu$  radians. This, however, constitutes sufficient intensity to be successfully processed by the receiver.

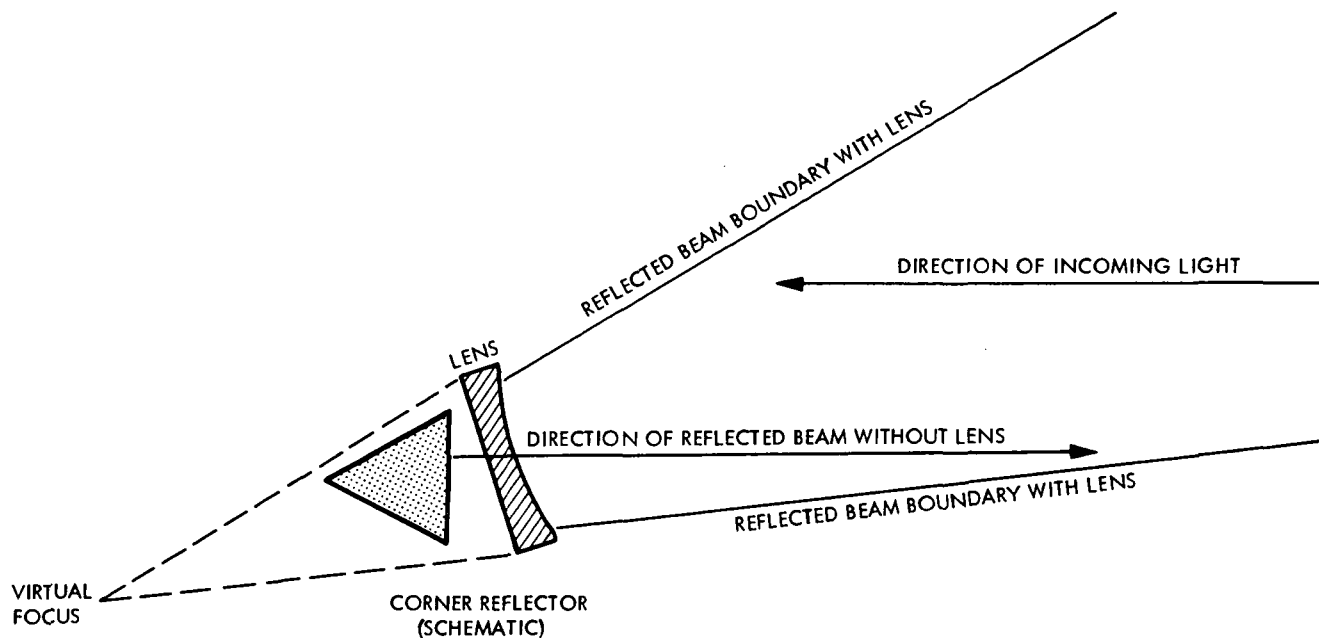


Figure N-1. The Idealized Configuration for the Optical System Consisting of a Corner Reflector and a Beam Spreading Lens

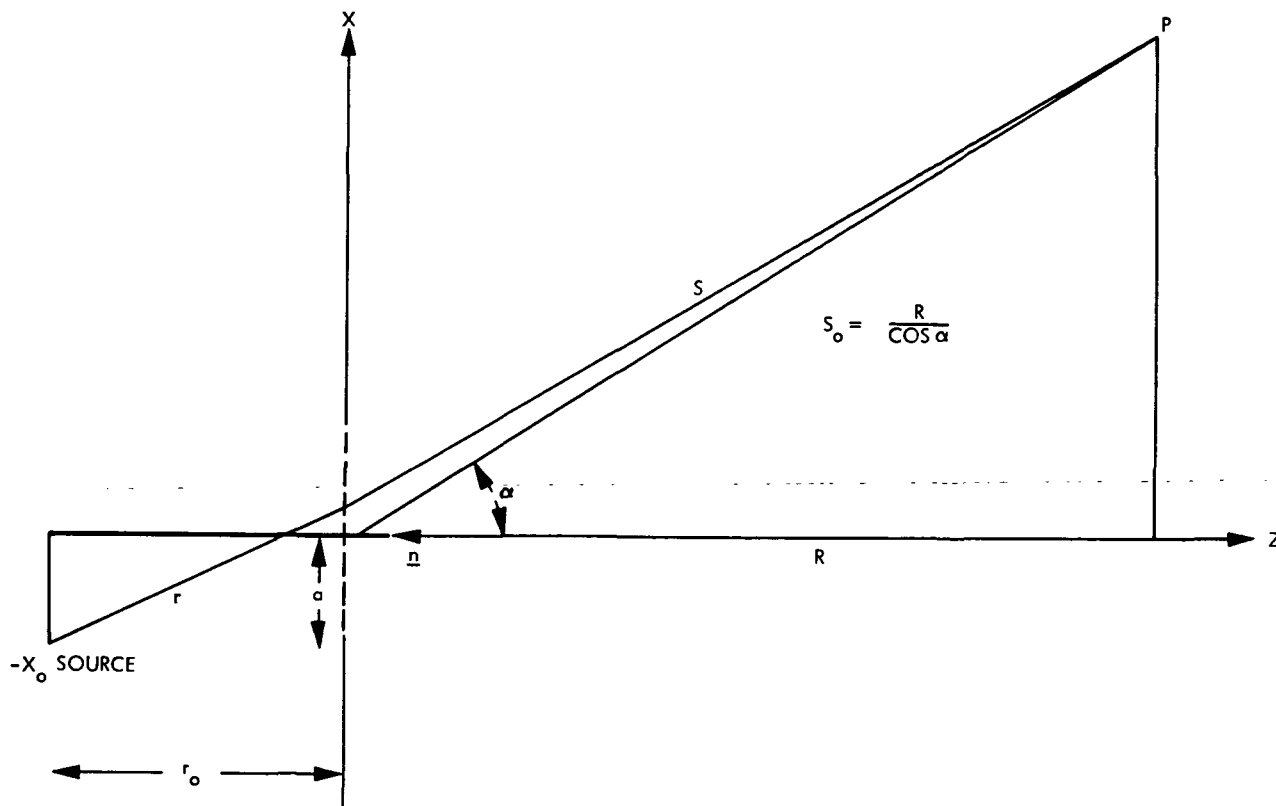


Figure N-2. The Mathematical Model Simulating Fig. N-1. Source is the virtual focus of the lens on Fig. N-1. The corner reflector is simulated by a circular aperture of radius  $a$ . The far field diffraction pattern is calculated by standard means (Ref. A(N-1)).

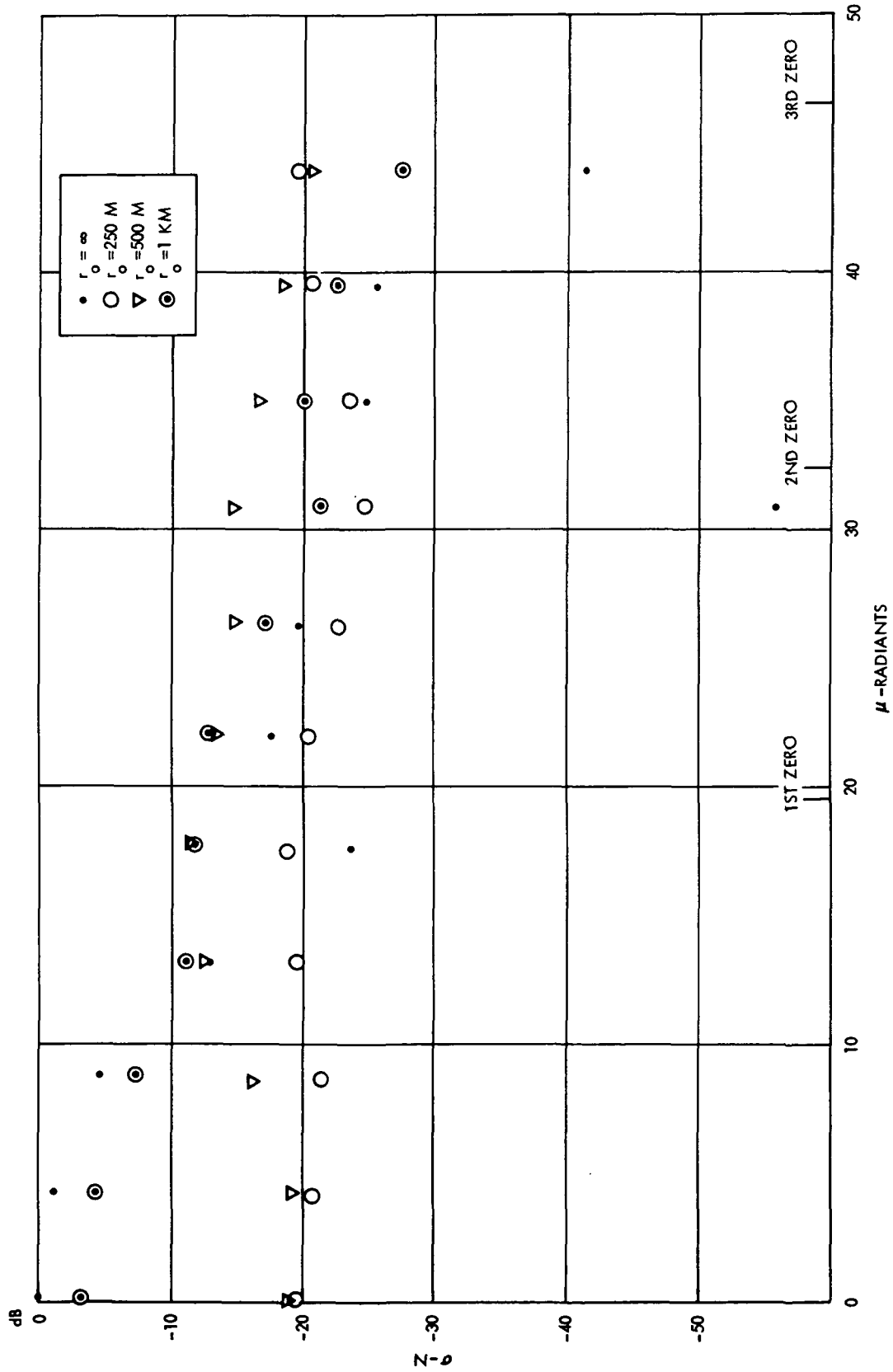


Figure N-3. Fraunhofer ( $r_o = \infty$ ) and Fresnel Diffraction. Explanations in the text

## TECHNICAL REPORT STANDARD TITLE PAGE

1. Report No. 33-605	2. Government Accession No.	3. Recipient's Catalog No.	
4. Title and Subtitle 3-D MULTILATERATION: A PRECISION GEODETIC MEASUREMENT SYSTEM		5. Report Date March 15, 1973	
		6. Performing Organization Code	
7. Author(s) P.R.Escobal, K.M.Ong, O.H.von Roos, M.S.Shumate, R.M.Jaffe, H.F.Fliegel, P.M.Muller		8. Performing Organization Report No.	
9. Performing Organization Name and Address JET PROPULSION LABORATORY California Institute of Technology 4800 Oak Grove Drive Pasadena, California 91103		10. Work Unit No.	
		11. Contract or Grant No. NAS 7-100	
		13. Type of Report and Period Covered Technical Memorandum	
12. Sponsoring Agency Name and Address NATIONAL AERONAUTICS AND SPACE ADMINISTRATION Washington, D.C. 20546		14. Sponsoring Agency Code	
15. Supplementary Notes			
16. Abstract  The systems analysis and laboratory demonstration described in this report indicate that a new technique of satellite geodesy, to be called 3-D Multilateration, can determine the relative three dimensional coordinates of ground stations within 1 centimeter over baselines of 20 to 10,000 kilometers. With this high accuracy, several crucial geodetic applications become possible. These applications include: earthquake hazards assessment, precision surveying, plate tectonics, and orbital applications.  Achievement of such accuracy can be attained through use of pulsed lasers to obtain simultaneous slant-ranges between an ensemble of ground stations and a moving retroreflector whose trajectory is known a-priori only to the accuracy necessary for aiming the lasers. Specifically, the positions of the satellite or airplane carried retroreflectors are eliminated from the equations which govern determination of station locations. However, once the station locations are determined, the trajectory of the retroreflector can be obtained as a direct by-product.  Numerical analysis has shown that suitably chosen multistation configurations result in well-conditioned solutions, with very small error magnification of the inherent ranging errors occasioned by the hardware subsystem.			
17. Key Words (Selected by Author(s)) Earth Surface Environmental Sciences Masers and Lasers Tracking		18. Distribution Statement Unclassified -- Unlimited	
19. Security Classif. (of this report) Unclassified	20. Security Classif. (of this page) Unclassified	21. No. of Pages N-8	22. Price

## HOW TO FILL OUT THE TECHNICAL REPORT STANDARD TITLE PAGE

Make items 1, 4, 5, 9, 12, and 13 agree with the corresponding information on the report cover. Use all capital letters for title (item.4). Leave items 2, 6, and 14 blank. Complete the remaining items as follows:

3. Recipient's Catalog No. Reserved for use by report recipients.
7. Author(s). Include corresponding information from the report cover. In addition, list the affiliation of an author if it differs from that of the performing organization.
8. Performing Organization Report No. Insert if performing organization wishes to assign this number.
10. Work Unit No. Use the agency-wide code (for example, 923-50-10-06-72), which uniquely identifies the work unit under which the work was authorized. Non-NASA performing organizations will leave this blank.
11. Insert the number of the contract or grant under which the report was prepared.
15. Supplementary Notes. Enter information not included elsewhere but useful, such as: Prepared in cooperation with... Translation of (or by)... Presented at conference of... To be published in...
16. Abstract. Include a brief (not to exceed 200 words) factual summary of the most significant information contained in the report. If possible, the abstract of a classified report should be unclassified. If the report contains a significant bibliography or literature survey, mention it here.
17. Key Words. Insert terms or short phrases selected by the author that identify the principal subjects covered in the report, and that are sufficiently specific and precise to be used for cataloging.
18. Distribution Statement. Enter one of the authorized statements used to denote releasability to the public or a limitation on dissemination for reasons other than security of defense information. Authorized statements are "Unclassified-Unlimited," "U. S. Government and Contractors only," "U. S. Government Agencies only," and "NASA and NASA Contractors only."
19. Security Classification (of report). NOTE: Reports carrying a security classification will require additional markings giving security and downgrading information as specified by the Security Requirements Checklist and the DoD Industrial Security Manual (DoD 5220.22-M).
20. Security Classification (of this page). NOTE: Because this page may be used in preparing announcements, bibliographies, and data banks, it should be unclassified if possible. If a classification is required, indicate separately the classification of the title and the abstract by following these items with either "(U)" for unclassified, or "(C)" or "(S)" as applicable for classified items.
21. No. of Pages. Insert the number of pages.
22. Price. Insert the price set by the Clearinghouse for Federal Scientific and Technical Information or the Government Printing Office, if known.

## TECHNICAL REPORT STANDARD TITLE PAGE

1. Report No. 33-605	2. Government Accession No.	3. Recipient's Catalog No.	
4. Title and Subtitle		5. Report Date	
		6. Performing Organization Code	
7. Author(s)		8. Performing Organization Report No.	
9. Performing Organization Name and Address JET PROPULSION LABORATORY California Institute of Technology 4800 Oak Grove Drive Pasadena, California 91103		10. Work Unit No.	
		11. Contract or Grant No. NAS 7-100	
		13. Type of Report and Period Covered	
12. Sponsoring Agency Name and Address NATIONAL AERONAUTICS AND SPACE ADMINISTRATION Washington, D.C. 20546		14. Sponsoring Agency Code	
		15. Supplementary Notes	
16. Abstract  Laboratory tests have demonstrated that a laser hardware subsystem with a ranging accuracy of 3 centimeters can be built from commercially available components. By 1975, at the latest, an accuracy level of 1 centimeter can be achieved. Costs of the proposed systems are lower than other proposed systems on a station construction and implementation basis.			
17. Key Words (Selected by Author(s))		18. Distribution Statement	
19. Security Classif. (of this report)	20. Security Classif. (of this page)	21. No. of Pages	22. Price

## HOW TO FILL OUT THE TECHNICAL REPORT STANDARD TITLE PAGE

Make items 1, 4, 5, 9, 12, and 13 agree with the corresponding information on the report cover. Use all capital letters for title (item 4). Leave items 2, 6, and 14 blank. Complete the remaining items as follows:

3. Recipient's Catalog No. Reserved for use by report recipients.
7. Author(s). Include corresponding information from the report cover. In addition, list the affiliation of an author if it differs from that of the performing organization.
8. Performing Organization Report No. Insert if performing organization wishes to assign this number.
10. Work Unit No. Use the agency-wide code (for example, 923-50-10-06-72), which uniquely identifies the work unit under which the work was authorized. Non-NASA performing organizations will leave this blank.
11. Insert the number of the contract or grant under which the report was prepared.
15. Supplementary Notes. Enter information not included elsewhere but useful, such as: Prepared in cooperation with... Translation of (or by)... Presented at conference of... To be published in...
16. Abstract. Include a brief (not to exceed 200 words) factual summary of the most significant information contained in the report. If possible, the abstract of a classified report should be unclassified. If the report contains a significant bibliography or literature survey, mention it here.
17. Key Words. Insert terms or short phrases selected by the author that identify the principal subjects covered in the report, and that are sufficiently specific and precise to be used for cataloging.
18. Distribution Statement. Enter one of the authorized statements used to denote releasability to the public or a limitation on dissemination for reasons other than security of defense information. Authorized statements are "Unclassified-Unlimited," "U. S. Government and Contractors only," "U. S. Government Agencies only," and "NASA and NASA Contractors only."
19. Security Classification (of report). NOTE: Reports carrying a security classification will require additional markings giving security and downgrading information as specified by the Security Requirements Checklist and the DoD Industrial Security Manual (DoD 5220.22-M).
20. Security Classification (of this page). NOTE: Because this page may be used in preparing announcements, bibliographies, and data banks, it should be unclassified if possible. If a classification is required, indicate separately the classification of the title and the abstract by following these items with either "(U)" for unclassified, or "(C)" or "(S)" as applicable for classified items.
21. No. of Pages. Insert the number of pages.
22. Price. Insert the price set by the Clearinghouse for Federal Scientific and Technical Information or the Government Printing Office, if known.